ALGORITHM FOR SPECTRAL MATCHING OF EARTHQUAKE GROUND MOTIONS USING WAVELETS AND BROYDEN UPDATING

Armen Adekristi

Thesis submitted to the faculty of the

Virginia Polytechnic Institute and State University

in partial fulfillment of the requirements for the degree of

Master of Science

In

Civil Engineering

Matthew R. Eatherton

Roberto T. Leon

Adrian Rodriguez-Marek

April 22, 2013

Blacksburg, VA

Key words: Spectral Matching, Broyden Updating, Wavelets, Spectrum Compatible Acceleration, Frequency Content

ALGORITHM FOR SPECTRAL MATCHING OF EARTHQUAKE GROUND MOTIONS USING WAVELETS AND BROYDEN UPDATING

by

Armen Adekristi

ABSTRACT

This study focuses on creating a spectral matching algorithm that modifies the real strong ground motions in the time domain by adding wavelets adjustment to the acceleration time series. The spectral matching procedure is at its core a nonlinear problem, thus a nonlinear solving method was employed in the proposed algorithm. The Broyden updating method was selected as the nonlinear solving method because it does not require a differentiation analysis. The Broyden updating also makes use the information associated with the change in spectral misfit due to wavelet modifications to approximate the Jacobian matrix which is expected to be an efficient calculation compared to Newton or other nonlinear solution schemes.

A parametric study was numerically conducted to obtain a set of gain factors that reduce the computational time and minimize the spectra misfit. The study was conducted using ten different ground motions, taken from FEMA P-695 (FEMA, 2009), which represent far field, near field-pulse and near field-no pulse earthquake ground motions.

A study of compatible wavelet functions was carried out to determine the appropriate wavelet function for the proposed method. The study include the baseline drift, the frequency and time resolution, and the cross correlation between wavelet adjustments during the spectra matching procedure. Based on this study, the corrected tapered cosine wavelet was selected to be used in the proposed algorithm.

The proposed algorithm has been tested and compared with other methods that are commonly used in spectral matching; the RSPMatch method and the frequency domain method. The comparing parameters were the computational time, the average misfit, the maximum misfit and error, the PGA, PGV, PGD, the Arias Intensity and the frequency content for both acceleration and displacement time histories. The result showed that the proposed method is able to match the target while preserving the energy development and the frequency content of the original time histories.

ACKNOWLEDGEMENTS

I would like to express my appreciation and deep sense of gratitude to the Fulbright fellowship for giving me the opportunity to pursue my master degree in the United States. Without their supports, I would not be able to savor the luxury of studying at the Virginia Tech.

I also would like to thank Dr. Matthew Roy Eatherton, the chairman of my research committee for his guidance and faith that make the completion of this research possible. Dr. Eatherton has taught me a great deal through his extensive understanding on the topics and unwavering patience in communicating it with me. I would like to extend my sincerely gratitude to Dr. Roberto T. Leon and Dr. Adrian Rodriguez-Marek, for their time, insight and rich assistance as my committee members. I also would like to thank Dr. Martin C. Chapman for his input in this thesis. My sincere thanks to Jonathan Hancock and Julian Bommer, who provided the source code for the RSPMatch2005.

I am very grateful for the opportunities provided to me by the Charles E. Via, Jr. Department of Civil and Environmental Engineering and the Graduate School of Virginia Tech, for the great knowledge that they transferred to me during my years here. I would like to express my thanks to my fellow friends in Virginia Tech for their support and sharing. It has been my pleasure to meet and study with the talented and kind people while at Virginia Tech. I also would give my thanks to the Indonesian Student Association (PERMIAS) in Blacksburg for their kindness during my stay here. My sincere thanks to the fellow Fulbright grantees who being such good friends all this time.

I owe thanks to my friends in Indonesia, especially to the ITB civil engineering society, for giving me the courage to pursuit my dream, and also for sharing me the joy and thought. Adrianto and Diego, I still remember our promises three years ago. I am on my way to make it happen.

I am also forever grateful for my parents, for their endless love and pray, for their patience and support throughout my life. It was them that give me strength to finish this thesis. I would also give thanks to my brothers and sister, Christianto Tonggo Sigalingging, Grace Christiani Sigalingging and Agung Chris Setiadi Sigalingging, for they share their laugh and warm support.

Finally, I would like to thank Jesus Christ, God Almighty, for all His blessing in my life. Only through Him is everything possible.

TABLE OF CONTENTS

LIST OF FIGURES

LIST OF TABLES

List of Symbols

$a(t)$	Acceleration time series
b_j	Amplitude of the adjustment function/wavelet function with period T_j
$b^{initial}$	Initial solution for Broyden iteration, initial vector b
b^M	Updated vector b at M^{th} iteration of Broyden loop
C	Spectra sensitivity matrix
$\hat{C}_{norm-i}$	Normalized norm of the off diagonal of C matrix
c_{ij}	Element of spectra sensitivity matrix C, describes the acceleration response at time peak t_i of SDOF oscillator with period T_i due to wavelet adjustment $\psi_j(t)$
D_{rms}	Spectra shape similarity measurement based on the average root-mean-square deviation of the observed spectrum from the target design spectrum
$\hat{d}_{drift}$	Normalized displacement drift
g_b	Gain factor applied to Δb^M
g_C	Gain factor applied for updating C matrix during the Broyden iteration
$h_i(t)$	SDOF oscillator with period T_i acceleration response time series
I_A	Arias Intensity
PGA_{GM}	Peak ground motion acceleration of the records
PGA_{target}	Zero period anchor point of the target spectrum
r	Pearson's correlation of coefficient
S	Wavelet scale
S_{ai}	Peak response of SDOF oscillator with period T_i as subjected to the acceleration time series
$S_{amisfit-i}$	The ordinate difference between target spectra and acceleration spectra at period T_i
$S_{atarget-i}$	Target spectra at period T_i
S_{ai}^M	Updated SDOF oscillator with period T_i at M^{th} iteration of Broyden loop
$S_{amisfit-i}^M$	Updated spectra misfit of period T_i at M^{th} iteration of Broyden loop
SE	Spectra shape similarity measurement based on the sum of errors between the logarithms of the original ground motion's spectra and the target spectra
SSE	Spectra shape similarity measurement based on the sum of squared errors between the logarithms of the original ground motion's spectra and the target spectra
t_i	Time of peak response of oscillator T_i
t_d	Duration of ground motion
$u_{GMi}(t)$	Oscillator with period T_i response as subject to ground motion time series

$u_{ti}(t)$	Total response of oscillator T_i, $u_{ti}(t) = u_{GMi}(t) + u_{t\Psi i}(t)$
$u_{ti-peak}$	Peak of $u_{ti}(t)$
$u_{\Psi ij}(t)$	Oscillator with period T_i response as subjected to wavelet adjustment $\psi_j(t)$
$u_{t\Psi i}(t)$	Sum of $u_{\Psi ij}(t)$
$\hat{v}_{drift}$	Normalized velocity drift
α_C	Gain factor applied on initial *C* matrix
α_j	The frequency-dependent factor,should be selected such that the adjustment wavelet and the reference time histories have consistent duration at frequency ω_j. Used in the tapered cosine wavelet
$\alpha_{\text{off-C}}$	Reduction factor applied on the off-diagonal terms of *C* matrix
$\delta a(t)$	Adjustment function time series that is added to the original time series to match the target spectra
$\delta\Psi_i$	Oscillator acceleration response of adjustment function $\delta a(t)$ for period T_i and damping ζ at time peak t_i
$\gamma(f)$	The frequency-dependent coefficient of the tapered cosine function
Ω	Time controlling parameter in the Suarez and Montejo wavelet
$\boldsymbol{\psi}(t)$	Mother wavelet function with period T_i
$\boldsymbol{\psi}(\omega)$	Fourier transform function
$\psi_i(t)$	Wavelet adjustment time series with period T_i
$\psi_{total}(t)$	Sum of wavelet adjustments, $\sum \psi_j(t)$
ζ	Damping ratio, usually taken as 0.05
ω_i	Angular frequency of period T_i, calculated as $2\pi / T_i$
ω'_i	Damped angular frequency of ω_i, calculated as $\omega_i\sqrt{1-\zeta^2}$
Δb^M	Change on the vector *b* matrix at M^{th} iteration of Broyden loop
Δt_j	Difference between the time peak response t_j and the wavelet time axis
$\Delta S^M_{amisfit-i}$	Change of spectra misfit of period T_i at M^{th} iteration of Broyden loop

CHAPTER 1. INTRODUCTION

1.1 Problem Statement

Seismic analysis for design of buildings and bridges requires determination of seismic loads. Depending on the method of analysis, the seismic loads can be defined in the form of a design response spectrum or a suite of representative ground motions. Response spectra, presented in the frequency domain, are simple, well defined and are the most common approach to characterizing seismic hazard for use in static analysis. However, the application of the design response spectrum for use with dynamic analysis is not necessarily straightforward. In many cases, including design of critical facilities, high rise building and irregular structures, the use of dynamic analysis is required, and the seismic load input needs to be defined in terms of acceleration time histories.

There are many approaches to obtain suitable acceleration time histories for dynamic analysis. If available, engineers can use a set of several recorded ground motions with appropriate magnitudes, fault characteristic, fault distance, and site condition that are consistent with those associated with the maximum considered earthquake for a site. ASCE 7-10 Section 16.1.3 requires that not less than three appropriate ground motions shall be used in the time histories analysis if the structure is designed based on the maximum response from the three analyses. ASCE 7-10 Section 16.1.4 and Section 16.2.4 permit the use average response quantities for design when at least 7 ground motions are used in response history analysis. However, there are few regions of the world where sets of recorded acceleration time histories are available with a wide range of site and source characteristics. It can therefore be desirable to either scale existing ground motions or develop artificial earthquake acceleration time histories. This report focuses on methods for creating artificial ground motions from the existing ground motion records.

The most widely used approaches for creating spectrum-compatible ground motions are generating artificial ground motions from white noise signals, and manipulating real acceleration time histories (Bommer and Acevedo, 2004). Artificial records constitute a convenient tool because it is possible to obtain one acceleration time history that is almost completely compatible with a target design spectrum.

However, spectrum-compatible artificial time histories have some shortcomings for nonlinear dynamic analysis, especially because of their dissimilarity with real earthquake ground motions and issues related to matching a uniform hazard spectrum that is not meant to represent a single earthquake scenario. The differences between artificial and real ground motions can be in form of number of cycles, phase content,

duration and also the energy content. Artificial acceleration time histories may have a large number of cycles and thus possess very high energy content. This problem can be partially mitigated by spectral matching methods that use real strong-motion acceleration time histories.

Spectral matching can be conducted in the frequency domain or the time domain. One common approach to spectral matching in the frequency domain consists of adjusting the Fourier amplitude spectra. However adjusting the Fourier amplitude spectral may corrupt the velocity and displacement time histories; although several base line correction methods can be employed to overcome this problem.

Furthermore, it is known that earthquake ground motions are non-stationary in that the statistical characteristics of the motion vary with time. This nonstationarity of a ground motion is associated with time dependent variation of the frequency (spectral non-stationary) and the time dependent variation of magnitude (amplitude non-stationary). Spectral nonstationarity can be partly associated to the arrival times of the different types of waves; P waves (primary), S waves (secondary), and surface waves (Rayleigh). Generally, the high frequency content arrives sooner which means there is a tendency for the dominant frequencies in the ground motion to shift to lower frequencies as time increases. By using direct adjustment on the Fourier amplitude spectra, the variation of frequency content of the ground motion tends to be not well preserved.

An alternative approach of spectral matching is in the time domain by adding wavelets to the acceleration time histories. A wavelet is a mathematical function that defines a waveform of effectively limited duration that has a zero average. The wavelet amplitude typically starts out at zero, increases, and then decreases back to zero. Wavelet adjustment of recorded accelerations leads to more focused corrections in acceleration time histories. Thus less energy is introduced into the ground motion and the velocity and displacement time histories are better preserved. A method for spectral matching using reserve impulse wavelet function was introduced by Lilhanand and Tseng (1987). Later Abrahamson developed a method of spectral matching using corrected cosine wavelet (Abrahamson 1992) by first approximating it as a linear system. A fundamental assumption of this method is that the time of peak response of the single degree of freedom oscillator used to compute each spectral ordinate will not change after spectral matching. This method then was implemented in the RSPMatch software (Manual for Program: RSPMatch2005, 2005). Refinements to the algorithm were made (Hancock, et al 2006) to overcome the time of peak response shifting by adding correction wavelet or applying a reduction factor to the target response spectrum to aid numerical stability and solution convergence. Al Altik and Abrahamson (2010) developed a new wavelet adjustment function that has a functional form that readily integrates to zero velocity and displacement without including any baseline correction in its functional form.

The process of spectral matching is an inherently nonlinear process. Adding wavelets to the acceleration history has a nonlinear effect on the spectral ordinates because the time of peak response of the elastic single degree of freedom system used to calculate the spectral ordinate may shift. As introduced briefly above, and discussed in more detail in the following two chapters, current methods for time-domain spectral matching approximate the spectral matching process as a linear system of equations and in some cases uses corrections to minimize the effect of nonlinearity. This report presents a proposed method of spectral matching using wavelets that embraces the inherent nonlinearities in the algorithm. Two major differences between the proposed method and the RSPMatch method are that the proposed method allows the time of peak response to be shifted and a nonlinear solution algorithm is employed.

1.2 Study Objectives

The objective of this study is to develop a method of spectral matching using wavelets coupled with a nonlinear solution algorithm. The method used in this study adds wavelets to a real strong ground motion to match a target response spectrum while preserving the spectral nonstationary character of the original ground motion. The proposed method accounts for the nonlinearity in the solution of the system of equations to determine the wavelet magnitudes used to modify the acceleration history. This is implemented using the Broyden updating method for solving nonlinear sets of equations. The proposed algorithm has been implemented and shown successful in its objective. The concepts, algorithm, its implementation, refinement of variables to improve convergence, and application examples are presented. Velocity and displacement time histories after spectral matching are analyzed to determine if the resulting ground motion is representative of a realistic ground motion.

A parametric study was performed to obtain a set of gain factors used in the algorithm that improve convergence time and reduce spectra misfit. A study was also conducted to examine the applicability of several wavelet bases for use in the proposed spectral matching procedure. Conclusions about the suitability of different wavelet bases is based on general criteria that make the conclusions from that study useful for wavelet selection with any time domain spectral matching method.

The energy in the ground motions before and after spectral matching was investigated using Arias Intensity to examine how much energy is input in the ground motion for different approaches to spectral matching. Non-stationary content of the matched acceleration were analyzed using wavelet spectrograms to observe how spectral matching changes the frequency content. Finally, the new spectral matching algorithm was compared to existing methods.

1.3 Report Organization

This report contains nine chapters. Chapter 1 gives the introduction of the project introduction, including the problem statement, objective of the project and the report organization. Chapter 2 presents the literature review and background of spectral matching for a ground motion. Chapter 3 explains the algorithm and presents the results of the RSPMatch method of spectral matching using wavelets. Chapter 4 describes the concept and algorithm of the proposed method. Chapter 5 shows a preliminary study on stability and convergence in correlation with some gain factors and coefficients used in the algorithm. Chapter 6 presents the numerical parametric study to obtain a good gain factor/coefficient set that is proposed for use in the algorithm. Chapter 7 analyzes some wavelet bases that are compatible to be used in the algorithm. Chapter 8 shows the numerical result and comparison with other methods. Chapter 9 presents the conclusions and recommendations.

CHAPTER 2. LITERATURE REVIEW

2.1 Existing Methods of Spectral Matching

Although spectral matching is becoming a common approach to produce a spectrum compatible time series, it is noted that at the outset that there is no consensus about the use of spectrum compatible acceleration histories in design to represent the hazard associated with a response spectrum. Because design response spectra are often a uniform hazard spectrum, the design spectrum represents more than one earthquake scenario. A spectrum matched ground motion therefore represents hazard coming from multiple earthquake events rolled together. It is generally believed that such time histories overestimate the structural response or are not realistic. Solutions have been proposed (e.g. the conditional mean spectrum (Baker 2011)), but are not the subject of this report.

Apart from the selection of an appropriate target spectrum, there are several approaches to developing an artificial spectrum-compatible acceleration time histories. A review of spectral matching methods is given by Preumont (1984) and Bommer and Acevedo (2004). There are three basic approaches for spectral matching: the frequency domain method, the frequency domain method with random vibration theory (RVT), and the time domain method.

Frequency Domains Methods

One common way to perform spectral matching using real earthquake ground motions is in the frequency domain by adjusting the Fourier amplitude spectra (Silva and Lee, 1987). The frequency domain approach adjusts the Fourier amplitude spectrum based on the ratio of the target response spectrum to the actual response spectrum while keeping the Fourier phase of the reference time series fixed.

While this approach is straightforward, it has several drawbacks. First, this approach often alters the non-stationary character of the time series to such a large degree that it no longer represents a real earthquake ground motion and tends to increase the total energy in the ground motion. Second, matching in the frequency domain with multiplicative scale functions applied to the Fourier amplitude spectra corrupts the velocity and displacement time histories which can be obtained by integrating the acceleration record. The corruptions are evident in the velocity time history as a nonzero value offset at the end of motions and in the displacement time history as a linearly increasing (or decreasing) displacement after the ground motion ceases.

Baseline correction methods are often necessary to correct the resulting ground motions. Shahbazian A. and Pezeshk S. (2010) proposed a technique that can be applied in the frequency domain method to appropriately manipulate the velocity and displacement time histories, such that a time domain baseline correction is no longer required. The technique makes use of filters that account for the high sensitivity of the displacement time history to the Fourier amplitude spectra scaling, and modifies the spectral scaling to accurately remove displacement offset. Their study also discussed that zero padding at ends of the ground motions may reduce the displacement distortion in the frequency domain.

Frequency Domain with Random Vibration Theory Method

This approach uses random vibration theory to make initial large adjustments to the Fourier amplitude spectrum, followed by the frequency domain method for small-scale adjustment (Preumont, 1984). This method generates a power spectral density function from the smoothed response spectrum and derives sinusoidal signals having random phase angles and amplitudes. The sinusoidal signals are then summed and iterative procedure is employed to improve the matching level with the target response spectrum by calculating the ratio between the target and generated acceleration response. The power spectral density function is then adjusted by this ratio. This method usually works well in terms of the acceleration and velocity time histories, but often changes the character of the displacement time histories. This method has a problem that the artificial acceleration time histories generally possess an excessive number of cycles, and consequently the resulting spectrum matched ground motions can have unreasonably high energy content.

Time Domain Method

The time domain method is generally considered a better approach for spectral matching since this method adjusts the acceleration time histories in the time domain by adding wavelets. A wavelet is a mathematical function that defines a waveform of effectively limited duration which has a zero average. The wavelet amplitude typically starts out at zero, increases, and then decreases back to zero. Adding discrete length wavelets to the acceleration records tends to better preserve the non-stationary character of the original time histories.

The time domain method was first introduced by Lilhanand and Tseng (1987, 1988). Lilhanand proposed an algorithm that uses reserve impulse wavelet functions to modify the initial time histories such that its response spectrum is compatible with a target spectrum. A fundamental assumption of this methodology is that the time of the peak response does not change as a result of the wavelet adjustment. This assumption is not

always valid as the time of peak response may be shifted by adding the wavelet adjustments to the acceleration time history. This method and the ensuing refinements will be discussed in the following chapter.

Zhou and Adeli (2003) decomposed earthquake records using the Mexican Hat wavelets. It was proposed that ground motions in earthquakes can be represented as a sequence of simple penny shaped ruptures at different locations along a fault line and occurring at different times. The single point source displacement of ground motion is idealized by a Gaussian function. The same idea can be applied for spectral matching with different wavelet forms.

Suarez and Montejo (2005) uses continuous wavelet transform to decompose the original acceleration time-series into number of time series which have non-overlapping frequency bands. Each time series is then being scaled iteratively so that the sum of all time series produces a spectrum compatible ground motion.

Amiri and Asadi (2010) proposed a new method of constructing artificial ground motions using neural-networks and wavelet packets capable of generating an earthquake acceleration time histories from a response spectrum. In the proposed method, the neural networks learn the inverse mapping directly from the actual recorded earthquake acceleration time histories and their response spectra.

Nakhaei and Mohraz (2010) studied inelastic spectral matching using wavelet transformations and the damage index proposed by Park and Ang (1985) for inelastic spectral matching. This approach will assist the selection of records to match a predetermined level of damage.

Shama (2012) showed that the Morlet wavelet can be used successfully to represent the mother wavelet for spectral matching. The procedure is illustrated by scaling a number of earthquake records to match the ASCE-7 Standard design spectrum at different seismic zones.

2.2 Wavelet Bases in the Time Domain Method

Wavelet analysis is becoming a powerful tool for analyzing localized variation of energy within earthquake time histories. By decomposing the time histories into the time-frequency domain, the dominant modes of variability and how the modes vary in time can be determined. Several studies on wavelet transform in seismic and geophysics area have been conducted during the past years. Application of wavelet transform itself started in 1981 with Morlet's studies. Morlet (1981, 1983; Goupillaud et al 1984) applied wavelet transform to seismic data analysis and developed the wavelet that still bears his name.

The development of spectral matching using wavelet transforms was started by Lilhanand and Tseng (1987, 1988). Wavelets were employed by using the response of an elastic SDOF system to simultaneously match

spectra with multiple damping ratios. Although their wavelet adjustment function introduced drift to the resulting velocity and displacement time histories, the method become a fundamental base for further development of spectral matching methods. Abrahamson (1992), based on the techniques presented by Lilhanand and Tseng (1987), developed the RSPMatch program that had been enhanced several times (Hancock et al. 2006; Al Atik and Abrahamson 2010). The RSPMatch adjustment preserves the nonstationary character of the reference ground motion. Suarez and Montejo (2005) developed their own wavelet based on the impulse response function.

In general, the wavelet used in time domain spectral matching methods should be selected to produce realistic spectrum compatible acceleration time histories. The wavelet should be compactly supported in which the value tends toward zero on both ends. The velocity and displacement time series, calculated by direct integration of the wavelet acceleration time history, should also be compactly supported. Numerical stability is also considered in selecting a wavelet basis. One of the challenges is adjusting the acceleration time history record in a way that the integrated velocity and displacement still have a zero value at the end. In the development of the time domain spectral matching method, there are several proposed wavelet forms. Some of them include the Lilhanand and Tseng wavelet, the tapered cosine wavelet, the improved tapered cosine wavelet and the Suarez and Montejo wavelet. The different wavelet bases are discussed in the following sections.

Lilhanand and Tseng Wavelet

The original wavelet used by Lilhanand and Tseng (1987) consists of the true acceleration impulse response function in reverse time order given by:

$$\boldsymbol{\psi}_j(t) = h_j(t_j - t) = e^{(-\omega_j \zeta_j (t_j - t)} \left[\left(2{\zeta_j}^2 - 1\right) sin(\omega_i{}'\left(t_j - t\right)) - 2\zeta_j \sqrt{1 - {\zeta_j}^2}\, cos(\omega_i{}'\left(t_j - t\right)) \right] \quad (2.1)$$

where t_j is the time of the peak response of the j^{th} oscillator under the action of the j^{th} wavelet.

The wavelet form used by Lilhanand and Tseng has a desirable numerical feature in that if the response amplitudes for a set of single degree of freedom oscillators with period i as subjected to a wavelets with period *j* are organized into a square matrix with identical sets of periods *i* and *j*, that the matrix is symmetric. This symmetric matrix of wavelet adjustment amplitudes helps aid the stability of the solution algorithm. The Lilhanand wavelet is emergent and stops abruptly, which encourages an SDOF oscillator subjected to the wavelet as an acceleration to have peak response at a constant time t_j. However this abrupt stop leads to an undesirable feature because it is contrary to the behavior of real strong ground motions that generally have a

sharp initiation and gradual decay. Figure 2-1 shows the Lilhanand and Tseng wavelet with a period of 1 sec and the associated time integrations resulting in velocity and displacement histories.

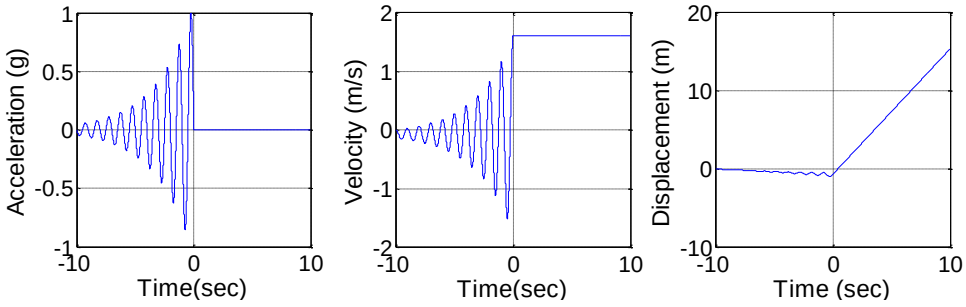

Figure 2-1 Lilhanand and Tseng Wavelet, T=1sec

Tapered Cosine Wavelet

The tapered cosine wavelet can be described by:

$$\boldsymbol{\psi}(t) = e^{[-|t-t_j+\Delta t|\alpha_j]} cos\left(\omega'_j\left(t - t_j + \Delta t_j\right)\right) \tag{2.2}$$

where Δt_j is the difference between the time peak response t_j and the reference origin of the wavelet. The value of Δt_j is given by

$$\Delta t_j = \frac{tan^{-1}\left[\frac{\sqrt{1-\zeta_j{}^2}}{\zeta_j}\right]}{\omega'_j} \tag{2.3}$$

The frequency-dependent factor, α_j, should be selected such that the adjustment wavelet and the reference time histories have consistent duration at a frequency ω_j. In other words, if the reference time-history has a short duration, the α_j should be selected such that the adjustment function at that frequency will also have a short duration (Hancock et. al 2006). This is purposed to ensure that the wavelet adjustment has a proper duration such that it starts and ends with zero value, which leads to zero drift in velocity and displacement drift. A tri-linear model for $\alpha(f)$ is given by:

- $\alpha(f)=a_1 f$ for $f < f_1$ (2.4a)
- $\alpha(f) = \left(a_1 + (a_2 - a_1)\frac{(f-f_1)}{(f_2-f_1)}\right) f$ for $f_1 < f < f_2$ (2.4b)
- $\alpha(f)=a2\, f$ for $f > f_2$ (2.4c)

The use of the tapered cosine wavelet as an adjustment to the acceleration history has the advantage of preserving the non-stationary character of the acceleration time histories. However, this adjustment function introduces drift to the velocity and displacement time histories. This drift is due to the functional form of the adjustment function and not to numerical errors. Thus, the application of the tapered cosine wavelet requires

applying baseline correction to the adjusted acceleration time histories. Figure 2-2 shows the Tapered Cosine Wavelet with period 1 sec and the associated time integrations resulting in velocity and displacement histories.

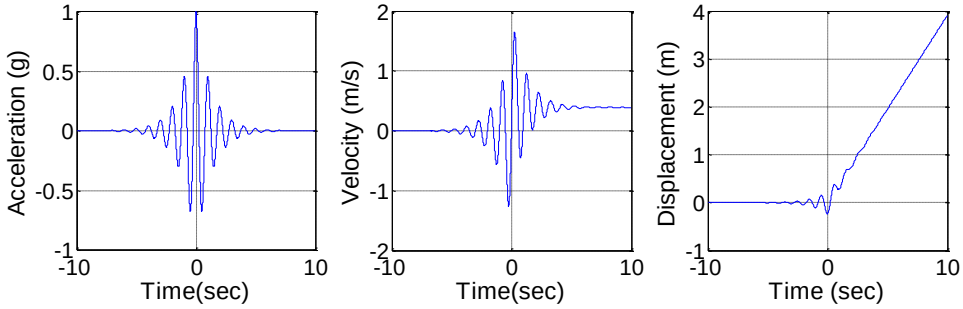

Figure 2-2 Tapered Cosine Wavelet, T=1sec

Corrected Tapered Cosine Wavelet (Al Atik and Abrahamson, 2010)

In order to prevent drift in the adjusted velocity and displacement time histories, the improved tapered cosine wavelet was developed such that its functional form integrates to zero velocity and displacement. The corrected tapered cosine wavelet differs from the tapered cosine wavelet proposed in Hancock et.al (2006) in terms that the wavelet has a functional form that readily to integrates to zero velocity and displacement without requiring any baseline correction form. The corrected tapered cosine wavelet can be described by:

$$\boldsymbol{\psi_j}(t) = e^{-\left[\frac{\left(t-t_j+\Delta t_j\right)}{\gamma_j}\right]^2} cos\left(\omega'_j\left(t-t_j+\Delta t_j\right)\right) \tag{2.5}$$

Where Δt_j is the differences between the time of peak response with the reference time of the wavelet (t_j). The correction factor γ_j is a frequency dependent coefficient used to adjust the duration of the adjustment function. The *γ(f)* was developed to ensure a smooth taper and lead to zero velocity and displacement at the end of the wavelet. The adjustment at all frequencies, *γ(f)* is given by:

$$\gamma(f) = 1.178 f^{-0.93} \tag{2.6}$$

The corrected tapered cosine wavelet result no drift in the velocity and displacement time series when the duration of the wavelet is long enough to start and end with zero value. However, this depends on the wavelet reference time t_j. The frequency-dependent coefficient of the tapered cosine function *γ(f)* was selected to ensure that drift in the velocity and displacement time histories of the wavelet does not occur for most t_j values at different frequencies. The minimum t_j values required to prevent drift is described by Eqn. 2.7.

$$t_{j\,min} = 3.9223\, f^{-0.845} \tag{2.7}$$

If the wavelet adjustment is centered at a time that is before $t_{j\,min}$ or close to the beginning of time history, part of the wavelet is truncated which leads to drift in velocity and displacement time history. The same is possible if t_j is near the end of the time history. For this case, it is required to zero pad the time history at the beginning or end of time history.

The acceleration, velocity and displacement time histories of corrected tapered cosine wavelet can be seen in Figure 2-3.

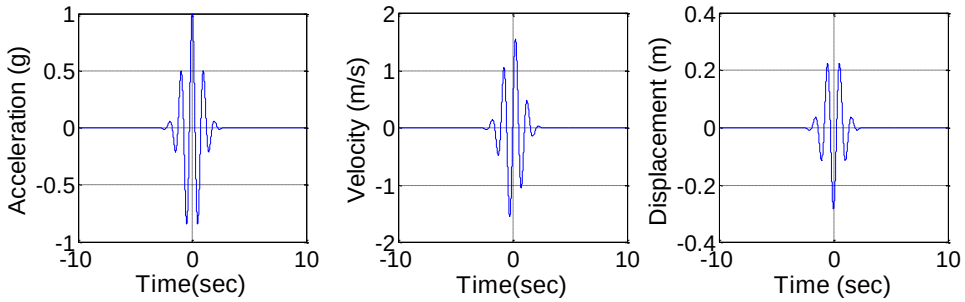

Figure 2-3 (a) Acceleration Time Histories, (b) Velocity Time Histories, (c) Displacement Time Histories of the Corrected Tapered Cosine Wavelet

Suarez and Montejo Wavelet

Suarez and Montejo (2005) identified the selection of a proper wavelet base as critical in the spectral matching process. They developed their own wavelet based on the impulse response function. The wavelet used by Suarez and Montejo resulted in baseline shifts and thus required baseline correction as part of the implementation scheme. The wavelet function of the Suarez and Montejo wavelet is given by:

$$\boldsymbol{\psi}(t) = e^{-\zeta\,\pi\,|t|}\ sin(\pi\,t) \tag{2.8}$$

Figure 2-4 shows the Suarez and Montejo wavelet with period 1 sec and its integrations.

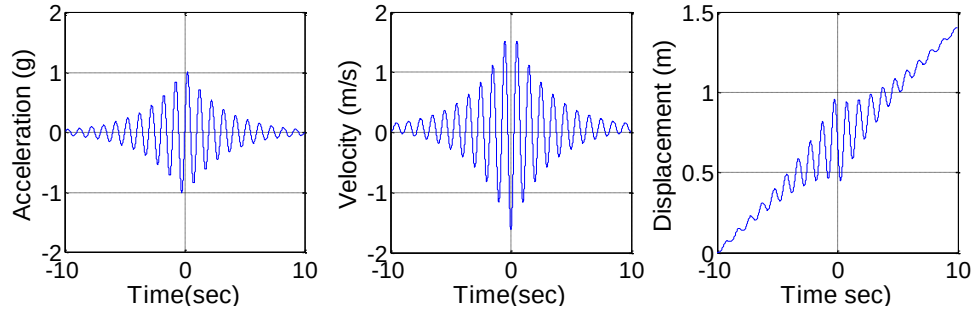

Figure 2-4. Suarez and Montejo Wavelet, T=1sec

CHAPTER 3. RSPMATCH METHOD OF SPECTRAL MATCHING USING WAVELETS

3.1 Introduction

Abrahamson (1992) developed the RSPMatch software based on the technique by Lilhanand and Tseng (1987). This method uses wavelet functions to modify the original acceleration time series such that its response spectra match in certain level with the target spectra. This methodology assumes that the time of peak response of the elastic SDOF oscillator does not change as the result of wavelet adjustments. Several enhancements have been made to this program over the years (Hancock et al. 2006, Al Atik and Abrahamson 2010). The latest enhancement uses the corrected tapered cosine wavelets. The basic steps of the methodology are as follows (a more detailed description of the algorithm and equations will be presented in the following pages):

(1) Calculate the response of an elastic SDOF system subjected to an acceleration time-series for each period and damping ratio to be matched.
(2) Compare the resulting response spectrum ordinate (peak response of the SDOF oscillator) with the target value. Determine the mismatch for each period and damping ratio, $S_{amisfit}$.
(3) Calculate the spectral sensitivity matrix *C,* which element c_{ij} describes the amplitude of acceleration response at time peak t_i of SDOF oscillator with period T_i due to wavelet adjustment with period T_j.
(4) Calculate the set of wavelet magnitudes, *b*, by solving the linear set of equation $\{S_{amisfit}\} = [C] \{b\}$.
(5) Add wavelets to the acceleration time histories with the appropriate phase and amplitude with objective of modifying the spectral ordinates. One wavelet is added for each period to be matched.
(6) Iterate by repeating the above steps until the largest spectral mismatch is below a given tolerance.

Each wavelet is shifted in time so that the time of SDOF oscillator peak response as subjected to the wavelet, is the same as the time of the peak response as subjected to the original acceleration time-series. As mentioned previously, the fundamental assumption of this methodology is that the time of peak response is not shifted as the result of adding the wavelet adjustment to the acceleration time series. However, this assumption is not always valid and can lead to a divergent solution as discussed later.

The spectral misfit, $S_{amisfit-i}$, is defined as the difference between the target spectrum ordinate, $S_{atarget-i}$, and the ground motion spectrum ordinate, S_{ai}, at a given period T_i and one particular damping ratio. The equation for spectral misfit is given by:

$$S_{amisfit-i} = \left(S_{atarget-i} - S_{ai}\right) \tag{3.1}$$

It is noted that although S_{ai} and $S_{atarget-i}$ is defined as the absolute value, the sign of the peak response can be positive or negative. Thus, the sign of $S_{amisfit-i}$ should be adjusted accordingly to the sign of the peak response.

By assuming that the time of peak response t_i will not change due to adding a small adjustment to the initial ground motion time series *a(t)*, the approach is to determine the adjustment function time series $\delta a(t)$, such that the oscillator response at t_i is the equal to $S_{amisfit-i}$. The adjustment function, $\delta a(t)$, can be written as the summation over the set of periods to be matched, *j*, of a set of wavelets, $\Psi_j(t)$, that have already been shifted appropriately in time as given in Chapter 2 (the corrected tapered cosine wavelet is used), and multiplied by a scale factor b_j.

$$\delta a(t) = \sum_{j=1}^{N} b_j \Psi_j(t) \tag{3.2}$$

Using Duhamel's integral, the acceleration response, $\delta\Psi_i$, for an elastic oscillator with period T_i, subjected to the adjustment function $\delta a(t)$ at time t_i is given by

$$\delta\Psi_i = \int_0^{t_i} \delta a(\tau) h_i(t_i - \tau) d\tau \tag{3.3}$$

where $h_i(t)$is the acceleration impulse response of SDOF oscillator with period T_i. By substituting Eqn. 3.2 into Eqn. 3.3 gives

$$\delta\Psi_i = \sum_{j=1}^{N} b_j \int_0^{t_i} \Psi_j(\tau) h_i(t_i - \tau) d\tau \tag{3.4}$$

The acceleration impulse response function $h_i(t)$ is given by

$$h_i(t) = \frac{-\omega_i}{\sqrt{1-\zeta^2}} e^{(-\omega_i \zeta t)} \left[(2\zeta^2 - 1) sin(\omega'_i t) - 2\zeta\sqrt{1-\zeta^2} cos(\omega'_i t) \right] \tag{3.5}$$

where ω_i is the angular frequency of period T_i and ω'_i is the damped angular frequency of period T_i.

Define the acceleration amplitude of SDOF oscillator response with period T_i at time t_i due to wavelet adjustment, $\Psi_j(t)$, with period T_j as c_{ij}

$$c_{ij} = \int_o^{t_i} \Psi_j(\tau)\, h_i(t_i - \tau) d\tau \tag{3.6}$$

The c_{ij} is one of the important variables here because it defines the amount that the wavelet adjustment $\Psi_j(t)$ will affect the spectral ordinate for period T_i. Furthermore, by substituting Eqn. 3.6 into Eqn. 3.2 gives

$$\delta\Psi_i = \sum_{j=1}^{N} b_j\, c_{ij} \tag{3.7}$$

This equation implicitly defines the change in the spectral ordinate at period T_i due to all scaled wavelet $\Psi_j(t)$.

By letting the response of adjustment function $\delta\Psi_i$ at time t_i is equal to the spectra misfit $S_{amisfit-i}$, then

$$S_{amisfit-i} = \sum_{j=1}^{N} b_j\, c_{ij} \tag{3.8}$$

For a spectral sensitivity matrix *C,* which element c_{ij} describes the acceleration response at time peak t_i of SDOF oscillator with period T_i due to wavelet adjustment $\psi_j(t)$ with and period T_j, Eqn. 3.8 can be written as

$$\{S_{amisfit}\} = [C]\{b\} \tag{3.9}$$

The amplitude of each wavelet used in the adjustment is determined by the solution of a set of simultaneous equations that account for the cross correlation of each wavelet with each response period to be matched. This can be described in matrix form as:

$$\{b\} = [C]^{-1}\, \{S_{amisfit}\} \tag{3.10}$$

Using an iterative procedure, the spectral misfit can be minimized to match the target spectra and the modified acceleration time series for each iteration can be calculated as:

$$a^r(t) = a^{r-1}(t) + \sum_{j=1}^{N} b_j \Psi_j(t) \quad (3.11)$$

where *r* is the iteration number.

3.2 Important Features

One of the important features in the RSPMatch method is the adjustment function. The adjustment function should be selected to yield a realistic spectrum compatible time series and also promote numerical stability. The time shifting of the wavelet acceleration adjustment $\Psi_j(t)$ should be conducted such that the associated peak response is in phase with the peak of response due to the original acceleration time series. For computational time efficiency, the wavelet adjustment $\Psi_j(t)$ should be chosen such that the spectra sensitivity matrix *C* can be computed analytically. For numerical stability, the cross correlation of the wavelet adjustment functions which is characterized by the off-diagonal terms of the *C* matrix also should be as small as possible.

Hancock et.al (2006) proposed the tapered cosine wavelet to be used in the spectral matching procedure and later, Al Atik and Abrahamson (2010) proposed a new adjustment function using the corrected tapered cosine wavelet as described by Eqn. 2.5 to 2.7.

To preserve the original character and the frequency content of the original accelerations, it is recommended that the adjustment is applied in stages over a progressively wider frequency band. Hancock et al. (2006) give an example of how the RSPMatch matches the target while preserving the frequency content by using 2 stages (or two subsets of periods).

The RSPMatch method is also able to simultaneously match several target spectrums with different damping levels. However, for numerical efficiency, if required, the method may subdivide the set of target periods into frequency bands. The flowchart procedure of the RSPMatch method is shown in Figure 3-1.

3.3 Challenges and Refinements to the Algorithm

The original procedure for RSPMatch was not always stable and may diverge, especially if the periods being matched are closely spaced. Several enhancements have been implemented to improve the stability and efficiency. Hancock et al (2006) made several enhancements to the original RSPMatch method based on issues that are discussed in the next paragraphs.

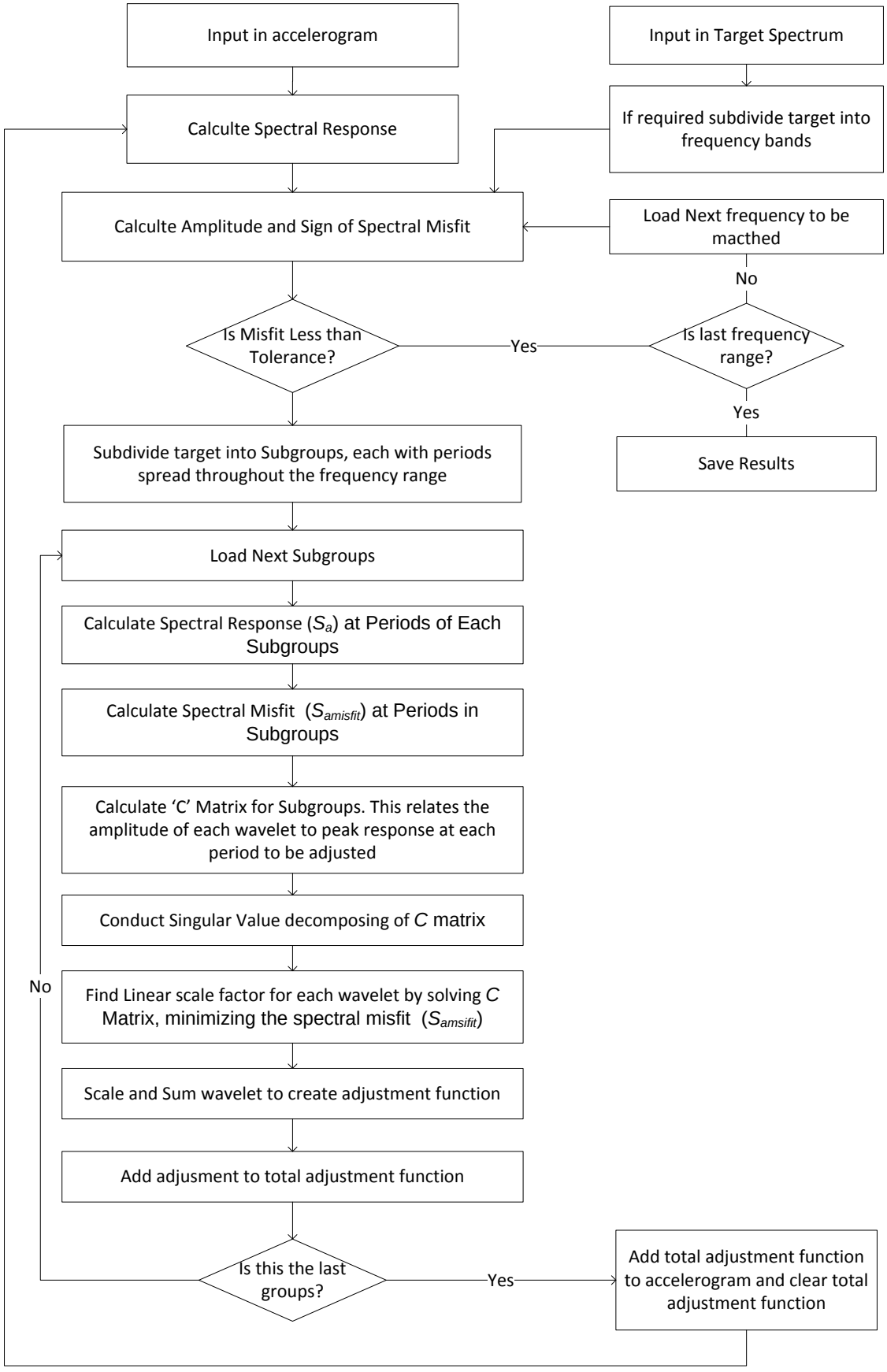

Figure 3-1 Original Algorithm for RSPMatch Method (Hancock, 2006)

3.3.1 Numerical Stability

As described before, the fundamental assumptions of this method is that the time of peak response is the same before and after each the wavelet adjustment is applied. If this assumption was always valid, the problem would be linear and could be solved exactly with a single iteration. However, the spectral matching procedure is a nonlinear problem. The nonlinearity is exacerbated when the algorithm is asked to match a set of closely spaced periods, since the added wavelets tend to interact with one another. In this case, a secondary peak may overshadow the original peak in the oscillator response. This secondary peak may occur due to the cross correlation between the wavelet adjustments. To put it simply, a wavelet adjustment that corresponds to one oscillator period can affect the peak response of an oscillator with other periods in a nonlinear way.

The cross correlation of the wavelets adjustment is defined in the procedure as the off-diagonal values of *C* matrix. The original RspMatch method subdivides the *C* matrix into several sub-matrices, and then sets some of the off-diagonal terms to zero. This procedure aids the numerical stability but it losses the solution accuracy because the cross correlation of some wavelet adjustment are not taken into account.

The RSPMatch ver. 2005b overcomes this issue by using the full *C* matrix and applying a constant reduction factor to the off-diagonal terms. Hancock et. al (2006) conducted trials with different off-diagonal factors and proposed that reducing the off-diagonal elements by 30% is effective in providing numerical stability.

3.3.2 Secondary Peak

Even though the reduction of the off-diagonal elements of the *C* matrix improves numerical stability, it does not reduce the occurrence of the secondary peaks. Hancock (2006) proposed that if the secondary peaks occur, a correction wavelet could be added at the period and time of the secondary peak that have worst miss-matched misfit. The solution can sometimes still diverge, even with the secondary peaks correction. This was found to occur when the cross correlation of the wavelet responses causes a shift in the phase of the response peak. Figure 3-2 demonstrates an example of when a second peak becomes larger than the original peak in response after an iteration of the spectral matching algorithm. The algorithm can match the target values at t_j = 6.12 sec. However, second peak occurs at t=6.88 sec which overshadow the original peak at 6.12 sec.

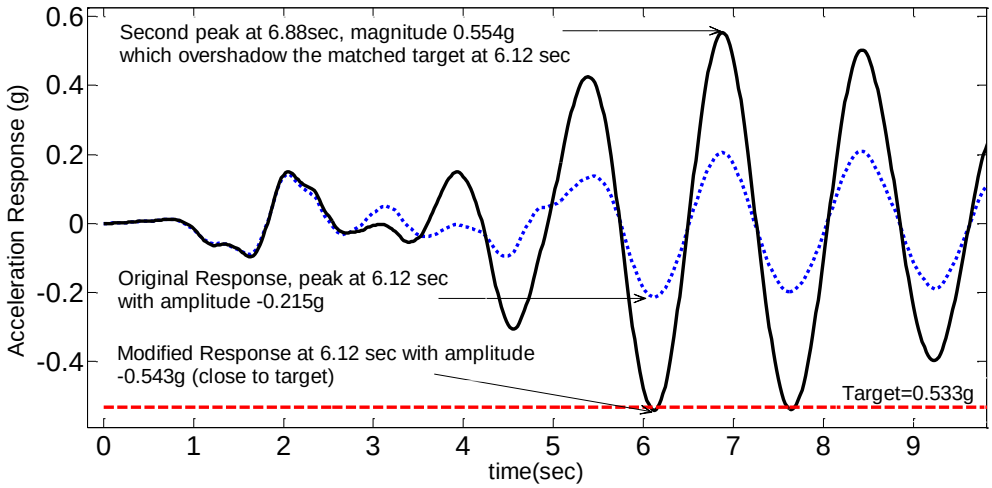

Figure 3-2 Illustration of Second Peak

To overcome the potential for phase shifting, a correction wavelet should be added if the time shifting is larger than one quarter cycle of the period being corrected. Moreover, if the time shifting of the worst miss-matched point is larger than a quarter cycle, it is desirable to increase the importance of the SDOF response that causes the diverging solution (the period that has worst misfit). This is achieved by reducing the amplitude of the adjustment correction $S_{amisfit}$ by 30% for all the points to be matched except the point causing divergence.

3.3.3 Pseudo-acceleration Spectra

Based on the types and the periods of the structure, the displacement spectra are sometimes used in the analysis. For instance: long period structures, base isolated structures, the direct displacement design method and the nonlinear static pushover analysis may require the displacement spectra. The displacement spectrum is directly related to the pseudo acceleration spectrum. Based on this reason, the RSPMatch ver. 2005b has an option to use the pseudo spectra acceleration. For small damping, the difference between the pseudo and the absolute acceleration spectra is not significant.

3.4 Improved Algorithm

A flowchart detailing the enhanced algorithm of the RSPMatch 2005b is shown in Figure 3-3. Hancock et al. (2006) discusses that although the new algorithm prevents the solution from diverging, it does not guarantee that the solution will converge to within the requested tolerance. For a set of closely spaced periods and multiple damping levels, it may be required to accept less stringent tolerance criteria.

Al Atik and Abrahamson (2010) proposed a new adjustment function which is the corrected tapered cosine wavelet that allows the use of an analytical solution in the spectral matching algorithm. This new adjustment function is readily integrated to zero velocity and displacement drift without performing any base-line

correction. The enhancement provides a more stable and efficient solution. It also allows matching the records to pseudo-acceleration response spectra, and ensures convergence and stability of the solution.

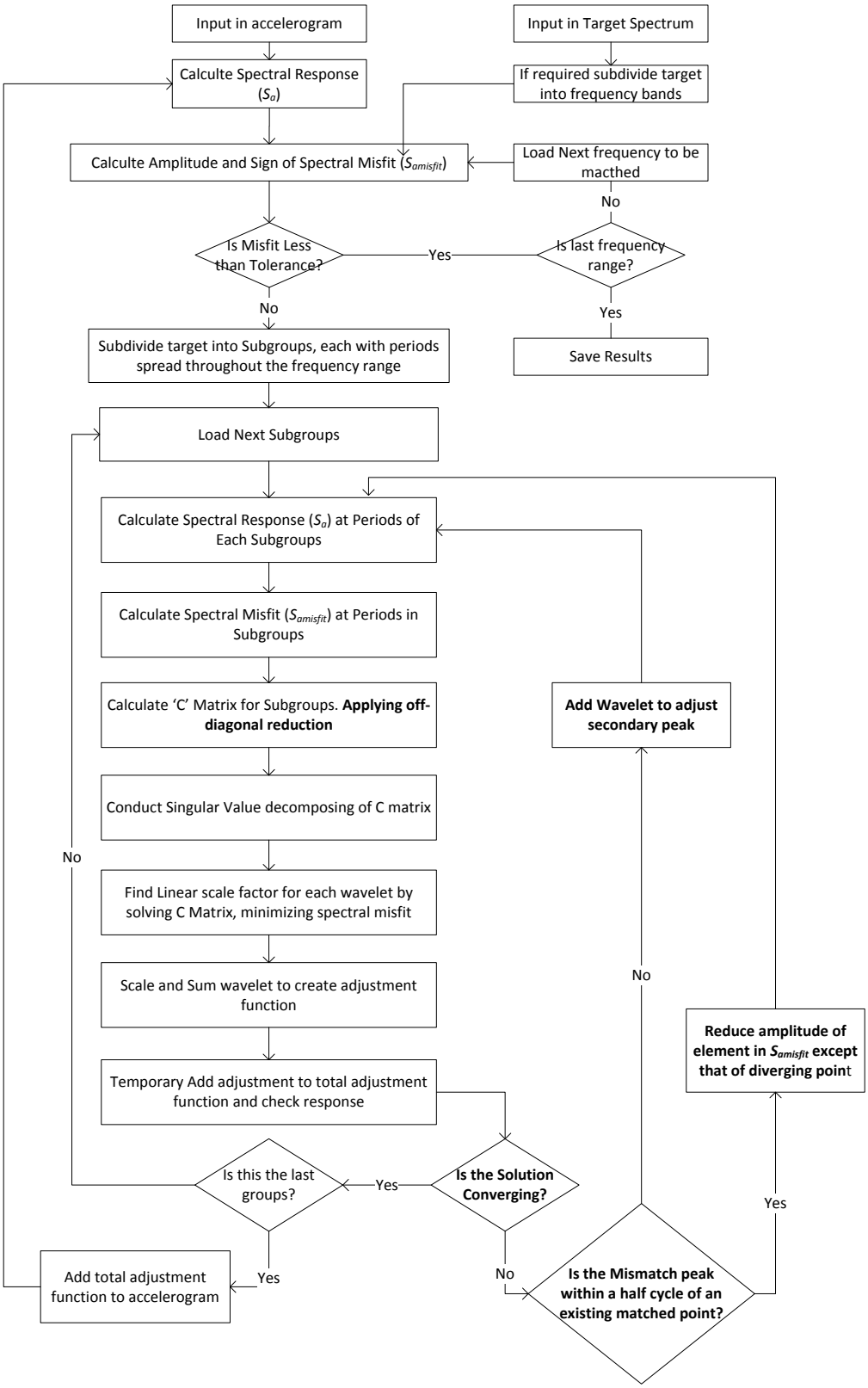

Figure 3-3 Improved Algorithm of RSPMatch ver. 2005b Method (Hancock, 2006)

3.5 RSPMatch Sample Result

The spectral compatible acceleration time series resulted from RspMacth ver. 2005b is shown in Figure 3-4. It takes approximately 32 sec to run the program using a personal laptop with Intel® i3 U380 1.33 GHz Processor, 4096MB DDR3 RAM. The ground motion used in this example was from the 1989 Loma Prieta earthquake, as recorded at the Diamond Heights station, 090 components (CDMG Station 58130). A 5% damping was used. The target response spectrum used in this example was defined as the Dmax hazard level in the FEMA P695 (FEMA 2009) associated with a generic high seismic area of California.

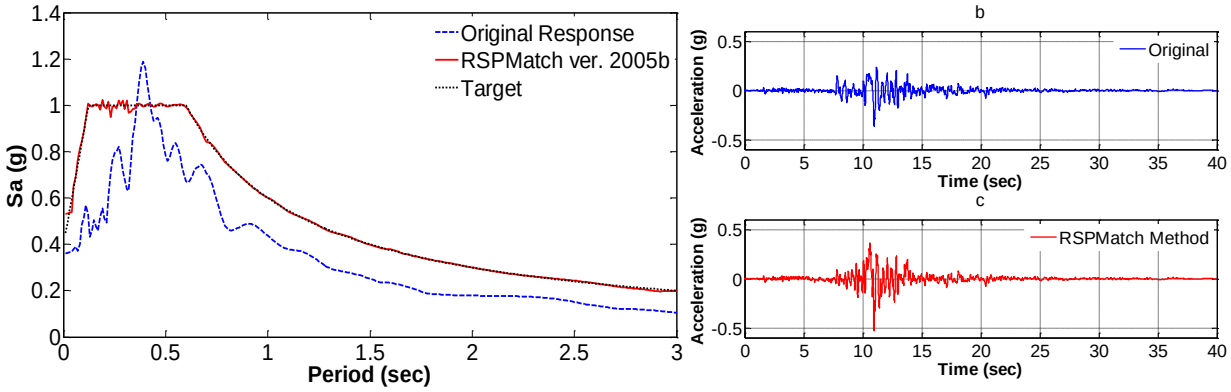

Figure 3-4 (a) Response Spectra (b) Original Acceleration Time Series, (c) Modified Acceleration Time Series for Loma Prieta, Diamond Height Ground Motion using RSPMatch ver. 2005b with 5% Damping

The velocity and displacement time series were obtained by integrating the acceleration time series using Matlab (Mathwork R2009a), and is given on Figure 3-5. As expected, RSPMatch ver. 2005b does not yield drift in the velocity and displacement time series.

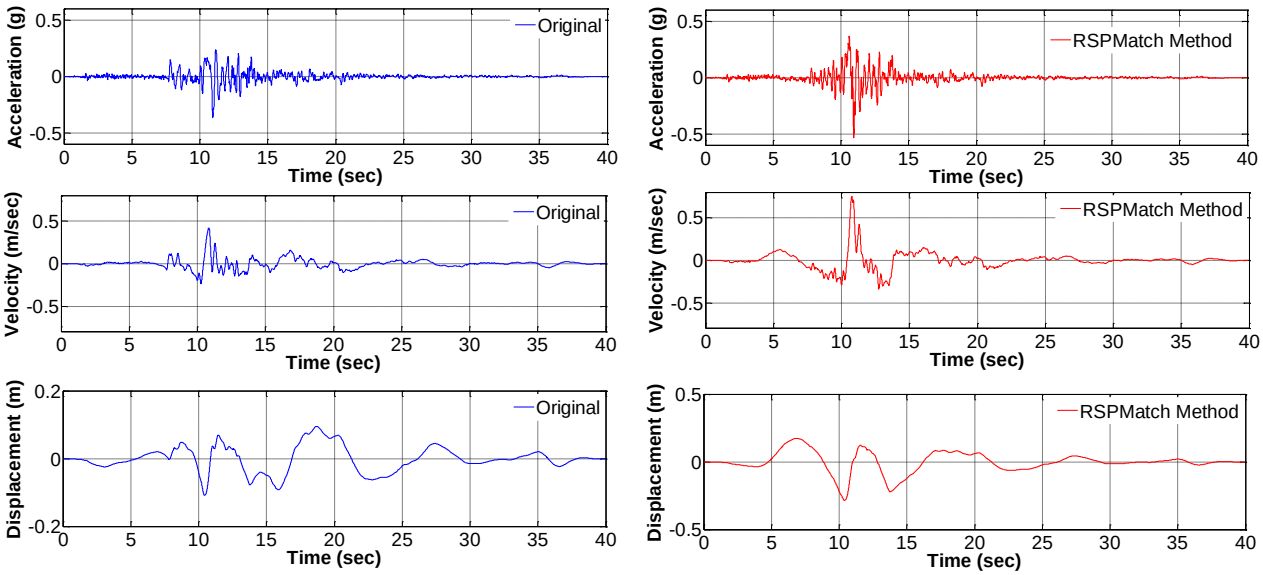

Figure 3-5 Time Series Comparison for 1989 Loma Prieta, Diamond Height Ground Motion using RSPMatch ver. 2005b with 5% Damping

CHAPTER 4. PROPOSED METHOD USING BROYDEN UPDATING

4.1 Introduction

From the previous discussion of RSPMatch method, it is observed that the relationship between the *b* vector and the spectra misfit $S_{amisfit}$ can be nonlinear, especially for a set of close spaced periods to be matched. That is, the spectral sensitivity matrix, *C* in Eqn. 3.9 is nonlinear. This nonlinearity comes from shifting in the time of peak response as the acceleration time histories is altered. A new method is proposed here that will take this nonlinearity into account by allowing the time of peak response to be shifted.

Kopecky (2007) discusses several methods to solve a nonlinear equation. The Newton method is one of the most popular methods. It is based on the principle of successive linearization, a technique in which the harder nonlinear problem is replaced by a succession of linear problems, whose solutions converge to the solution of the nonlinear problem. In order to use the Newton method, all the functions must be differentiable and, in addition, the derivative must be supplied. Another challenge associated with using the Newton method is that there is no guarantee of convergence. The Newton method may not converge if started too far away from a root/solution.

An alternative method for solving nonlinear equations is the quasi-Newton method. This method is similar to the Newton method in that they consist of iterations over successive linear-equation solving problems. However they are different in that the quasi-Newton method does not require an analytical Jacobian. The secant method is the most popular quasi-Newton method for the uni-variate case. It is identical to the Newton method, except that it approximates the derivative of the function at each iteration with a finite difference. On the down side, like Newton Method, the secant method is not very robust, especially when the initial guesses are far from root.

For the multivariate case, one the most popular quasi-Newton approaches is the Broyden method. The purpose of Broyden method, like other quasi-Newton methods is to determine a zero of a function *F* or minimize a function *G* using approximations of the Jacobian of *F* or the Hessian of *G* or their inverse. If the derivative is costly to be evaluated or approximated, the Broyden method is usually more efficient.

4.2 Broyden Updating Method

The goal of the Broyden method is to determine a zero of a function *F* or minimize a function *G* using approximations of the Jacobian of *F*, or the Hessian of *G*, or their inverse. If function *F* is defined by $F(x) = Ax-b$,

then its Jacobian matrix is *A*. Broyden (1965) suggested using the current approximation of the Jacobian matrix *J* and improving/updating the Jacobian matrix by taking the solution to the secant equation.

$$[J_k] = [J_{k-1}] + \frac{\{\Delta F\} - [J_{k-1}]\{\Delta x\}}{\|\{\Delta x\}\|^2}\{\Delta x\}^T \quad (4.1)$$

where *k* is the index of iteration, $\{\Delta F\}$ is the a vector of the changes in the function *F* caused by the change in $\{x\}$,$\{\Delta x\}$ as described by:

$$\{\Delta x\} = \{x_k\} - \{x_{k-1}\}$$
$$\{\Delta F\} = \{F_k\} - \{F_{k-1}\}$$

then the Broyden method proceeds to $\{x_{k+1}\} = \{x_k\} - [J_{k-1}]^{-1}\{F(x_k)\}$

Broyden also introduced similar steps that approximate A^{-1} and can be obtained by applying the Sherman-Morrison formula. The general algorithm for this type of Broyden method is given by:

- Define H_k which approximates A^{-1}
- Initialize arbitrary x_o and H_o
- Calculate $r_0 = b - A\ x_0$
- for k = 0,1,…:

$$\{\Delta x\} = [H_k]\{F_k\}$$
$$\{\Delta F\} = A\{\Delta x\}$$
$$\{x_{k+1}\} = \{x_k\} + \alpha_k\{\Delta x\}$$
$$\{F_{k+1}\} = \{F_k\} - \alpha_k\{\Delta F\}$$
$$[H_{k+1}] = [H_k] + \frac{(\{\Delta x\} - [H_k]\{\Delta F\})}{\{f_k^H\}\{\Delta F\}}\{f_k^H\}$$

- end

By substituting $[H_k]$ to $[J_k]^{-1}$ and taking $\{f_k\}$ equals to $\{\Delta x\}^T[J_{k-1}]^{-1}$, the updating Jacobian inverse matrix can be written as:

$$[J_k]^{-1} = [J_{k-1}]^{-1} + \frac{\{\Delta x\} - [J_{k-1}]^{-1}\{\Delta F\}}{\{\Delta x\}^T[J_{k-1}]^{-1}\{\Delta F\}}\{\Delta x\}^T[J_{k-1}]^{-1} \quad (4.2)$$

The proposed spectral matching algorithm implements the Broyden method concept for solving equation $S_{amisfit} = [C]\{b\}$. To be able to apply the Broyden method to the spectral matching problem, the calculated spectral sensitivity matrix *C* has to locate the peak response, regardless of the time it occurs, for each structure period (T_i) as it shifts.

A conceptual illustration of the Broyden method applied to spectral matching for one target period is shown in Figure 4-1. The Broyden method starts with initial *C* matrix, *b* vector, and spectra misfit. The Broyden method

will update the *C* matrix based on the amount that the wavelets with magnitude, *b*, affected the spectral misfit. After updating the *C* matrix, a new misfit $S_{amisfit}$, and a new vector *b* is calculated for the next iteration. The procedure will continue until the misfit is less than some tolerance. The Broyden method is especially useful in this context because the results from each iteration are used to update the sensitivity matrix, *C*. In this way the *C* matrix can be updated in a nonlinear manner.

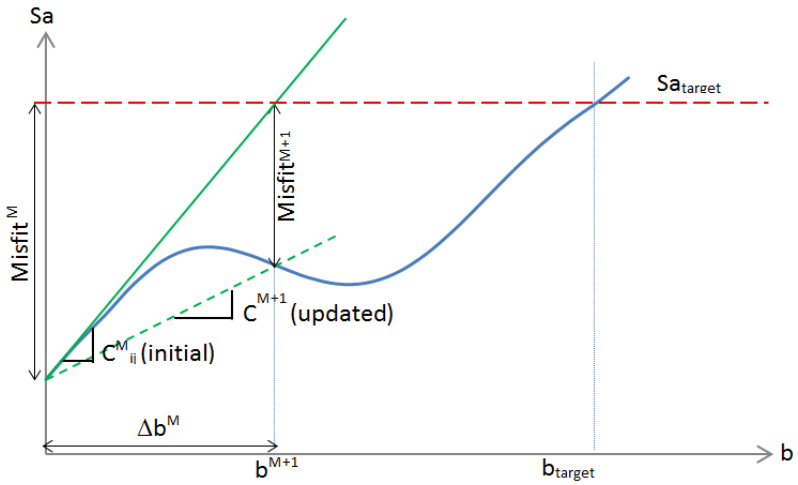

Figure 4-1 Illustration for Broyden Method to Solve Non Linear System

It is noted that the solution is not unique. There may be several solutions that can minimize the misfit below the tolerance. A demonstration will be given in the next chapter. At this step, it can be summarized that some of the key improvements in the proposed method compared to the RSPMatch approach is that the proposed method makes use of the information about the effect of wavelets on misfit during the Broyden iteration by updating the *C* matrix. The proposed method also takes into account the nonlinearity in the basic equation $S_{amisfit} = [C]\{b\}$.

4.3 Proposed Algorithm

The proposed algorithm is described in detail in this section. The improved tapered cosine wavelet is selected to be used in this proposed method to prevent drift in the displacement and velocity time histories. The selection of the wavelet adjustment function is discussed in detail in 0. The algorithm is implemented in Matlab 2009a (Matlab 7.9 , "The Language of Technical Computing," The Mathworks, Inc). A flowchart of the proposed algorithm can be seen in Figure 4-2. Figure 4-3 shows the Broyden algorithm for solving nonlinear system.

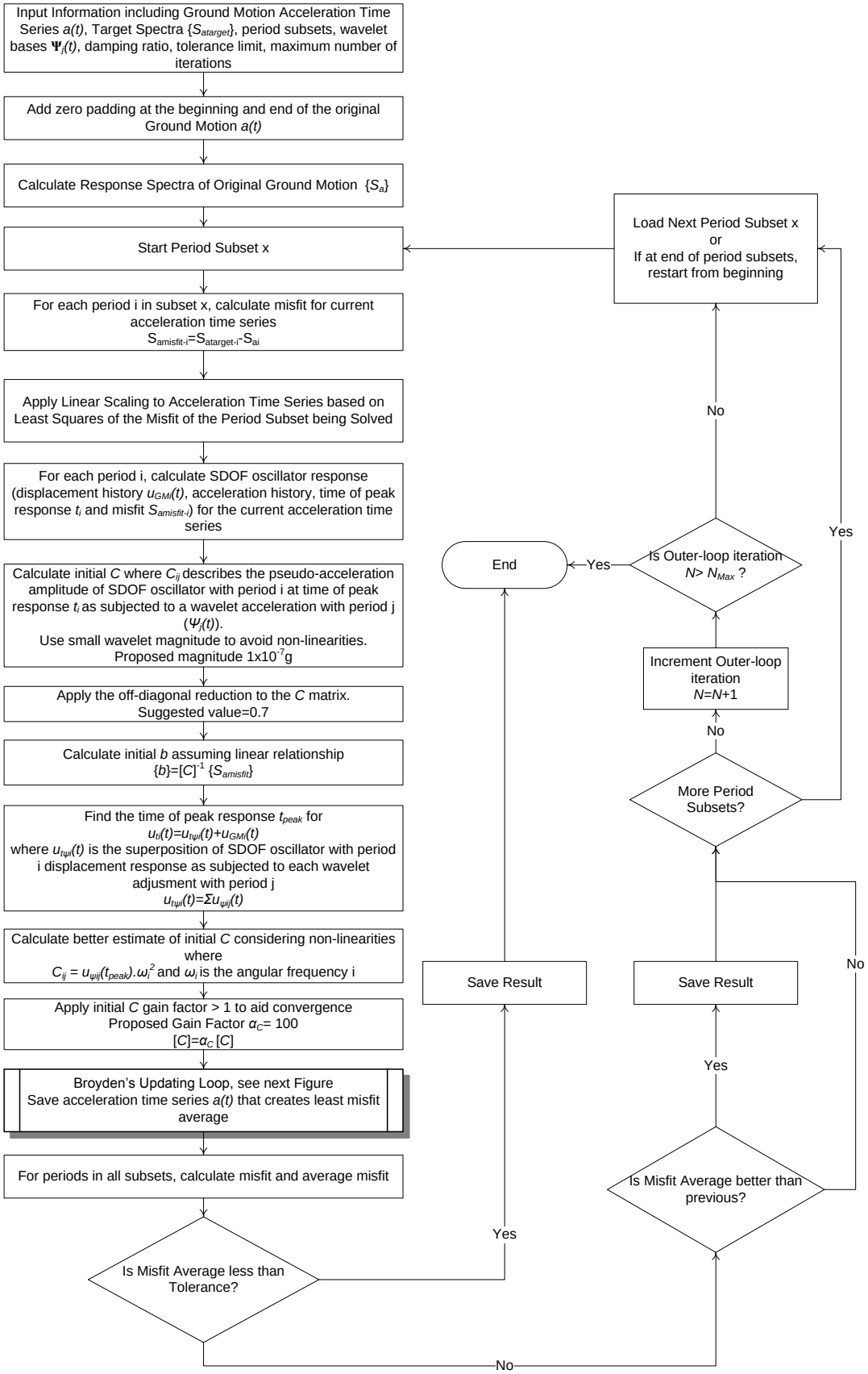

Figure 4-2 Algorithm for Proposed Method

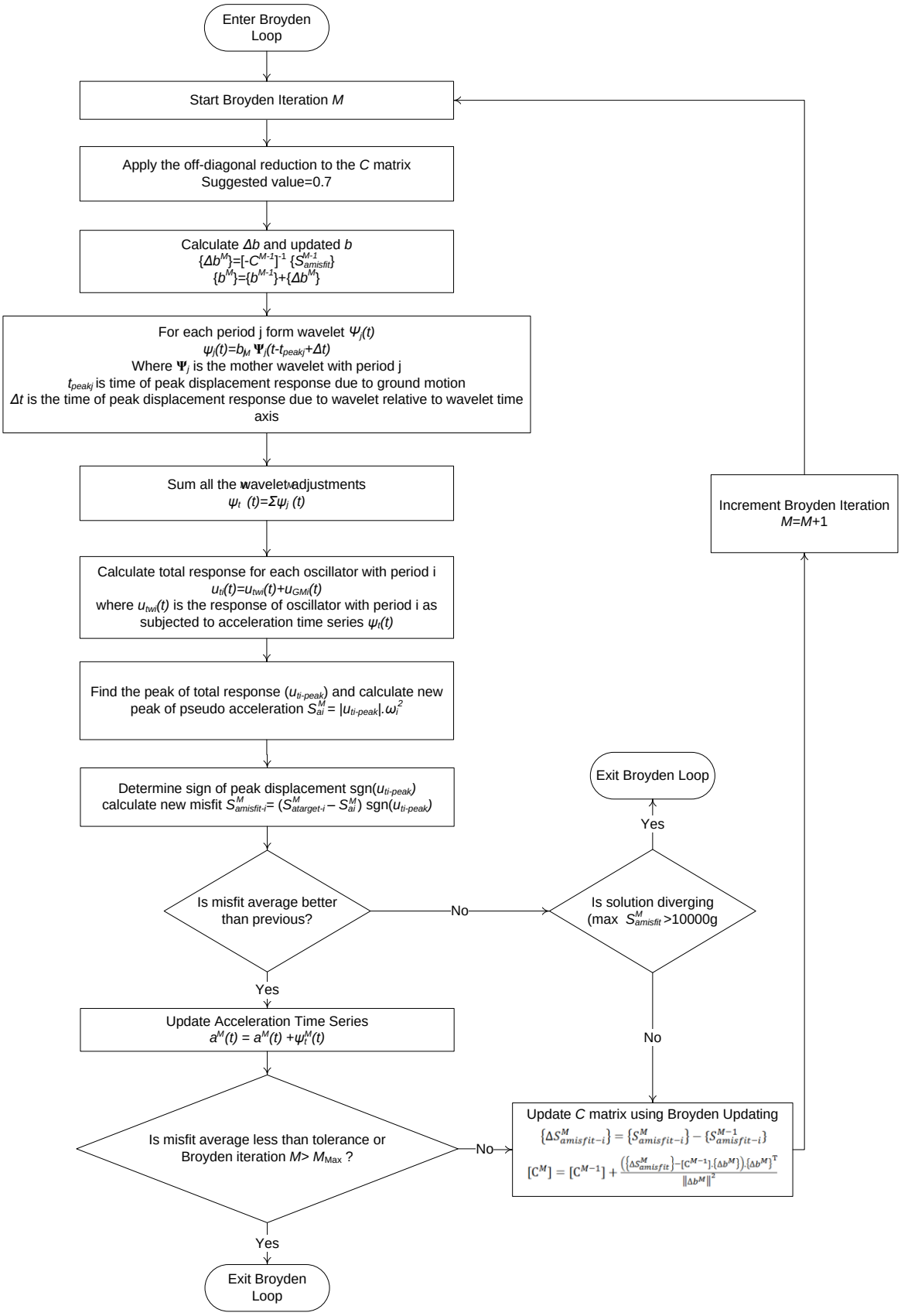

Figure 4-3 Algorithm for Broyden Method

Step 1: Information Input

The first step of the proposed algorithm is inputting the required information which includes the ground motion acceleration ($a(t)$), the target spectra ($S_{atarget}$), the damping ratio (ζ), the period subset, tolerance limit, the maximum number of iteration, and the duration of zero padding.

To minimize the magnitude of the adjustments required during spectral matching, the selected ground motion should be considered appropriate for the site in terms of earthquake magnitude, fault characteristics, fault distance, and site conditions. It is also beneficial if the ground motion has good similarity on its spectra compared to the target spectra. Bommer and Acevedo (2004),Haselton (2012) and NIST GCR 11-917-15 discuss the criteria of selecting and scaling earthquake ground motion for performing response-history analyses.

The proposed algorithm is able to match one damping ratio at a time; a common damping ratio is 5% as inherited from typical design response spectra. The period subset is the group(s) of period bands in which the algorithm will match in sequence. To avoid a divergent solution, it is recommended to divide the periods in to several subsets. For medium range period (0.05sec to 3sec), it is recommended to use 2 period subsets, which is from the smallest period to the mean period and from the smallest period to the maximum period. In the case of small set of period which closes together, user may use 1-2 period subsets. For large set of periods, it might be better to use more period subsets (3-4), depends on the periods range. For this case, it is not recommended to use only one period subset, since it may give more chance of solution diverging and may generate major changes of the original time series

The periods can be linearly or log scale spaced. However, since the bandwidth of the oscillator response is a ratio of the forcing frequency to the natural frequency; fewer points are required at long periods (low frequencies) to obtain a smooth spectral match. Thus for efficiency, it is proposed that the period spacing is in log scale.

The tolerance limit is the average of the absolute value of spectra misfits $S_{amisfit}$. The value for the limit used in this work is 0.005g which is considered to be small. Closely spaced periods may require a larger tolerance. The algorithm consists of 2 major loops: the outer-loop and the Broyden loop. The outer-loop is the looping where the period subsets are being matched in sequence. The Broyden loop is the inner loop that is matching each period subset by applying the Broyden updating. It is required to define the maximum number of iterations for each loop. Closely spaced period and small tolerance limit may require more iteration.

Zero padding is required to reduce the distortion and minimize the chance of baseline drift during the spectral matching. Note that because the wavelet can be shifted during the spectral matching procedure, zero padding

also ensures that the ground motion has long enough duration so that the shifted wavelet adjustments will start and end with zero value.

Step 2: Calculate Initial Response Spectra

The next step is to calculate the original response spectra based on an elastic SDOF oscillator response. The pseudo acceleration spectrum is calculated. Newmark method with average acceleration is implemented to calculate the oscillator response.

Step 3: Acceleration Scaling

The outer-loop iteration will match the spectral acceleration for each period subset in sequence. For each period subset, the algorithm will calculate the spectral misfit $S_{amisfit}$ of the current acceleration time series. The misfit is used to scale the acceleration time series based on a least square fit over the misfit values. The least squares method is selected because it generally yields lower scale factors than using the average misfit or the PGA scaling. The issues in scaling the original ground motion are out of the scope of this study. Watson-Lamprey and Abrahamson (2006) found that a spectral matched acceleration time histories with large scale factors (over a factor of 10) could be used without causing a bias in nonlinear response if the reference ground motion is selected based on the properties of the scaled ground motion rather than just selecting time histories based on magnitude, distance, and site.

After the acceleration time series is scaled, the algorithm calculates the SDOF response which includes the displacement time series $u_{GMi}(t)$, acceleration time series, time of peak response t_i, and the spectra misfit $S_{amisfit}$.

Step 4: Calculate Initial *C* Matrix and Initial Vector *b*

The algorithm then calculates the initial *C* matrix in which element C_{ij} describes the pseudo-acceleration response amplitude of a SDOF oscillator with period T_i at time of peak response t_i as subjected to a wavelet adjustment with period T_j, denoted as $\psi_j(t)$. To reduce the effect of nonlinearities, it is proposed to use a small wavelet magnitude for the initial calculation of the *C* matrix. The proposed wavelet magnitude is $1\text{x}10^{-7}$g. Once the *C* matrix is calculated, the next step is to calculate the initial solution (initial vector *b*) by assuming a linear relationship between the $S_{amisfit}$ and the wavelet adjustment, as described in Eqn. 4.3.

$$\{b^{initial}\} = [C]^{-1}\{S_{amisfit}^{initial}\} \tag{4.3}$$

The reduction of the off-diagonal terms of the *C* matrix is also being employed in the algorithm and will be shown to aid the stability. It is noted that the *C* matrix and vector *b* were calculated here using the same

procedure as the RSPMatch. A parametric study of wavelet magnitude, off-diagonal reduction factor, and other parameters is discussed later.

As discussed previously in the RSPMatch method, the *b* vector may cause a second peak to overshadow the original peak. This is where the proposed method has the potential to more efficiently solve the nonlinear problem. The next step is to calculate a better estimate of initial spectral sensitivity *C* matrix that is able to locate the time of peak response regardless of the shifting on time of the peak.

Step 5: Calculate Better Estimate of Initial *C* matrix

To calculate a better estimate of the initial *C* matrix, the algorithm calculates the sum of the SDOF oscillator responses, $u_{\Psi ij}(t)$, with period T_i subjected to each wavelet adjustment as described in Eqn. 4.4

$$u_{t\Psi i}(t) = \sum_j u_{\Psi ij}(t) \tag{4.4}$$

The algorithm then calculates the total response $u_{ti}(t)$ described as the superposition of ground motion response $u_{GMi}(t)$ with the total response of wavelet adjustments $u_{t\Psi i}(t)$

$$u_{ti}(t) = u_{GMi}(t) + u_{t\Psi i}(t) \tag{4.5}$$

Once the total response $u_{ti}(t)$ is calculated, the algorithm finds the time of peak response t_i. The c_{ij} element of better estimate *C* matrix is calculated by Eqn. 4.6

$$c_{ij} = u_{\Psi ij}(t_i)\ \omega_i^2 \tag{4.6}$$

From an illustration of the Broyden method presented before, it is noticed that the initial *C* is affecting the stability of the Broyden iteration. Large values in the initial *C* matrix will aid the algorithm not to overshoot the solution and improves the convergence. The proposed method employs a gain factor α_C that is applied to the initial *C* as defined in Eqn. 4.7. The concept and parametric study of gain factor α_C is discussed later.

$$[C] = \alpha_C\,[C] \tag{4.7}$$

Step 6: Broyden Loop

The first step of each Broyden iteration starts with updating the initial vector *b* based on the misfit and spectra sensitivity matrix *C*. As for the first iteration, the misfit and matrix *C* are the initial misfit and the initial matrix *C* that already calculated on the previous step on the outer-loop. The vector *b* is being updated as described in Eqn. 4.8 and 4.9.

$$\{\Delta b^M\} = [-C^{M-1}]^{-1}\,\{S_{amisfit}^{M-1}\} \tag{4.8}$$

$$\{b^M\} = \{b^{M-1}\} + \{\Delta b^M\} \tag{4.9}$$

where *M* is the sequence of Broyden iteration. After the *b* vector is updated, the new wavelet adjustments are formed for each period *j*. The wavelet adjustment $\psi_j(t)$ is multiplied by the updated b_j^M and shifted in time so

that the time of maximum SDOF response under the action of the wavelet is the same as the time of the peak response. Wavelet acceleration adjustment $\psi_j(t)$ is defined by Eqn. 4.10.

$$\psi_j(t) = b_j^M \, \boldsymbol{\psi}_\mathbf{j}\left(t - t_j + dt\right) \tag{4.10}$$

where wavelet $\boldsymbol{\psi}_\mathbf{j}$ is the mother wavelet function, t_j is the time of peak response and dt is the time adjustment. It is noted that the formulation of the corrected tapered cosine wavelet as written in Chapter 2 already includes the time shifting. Although several wavelet bases are investigated in Chapter 7, the corrected tapered cosine wavelet is used for the rest of the studies in this thesis

The next step of the Broyden iteration is to sum all the wavelet adjustments $\psi_j(t)$ and calculate the SDOF oscillator response due to the total wavelet adjustment ($\psi_t(t)$), denoted as $u_{t\psi i}(t)$.

$$\psi_t(t) = \sum \psi_j(t) \tag{4.11}$$

The algorithm then continues with calculating the total response $u_{ti}(t)$ described as the superposition of the ground motion response $u_{GMi}(t)$ with the response of total wavelet adjustment $u_{t\psi i}(t)$.

$$u_{ti}(t) = u_{GMi}(t) + u_{t\psi i}(t) \tag{4.12}$$

Once the total response $u_{ti}(t)$ is calculated, the algorithm finds the peak response $u_{ti\text{-}peak}$ and calculates the peak pseudo-acceleration S_{ai}^M as:

$$S_{ai}^M = u_{ti-peak}\, \omega_i^2 \tag{4.13}$$

where ω_i is the angular frequency associated with period T_i.

The algorithm then determines the sign of $u_{ti-peak}$ and calculates new misfit as:

$$S_{amisfit-i}^M = \left(S_{atarget-i} - Sa_i^M\right) sgn(u_{ti-peak})^T \tag{4.14}$$

If the average of the absolute value of new misfit $S_{amisfit-i}^M$ is less than previous, the algorithm saves the acceleration time series then checks if the average misfit is less than the tolerance. If this condition is true, then the Broyden loop will end. In case that the average of the absolute value of new misfit $S_{amisfit-i}^M$ is larger than previous, the algorithm will check if the solution is diverging by checking whether the maximum new misfit $S_{amisfit-i}^M$ is larger than 1x10^{4}g. If this condition is true, then the Broyden loop will stop. If not then, the Broyden loop will calculate the change in the spectra misfit (denoted as $\Delta S_{amisfit-i}^M$) and update the C matrix.

$$\left\{\Delta S_{amisfit}^M\right\} = \left\{S_{amisfit}^M\right\} - \left\{S_{amisfit}^{M-1}\right\} \tag{4.15}$$

$$[\mathrm{C}^M] = [\mathrm{C}^{M-1}] + \frac{\left(\left\{\Delta S_{amisfit}^M\right\} - [\mathrm{C}^{M-1}]\{\Delta b^M\}\right)\{\Delta b^M\}^{\mathrm{T}}}{\|\Delta b^M\|^2} \tag{4.16}$$

Once the sensitivity matrix C^M is updated, the Broyden loop starts from the beginning and increments the number of Broyden iteration, M=M+1.

Step 7: Acceleration-Misfit Updating and Termination Condition

After the misfit for the current period subset is less than tolerance or the maximum number of Broyden iterations, M_{max}, is reached, the Broyden loop will stop and runs the next period subset. Every time the Broyden iteration stops, the acceleration time histories and misfit are updated.

$$a^N(t) = a^{N-1}(t) + \psi_t^{N-1}(\mathrm{t}) \tag{4.17}$$

where $a^N(t)$ is the updated acceleration time series for the period subset being macthed, $a^{N-1}(t)$ is the acceleration time series from the previous period subset, $\psi_t^{N-1}(t)$ is the best total wavelet adjusment function from the previous period subset.

CHAPTER 5. PRELIMINARY STUDIES ON STABILITY AND CONVERGENCE

The Broyden algorithm was applied to solve the nonlinear system of spectral matching equations. As expected in a typical nonlinear system, there is no unique solution. A different initial value of the *b* vector and the initial spectral sensitivity matrix *C* may lead to a different solution. The updating rate at each of the Broyden iterations, which can be manipulated by several gain coefficients, may also influence the solution. Preliminary studies were conducted to examine the non-unique solution and the stability/convergence of the algorithm.

To give an illustration that the algorithm yields no unique solution, a numerical sample was carried out. For simplicity, 2 periods were being matched to a target spectrum simultaneously: 0.5 sec and 3.0 sec. The Broyden algorithm was applied to modify the 1999 Hector Mine ground motion, Hector Station Component 000. The tolerance was set as either 0.005g on the average misfit or 10% of the spectral ordinate on any particular misfit value. The damping ratio was taken as 5% of critical damping and the target response spectrum was the Dmax spectrum from FEMA P695 (FEMA 2009) associated with a high seismic area of California. There were 2 different initial *b* vectors used in matching the response: [1.0 1.0] for Table 5-1 and [0.1 0.1] for Table 5-2. Table 5-1 and Table 5-2 show the numerical results including all the elements of the C matrix, the *b* vector, the misfit and time of peak response.

Table 5-1 Numerical Sample Result using Proposed Method Set 1

	Spectra Sensitivity C Matrix				b		Misfit (g)		Time peak (sec)	
iteration	C_{11}	C_{12}	C_{21}	C_{22}	Tn=0.5 sec	Tn=3.0 sec	Tn=0.5 sec	Tn=3.0 sec	Tn=0.5 sec	Tn=3.0 sec
initial							0.591764	-0.137	12.13	21.09
1	4.2277	-0.00264	1.20E-05	3.8843	1	1	-4.23199	-3.5289	12.13	21.09
2	-0.40836	-4.208	-3.8659	0.37759	2.001572	1.908509	-8.46398	-7.0578	12.13	21.09
3	-0.40836	-4.208	-3.8725	0.3716	-0.00157	0.091491	-1.70E-12	0.024105	12.13	19.53
4	-4.5969	-3.8015	-0.36286	0.031012	0.004596	0.090892	-0.02608	0.021849	12.13	19.53
5	-6.2893	-1.5402	-1.1415	1.0714	0.058636	0.018685	-0.25474	-0.1172	12.13	21.08
6	-6.0136	-1.8116	-0.66569	0.60305	0.005268	0.071216	-0.02897	-0.05	12.13	22.78
7	-6.0996	-1.5876	-1.6305	3.1155	-1.71E-02	1.29E-01	0.014966	0.167862	11.1	19.56
8	-6.0898	-1.6189	-1.6753	3.2587	-0.00259	0.083153	0.001588	-0.00728	11.1	19.52

Table 5-2 Numerical Sample Result using Proposed Method Set 2

	Spectra Sensitivity C Matrix				b		Misfit (g)		Time peak (sec)	
iteration	C11	C12	C21	C22	Tn=0.5 sec	Tn=3.0 sec	Tn=0.5 sec	Tn=3.0 sec	Tn=0.5 sec	Tn=3.0 sec
initial							0.591764	-0.137	12.13	21.09
1	0.42277	-0.00026	-1.38E-06	-0.37808	0.1	0.1	-0.4294	0.056239	12.13	21.09
2	-4.1297	-0.66692	0.59938	-0.29031	1.115756	0.248745	-4.72337	0.621883	12.13	19.59
3	-4.1292	-0.66684	0.60203	-0.28992	-0.00144	0.084286	-5.75E-04	-0.00302	12.13	19.52

It can be seen in Table 5-1 and Table 5-2 that although the algorithm started with a different *b* vector, it yields a solution which satisfies the tolerance limit. It is noticed that a different initial *b* vector may lead to a different solution. It is also observed from this illustration that the algorithm efficiency is sensitive to the initial *b* vector. On closer inspection, it is observed in Table 5-1, that the wavelet amplitudes, *b*, on the second iteration were much larger than the final value. This excessively large value for the wavelet amplification leads to more iterations, which has more chance of producing a combination that causes a time shift in peak response. It is also noted that when the time of peak response is shifted, there is the potential for the solution to diverge; although this is not always the case.

On a brief examination, the numerical stability and the efficiency of the proposed algorithm depends on several important elements, i.e. the method for computing the initial *C* matrix, the method for computing the initial *b* vector, and the method for updating the *C* matrix. These important elements can be modified using some multiplier gain factors, such as α_c demonstrated above. The following section discusses the preliminary study of the effect of the gain factors.

5.1 Gain Factor on the Initial Spectral Sensitivity Matrix (α_C)

The initial *C* matrix gain factor (α_C), described in Eqn. 4.7, is intended to be larger than one and produce a larger magnitude of the initial *C* matrix in order to get a smaller initial increment of the Δb vector. This will in turn reduce the potential of overshooting the solution and thus aid convergence. A study was conducted to examine the convergence rate by varying the α_c values for one ground motion.

$$[C] = \alpha_C [C] \tag{4.7}$$

The study was conducted using the 1999 Hector Mine, Hector Station Component 000. The tolerance was set as either 0.015g on the average misfit or 5% of the spectral ordinate on any particular misfit value. The period set being solved ranges from 0.1sec to 1.0sec with 0.1sec increments. The damping ratio was taken as 5% of critical and the target response spectrum was the Dmax spectrum from FEMA P-695 (FEMA 2009) associated with a high seismic area of California. Considering time-efficiency, the maximum number of Broyden iteration was limited to 200 iterations. The average misfit and the maximum error in the spectral ordinate are presented in Figure 5-1 and Figure 5-2 respectively.

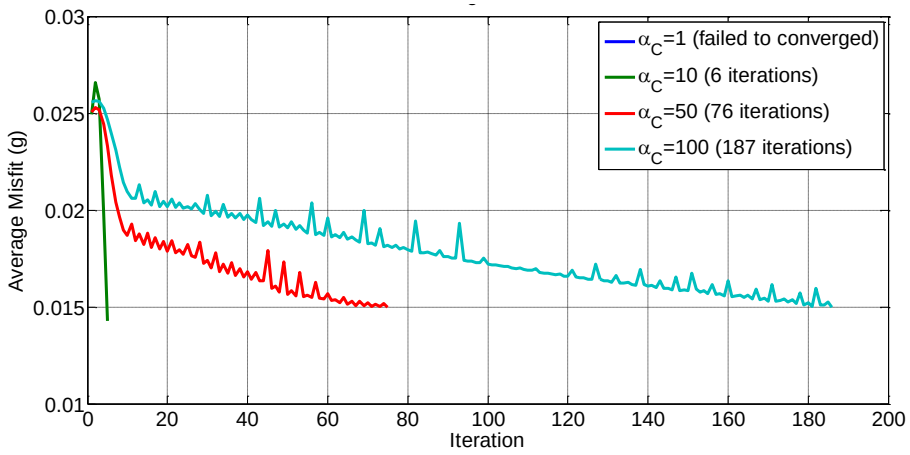

Figure 5-1 Gain Factor α_C vs Average Misfit

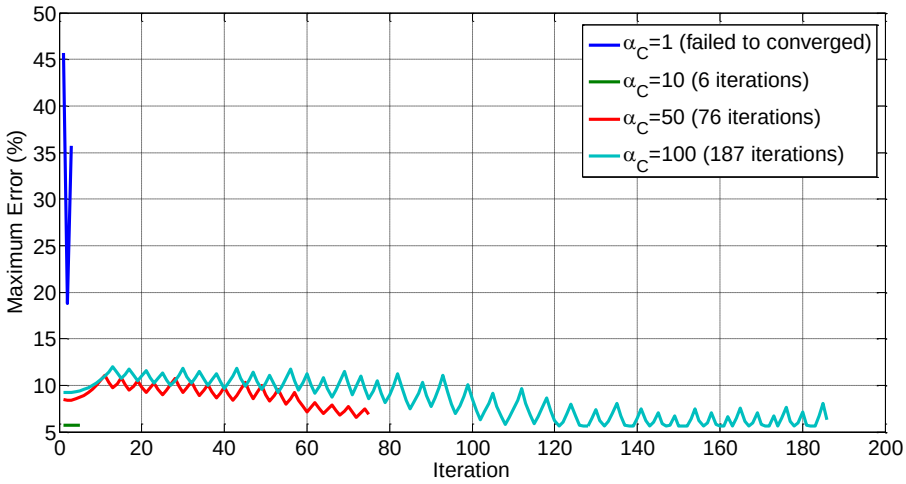

Figure 5-2 Gain Factor α_C vs Maximum Error

On the first iteration, the acceleration time history has been scaled to get a better match with the target spectra, and the misfit has been reduced by the initial wavelet adjustments (correspond to the linear relationship between $S_{amisfit}$ and b vector). The first wavelet adjustments of the Broyden iteration, affected by the initial gain factor, α_c, were applied on the first result. Thus, the initial iteration shows a different result for different values of the gain factor α_c.

The spikes in the misfits are associated with the shifting on the time of peak response and also associated with the change in b vector. When the b vector is greatly changed from the previous values, the resulting misfits tend to increase. The Broyden method then updates the C matrix to reduce the misfits.

It is observed that the gain factor α_C is affecting solution convergence. It can be seen that, for this case, with a gain factor α_C =1 the solution diverged. The solution started with a high error in misfit then failed to reduce the error. The gain factor α_C =1 yields a large average misfit and thus it is not shown in Figure 5-1. The gain factor α_C = 10 shows a better converging solution where the algorithm reached the tolerance limit within only 6 iterations. It is also observed that although a gain factor α_C >1 aids the solution convergence; a large α_C may

require the algorithm to run more iterations. For instance, the gain factor α_C=50 and α_C=100 require 76 iterations and 187 iterations respectively to reach the tolerance limit. Having a large number of the Broyden iterations is not considered time-effective. Different cases (ground motion, period set, damping level, and target spectra) may result different solution convergence.

Based on this preliminary study, it is desirable to conduct a more detail study to obtain a good value of the gain factor α_C. Such study will be discussed in the next chapter.

5.2 Gain Factor Applied to the *Δb* Vector (g_b)

A preliminary study was conducted to examine the effect of the gain factor applied to the *Δb* vector on the solution convergence as described in Eqn. 5.1. This equation is replacing Eqn. 4.8 in previous chapter.

$$\{\Delta b^M\} = g_b[-C^{M-1}]^{-1}\{S_{amisfit}^{M-1}\} \quad (5.1)$$

This gain factor g_b controls how the vector *b* changed during the Broyden iteration. A constant factor was proposed in this preliminary study. The study was conducted using the 1999 Hector Mine, Hector Station Component 000. The tolerance of the average misfit was set to 0.015g or 5% on the maximum misfit, whichever is reached first. The period set being solved ranges from 0.1sec to 1.0sec with 0.1sec increment. The damping ratio was taken as 5% of critical damping and the target response spectrum was the Dmax spectrum from FEMA P695 (FEMA 2009) associated with a high seismic area of California. The gain factor α_C was set as 50. Figure 5-3 and Figure 5-4 show the changing rate of average misfit and maximum error throughout iterations for different gain factor g_b.

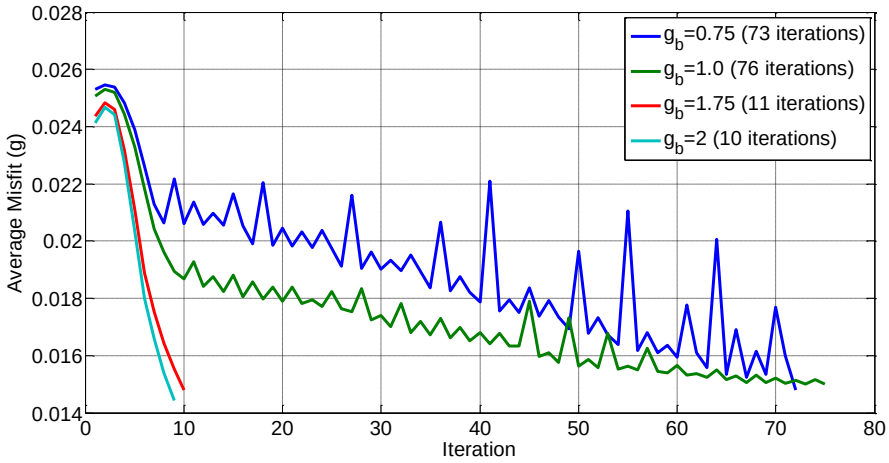

Figure 5-3 Gain Factor g_b vs Average Misfit

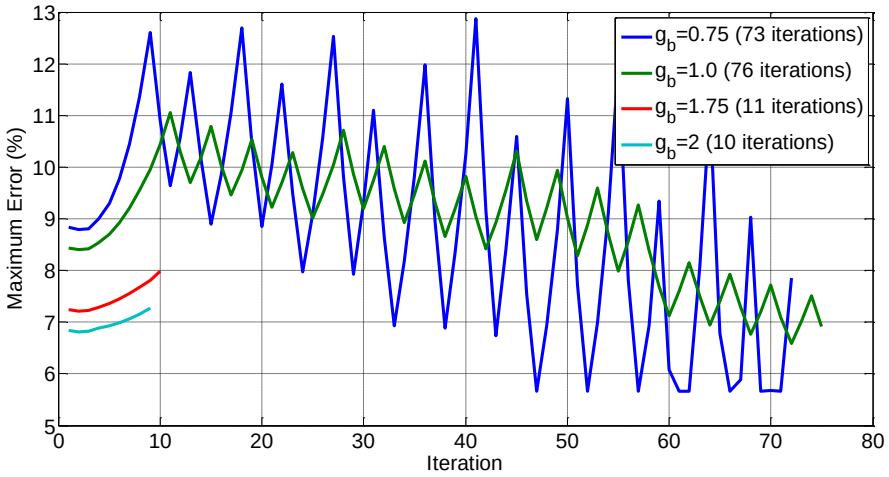

Figure 5-4 Gain Factor g_b vs Maximum Error

On the first iteration, the acceleration time history has been scaled to get a better match with the target spectra and the misfit has been reduced by the initial wavelet adjustments (correspond to the linear relationship between $S_{amisfit}$ and b vector). The first wavelet adjustments of the Broyden iteration, affected by the gain factor on the Δb vector, were also applied on the first result. Thus, the initial iteration shows a different result for different g_b.

It can be seen that the gain factor g_b is affecting solution convergence. For this case, it is observed that a smaller gain factor g_b tends to make the solution requires more iterations. This is because the solution b vector is being updated with a small increment. A large gain factor g_b makes the solution updated in more rapid increment thus the algorithm may requires less iteration. However, it should be noticed that, depends on the case, at a large gain factor g_b, the algorithm may overshoot the solution. Hence it is desirable to conduct more detailed study to obtain a good estimate of the gain factor g_b.

5.3 C Matrix Updating Gain Factor (g_c)

The sensitivity of convergence to the gain factor g_c that is applied on the C matrix updating procedure has also been studied. Eqn. 5.2 describes the application of gain factor g_C. This equation is replacing Eqn. 4.16 in previous chapter.

$$[C^M] = [C^{M-1}] + g_C \frac{\left(\left\{\Delta S^M_{amisfit}\right\} - [C^{M-1}]\{\Delta b^M\}\right)\{\Delta b^M\}^{\mathrm{T}}}{\|\Delta b^M\|^2} \tag{5.2}$$

The study was conducted using the 1999 Hector Mine, Hector Station Component 000. The tolerance of the average misfit was set to 0.015g or 5% on the maximum misfit corresponds to the target, whichever is reached first. The period set being solved ranges from 0.1sec to 1.0sec with 0.1sec increment. The damping ratio was taken as 5% of critical and the target response spectrum was the Dmax spectrum from FEMA P695 (FEMA 2009) associated with a high seismic area of California. The gain factor α_C and g_b were set as 50 and 1

respectively. Figure 5-5 and Figure 5-6 show the changing rate of the average misfit and the maximum error throughout iterations for a different gain factor g_C.

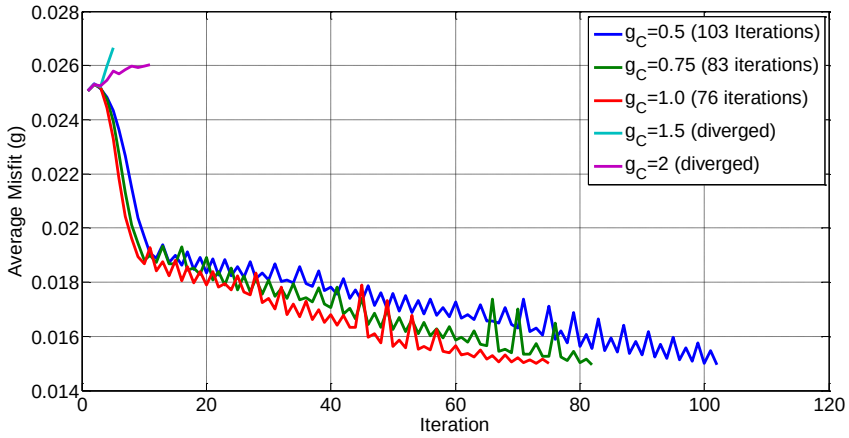

Figure 5-5 Gain Factor g_C vs Average Misfit

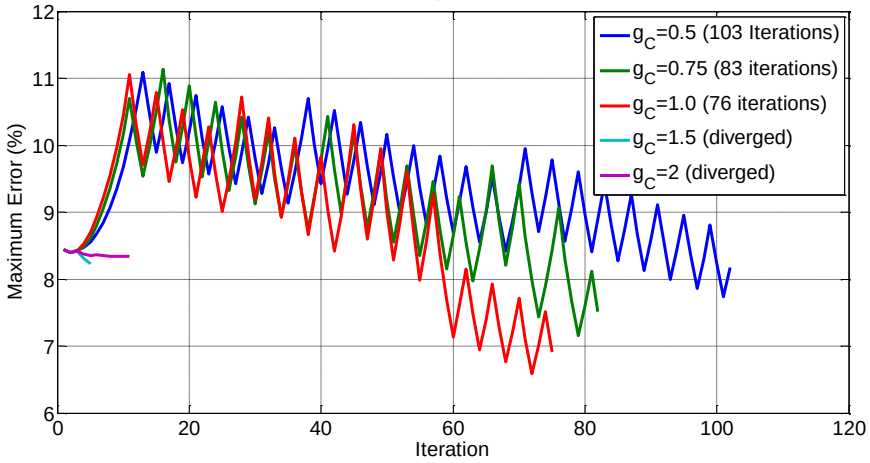

Figure 5-6 Gain Factor g_C vs Maximum Error

On the first iteration, the acceleration time history has been scaled to get a better match with the target spectra and the misfit has been reduced by the initial wavelet adjustments (correspond to the initial *b* vector). The first wavelet adjustments of the Broyden iteration were also applied on the first result. However, since g_C is applied after the wavelet adjustment calculation, the initial iteration of different g_C show the same results.

It is observed that the gain factor g_c is affecting solution convergence. It can be seen here that for this particular case a small gain factor g_c tends to make the algorithm runs with more iterations. This may happen because the spectra sensitivity *C* matrix is being updated in smaller increment. It is also observed that, depends on the case, a large gain factor g_c may make the algorithm overshoot the solutions, as can be seen for the g_c=1.5 and 2.0. For these values, the average misfits start to increase at the initial iteration.

This illustration shows how important the gain factor g_c to the solution convergence. Different cases (ground motion, period set, damping level, and target spectra) may result different solution convergence. Hence a

parametric study will be conducted in the next chapter to obtain a good value of the g_c in conjunction with the other the gain factors.

5.4 Off-diagonal Terms of *C* Matrix for Broyden Updating

Hancock et.al (2006) discusses the benefit of reducing the off-diagonal terms of the spectra sensitivity *C* matrix. While the off-diagonal reduction of *C* matrix was already implemented on the initial vector *b* calculation, the same concept was applied during the Broyden updating iteration as described in Eqn. 5.3. Here $C_{reduced}$ is the full *C* matrix which off-diagonal terms had been multiplied by constant reduction factor, $\alpha_{off\text{-}C}$.

$$\{\Delta b\} = g_b[-C_{reduced}]^{-1}\{S_{amisfit}\} \tag{5.3}$$

The study was conducted using the 1992 Cape of Mendocino, Petrolia Component 000 based on trials which shown that the effect of off-diagonal reduction is showed clearer on this ground motion. The tolerance of the average misfit was set to 0.010g or 7.5% on the maximum misfit corresponds to the target, whichever is reached first. The period set being solved ranges from 0.1sec to 1.0sec with 0.1sec increment. The damping ratio was taken as 5% of critical damping and the target response spectrum was the Dmax spectrum from FEMA P695 (FEMA 2009) associated with a high seismic area of California. The gain factor α_C, g_b and g_C were set as 500, 1 and 1 respectively. Figure 5-7 and Figure 5-8 show the evolution of the average misfit and the maximum misfit throughout iterations for different reduction coefficients of the off-diagonal of *C* matrix.

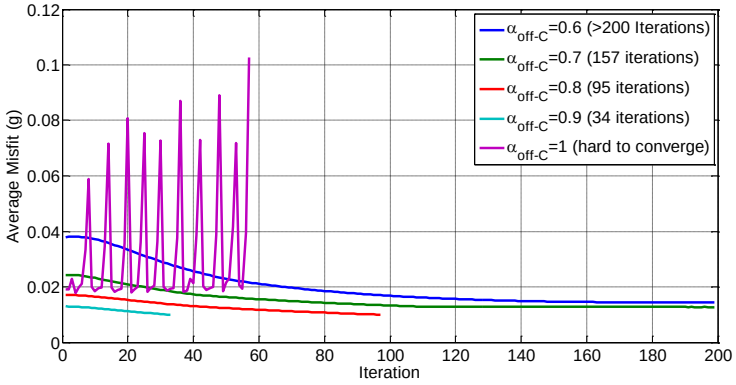

Figure 5-7 Off-diagonal terms Reduction ($\alpha_{off\text{-}C}$) vs Average Misfit

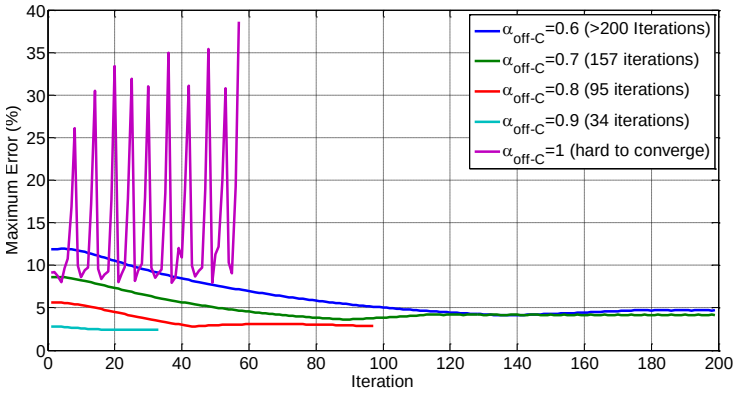

Figure 5-8 Off-diagonal terms Reduction ($\alpha_{off\text{-}C}$) vs Maximum Error

On the first iteration, the acceleration time history has been scaled to get a better match with the target spectra and the misfit has been reduced by the initial wavelet adjustments (correspond to the initial *b* vector). The first wavelet adjustments of the Broyden iteration, affected by the reduced off-diagonal terms of *C* matrix, were applied on the first result. Thus, the initial iterations show different results for different values of $\alpha_{off\text{-}C}$.

It is observed that the reduction of the off-diagonal terms is affecting solution convergence. It can be seen here that the reduction of the off-diagonal terms of *C* matrix reduces the solution accuracy, which is indicated by the large average misfit on the beginning of iteration. This may happen because by reducing the off-diagonal terms of *C* matrix, the cross correlation between the wavelet acceleration adjustment function is being underestimated. It is also noticed that although a small factor on the off-diagonal terms of *C* matrix makes the algorithm starts with higher misfit, the reduction rate is faster. For instance, for the reduction factor $\alpha_{off\text{-}C}$=0.6 the average misfit starts at 0.038g, and after 50 iterations the average misfit is 0.019g (50% of initial). While for $\alpha_{off\text{-}C}$=0.7 the initial average misfit is 0.024g, and after 40 iterations the average misfit is 0.0156g (65% of initial). It is also shown that, for this case, without the off-diagonal terms reduction, the algorithm is hard to converge. Different cases (ground motion, period set, damping level, target spectra) may result different solution convergence.

A parametric study of this reduction of the off-diagonal terms of *C* matrix with conjunction with other gain factors is presented in next chapter.

5.5 Test Case for Spectral Matching using the Broyden Updating Method

To illustrate the use of the Broyden updating method in the spectral matching, an example was conducted using the 1999 Hector Mine, Hector ground motion. The periods being solved ranges from 0.1sec to 3.0sec with 0.1sec increments (total 30 periods). The tolerance limit was set as 0.015g on the average misfit or 10% on the maximum misfit corresponds to the target, whichever is reached first. The damping ratio was taken as 5% of critical and the target response spectrum was the Dmax spectrum as before. The gain factors α_C, g_b, g_C, and $\alpha_{off\text{-}C}$ were set as 50, 1, 1 and 0.7 respectively. The spectral matching was conducted by using the Broyden updating method without any outer loop. The maximum number of Broyden iterations was set as 6000.

No period subset was applied for this study; the 30 periods were solved simultaneously. Only one linear scaling to the original acceleration time series was applied before the first iteration. The spectrum compatible acceleration and the convergence rate are presented in Figure 5-9 and Figure 5-10.

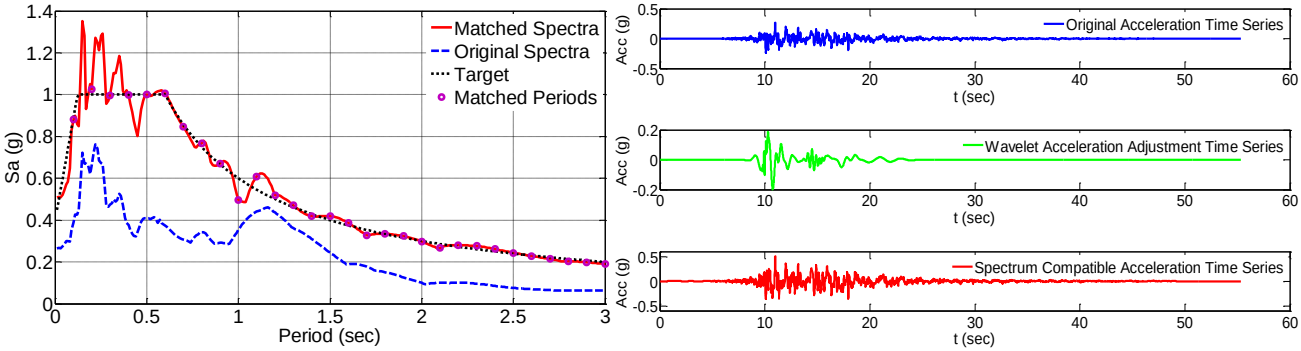

a b

Figure 5-9 Spectrum Compatible Result using Broyden Method Test 1 with Linearly Spaced Period
(a) Spectra Comparison (b) Acceleration Time Series Comparison

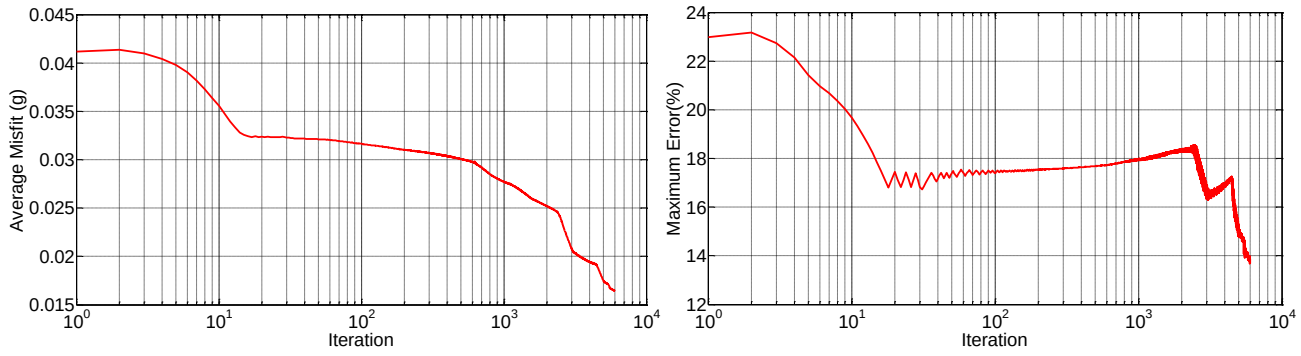

a b

Figure 5-10 Convergence Rate of Broyden Method Test 1 for 1999 Hector Mine, Hector Spectral matching
(a) Average Misfit Reduction Rate (b) Maximum Error Reduction Rate

It can be seen that the Broyden method is able to match the given target. Based on visual observation, the wavelet adjustments cause only a minor change to the spectrum compatible acceleration time series, thus producing a realistic spectra compatible acceleration time series. In Figure 5-10 it can be seen that the Broyden method is converged for the given problem.

Another attempt was conducted using the Broyden method for the same ground motion with a closer spaced periods; from 0.1-1.0sec with 0.05 log scale increments and 1.0sec-3.0sec with 0.025 log scale increments (total 40 periods). The tolerance limit and the spectra target were the same with the previous sample. The maximum numbers of the Broyden iteration was 10000 iterations. The spectrum compatible acceleration and the convergence rate are presented in Figure 5-11 and Figure 5-12.

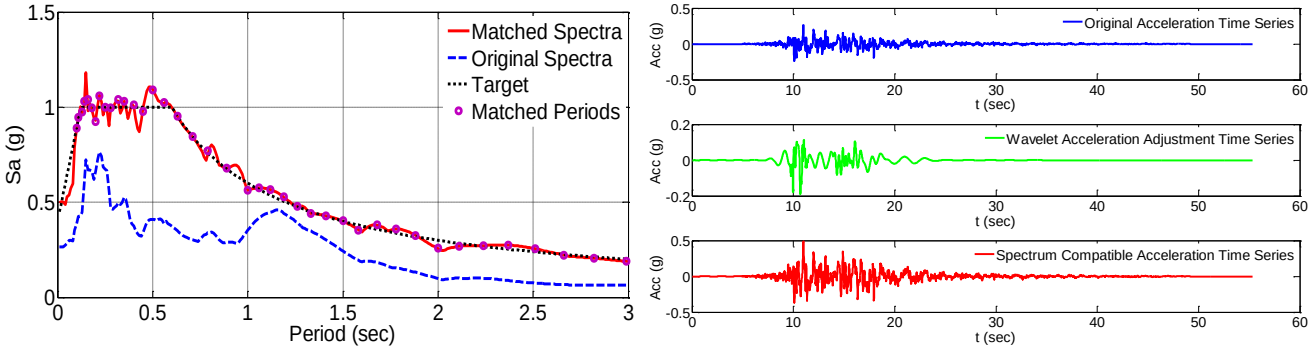

a b

Figure 5-11 Spectrum Compatible Result using Broyden Method Test 2 with Log Spaced Period
(a) Spectra Comparison (b) Acceleration Time

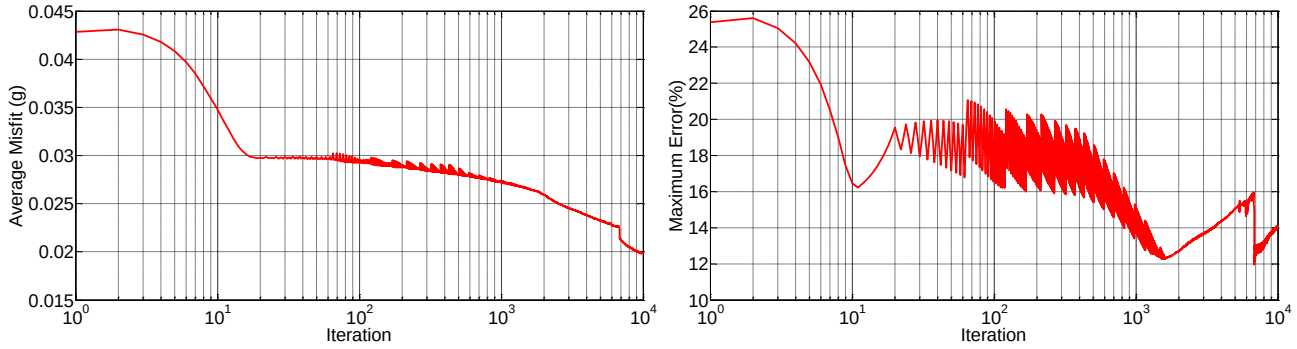

Figure 5-12 Convergence Rate of Broyden Method Test 2 for 1999 Hector Mine, Hector Spectral matching
(a) Average Misfit Reduction Rate (b) Maximum Error Reduction Rate

The presented response spectra in Figure 5-11 are from 0.01sec to 3.0sec with 0.01sec increments, which considered being a closed spaced periods. Here it can be seen that the Broyden updating method is capable of matching the target spectral ordinates.

Although the Broyden updating method works on the previous samples, it should be noted that the number of iterations are too large to be a computationally efficient option. By a closer examination on Figure 5-10 and Figure 5-12, it is observed that the convergence rate is rapid on the first 20 iterations. This fact leads to the proposed method, presented in the previous chapter, where the Broyden method is truncated by a maximum number of iterations (proposed value is 5-20 iterations), and then starts over again for the next period subset.

5.6 Solution Divergence

The previous examples show that the Broyden updating method is good for solving the nonlinear problem on spectral matching. However for a very close spaced period, there is a chance that the algorithm will diverge. To study this diverging behavior, one should look at the general form of the Broyden formula (Yang, 1995) given as:

$$[\mathrm{J_k}] = [\mathrm{J_{k-1}}] + \frac{\{\Delta \mathrm{F}\} - [\mathrm{J_{k-1}}]\{\Delta \mathrm{x_k}\}}{\{\mathrm{g_k}\}^{\mathrm{T}}\{\Delta \mathrm{x_k}\}}\{\mathrm{g_k}\}^{\mathrm{T}}$$

where *k* is the iteration number. By using the Sherman-Morrison formula leads to a direct Broyden updating (Jacobian inverse updating) :

$$[J_k]^{-1} = [J_{k-1}]^{-1} + \frac{\{\Delta x_k\} - [J_{k-1}]^{-1}\{\Delta F\}}{\{f_k\}^T\{\Delta F\}}\{f_k\}^T$$

By taking $\{g_k\}$ equals to $\{\Delta x_k\}$ and $\{f_k\}$ equals to $\{\Delta x\}^T[J_{k-1}]^{-1}$, one can find the common Broyden formula as given by:

$$[J_k] = [J_{k-1}] + \frac{\{\Delta F\} - [J_{k-1}]\{\Delta x_k\}}{\|\{\Delta x_k\}\|^2}\{\Delta x_k\}^T$$

$$[J_k]^{-1} = [J_{k-1}]^{-1} + \frac{\{\Delta x_k\} - [J_{k-1}]^{-1}\{\Delta F\}}{\{\Delta x_k\}^T[J_{k-1}]^{-1}\{\Delta F\}}\{\Delta x_k\}^T[J_{k-1}]^{-1}$$

However, it is noticed that $\{g_k\}$ should be selected in a way such that $\{g_k^T\}\{\Delta x_k\} \neq 0$, and $\{f_k\}$ needs to be chosen such that $\{f_k^T\}\{\Delta F\} \neq 0$ and $\{g_k\} = [J_k]^T\{f_k\}$. Yang (1995) provides a comprehensive discussion how to select these terms. Although the Broyden method may converge by taking $\{g_k\}$ equals to$\{\Delta x\}$, and for some cases are working faster, it should be noted that this type of Broyden family may diverge. Gay and Schanabel (1978) independently developed two methods to choose $\{f_k\}$, one of them is described as:

$$\{f_k\} = [J_k]^{-1}\left(\{\Delta x_k\} - \sum_{i=0}^{k-1} \tilde{p}_i^H p_k \tilde{p}_i\right)$$

where the vectors $\tilde{p}_0, \ldots, \tilde{p}_{k-1}$ are the orthonormal basis of the space spanned by $\{\Delta x_i\}$, *i*=0,….,*k*-1. This variant of Broyden method is called the dual Projected Broyden Method. However, since this calculation requires more computational effort, it is considered more efficient to use the basic Broyden and terminate the updating procedure if the solution greatly diverged or reached prescribed maximum iterations.

Another source of a diverging solution is the error matrix *E*, defined as $E_k = I - A\,[J_k]^{-1}$ where *I* is the identity matrix, and *A* is the coefficient of function *F(x) = Ax-b* being solved. It is mentioned before that the Broyden updating is approximating the Jacobian *A* by a matrix *J*. Yang (1995) provides a comprehensive study on how selecting $\{f_k\}$ and also $\{g_b\}$ (which defined as α_k on her report) may leads to a difference convergence (or divergence) behavior of the Broyden method.

CHAPTER 6. PARAMETRIC STUDY

The Broyden method was applied to solve the nonlinear system of spectral matching, and as proven previously in Chapter 5 that, as expected in a typical nonlinear system, the solution is not unique. It was also observed in the preliminary study that the solution is sensitive to the initial *b* vector and the *C* matrix as well as the other coefficient parameters in the Broyden updating set. Parametric study was carried out to investigate the effect of some coefficients that are used in the algorithm, and to get a good combination that leads to a more effective calculation and minimize the spectra misfit $S_{amisfit}$.

This preliminary study was conducted using several different gain factor combinations, including:

- 8 values of the gain factor on the initial spectral sensitivity *C* matrix (α_C)
- 12 values of magnitudes of the wavelet adjustment (Ψ_M), which is the peak acceleration (*g*) of the mother wavelet function
- 12 values of the off-diagonal of *C* matrix reduction ($\alpha_{off\text{-}C}$)
- 7 values of gain factor g_b
- 13 values of gain factor g_C
- 6 values of maximum number for Broyden iterations (*M*)
- 12 values of maximum number for outer-loop iterations (*N*)

The parametric study was conducted using separate studies instead of using every possible combination of the gain factors. Ten different ground motions taken from FEMA P695 (FEMA 2009) were being used in this parametric study. The ten ground motions were chosen to represent far field, near field-pulse like, and near field-no pulse like earthquake motions. Table 6-1 shows the selected ground motions. The magnitudes of the selected events range from M6.5 to M7.4 with an average magnitude of M6.9. The variation of soil conditions and shear wave velocity (V_{s30}) were also being considered in selecting the ground motions. The Peak Ground Acceleration (PGA) of the selected ground motions range from 0.13g-0.98g with an average of 0.41g. The source distance was taken as the closest distance to the fault plane. The damping ratio was taken as 5% of the critical damping and the target response spectrum was the Dmax spectrum from FEMA P695 (FEMA 2009), associated with a high seismic area of California. All operations in the parametric study were executed using a personal laptop with i7-2760QM 2.4Gz processor and 8192Mb DDR3 RAM.

According to Bommer and Acevedo (2004), one of the criteria in selecting the ground motion as an input of time histories analysis is the similarity between the spectral shapes to the shape of the target spectrum. The

quantified shape similarity (denoted as D_{rms}) is based on the average root-mean-square deviation of the observed spectrum from the target design spectrum.

$$D_{rms} = \frac{1}{N}\sqrt{\sum_{i=1}^{N}\left(\frac{S_{ai}}{PGA_{GM}} - \frac{S_{atarget-i}}{PGA_{target}}\right)^2} \quad (6.1)$$

- N is the number of periods at which the spectral shape is specified
- S_{ai} is the spectral acceleration from the record at period T_i
- $S_{atarget-i}$ is the target spectral acceleration at the same period
- PGA_{GM} is the peak ground motion acceleration of the records
- PGA_{target} is zero-period anchor point of the target spectrum

A small D_{rms} value represents a better match between the shape of the record and the target spectrum. For instance, Bommer and Avecedo (2004) proposed that values of D_{rms} of the order of 0.15 were needed for matching ordinates in the period range of 0.4-0.8 second, whereas values as low as 0.06-0.07 could be used for matching the spectral ordinates from 0.1 to 0.3s second. However, there are no acceptance criteria of D_{rms} for wide range of periods yet.

The D_{rms} values for the selected ground motions are also presented in Table 6-1. It can be seen here that some of the near field ground motions have a large D_{rms}, which in practice might make the use of these ground motions to match the target questionable. However, in this study, the purpose of using these ground motions was to examine how well the algorithm can match the target using various types of ground motion.

Baker (2011) proposes one criteria of selecting ground motion based on shape similarity between original spectra and target spectra. The shape similarity is determined by the sum of squared errors (SSE) between the logarithms of the original ground motion spectra and the target spectra, defined as:

$$SSE = \sum_{j=1}^{n}\left(ln\, S_{ai} - ln\, S_{atarget-i}\right)^2 \quad (6.2)$$

where ln S_{ai} is the log spectral acceleration of the original ground motion at period T_j, and ln $S_{atarget-i}$ is the log of target spectra. A small SSE represents a good similarity between the original ground motion spectra with the target. Both shape similarity measurements are presented and used in the further analysis.

Table 6-1 Selected Ground Motions for Parametric Study

Ground Motion #	Event Name/Year	Mag-nitude	Recording Station/ Component	PGA (g)	Site Class/V_{S30} (m/s)	Source Distance (km)	Ground Motion Type	D_{rms}	SSE
1	Hector Mine/1999	7.1	Hector/ Component 000	0.23	C/685	11.7	Far Field	0.029	230
2	Landers/1992	7.3	Yermo Fire Station/ Component 270	0.25	C/523	23.6	Far Field	0.028	88
3	Manjil, Iran/1990	7.4	Abhar/ Component 057	0.13	C/724	13	Far Field	0.021	359
4	San Fernando/1971	6.6	LA-Hollywood Stor/ Component 090	0.21	D/219	22.8	Far Field	0.028	317
5	Imperial Valley-06/ 1979	6.5	El Centro Array#6/ Component 140	0.41	D/203	1.4	Near Field-Pulse	0.028	36
6	Erzican, Turkey/1992	6.7	Erzincan/ Component EW	0.50	D/275	4.4	Near Field-Pulse	0.020	8
7	Cape Mendocino/1992	7	Petrolia/ Component 000	0.59	C/713	8.2	Near Field-Pulse	0.033	79
8	Loma Prieta/1989	6.9	BRAN/ Component 000	0.48	C/376	10.7	Near Field-No Pulse	0.027	113
9	Nahanni, Canada/1985	6.8	Site 1/ Component 019	0.98	C/660	9.6	Near Field-No Pulse	0.053	189
10	Northridge-01/1994	6.7	Northridge-Saticoy/ Component 090	0.37	C/380	8.4	Near Field-No Pulse	0.023	60

6.1 Gain Factor on the Initial Spectral Sensitivity *C* Matrix (α_C)

It was observed in the preliminary study that the selection of the initial spectral sensitivity *C* matrix may cause the algorithm to overshoot the solution. A higher initial spectral sensitivity *C* matrix is expected to give a small initial *b* vector increment in the first Broyden iterations, hence reducing the chance of overshooting the solution. The magnitude of the initial *C* matrix is controlled by the gain factor α_C as defined in Eqn 4.7. Eight different values of α_C were studied in this parametric study. The eight values of gain factor α_C were 1, 5, 10, 100, 500, 1000, 5000, and $1x10^4$.

The criteria for selecting the best values in the parametric study include the computational time, the average misfit, and the maximum misfit. The parametric study was conducted while keeping the wavelet magnitude (Ψ_M), the reduction of the off diagonal of the *C* matrix ($\alpha_{off\text{-}C}$), the gain factor g_b, the gain factor g_c constant as $1x10^{-6}$g, 0.7, 1, and 1 respectively. The maximum number of the Broyden iteration and the outer loop iteration were set as 10 and 5 respectively. The tolerance limit was 0.005g of the average misfit. The wavelet magnitude was 10^{-6}g. Figure 6-1 to Figure 6-4 show the graphical results of parametric study on the gain factor α_C.

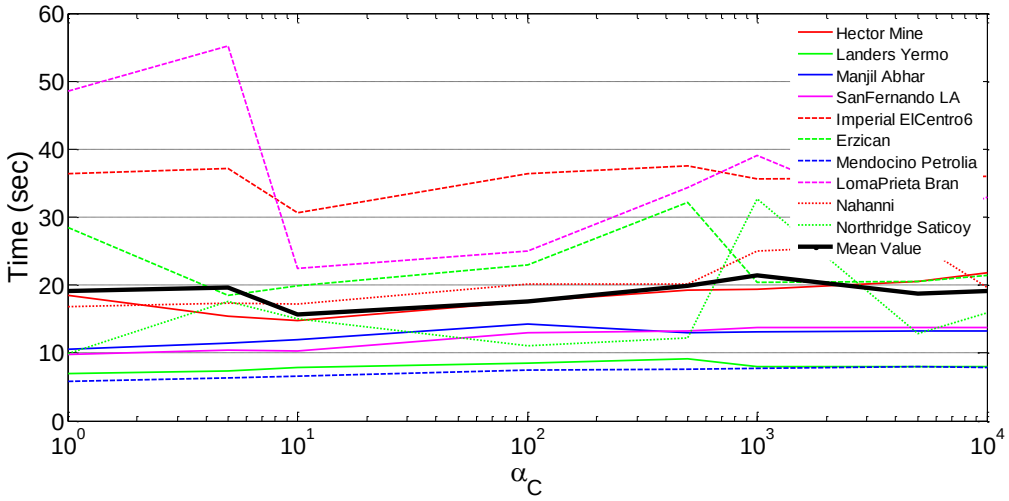

Figure 6-1 Gain Factor α_C vs Computational time

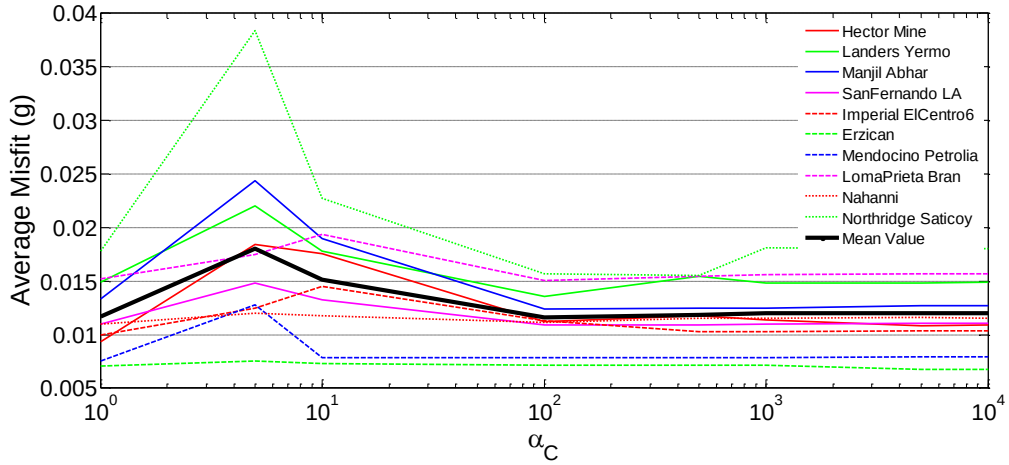

Figure 6-2 Gain Factor α_C vs Average Misfit

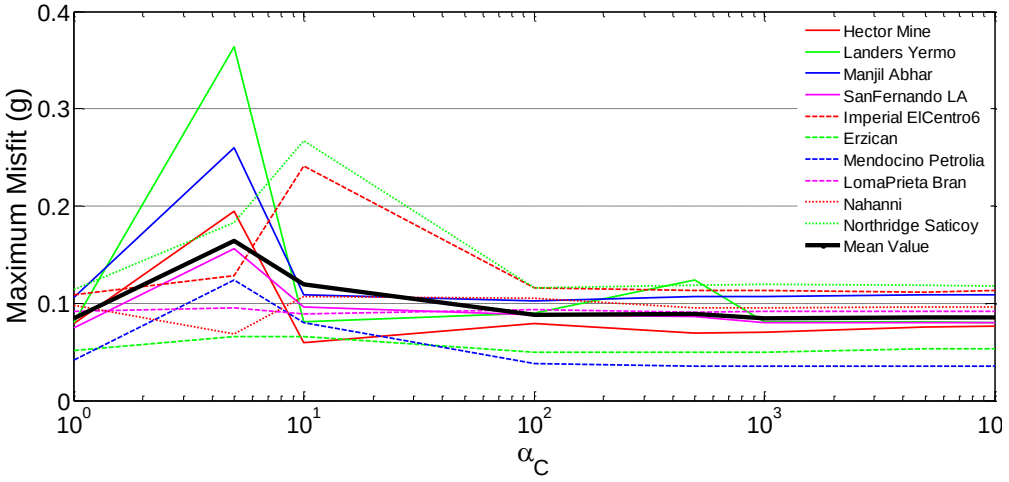

Figure 6-3 Gain Factor α_C vs Maximum Misfit

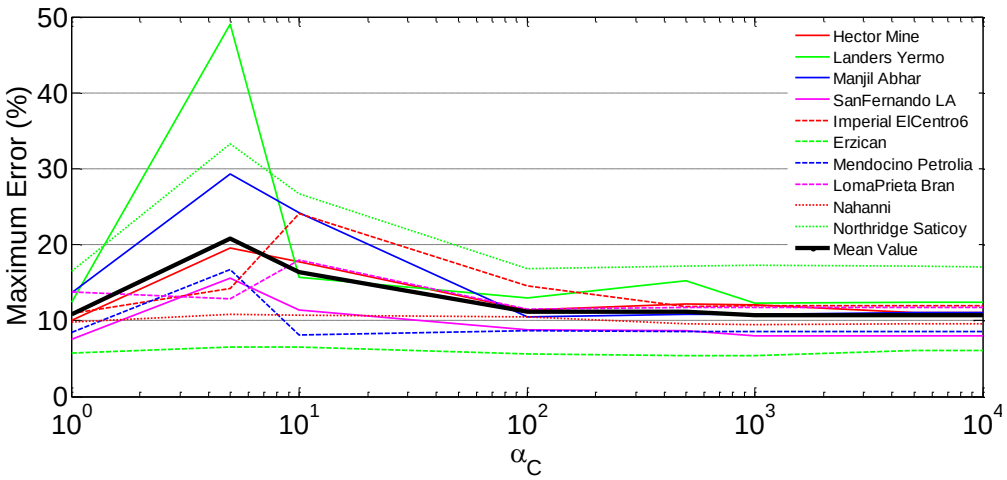

Figure 6-4 Gain Factor α_C vs Maximum Error

The comparison of the computational times is presented in Figure 6-1, where it is hard to see the trends. Figure 6-2 presents the average misfit versus various values of α_C. It is showed that the average misfits are relatively small for α_C =1 and yields a large misfit between α_C =5 and 100. The average misfit also seems to be small for α_C =100 and relatively stable after α_C >500. This implies that α_C greater than 100 gives less nonlinearity to the solution than a smaller α_C. Another cause for this difference in the average misfit is due to the $\Delta b^{initial}$ vector, given by

$$\{\Delta b^{initial}\} = \mathrm{g}_b \left[C^{initial}\right]^{-1} \{S^{initial}_{amisfit}\}$$

A high initial *C* matrix yields a small $\Delta b^{initial}$ vector and leads the Broyden iteration to start with a *b* vector that is close to the initial *b*.

Figure 6-3 plots the maximum misfit versus α_C. It can be observed that there are similar patterns with the average misfit in which the maximum misfits are higher between α_C =5 and 100. The maximum misfits are relatively constant after α_C=100. A similar pattern is also observed for the maximum error, as can be seen in Figure 6-4 where the error reaches up to 20% of the target for α_C less than 100, then becomes stable at about 10% for α_C greater than 100.

It is observed that the trends on average misfit and maximum misfit are not decreasing monotonically. For instance at $5 \leq \alpha_C \leq 10$ the misfit is increased then reduced again at $\alpha_C \geq 100$. It is hard to examine the causes since this parametric study compares several parameters (computational time, average misfit, maximum misfit and maximum error) and uses multiple tolerances at the same time. An alternative parametric study can be conducted by using a fixed tolerance, i.e. the average misfit, with unlimited number of outer loop iteration and then compares only the computational time.

Based on the observed figures, there are three potential candidates of α_C from the set analyzed that yield a short computational time, a small average misfit and a small maximum misfit. The three α_C candidates are 1, $1x10^2$, and $1x10^3$. The quantified values of the computational time, the average misfit, and the maximum misfit for these three α_C candidates are presented in Table 6-2 where the mean and standard deviation are being compared.

Table 6-2 Comparison of Parametric Study on Gain Factor α_C with Wavelet Magnitude $1x10^{-6}$g

α_C	Wavelet Magnitude = $1x10^{-6}$g							
	Time (s)		Average Misfit (g)		Max Misfit (g)		Max Error (%)	
	Mean	σ	Mean	σ	Mean	σ	Mean	σ
1	19	14	0.01172	0.00349	0.08468	0.02410	10.88	3.26
$1x10^2$	17	9	0.01164	0.00276	0.08782	0.02611	11.12	3.17
$1x10^3$	21	11	0.01203	0.00339	0.08526	0.02709	11.12	3.21

Here it can be seen that in term of computational time, α_C=$1x10^2$ gives a slightly better result. It is also shown that in term of the average misfit, α_C=$1x10^2$ yields the smallest average misfit (both in mean and standard deviation). This small misfit indicates that a smooth spectra response. The second best combination is α_C=1 which gives less than 1% higher means value but the standard deviation is 26% higher than the best candidate.

It is also shown that for the maximum misfit, α_C=1 gives the smallest value in mean and standard deviation. The second best combination is α_C =$1x10^3$ which gives only 0.7% higher value of mean but 12% higher standard deviation. The gain factor α_C =$1x10^2$ resulted a 4% higher mean value and 8% higher standard deviation compared to α_C=1.

In terms of maximum error percentage, α_C =1 gives a better result with 10.88% mean error. The second best combination is α_C =$1x10^2$ with 11.12% error. Gain factor α_C =$1x10^3$ gives the same maximum error with α_C =$1x10^2$ but has a higher standard deviation.

The α_C = 1 is also showing a good result, however based on this comparison; the proposed value of α_C is $1x10^2$. This is because the fact that, in general, it yields a short computational time and a smaller average misfit. Although the maximum misfit for α_C = $1x10^2$ is higher than α_C =1, this maximum misfit is considered to be small in terms of error.

6.2 Wavelet Magnitude (Ψ_M)

The wavelet magnitude (Ψ_M) is defined as the peak acceleration of mother wavelet. It determines the order of the *b* vector and *C* matrix. Figure 6-5 shows the corrected tapered cosine wavelet with magnitude 1g. As discussed in Chapter 4, on Eqn. 4.4 to 4.6, the initial *C* matrix is calculated based on the superposition of the ground motion response $u_{GMi}(t)$ with the total response of the wavelet adjustment $u_{t\psi i}(t)$. Hence, a high Ψ_M

tends to shift the original time of peak response and creates an initial *C* matrix that is greatly different than the original *C* matrix (before the original time of peak response shifted). It was observed on the previous chapter that the initial Broyden iteration is sensitive to initial *C* matrix.

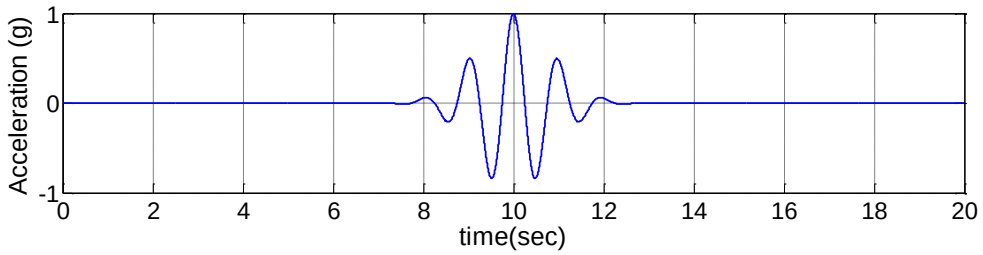

Figure 6-5 The Corrected Tapered Cosine Wavelet with Magnitude 1g

The wavelet magnitude (Ψ_M) basically defines the order of the initial vector *b*. It was discussed before that a wavelet magnitude that is smaller than 1g is expected to reduce the solution sensitivity during the initial Broyden iteration. Twelve values of Ψ_M were studied; 1g, 0.1g, 0.05g, 0.01g, $5x10^{-3}$g, $1x10^{-3}$g, $5x10^{-4}$g, $1x10^{-4}$g, $5x10^{-5}$g, $1x10^{-5}$g; $1x10^{-6}$g, $1x10^{-7}$g. The parametric study was conducted while keeping the gain factor α_C, the reduction of the off diagonal of the C matrix ($\alpha_{off\text{-}C}$), the gain factor g_b, the gain factor g_c constant as $1x10^2$, 0.7, 1, and 1 respectively. The maximum number of the Broyden iteration and the outer loop iteration were set as 10 and 5 respectively.

The tolerance limit was set as 0.005g on the average misfit. Figure 6-6 to 6-9 show the graphical results of the parametric study on wavelet magnitude. The required computational time, the average misfit, the maximum misfit and the error were observed in this study.

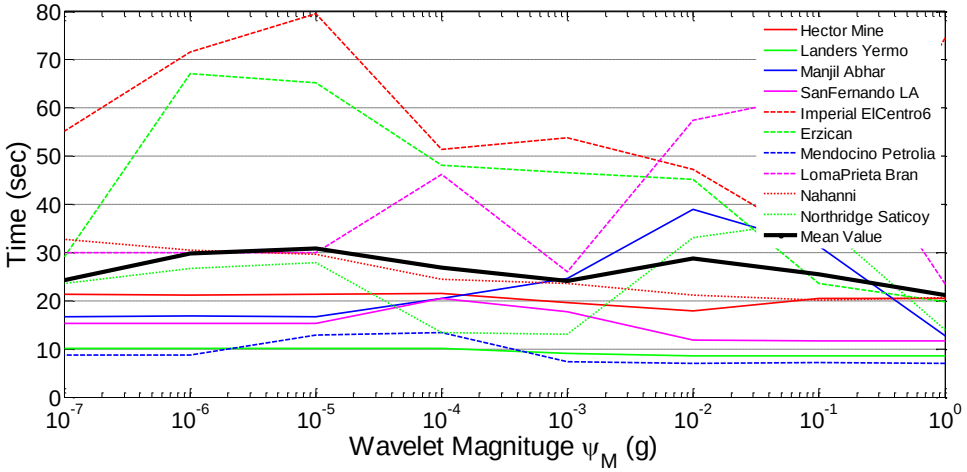

Figure 6-6 Wavelet Magnitude Ψ_M vs Computational time

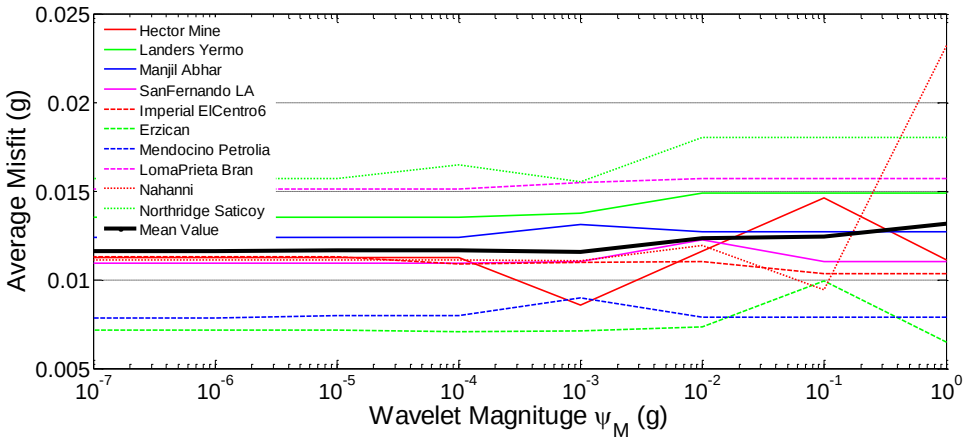

Figure 6-7 Wavelet Magnitude Ψ_M vs Average Misfit

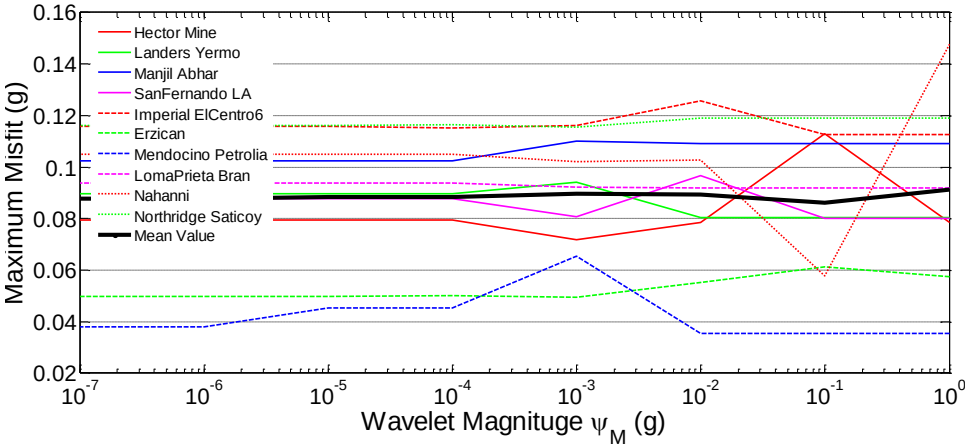

Figure 6-8 Wavelet Magnitude Ψ_M vs Maximum Misfit

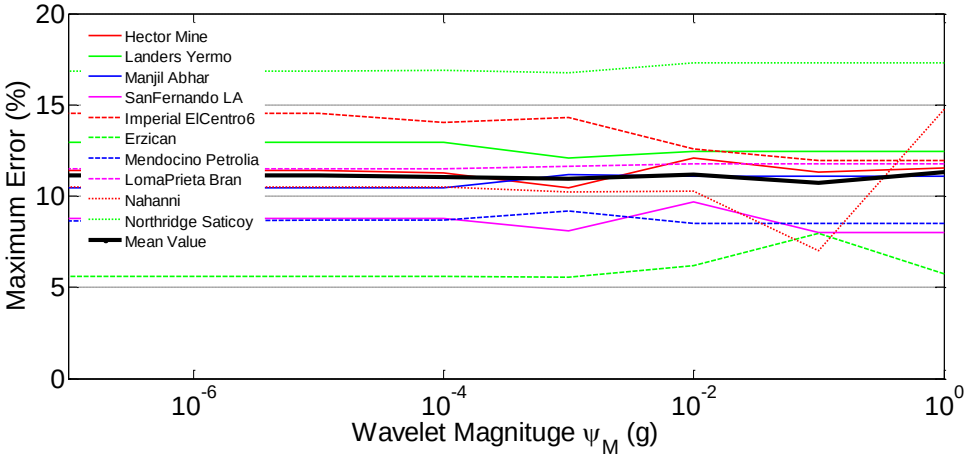

Figure 6-9 Wavelet Magnitude Ψ_M vs Maximum Error

Figure 6-6 plots the computational time versus the wavelet magnitude Ψ_M. It is hard to see the trends here. There are 3 special cases where the algorithm runs faster on Ψ_M near 1g: the 1990 Manjil, Abhar (GM #3); the 1979 Imperial ElCentro6 (GM #5); and the 1992 Erzican, Erzican (GM #6) ground motions. On the contrary, for the 1989 Loma Prieta, Bran (GM #8) ground motion, the algorithm runs slower on Ψ_M near 1g.

Figure 6-7 presents the average misfit versus the wavelet magnitude Ψ_M. It is observed that the algorithm yields a high average misfit for Ψ_M near 1g, and becomes constant for Ψ_M less than $1x10^{-5}$g. There is an exceptional case for the 1992 Erzican, Erzican (GM #6) ground motion where the Ψ_M=1g yields a small misfit. However, in general, a high Ψ_M tends to yield a high average misfit. This implies that a small wavelet magnitude (less than 0.001g) gives less nonlinearity to the initial solution for the C matrix, especially in the first Broyden iterations.

To understand this behavior, we should take a closer examination of the initial *C* matrix calculation. The initial *C* matrix approximates the Jacobian in the solution. The Broyden method updates the *C* matrix during the iteration, hence it is considered better if the iteration starts with an appropriate *C* matrix.

It is discussed before that a large wavelet magnitude leads to a *C* matrix that is greatly different than the original *C* matrix due to the time shifting. At some level of low Ψ_M, the chance of time shifting is reduced. It can be seen on Figure 6-7 that Ψ_M which less that 10^{-5}g have a constant average misfit. This is due to absence of time shifting on the initial *C* matrix for these small Ψ_M.

The comparison of the maximum misfit is presented on Figure 6-8. The similar trends with the average misfit are also occurring here where the maximum misfits are higher at a larger Ψ_M. There is one special case for the 1992 Cape of Mendocino, Petrolia (GM #7) ground motion where the maximum misfits are smaller on Ψ_M greater than 10^{-2}g. However, most of the maximum misfits are relatively stable at Ψ_M less than $1x10^{-4}$g. Where the maximum errors are plotted on Figure 6-9, it can also be seen that the errors become relatively stable for Ψ_M less than $1x10^{-4}$g.

It is observed on the previous figures that there are at least three candidates of Ψ_M that require a faster computational time and yield a small misfit. Based on the values analyzed, the three candidates for the factor Ψ_M are: $1x10^{-5}$g, $1x10^{-6}$g and $1x10^{-7}$g. Ψ_M=1g is also being presented here for comparison. The quantified values of the computational time, the average misfit, the maximum misfit and the error for these Ψ_M are presented in Table 6-3.

Table 6-3 Comparison of Parametric Study on Wavelet Magnitude

Wavelet Magnitude (g)	Time (s)		Average Misfit (g)		Max Misfit (g)		Max Error (%)	
	Mean	σ	Mean	σ	Mean	σ	Mean	σ
1	22	20	0.013139	0.004980	0.091306	0.03233	11.31	3.32
$1x10^{-5}$	31	23	0.011650	0.002735	0.088539	0.02463	11.12	3.17
$1x10^{-6}$	29	22	0.011635	0.002756	0.087816	0.02611	11.12	3.17
$1x10^{-7}$	24	14	0.011635	0.002756	0.087816	0.02611	11.12	3.17

It can be seen in Table 6-3 that the best candidates in terms of the computational time are Ψ_M =1g and $1x10^{-7}$g. However, Ψ_M =$1x10^{-7}$g is considered better than 1g because its results have smaller standard deviation.

In terms of the average misfit, Ψ_M=$1x10^{-6}$g and $1x10^{-7}$g give the same results. The second best candidate is Ψ_M=$1x10^{-5}$g which gives only slightly (less than 1%) higher mean value and standard deviation. It is shown here that Ψ_M= 1g gives a 13% higher mean value and the standard deviation is 81% larger than the best candidates.

In terms of the maximum misfit, the best candidates are Ψ_M=$1x10^{-6}$g and $1x10^{-7}$g. The second best candidate is Ψ_M=$1x10^{-5}$g which gives only 1% higher on the mean value, but 6% lower standard deviation than the best candidates. Ψ_M=1g gives 4% higher on the mean value and the standard deviation are 24% higher compared to the best candidates. In terms of the error percentage, Ψ_M=$1x10^{-5}$g, $1x10^{-6}$g and $1x10^{-7}$g yield the same maximum error while Ψ_M=1g gives a higher error.

Based on these comparisons, the proposed value of Ψ_M is $1x10^{-7}$g. This is based on the fact that this wavelet magnitude yields a smaller average misfit with lower standard deviation and only a slightly higher maximum misfit. Further parametric study is discussed in the next paragraphs to examine the better combination with other parameters using the proposed α_C=$1x10^{2}$ and Ψ_M=$1x10^{-7}$g.

6.3 Coefficient of the Off-diagonal Terms of *C* Matrix

The cross correlation of the wavelets adjustment implicitly defines the off-diagonal terms of the spectral sensitivity *C* matrix, and it is the source of solution nonlinearity. A parametric study to observe the effect of the off-diagonal terms of the *C* matrix was carried out using twelve different reduction coefficients ($\alpha_{off\text{-}C}$), which range from 0.2 to 1.0 with 0.1 increments, 0.65, 0.75 and 0.85. The parametric study was conducted while keeping the gain factor α_C, the wavelet magnitude Ψ_M , the gain factor g_b, the gain factor g_c constant as $1x10^{2}$ and $1x10^{-7}$g, 1, and 1 respectively. The maximum number iteration of the Broyden and the outer loop were set as 10 and 5 respectively. The tolerance limit was 0.005g on the average misfit. Figure 6-10 to Figure 6-13 show the graphical results of parametric study on the off-diagonal terms of the *C* matrix.

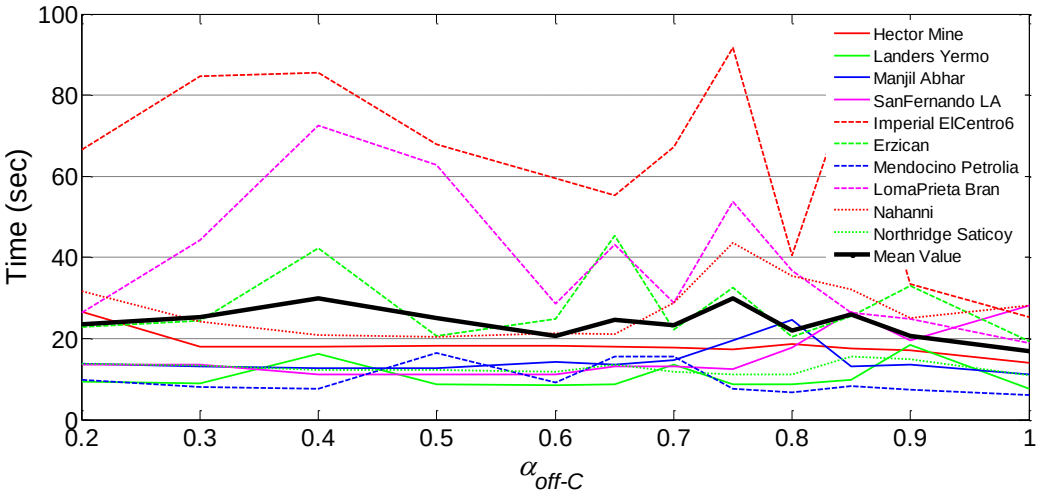

Figure 6-10 Reduction Coefficient of the Off-diagonal Terms of C Matrix vs Computational time

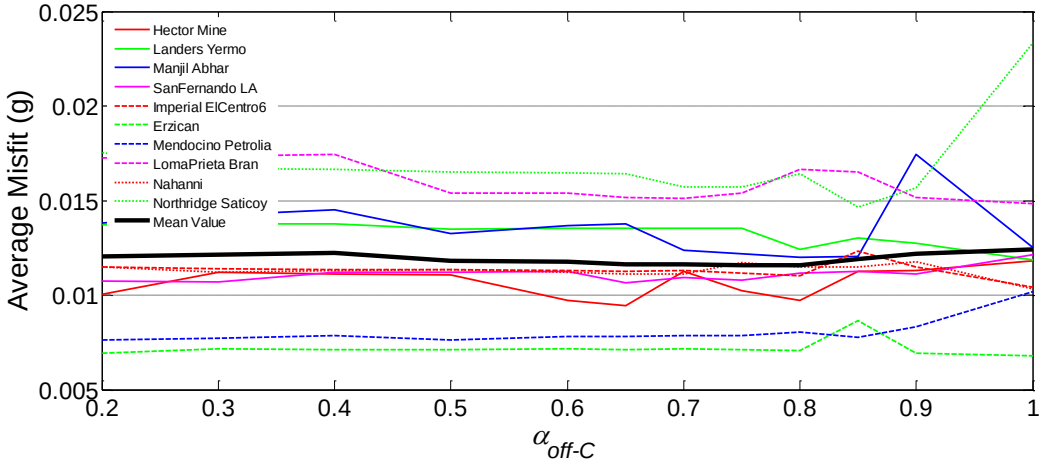

Figure 6-11 Reduction Coefficient of the Off-diagonal Terms of C Matrix vs Average Misfit

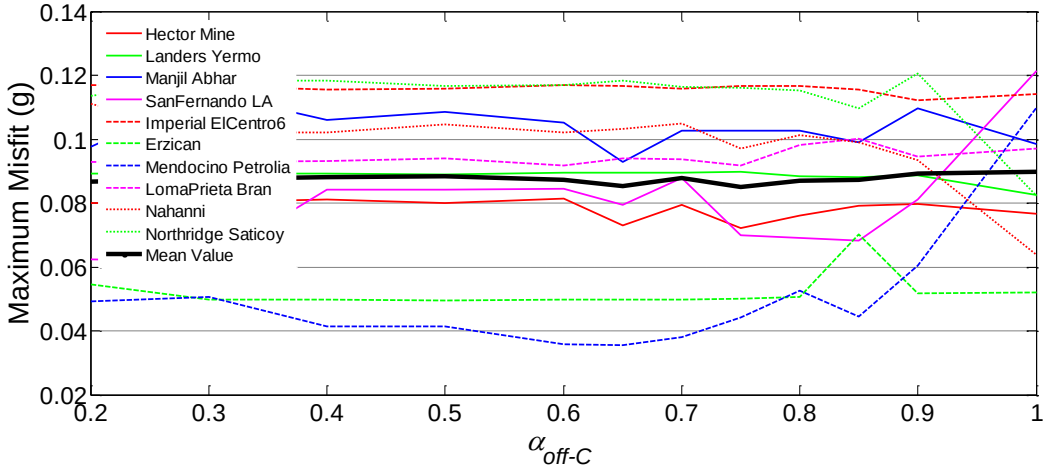

Figure 6-12 Reduction Coefficient of the Off-diagonal Terms of C Matrix vs Maximum Misfit

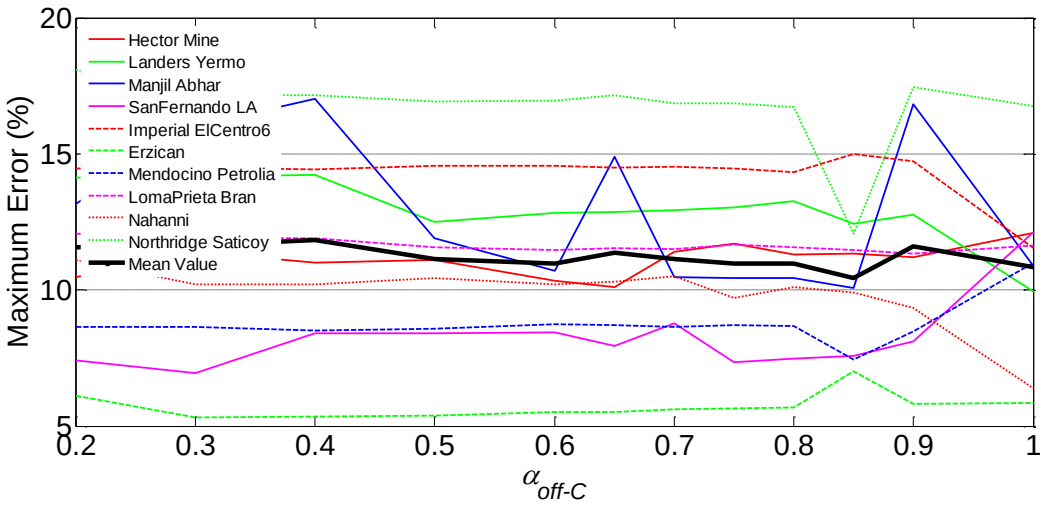

Figure 6-13 Reduction Coefficient of the Off-diagonal Terms of C Matrix vs Maximum Error

The computational time is plotted in Figure 6-10. It is observed that the algorithm runs faster on a $\alpha_{off\text{-}C}$ near 1. Figure 6-11 plots the average misfit versus $\alpha_{off\text{-}C}$. It can be seen here that the average misfit becomes small between 0.5< $\alpha_{off\text{-}C}$ <0.8. The average misfit is larger for $\alpha_{off\text{-}C}$ less than 0.5. This is happening because by underestimating the cross correlation between the wavelet adjustments, the calculation lost its solution accuracy. There are two ground motions, the 1971 San Fernando, LA Store (GM #4) and the 1992 Cape of Mendocino, Petrolia (GM #7), that yield a large average misfits at $\alpha_{off\text{-}C}$ equals to 1. These large misfits may happen because, for these particular ground motions, the wavelets cross correlation are high and producing more nonlinearities to the solution. This implies that reducing the off-diagonal terms may aid the solution convergence.

Figure 6-12 shows the plot of the maximum misfit versus $\alpha_{off\text{-}C}$. It can be seen here that the maximum misfit is relatively constant as $\alpha_{off\text{-}C}$ varies. The maximum error is presented on Figure 6-13. It is shown here that, in average, the errors are relatively small for 0.5< $\alpha_{off\text{-}C}$ <0.8. However, it is hard to see the correlation between the maximum error and the maximum misfit. Even though the maximum misfit is small for 0.5< $\alpha_{off\text{-}C}$ <0.8, the pattern for error is not necessarily the same. For instance, on the 1990 Manjil, Abhar (GM #3) ground motion the maximum misfit is decreased at $\alpha_{off\text{-}C}$ equals to 0.65, but apparently this maximum misfit occurs at a smaller target spectra $S_{atarget\text{-}i}$, thus yielding a larger error.

Based on the observation on the previous figures, there are two candidates of $\alpha_{off\text{-}C}$ which result a short computational time and a small misfit; 0.6 and 0.7. The quantified parameters of these two candidates are presented in Table 6-4 where the mean and the standard deviation are being compared.

Table 6-4 Comparison of Parametric Study on the Reduction Coefficient of the Off-diagonal of *C* matrix $\alpha_{off\text{-}C}$

Off diagonal reduction of *C* matrix $\alpha_{off\text{-}C}$	Time (s)		Average Misfit (g)		Max Misfit (g)		Max Error (%)	
	Mean	σ	Mean	σ	Mean	σ	Mean	σ
0.6	21	15	0.01175	0.00305	0.08736	0.02669	10.98	3.23
0.7	23	17	0.01164	0.00276	0.08782	0.02611	11.12	3.17

It can be seen here that in term of computational time, $\alpha_{off\text{-}C}$=0.7 is 2sec longer and the results are more distributed (13% higher standard deviation). The best combination in term of average misfit is $\alpha_{off\text{-}C}$=0.7, which has 1% smaller on mean value but has 11% smaller standard deviation compared to $\alpha_{off\text{-}C}$=0.6. It is also observed that $\alpha_{off\text{-}C}$= 0.7 yields only a 0.5% larger maximum misfit but has a 2% less distributed standard deviation compared to the $\alpha_{off\text{-}C}$=0.6. In terms of error, $\alpha_{off\text{-}C}$=0.6 gives a better result but the standard deviation is higher.

Based on this comparison, the proposed value of $\alpha_{off\text{-}C}$ is 0.7 since this value yields a small average misfit and only a slightly higher maximum misfit with better distribution. Further parametric study is discussed in the next paragraphs to examine the better combination with other parameters.

6.4 Gain Factor Applied to the *Δb* Vector (g_b)

The gain factor applied to the vector *Δb* is controlling how fast the vector *b* changes during the Broyden iteration. Recall Eqn. 5.1 and Eqn. 4.9. In Eqn. 5.1, the changing rate *Δb* is controlled by the gain factor $g_{b,}$ while Eqn. 4.9 uses the *Δb* to update vector *b*.

$$\{\Delta b^M\} = g_b[-C^{M-1}]^{-1}\{S^{M-1}_{amisfit}\} \quad (5.1)$$

$$\{b^M\} = \{b^{M-1}\} + \{\Delta b^M\} \quad (4.9)$$

This parametric study was numerically conducted to get a good value of the gain factor g_b which aids the calculation stability. Seven values of the gain factor g_b were carried out in this parametric study; 0.1, 0.2, 0.5, 0.75, 1.0, 10 and 100. The value of the gain factor α_C, the wavelet magnitude (Ψ_M), and the coefficient of the off-diagonal *C* matrix ($\alpha_{off\text{-}C}$), and the gain factor g_C were taken as $1x10^2$, $1x10^{-7}$g and 0.7 respectively. The maximum number iteration of the Broyden and the outer loop were set as 10 and 5 respectively. The tolerance limit was 0.005g on the average misfit. Figure 6-14 to Figure 6-17 show the graphical results of this parametric study for the gain factor g_b.

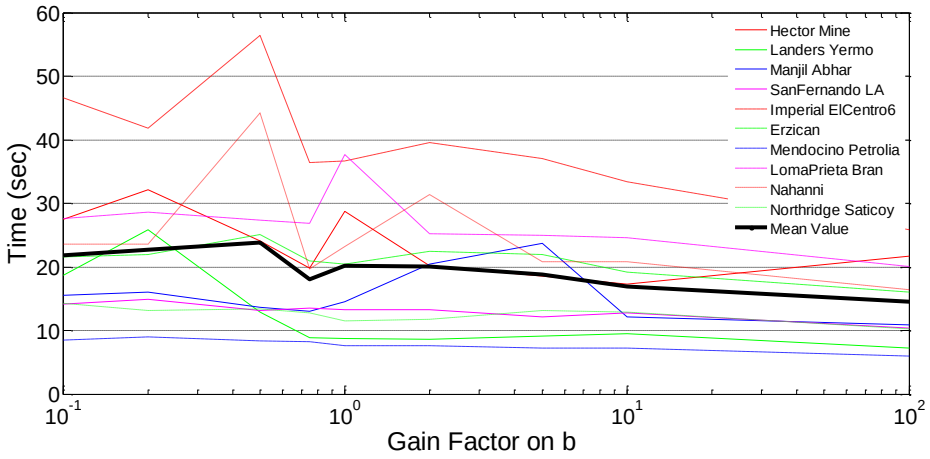

Figure 6-14 Gain Factor g_b vs Computational time

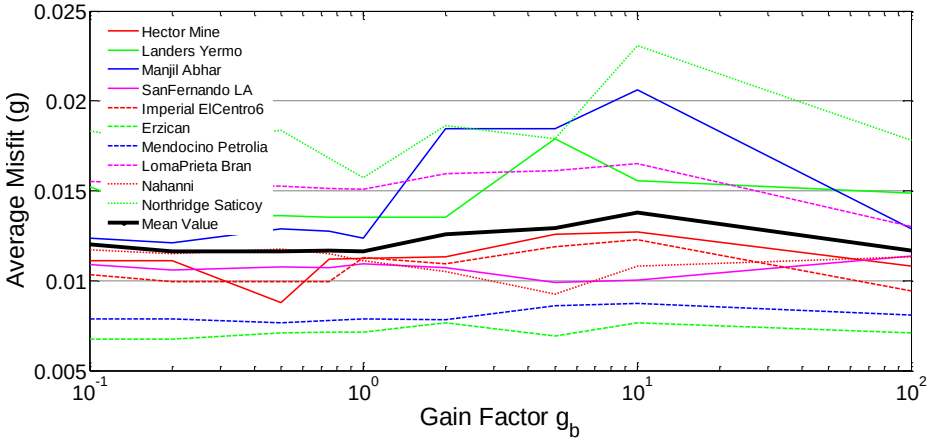

Figure 6-15 Gain Factor g_b vs Average Misfit

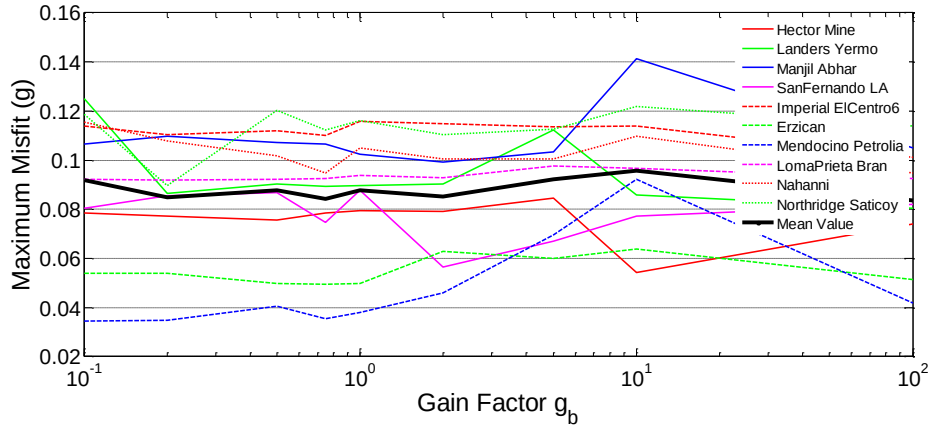

Figure 6-16 Gain Factor g_b vs Maximum Misfit

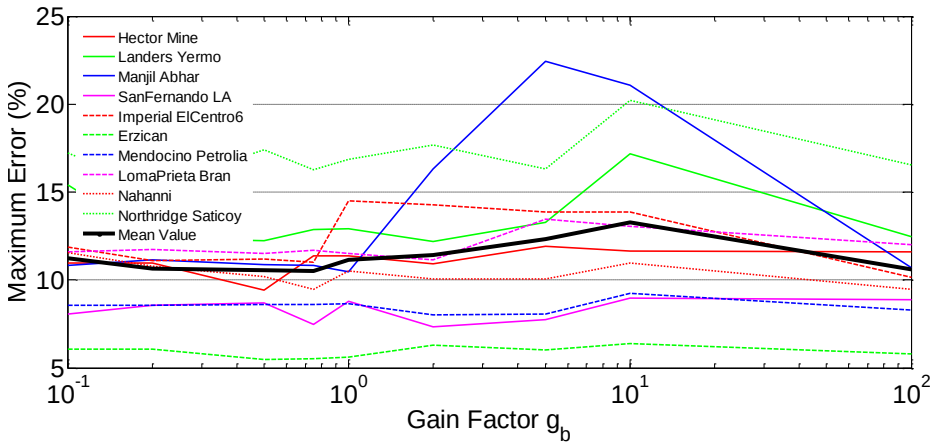

Figure 6-17 Gain Factor g_b vs Maximum Error

In Figure 6-14 it is shown that the algorithm runs faster on a large g_b. The average misfit is plotted in Figure 6-15. In general, the average misfit is relatively better on a small g_b. Figure 6-16 presents the maximum misfit versus the gain factor g_b. It is observed on this figure that the maximum misfits are relatively constant for various values of gain factor g_b. There is one special case for the 1992 Cape of Mendocino, Petrolia (GM #8) ground motion where the maximum misfit is increasing on high g_b. It is hard to see the trends on the error as presented in Figure 6-17. However, in general the errors are quite stable, except for the 1990 Manjil, Abhar (GM #3) where the error is high on large g_b.

Based on previous figures, there are two candidates of the gain factor g_b which result in a short computational time and a small misfit; 0.75 and 1. The quantified parameters of these two candidates are presented in Table 6-5, where the mean and standard deviation of each parameter are being compared.

Table 6-5 Comparison of Parametric Study on the gain factor g_b

Gain Factor	Time (s)		Average Misfit (g)		Max Misfit (g)		Max Error (%)	
g_b	Mean	σ	Mean	σ	Mean	σ	Mean	σ
0.75	18	9	0.011667	0.003031	0.08442	0.02553	10.61	2.99
1	19	11	0.011635	0.002756	0.08682	0.02611	11.12	3.17

In Table 6-5 it can be seen that both candidates result a close computational time. In term of average misfit, the best candidate is g_b=1.0. The g_b=0.75 yields about 1% larger value on mean and the standard deviation is 10% higher. This high standard deviation on g_b=0.75 indicates more potential variation on different ground motions (beside the ten selected ground motions).

In term of maximum misfit, g_b=0.75 yields the smallest value both on the mean and the standard deviation. The g_b=1.0 yields a 3% larger mean and the standard deviation is 2% higher. In term of error, g_b=0.75 also yields a better result.

Although the gain factor g_b=0.75 gives a slightly better maximum misfit and error, it has 10% higher standard deviation on the average misfit than on g_b=1.0. This implies that various results may occur on different ground motions. Therefore, for the sake of result consistency, the gain factor g_b=1.0 is selected in the algorithm.

6.5 Spectral Sensitivity C Matrix Updating Gain Factor (g_C)

The gain factor g_C that is applied in the spectral sensitivity *C* Matrix updating process controls how much the *C* matrix changed at each Broyden iteration, as defined in Eqn. 5.2.

$$[C^M] = [C^{M-1}] + g_C \frac{\left(\left\{\Delta S^M_{amisfit}\right\} - [C^{M-1}]\{\Delta b^M\}\right)\{\Delta b^M\}^{\mathrm{T}}}{\|\Delta b^M\|^2} \tag{5.2}$$

This parametric study was numerically conducted to find a value of g_C which aids the calculation stability. Thirteen values of g_C were carried out in this parametric study; from 0.1 to 1.0 with 0.1 increments, 2, 5 and 10. The value of the gain factor α_C, the wavelet magnitude (Ψ_M), the coefficient of the off-diagonal *C* matrix ($\alpha_{off\text{-}C}$) and the gain factor g_b were taken as 1x10^2, 1x10^{-7}g, 0.7 and 1.0 respectively as proposed from previous studies. The maximum number of the Broyden iteration and the outer loop iteration were set as 10 and 5 respectively. The tolerance limit was 0.005g on the average misfit. Figure 6-18 to Figure 6-21 show the graphical results of this parametric study on the gain factor g_C.

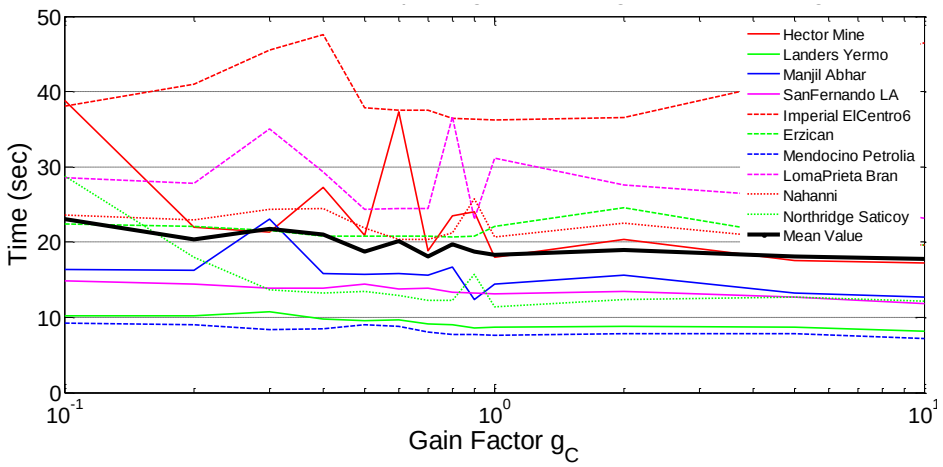

Figure 6-18 Gain Factor g_c vs Computational time

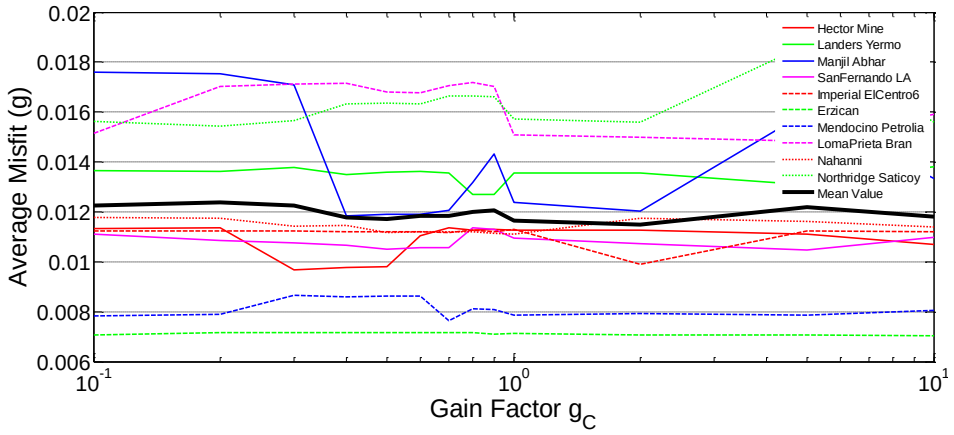

Figure 6-19 Gain Factor g_c vs Average Misfit

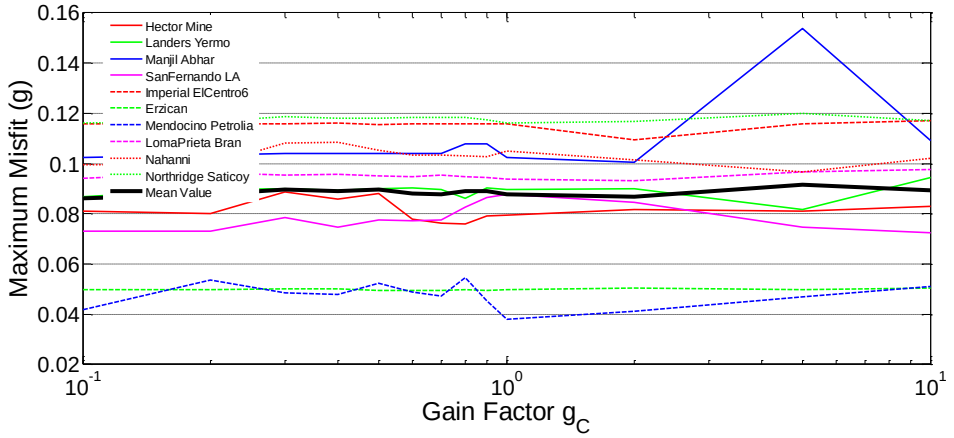

Figure 6-20 Gain Factor g_c vs Maximum Misfit

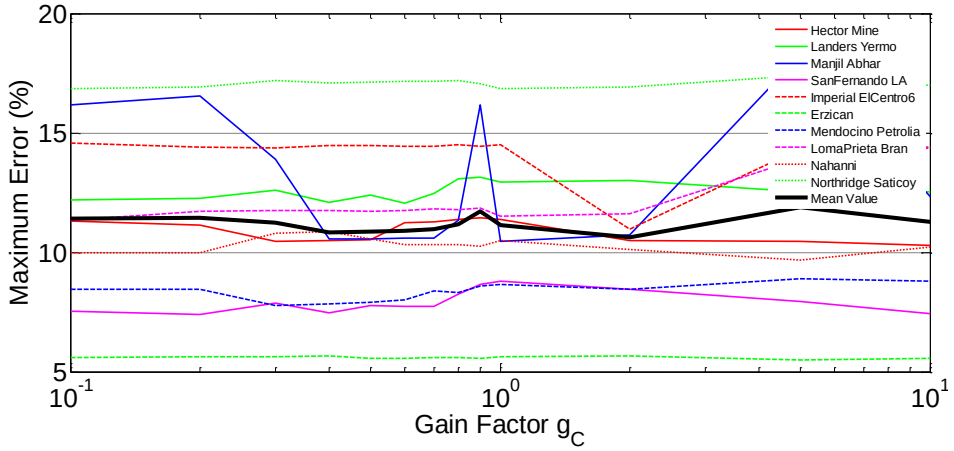

Figure 6-21 Gain Factor g_c vs Maximum Error

Figure 6-18 plots the computational time versus the gain factor g_C. It can be seen here that the computational time is relatively longer for a small g_C and becomes stable for g_C larger than 1.The average misfit is presented in Figure 6-19. It is observed that, in general, the average misfit is relatively constant. One special case happens for the 1990 Manjil, Abhar (GM #3) ground motion where the average misfit is large for $g_C < 0.4$ and $g_C > 2$.

Figure 6-20 shows the maximum misfit versus the gain factor g_C. It is shown that the maximum misfits are also relatively constant except for the 1990 Manjil, Abhar (GM #3) ground motion. For this ground motion, the algorithm yields large misfits for g_C larger than 2. The same pattern is shown in Figure 6-21, where the maximum errors are relatively constant, except on the 1990 Manjil, Abhar ground motion case.

Based on these observations, there are two candidates of the gain factor g_C which result in a short computational time and a small misfit; 0.6 and 1.0. The quantified parameters of these two candidates are presented in Table 6-6 where the mean and the standard deviation of each parameter are being compared.

Table 6-6 Comparison of Parametric Study on gain factor g_C

Gain Factor	Time (s)		Average Misfit (g)		Max Misfit (g)		Max Error (%)	
g_C	Mean	σ	Mean	σ	Mean	σ	Mean	σ
0.6	20	10	0.011842	0.00304	0.088059	0.02464	10.89	3.36
1.0	18	9	0.011635	0.002756	0.087816	0.02611	11.12	3.17

It can be seen that the two candidates of g_C yield similar computational times. In term of the average misfit, g_C =1.0 yields a better result since it has 2% less on mean and 10% higher on standard deviation. In term of the maximum misfit, the best candidate is g_C= 1.0 where the mean value is about the same with g_C= 0.6 but the standard deviation is 6% lower. In term of maximum error, g_C= 0.6 yields a better error but has a higher standard deviation. Based on this comparison, the selected value of the gain factor g_C is 1.0.

6.6 Maximum Number of Broyden Iteration

To examine the efficient number of Broyden iterations, a parametric study was conducted using six different numbers of maximum Broyden iteration: 1, 2, 5, 7, 10, 12 and 15. All other gain factors and coefficients were taken as the proposed values from the previous studies. The tolerance limit was 0.005g on the average misfit. Figure 6-22 to Figure 6-25 show the graphical results of parametric study on the maximum number of Broyden iteration.

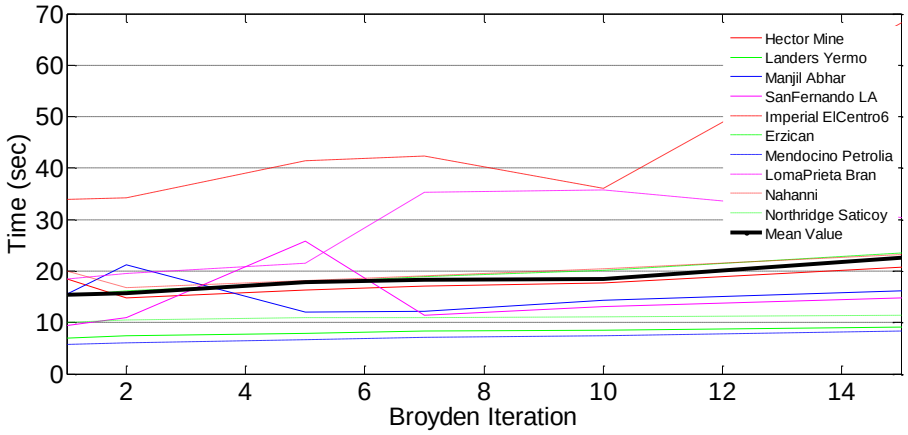

Figure 6-22 Broyden Iteration vs Computational time

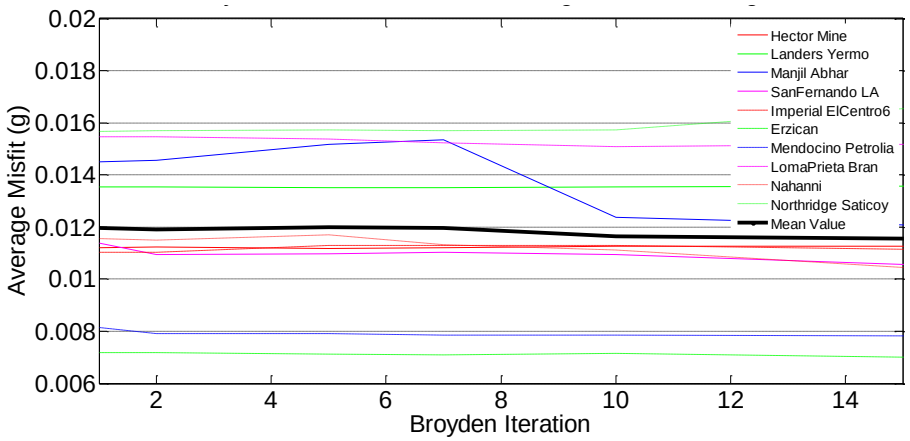

Figure 6-23 Broyden Iteration vs Average Misfit

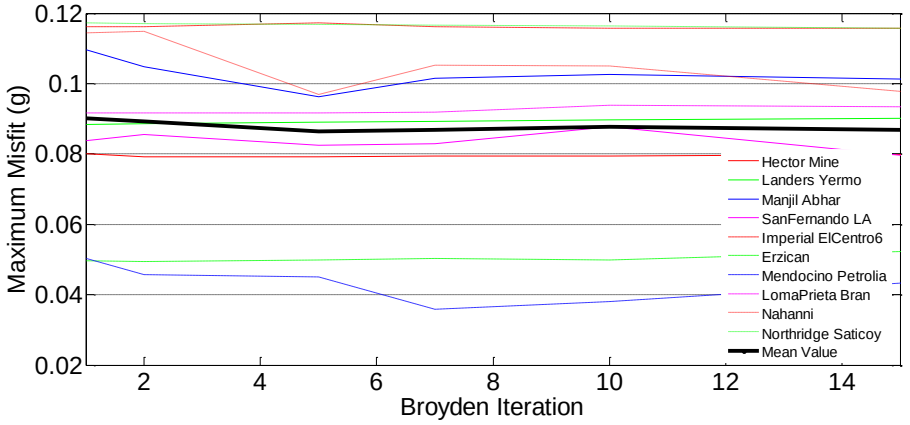

Figure 6-24 Broyden Iteration vs Maximum Misfit

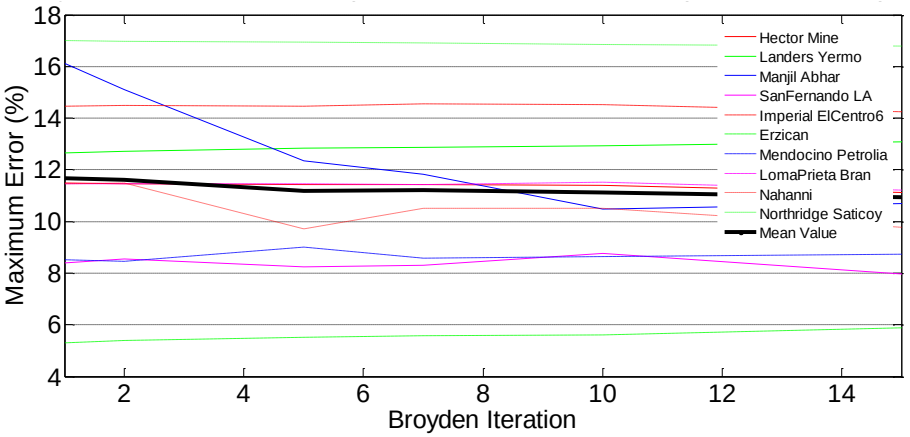

Figure 6-25 Broyden Iteration vs Maximum Error

In Figure 6-22 it can be seen that the computational time is longer as the Broyden iteration increased. Figure 6-23 shows that generally after 10 iterations, the average misfit are become constant. This implies that the Broyden iteration successfully reduces the misfit within the 15 first iterations.

Figure 6-24 shows about the same trend for the maximum misfit. The maximum errors are plotted in Figure 6-25. It can be seen here that the Broyden iteration is able to reduce the maximum error. There are 3 ground motions (GM #1, GM #6 and GM #8) where the maximum errors are constant. This implies that the initial solution guess (initial vector *b*) was quite accurate.

By observing these figures, there are three candidates of the Broyden iteration that results in a considerable fast computational time, a small misfit and a small error; the Broyden iteration #5, #10 and #15. The quantified values of these candidates are presented in Table 6-7 where the mean and the standard deviation of each parameter are being compared.

Table 6-7 Comparison of Parametric Study on Maximum Broyden Iteration

Maximum Broyden Iteration	Time (s)		Average Misfit (g)		Max Misfit (g)		Max Error (%)	
	Mean	σ	Mean	σ	Mean	σ	Mean	σ
5	17	10	0.011996	0.002989	0.08646	0.024135	11.19	3.26
10	19	10	0.011635	0.002756	0.08782	0.026111	11.12	3.17
15	23	17	0.011559	0.002968	0.08612	0.024185	10.95	3.17

It can be seen here that the three candidates show close computational time. Note that the time increment is not linear. This is because once the tolerance limit is reached; the algorithm is not required to run all the Broyden iterations (or also the outer-loop iterations). In term of average misfit, the 15 maximum Broyden iterations give the smallest mean value. However, the 10 maximum Broyden iterations are considered better because these iterations yield only 0.2% larger on mean value but the results are less distributed (7% lower standard deviation).

The 15 maximum Broyden iterations yield the best maximum misfit in term of mean value. The second best candidate is the 5 maximum Broyden iterations which yield only 0.4% higher mean and only 0.2% higher standard distribution. The 10 maximum Broyden iterations yield a 2% higher mean with 8% higher standard deviation. It is noticed here that the maximum misfits are slightly better on 5 Broyden iteration compared to 10 Broyden iterations. This is based on the fact that the during the Broyden loop, the algorithm saves the best acceleration time series which gives better average misfit. Moreover, in term of maximum error, a higher number of the maximum Broyden iteration gives a better error.

By considering the computational time and the average misfit, it is proposed to use a maximum 10 iterations in the Broyden loop.

6.7 Number of Outer Loop Iteration

This parametric study was conducted to examine the efficient number of the outer loop iteration. A large number of outer loop iteration may give a small average misfit, but may consider not efficient in term of computational time. The parametric study was carried out using the proposed gain factors from the previous studies. The target and tolerance limit were the same with previous studies. Figure 6-26 to Figure 6-29 show the graphical results of parametric study on the maximum outer-loop iteration.

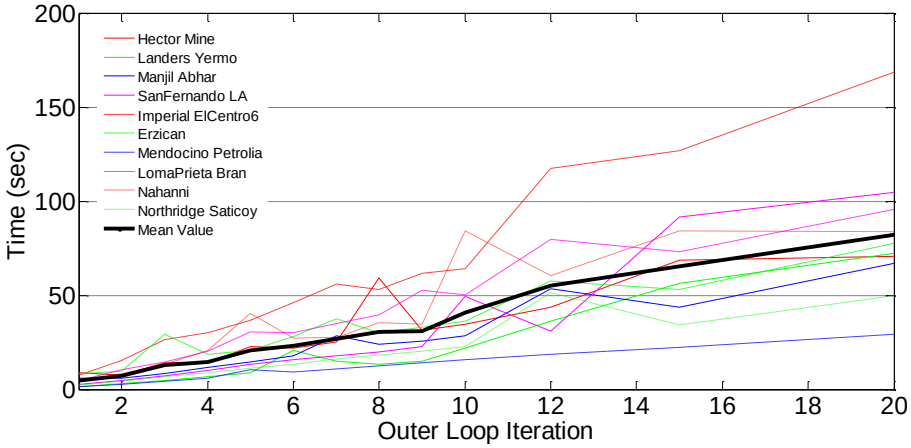

Figure 6-26 Outer-loop Iteration vs Computational time

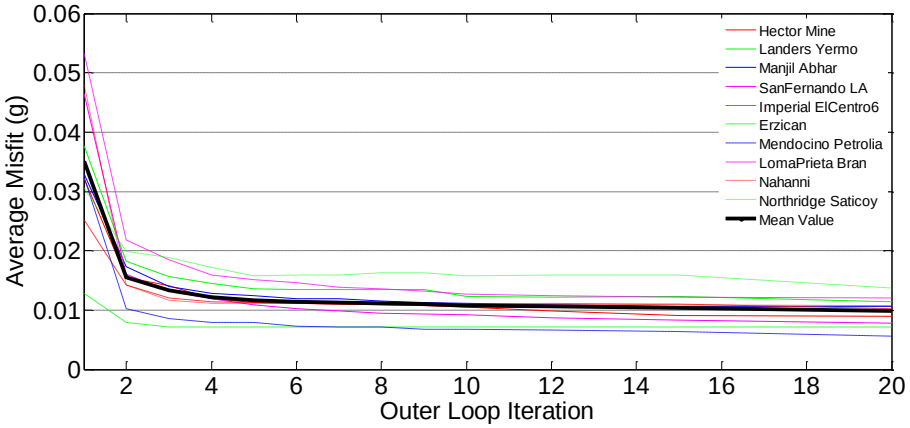

Figure 6-27 Outer-loop Iteration vs Average Misfit

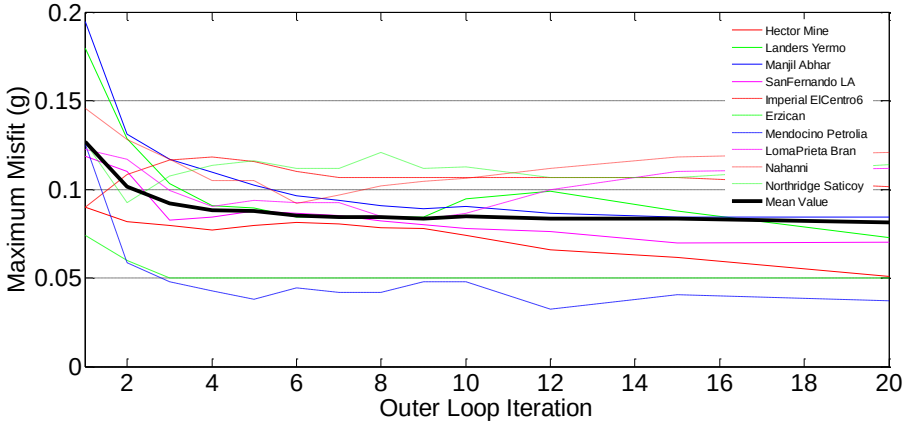

Figure 6-28 Outer-loop Iteration vs Maximum Misfit

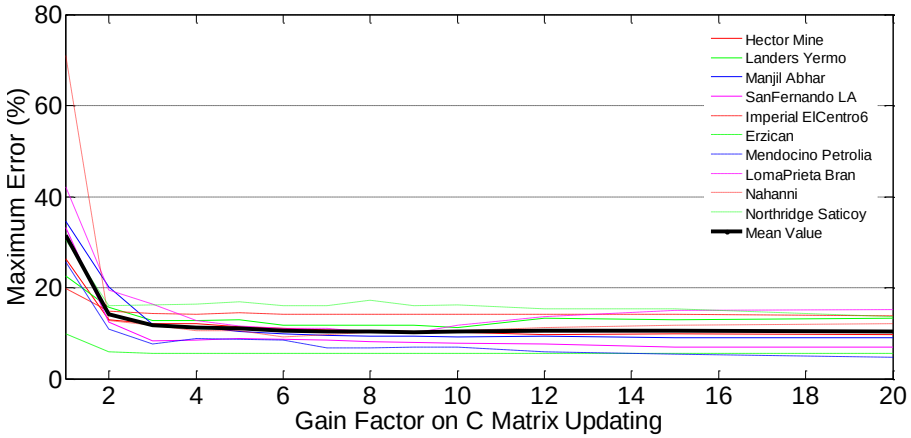

Figure 6-29 Outer-loop Iteration vs Maximum Error

The computational time is plotted in Figure 6-26, it can be seen that the computational time is increasing throughout the number of outer-loop iterations. Figure 6-27 presents the graphical result of the average misfit versus the number of outer loop iterations. It is observed in this figure that the average misfit is decreasing rapidly between the first and the third iteration, and then decreasing at a slower rate after the 4th outer-loop iteration. However, it is also observed that on the 1994 Northridge, Saticoy (GM #10) ground motion, the average misfit decrement rate is still high until the 5th outer-loop iteration.

The maximum misfit versus the maximum outer-loop iteration can be seen in Figure 6-28. It is observed in this figure that, in general, the maximum misfit is reduced rapidly within the 4 outer-loop iterations. It can also be seen that although the average misfit is reduced as the outer-iteration increased, there is a change that the maximum misfit will be increased. This is due the fact that the algorithm is set to optimize the average misfit, not the maximum misfit (the tolerance limit is set to 0.005g on average misfit). Only the solution that yields a smaller misfit compared to previous iteration was saved during the iteration.

The maximum errors are presented in Figure 6-29. It can be seen here that the errors are reduced rapidly between the 1st and 4th outer loop iteration, then it becomes stable after the 6th iteration. More iterations may be required to satisfy smaller tolerance, but overall 6 outer loop iterations is good enough to yield an approximately 10% on maximum error (only 3 ground motions that reach error more than 10% at this iterations).

Table 6-8 presents the quantified values of computational time, the average misfit and the maximum misfit for the maximum outer loop iteration of 5, 6 and 7. It can be seen that in term of the average misfit, the maximum outer-loop iterations of 6 yields a considerable small maximum misfit and error. Therefore, it is selected to use 6 maximum outer loop iterations.

Table 6-8 Comparison of Parametric Study on Outer-loop Iteration

Maximum Outer-loop Iteration	Time (s)		Average Misfit (g)		Max Misfit (g)		Max Error (%)	
	Mean	σ	Mean	σ	Mean	σ	Mean	σ
5	21	11	0.011635	0.00276	0.08782	0.02611	11.12	3.17
6	23	10	0.01142	0.00282	0.08499	0.02239	10.59	2.98
7	27	13	0.01127	0.002774	0.08428	0.02247	10.39	3.15

6.8 Summary of Parametric Study

Numerical parametric studies have been conducted to obtain a good combination of several gain factors that are used during the spectral matching procedure, to reduce the computational time and minimize the misfit. The summary of the proposed gain factors are presented in Table 6-9.

It is noted that these gain factors set were based on particular period set, target and tolerance limit. For other applications or specific objectives, the values could be modified. The values presented here are intended for general use. However, if computational time was the key importance and the misfit was not as important, the number of Broyden iteration and outer loop iteration could be reduced. Conversely, if the magnitude of misfit was of key importance, the number of iterations could be increased and the tolerance decreased.

Table 6-9 Proposed Value of Gain Factors

Gain Factor	Variable	Proposed Value
Gain Factor on Initial C Matric	α_C	$1x10^{2}$
Wavelet Magnitude	ψ_M	$1x10^{-7}$g
Off-diagonal terms of C Matrix Reduction Factor	$\alpha_{\text{off-C}}$	0.7
Gain Factor on vector b Updating	g_b	1
Gain Factor on C Matrix Updating	g_C	1
# of Maximum Broyden Iterations	M	10
# of Maximum Outer-loop Iterations	N	6

6.9 Comparison with Linear Relationship Algorithm between the Spectra Misfit and Vector *b*

This section discusses the implementation of the Broyden updating using the proposed gain factors. The results were being compared to the algorithm that represents the basic (original) version of RSPMatch, which in this paper will be called the 'Linear-Algorithm'. The current versions of RSPMatch have had many enhancements to improve numerical stability and efficiency, as discussed in Chapter 3. This comparison was not intended to be a direct comparison between the RSPMatch and the proposed method. A direct comparison will be presented in Chapter 8.

6.9.1 'Linear-Algorithm' Configuration

The spectral matching in the Linear-Algorithm was fully based on the linear relationship between the spectra misfit $S_{amisfit}$ and the vector b. Neither second wavelet corrections nor target reduction were applied to the Linear-Algorithm. The response of structure was calculated using Newmark method and the pseudo-acceleration was being matched.

There were two period subsets that were implemented in both algorithms; the first period subset ranges from 0.06 to 1.3sec and the second ranges from 0.06 to 3.0sec both with 0.025 increments in log scale. A linear scaling based on the least square fit of the misfit was applied to the acceleration time series.

There were two major loops in the Linear-Algorithm. The first one was the outer loop; this is where the period subsets are being solved in sequence. No maximum number of outer-loop iteration was implemented in this comparison. Another loop was the inner-loop, where each of period subset is being solved using the linear relationship between the spectra misfit $S_{amisfit}$ and b vector. For each period subset, the maximum number of the inner iteration was set as 5. This was based on the observation that after 5 iterations, the solution tends to diverge, especially on closed ranged periods.

The off-diagonal terms of C matrix was being multiplied by a factor 0.7. A detailed flow chart of the Linear Algorithm can be seen in Appendix C-1.

6.9.2 Result

The ten ground motions were being compared. The damping ratio was taken as 5% of the critical damping and the target response spectrum was the Dmax spectrum from FEMA P-695 (FEMA 2009) associated with a high seismic area of California. Both algorithms were executed using a personal laptop with i7-2760QM 2.4Gz processors and 8192Mb DDR3 RAM. The target was 0.0125g on the average misfit. The computational time comparisons are presented in Figure 6-30.

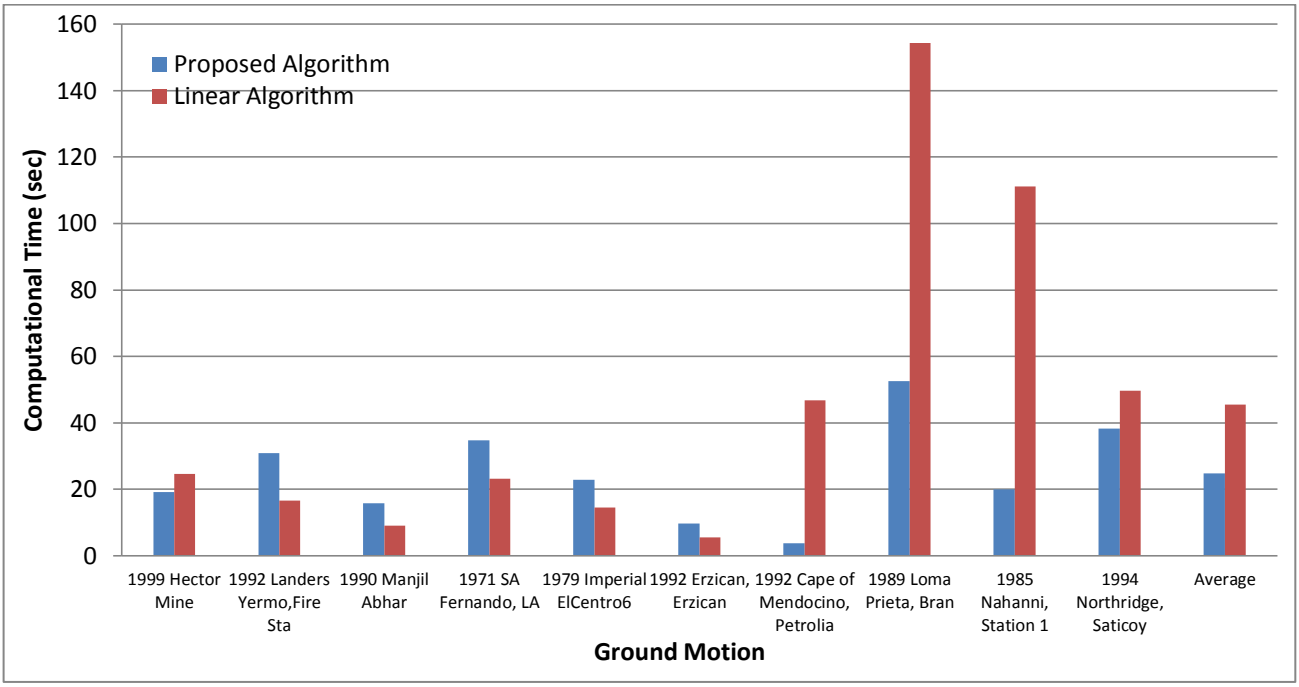

Figure 6-30 Computational Time Comparison between Proposed vs Linear Algorithm

It can be seen here that, in general, the proposed algorithm yields more effective computational time compared to the Linear-Algorithm. This is based on the fact that the Linear-Algorithm calculates the full *C* matrix for each inner iteration, while the proposed algorithm makes use the *b* vector and spectra misfit $S_{amisfit}$ to update the *C* matrix.

CHAPTER 7. STUDY OF COMPATIBLE WAVELET BASE FOR SPECTRAL MATCHING

A study of compatible wavelet functions was carried out to determine the most appropriate wavelet functions for the proposed method. The numerical stability and the calculation efficiency were the main concerns in selecting a wavelet base. Some wavelet features that were being studied include the frequency resolution, the time resolution, the off-diagonal terms of C matrix, the velocity and displacement time histories and also the analytical integration of the wavelet form. Seven existing wavelet bases were studied.

7.1 Wavelet Bases

Seven existing wavelet bases were studied; the Lilhanand and Tseng wavelet, the tapered cosine wavelet, the corrected tapered cosine wavelet, the Morlet wavelet, the Mexican Hat wavelet, the Suarez and Montejo wavelet and the Shannon wavelet. The forms and features of each wavelet base are discussed here.

7.1.1 Lilhanand and Tseng Wavelet

The original wavelet proposed by Lilhanand and Tseng (1987), consists of the true acceleration impulse response function in reverse time order given by Eqn. 7.1.:

$$\boldsymbol{\psi}_j(t) = h_j(t_j - t) = e^{(-\omega_j \zeta (t_j - t)}\left[(2\zeta^2 - 1)sin(\omega_i{}'(t_j - t)) - 2\zeta\sqrt{1-\zeta^2}cos(\omega_i{}'(t_j - t))\right] \quad (7.1)$$

where t_j is the time of the peak response of the j^{th} oscillator under the action of the j^{th} wavelet. Figure 7-1 shows the Lilhanand and Tseng Wavelet for period 1 sec and its integrations.

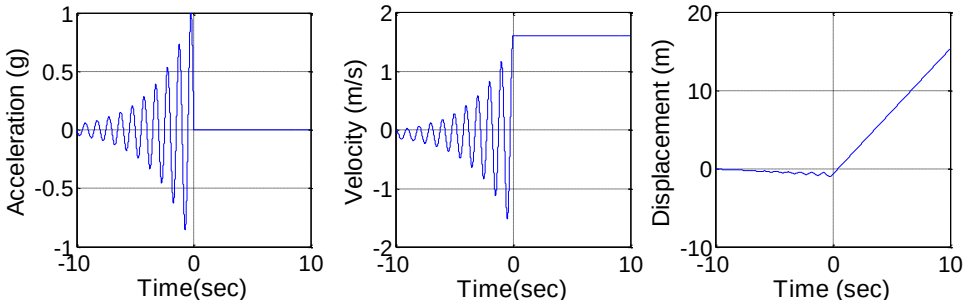

Figure 7-1 Lilhanand and Tseng Wavelet, T=1sec

7.1.2 Tapered Cosine Wavelet

The tapered cosine wavelet can be described by Eqn. 7.2.

$$\boldsymbol{\psi}_j(t) = e^{[-|t-t_j+\Delta t|\alpha_j]}cos\left(\omega'_j(t - t_j + \Delta t_j)\right) \quad (7.2)$$

where Δt_j is the difference between the time peak response t_j and the reference origin of the wavelet. Δt_j is given by:

$$\Delta t_j = \frac{tan^{-1}\left[\frac{\sqrt{1-\beta_j{}^2}}{\beta_j}\right]}{\omega'_j} \quad (7.3)$$

the frequency-dependent factor α_j should be selected such that the adjustment wavelet and the reference time histories have consistent durational at frequency ω_j. A tri-linear model for α_j as a function of frequency is given by:

- $\alpha(f) = a_1 f$ for $f < f_1$ (7.4a)
- $\alpha(f) = \left(a_1 + (a_2 - a_1)\frac{(f-f_1)}{(f_2-f_1)}\right) f$ for $f_1 < f < f_2$ (7.4b)
- $\alpha(f) = a_2 f$ for $f > f_2$ (7.4c)

Figure 7-2 shows the tapered cosine wavelet for period 1 sec and the associated time integrations resulting in velocity and displacement histories.

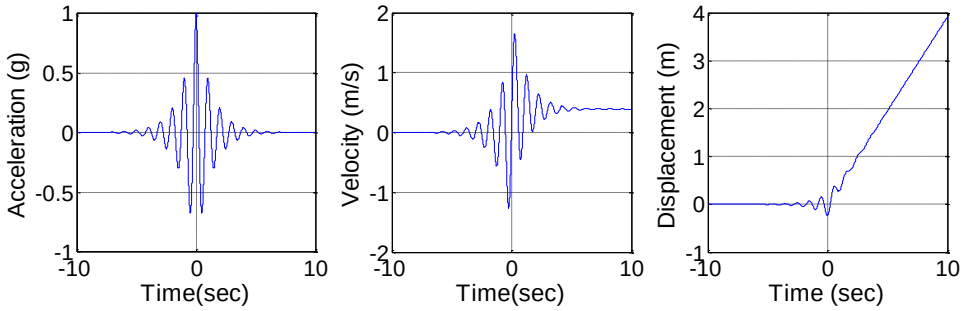

Figure 7-2 Tapered Cosine Wavelet, T=1sec

7.1.3 Corrected Tapered Cosine Wavelet

The corrected tapered cosine wavelet differs from the tapered cosine wavelet proposed by Hancock et.al (2006) in terms that the wavelet has a functional forms that readily to integrate to zero velocity and displacement without requiring any baseline correction. The corrected tapered cosine wavelet is described on Eqn. 7.5.

$$\boldsymbol{\psi}_j(t) = e^{-\left[\frac{(t-t_j+\Delta t_j)}{\gamma_j}\right]^2} cos\left(\omega'_j\left(t - t_j + \Delta t_j\right)\right) \quad (7.5)$$

Where Δt_j is the differences between the time of peak response with the reference time of the wavelet (t_j). The correction factor γ_j is a frequency dependent coefficient used to adjust the duration of the adjustment function, given by Eqn. 7.6.

$$\gamma(f) = 1.178 f^{-0.93} \quad (7.6)$$

Figure 7-3 shows the corrected tapered cosine wavelet with period 1 sec and the associated time integrations resulting in velocity and displacement histories.

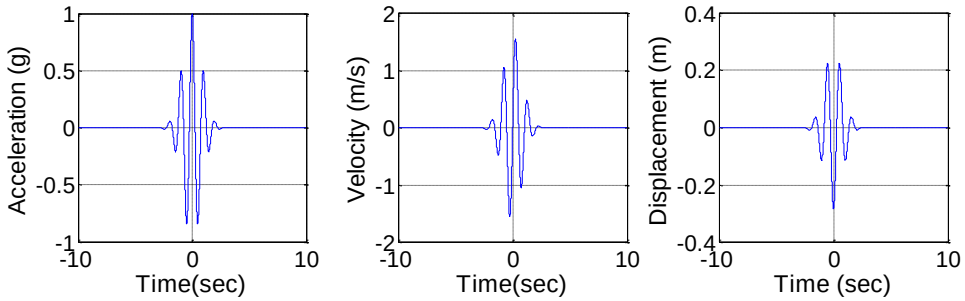

Figure 7-3 Corrected Tapered Cosine Wavelet, T=1sec

In this study, there were 2 approaches to scale the corrected tapered cosine wavelet. The first approach was by using the built-in scaling function as described in the Eqn. 7.5 where the corrected tapered cosine wavelet is automatically scaled as a function of ω_j. The second approach was by normalizing Eqn. 7.5 with period 1 sec, the wavelet base equation becomes

$$\boldsymbol{\psi}_j(t) = e^{-\left[\frac{(t-t_j+\Delta t_j)}{1.178}\right]^2} cos\left(t - t_j + \Delta t_j\right) \tag{7.7}$$

The corrected tapered cosine wavelet from Eqn. 7.7 then can be scaled and shifted using the general wavelet scaling function as discussed by Mallat (1999), described by Eqn. 7.8

$$\psi_{j_{s,p}}(t) = \frac{1}{\sqrt{s}}\boldsymbol{\psi}_{\mathrm{j}}\left(\frac{t-t_j+\Delta t_j}{s}\right) \tag{7.8}$$

where s > 0 is the wavelet scale.

7.1.4 Morlet Wavelet

Morlet (1981, 1983; Goupillaud et al 1984) applied wavelet transform to the seismic data analysis and developed his universal wavelet for this application. The continuous Morlet wavelet is expressed in the time domain as:

$$\boldsymbol{\psi}_0(t) = cos(5t)e^{-t^2/2} \tag{7.9}$$

where ω_0 and t are dimensionless frequency and time parameters. This wavelet has a similar mathematical function to the corrected tapered cosine wavelet. There are slightly differences in the coefficients. Also the corrected tapered cosine wavelet form in Eqn. 7.5 has the time shift included, whereas the form of the Morlet wavelet written here is meant to be used with typical wavelet scaling and time shifting as given in Eqn. 7.8.

This Morlet wavelet as shown in Figure 7-4 is assumed admissible, i.e. have zero mean and localized in both time and frequency space.

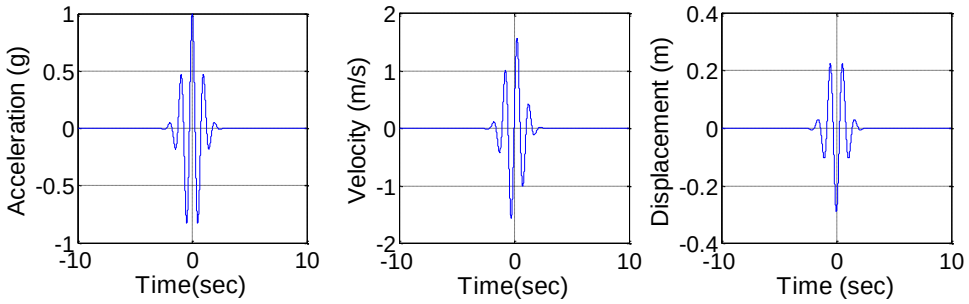

Figure 7-4. Morlet Wavelet, T=1sec

7.1.5 Mexican Hat Wavelet

Wavelet equals to the second derivative of a Gaussian are called the Mexican Hat wavelet. The mathematical function of the Mexican Hat wavelet is given by Eqn. 7.10.

$$\boldsymbol{\psi}(t) = \frac{2}{\sqrt{3}}\pi^{-0.25}(1 - t^2)\, e^{-t^2} \tag{7.10}$$

Figure 7-5 shows the Mexican Hat wavelet with period 1 sec and the associated time integrations resulting in velocity and displacement histories.

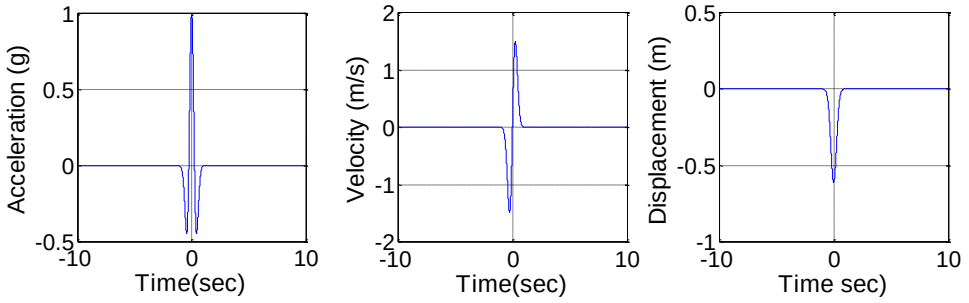

Figure 7-5. Mexican Hat Wavelet, T=1sec

7.1.6 Suarez and Montejo Wavelet

Suarez and Montejo (2005) developed a wavelet based on the impulse response function to be used for spectral matching. Their wavelet resulted in displacement baseline drift. The wavelet function of the Suarez and Montejo wavelet is given by Eqn. 7.11.

$$\boldsymbol{\psi}(t) = e^{-\zeta\, \Omega\, |t|}\ sin(\Omega\, t) \tag{7.11}$$

where Ω is the time controlling parameter.

Figure 7-6 shows the Suarez and Montejo wavelet with period 1 sec and the associated time integrations resulting in velocity and displacement histories.

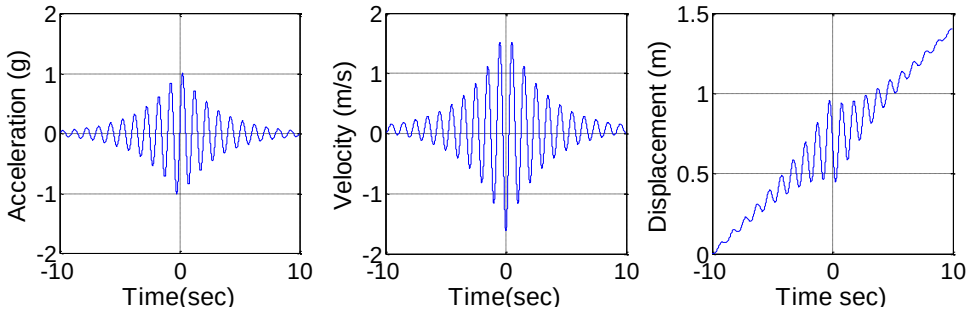

Figure 7-6. Suarez and Montejo Wavelet, T=1sec

7.1.7 Shannon Wavelet

The Shannon wavelet is constructed from the Shannon multi-resolution approximation (Mallat, 1999). This wavelet has infinite function in time histories and has slow asymptotic time decay. The wavelet function of the Shannon wavelet is given by Eqn. 7.12.

$$\boldsymbol{\psi}(t) = \frac{2\,sin(2\pi\,(t-0.5))}{2\pi\,(t-0.5)} - \frac{sin(\pi\,(t-0.5))}{\pi\,(t-0.5)} \tag{7.12}$$

Figure 7-7 shows the Shannon wavelet with period 1 sec and the associated time integrations resulting in velocity and displacement histories.

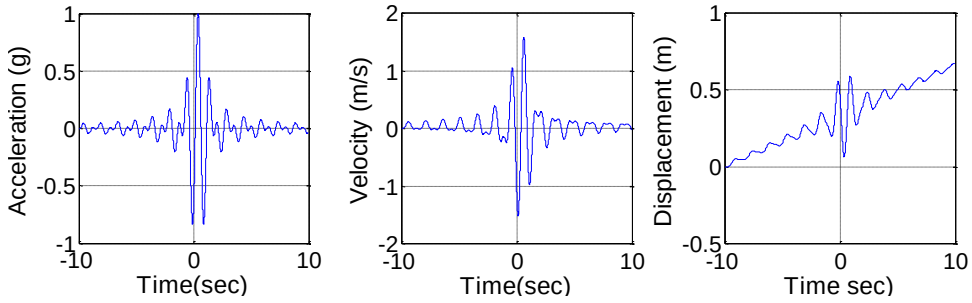

Figure 7-7. Shannon Wavelet, T=1sec

7.2 Selection of Wavelet Basis for Spectral Matching

In order to examine a compatible wavelet base which promotes stability and efficiency in calculation, some characteristic of wavelet base were observed including the frequency resolution, the time resolution, the off-diagonal terms of *C* matrix, the baseline drift as the products of wavelet integrations, and also the analytically integration form of the wavelet response.

7.2.1 Frequency and Time Resolution

The wavelet resolution defines the energy density of a finite signal using the Heisenberg box. The horizontal axis of the spectrogram corresponds to the time localization, and the vertical axis corresponds to the frequency localization (as a result from the Fourier transform). The area of the rectangle remains equal at all scales, but the resolution in time and frequency depends on wavelet scale *s*. Small wavelet scales decrease the

time spread but increase the frequency support, which is shifted toward higher frequency (Mallat,1999). Figure 7-8 shows the illustration for frequency and time resolutions.

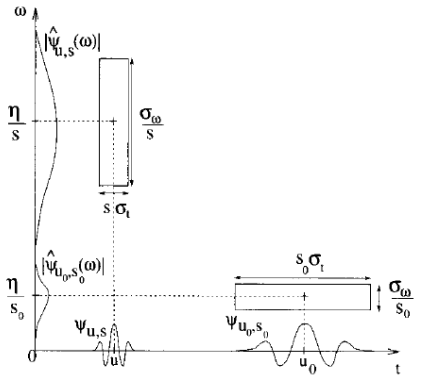

Figure 7-8 Illustration of Wavelet Resolution (fair use from Mallat, 1999)

A wavelet base with a narrow resolution in the frequency and time is expected to give a better numerical stability. The reason is that the wavelet base that has a narrow resolution that is being added to modify an oscillator with period *i* response is expected to give less influence to the other oscillator.

The frequency resolution was calculated by measuring the frequency bandwidth between frequencies with 10% of the peak Fourier Amplitude Spectra (FAS). In this study, the value of 10% FAS was chosen arbitrarily. The time resolution was calculated by measuring the time duration of between two points in the wavelet time series that have 1% of the peak magnitude. The 1% value was chosen arbitrarily. The Fourier transform $\boldsymbol{\psi}(\omega)$ of a wavelet function $\boldsymbol{\psi}(t)$ is defined by Eqn. 7.13. The values of frequency resolution and time resolution are given in Table 7-1 to Table 7-3.

$$\boldsymbol{\psi}(\omega) = F[\boldsymbol{\psi}(t)] = \int_{-\infty}^{\infty} \boldsymbol{\psi}(t) e^{-i\omega t} dt \tag{7.13}$$

7.2.2 Off-diagonal Terms of C Matrix

Both of the frequency and the time resolution implicitly determine the off-diagonal terms of *C* matrix which is the source of nonlinearity in the solution. These terms describe the cross correlation of the oscillator with period *i* response due to wavelet adjustment with period *j* with the other oscillators response which have different period.

To examine the cross correlation of different wavelets, it was necessarily to quantify the off-diagonal terms of *C* matrix. In this study these terms were being quantified by taking the first norm of the off-diagonal values of *C* matrix, and then normalized the value by the primary element of the *C* matrix as described by Eqn. 7.14.

$$\hat{C}_{norm-i} = \frac{\|C_{ij}\|_1}{C_{ii}}, i \neq j \tag{7.14}$$

Since the *C* matrix is unique for each particular ground motion, set of ground motions were observed. The average value of $\hat{C}_{norm-i}$ for each ground motion was also compared. A wavelet base with a small value on the average $\hat{C}_{norm-i}$ is expected to yield less nonlinear calculation. The study was conducted using the same 10 different ground motions as used in the parametric study. The periods that being observed range from 0.1 second to 3 second with 0.05 second increment. The values $\hat{C}_{norm-i}$ are given in Table 7-1 to Table 7-3.

7.2.3 Baseline Drift

The response spectrum compatible acceleration resulted from the spectral matching procedure has to be realistic; it has to preserve the similarity with the original acceleration in terms of duration, the non-stationary features and the velocity/displacement characteristics. The latter can be maintain if the wavelet base itself yields a zero velocity and zero displacement at the end of the time series. In this study, the velocity and displacement drift were normalized with respect to the peak pseudo-velocity ($\frac{a_{peak}}{\omega}$) and the peak pseudo-displacement ($\frac{a_{peak}}{\omega^2}$) respectively. To be equally weighted, on this comparison the wavelet amplitude a_{peak} for all wavelets time series was set to 1g. The normalized baseline drift for velocity and displacement were given by Eqn. 7.15 and Eqn. 7.16 respectively.

$$\hat{v}_{drift} = \frac{v_{end}}{\left(\frac{a_{peak}}{\omega}\right)} = \frac{v_{end}\,\omega}{a_{peak}} \tag{7.15}$$

$$\hat{d}_{drift} = \frac{d_{end}}{\left(\frac{a_{peak}}{\omega^2}\right)} = \frac{d_{end}\,\omega^2}{a_{peak}} \tag{7.16}$$

The values of the normalized baseline drift $\hat{v}_{drift}$ and $\hat{d}_{drift}$ are given in Table 7-1 to Table 7-3.

7.2.4 Analytically Integration

Another feature that was studied is the capability of SDOF oscillator response due to the wavelet to be analytically calculated to form a simple generic formula. This analytical calculated can be conducted using the Duhamel's integral. Being able to be analytically calculated is very convenient in terms of the calculation efficiency. However since some of the wavelet bases are complicated or form a complex integration formula, this feature is not mandatory.

7.3 Comparison of Wavelet Features

The features of the seven different wavelet bases were being compared using three different periods; 0.2 sec, 1.0 sec and 2.0 sec which represent the oscillator with short, medium and long period respectively. Table 7-1 to Table 7-3 shows the feature comparison. The 3rd column shows the velocity baseline drift that has been normalized to the peak of pseudo-velocity. The 4th column presents the displacement baseline drift that has

been normalized to the peak of pseudo-displacement. The 5th and 6th column show the frequency resolution and the time resolution respectively. The last column shows the average of $\hat{C}_{norm-i}$ resulted from the ten different ground motions.

Table 7-1 Comparison of Wavelet Features for T=0.25 sec

No	Wavelet Base	Velocity Baseline Drift $\frac{v_{end}*\omega}{a_{peak}}$ per sec	Displacement Baseline Drift $\frac{d_{end}*\omega^2}{a_{peak}}$ per sec	Frequency Resolution (Hz)	Time Resolution (sec)	Average $\hat{C}_{norm-i}$
1	Lilhanand and Tseng	1.053	265.060	6.767	7.282	n/a
2	Tapered Cosine	0.311	78.071	3.895	2.275	0.068
3	Corrected Tapered Cosine	0	0	2.978	1.320	0.060
4	Generalized Corrected Tapered Cosine with f=1Hz	0	0	3.281	1.262	0.065
5	Morlet	0	0.012	3.374	1.095	0.068
6	Mexican Hat	0	0	8.763	0.475	0.086
7	Shannon	-0.005	2.757	2.760	20.748	n/a
8	Suarez and Montejo	0	0.213	1.195	7.275	0.068

Table 7-2 Comparison of Wavelet Features for T=1.0 sec

No	Wavelet Base	Velocity Baseline Drift $\frac{v_{end}*\omega}{a_{peak}}$ per sec	Displ Baseline Drift $\frac{d_{end}*\omega^2}{a_{peak}}$ per sec	Freq Resolution (Hz)	Time Resolution (sec)	Average $\hat{C}_{norm-i}$
1	Lilhanand and Tseng	1.033	62.039	1.999	29.130	n/a
2	Tapered Cosine	0.251	15.741	0.791	11.164	0.135
3	Corrected Tapered Cosine	0	0	0.824	5.049	0.150
4	Generalized Corrected Tapered Cosine with f=1Hz	0	0	0.834	5.049	0.151
5	Morlet	0	0.003	0.869	4.382	0.150
6	Mexican Hat	0	0	2.151	1.893	0.197
7	Shannon	-0.019	2.700	0.669	82.994	n/a
8	Suarez and Montejo	0	5.646	0.299	30.068	0.129

Table 7-3 Comparison of Wavelet Features for T=2.0s

No	Wavelet Base	Velocity Baseline Drift $\frac{v_{end}*\omega}{a_{peak}}$ per sec	Displ Baseline Drift $\frac{d_{end}*\omega^2}{a_{peak}}$ per sec	Freq Resolution (Hz)	Time Resolution (sec)	Average $\hat{C}_{norm-i}$
1	Lilhanand and Tseng	0.853	19.800	0.999	58.261	n/a
2	Tapered Cosine	0.478	15.022	0.795	10.528	0.226
3	Corrected Tapered Cosine	0	0	0.447	8.714	0.201
4	Generalized Corrected Tapered Cosine with f=1Hz	0	0	0.415	10.098	0.200
5	Morlet	0	0.002	0.429	8.765	0.201
6	Mexican Hat	0	0	1.161	3.792	0.269
7	Shannon	-0.028	-4.705	0.389	165.99	n/a
8	Suarez and Montejo	0	13.906	0.150	60.137	0.153

In Table 7-1to Table 7-3, it can be seen that only 3 wavelets are giving a small/zero displacement drift; the corrected tapered cosine wavelet, the Morlet wavelet and the Mexican Hat wavelet. It is also observed that the Lilhanand and Tseng wavelet, and the Suarez and Montejo wavelet have a large displacement drift. Thus the implementation of these wavelets will generate a large baseline drift.

In Table 7-1to Table 7-3 it is shown that the Mexican hat wavelet is narrower in the time domain, yet broader in frequency than both the Morlet wavelet and the corrected tapered cosine wavelet. In term of time duration, the Shannon wavelet, the Suarez and Montejo wavelet, and Lilhanand and Tseng wavelet have long time resolution. This implies that the wavelet implementation on the spectral matching algorithm requires considerable large zero padding at ends of the ground motion time series to ensure that the shifted wavelet adjustment starts and ends with zero value, which is considered inefficient.

On the study of the off-diagonal terms of *C* matrix, only five wavelets bases were being compared. The Lilhanand and Tseng wavelet was neglected due to its form that stops abruptly, which is not representing a natural earthquake ground motions, and also due to its high baseline displacement drift. The Shannon wavelet was neglected because it has long duration/time resolution. It was hard to get the time of peak response due to wavelet coincides with the time of peak response of the original ground motions. This may happen because by shifting the Shannon wavelet may cause parts of the wavelet truncated.

Figure 7-9 shows the $\hat{C}_{norm-i}$ value of each wavelet base for different ground motions. The horizontal axis shows the oscillator period, while the vertical axis corresponds to the $\hat{C}_{norm-i}$ terms. In general, the Mexican hat wavelet has large $\hat{C}_{norm-i}$ while the Suarez and Montejo wavelet generally has smaller values. The tapered cosine wavelet has relatively small $\hat{C}_{norm-i}$ at short periods (less than 1.0 second), but it has large values on long periods. The corrected tapered cosine and the Morlet wavelet have approximately close values; this is because the two wavelets have similar function forms.

It is also observed that the $\hat{C}_{norm-i}$ corresponds to the frequency resolution; in which a wavelet that has a narrow frequency resolution tends to have a small $\hat{C}_{norm-i}$. However, in this paper no study was conducted about their correlation.

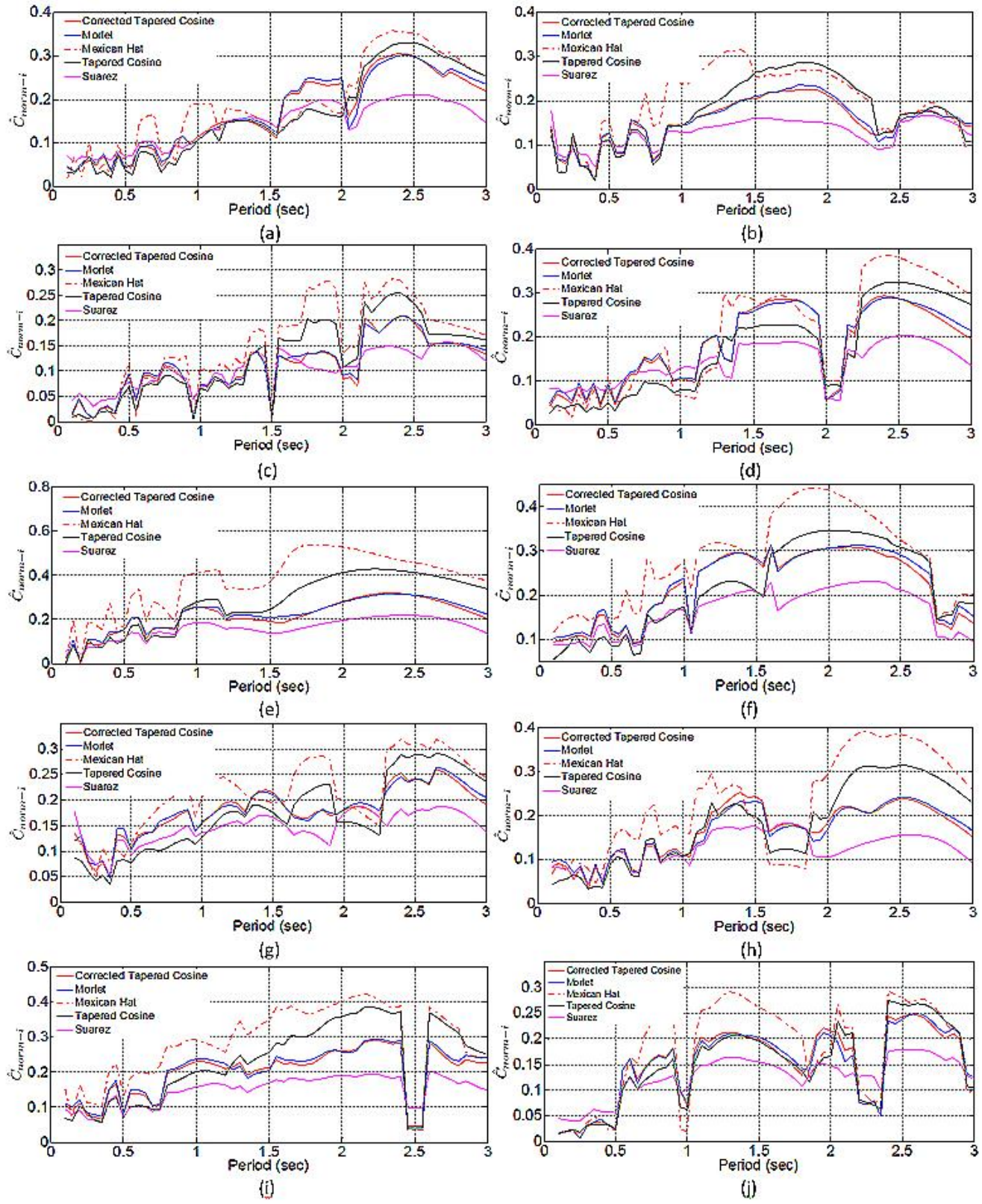

Figure 7-9 $\hat{C}_{norm-i}$ for the Selected Ground Motions.
(a) 1999 Hector Mine, Hector (b) 1992 Landers Yermo, Landers Fire Station (c) 1990 Manjil Abhar, Abhar
(d) 1971 San Fernando, LA Store (e) 1979 Imperial-1, ElCentro#6 (f) 1992 Erzican, Erzincan
(g) 1992 Cape Mendocino, Petrolia (h) 1989 Loma Prieta, BRAN (i) 1985 Nahanni, Station 1

(j) 1994 Northridge, Saticoy.

Based on this comparison, the corrected tapered cosine wavelet and the Morlet wavelet are expected to be good candidates. Although the Suarez and Montejo wavelet has small $\hat{C}_{norm-i}$, it has large base-line drift as showed on the previous comparison, this makes the use of the Suarez and Montejo wavelet on spectral matching requires a baseline drift correction.

7.4 Comparison of Spectrum Compatible Acceleration Time Histories using Different Wavelet Bases

The three candidates of wavelet bases (the corrected tapered cosine wavelet, the Morlet wavelet and the Mexican Hat wavelet) were implemented in the algorithm to compare the spectrum compatible acceleration time histories, resulted from each wavelet base. The same ten ground motions used in 0 were being used here. The damping ratio was set to 5% and the target response spectrum was the Dmax spectrum from FEMA P695 (FEMA 2009) associated with a high seismic area of California. The target periods range from 0.07 sec to 3.0 sec, equally spaced in log scale. The algorithm was executed using a personal laptop with i7-2760QM 2.4Gz processors and 8192Mb DDR3 RAM

The comparing parameters for this study were the computational time, the average misfit, the maximum misfit, the displacement drift, the PGA, PGV, PGD, the Arias Intensity and the frequency content of both acceleration and displacement time histories. The average misfit and the maximum misfit were taken as the mean and the maximum value of the absolute misfits respectively. The maximum error was also presented in this study; calculated by dividing the maximum absolute misfit with the corresponding target. The displacement drift was taken as the displacement value at the end of the ground motion. The PGA, PGV and PGD were the maximum of the absolute value of the acceleration, velocity and displacement time series respectively. The velocity and the displacement time series were calculated from the direct integrations of the acceleration time series.

The Arias Intensity (I_A) determines the shaking intensity and measures the strength of the ground motions. The Arias Intensity can also be used to capture the potential destructiveness of an earthquake. The Arias Intensity was firstly defined by Arias (1970) as the time integral of the square of the acceleration-time history.

$$I_A = \frac{\pi}{2g}\int_0^{t_d} a(t)^2 dt \tag{7.17}$$

where I_A is the Arias Intensity in units of length per time, *a(t)* is the acceleration time histories, t_d is the duration of the ground motion, and *g* is the acceleration of gravity. Besides comparing the cumulated energy, it was also desirable to examine the energy development of the resulted time histories, by using the normalized Arias Intensity. The Arias Intensity was normalized by dividing the Arias Intensity at each time with the total cumulative value of the Arias Intensity.

The preservation of the frequency content was evaluated by comparing the wavelet coefficients spectrograms of the original time histories with the modified ones. The wavelet coefficient spectrogram was calculated using Naga (2011) Matlab routine with complex Morlet wavelet of bandwidth 1 and frequency 1.5 Hz. Both acceleration and displacement time histories spectrogram were being compared in this study. Further, the spectrogram correlation between the original records and the modified ones were quantified using the Pearson's correlation of coefficient.

The Pearson's correlation of coefficient (r) is defined as the covariance of the two functions divided by the product of their standard deviations. The formula to calculate the Pearson's correlation of coefficient of the spectrograms is described as:

$$r = \frac{n \cdot m \sum_i^n \sum_j^m x_{ij} y_{ij} - \sum_i^n \sum_j^m x_{ij} \cdot \sum_i^n \sum_j^m y_{ij}}{\sqrt{n \cdot m \sum_i^n \sum_j^m x_{ij}^2 - \left(\sum_i^n \sum_j^m x_{ij}\right)^2} \sqrt{n \cdot m \sum_i^n \sum_j^m y_{ij}^2 - \left(\sum_i^n \sum_j^m y_{ij}\right)^2}} \quad (7.18)$$

where n and m are the number of samples series, x_{ij} is the absolute magnitudes of wavelet coefficients of original spectrogram, and y_{ij} is the absolute magnitudes of wavelet coefficients of modified spectrogram.

The absolute value of Pearson's correlation coefficients (r) are less than or equal to 1. A value of 1 implies that all data points on modified spectrogram are lying on the original spectrogram while a value of 0 implies that there is no linear correlation between the spectrograms.

The result comparisons are presented on Table 7-4 to Table 7-6. Table 7-4 shows the computational time, the average misfit, the maximum misfit and the maximum error for each acceleration time history resulted from the three different wavelet bases. Table 7-5 presents the PGA, PGV and PGD and the displacement drift comparison. Table 7-6 gives the comparison of the energy content and the correlation coefficient for the frequency contents.

Table 7-4 Comparison of Computational Time, Misfit and Displacement Drift

GM	Computational Time (sec)			Average Misfit (g)			Maximum Misfit (g)			Max Error (%)		
	CTCW*	Morlet	Mexican Hat	CTCW*	Morlet	Mexican Hat	CTCW*	Morlet	Mexican Hat	CTCW*	Morlet	Mexican Hat
1	31	34	33	0.011	0.012	0.014	0.075	0.067	0.120	10.17	11.79	14.99
2	20	15	25	0.015	0.014	0.020	0.117	0.105	0.103	14.46	10.48	12.00
3	21	17	25	0.011	0.013	0.018	0.092	0.083	0.111	9.22	11.64	18.53
4	19	27	35	0.010	0.014	0.014	0.086	0.113	0.091	8.62	14.28	11.5
5	46	35	60	0.011	0.011	0.033	0.105	0.104	0.149	10.53	10.42	19.34
6	33	21	36	0.007	0.006	0.015	0.051	0.062	0.150	5.69	6.25	14.97
7	19	14	18	0.008	0.008	0.010	0.057	0.046	0.009	8.84	9.58	12.52
8	37	39	60	0.016	0.018	0.015	0.093	0.115	0.107	11.21	14.42	15.52
9	30	36	64	0.011	0.010	0.016	0.116	0.136	0.081	11.62	13.61	13.69
10	23	22	41	0.016	0.016	0.022	0.087	0.110	0.169	14.61	12.89	16.89
Mean	27.9	26.0	39.7	0.012	0.012	0.018	0.088	0.094	0.109	10.50	11.54	15.00
Std	9.1	9.4	16.3	0.003	0.004	0.006	0.023	0.028	0.045	2.69	2.49	2.67

*CTCW=Corrected Tapered Cosine Wavelet

Table 7-5 Comparison of PGA, PGV and PGD

GM	PGA (g)				PGV (m/sec)				PGD (m)				Displacement Drift (m)		
	Original	CTCW	Morlet	Mexican Hat	Original	CTCW	Morlet	Mexican Hat	Original	CTCW	Morlet	Mexican Hat	CTCW	Morlet	Mexican Hat
1	0.23	0.52	0.51	0.43	0.29	0.64	0.62	0.64	0.23	0.37	0.35	0.37	0.00	-0.01	-0.01
2	0.25	0.49	0.6	0.77	0.51	0.85	0.85	0.93	0.44	0.67	0.68	0.77	-0.01	-0.02	-0.01
3	0.13	0.39	0.4	0.56	0.21	0.47	0.46	0.44	0.08	0.18	0.19	0.2	-0.02	-0.02	-0.02
4	0.21	0.52	0.48	0.53	0.19	0.43	0.43	0.44	0.13	0.25	0.23	0.21	0.00	0.00	0.01
5	0.41	0.44	0.44	0.41	0.65	0.64	0.65	0.62	0.28	0.25	0.25	0.25	0.00	0.00	-0.01
6	0.5	0.54	0.55	0.58	0.64	0.51	0.52	0.53	0.22	0.19	0.19	0.18	0.00	-0.01	0.00
7	0.59	0.55	0.63	0.61	0.48	0.55	0.59	0.56	0.22	0.25	0.24	0.26	0.00	-0.01	-0.02
8	0.48	0.4	0.39	0.49	0.56	0.51	0.53	0.48	0.12	0.14	0.13	0.12	0.01	0.00	0.00
9	0.98	0.51	0.51	0.67	0.46	0.5	0.44	0.46	0.1	0.17	0.14	0.15	0.00	0.00	0.00
10	0.37	0.45	0.47	0.43	0.29	0.38	0.37	0.36	0.08	0.14	0.14	0.13	0.00	0.01	0.01
Median	0.39	0.50	0.50	0.55	0.47	0.51	0.53	0.51	0.18	0.22	0.21	0.21	0.00	0.01	0.01
Mean	0.42	0.48	0.50	0.55	0.43	0.55	0.55	0.55	0.19	0.26	0.25	0.26	0.00	0.01	0.01
Std	0.25	0.06	0.08	0.12	0.17	0.13	0.14	0.16	0.11	0.16	0.16	0.19	0.01	0.01	0.01

Table 7-6 Comparison of Arias Intensity and Correlation on Frequency Content

GM	Arias Intensity (m/sec)				Coefficient of Correlation for Acceleration			Coefficient of Correlation for Displacement		
	Original	CTCW	Morlet	Mexican Hat	CTCW	Morlet	Mexican Hat	CTCW	Morlet	Mexican Hat
1	0.83	3.01	2.93	3.01	0.86	0.86	0.76	0.95	0.95	0.81
2	0.93	3.02	3.49	3.45	0.86	0.85	0.84	0.97	0.97	0.94
3	0.65	4.92	4.87	4.90	0.840	0.84	0.85	0.98	0.97	0.96
4	0.65	2.54	2.51	2.32	0.88	0.84	0.83	0.98	0.95	0.96
5	1.49	1.98	2.04	1.95	0.93	0.93	0.81	0.97	0.98	0.85
6	1.79	1.57	1.54	1.13	0.98	0.98	0.92	0.99	0.99	0.96
7	3.42	2.83	2.79	2.87	0.83	0.83	0.75	0.95	0.95	0.82
8	5.36	2.99	2.96	2.78	0.79	0.80	0.79	0.93	0.89	0.90
9	4.45	1.62	1.54	1.46	0.71	0.74	0.69	0.91	0.91	0.90
10	1.97	3.03	2.97	2.85	0.86	0.87	0.70	0.85	0.83	0.74
Median	1.64	2.91	2.86	2.82	0.86	0.85	0.80	0.96	0.95	0.90
Mean	2.15	2.75	2.76	2.67	0.85	0.85	0.79	0.95	0.94	0.88
Std	1.68	0.96	0.98	1.07	0.07	0.07	0.07	0.04	0.05	0.08

It can be seen that, in general, the three wavelet base candidates are able to match the target spectra. It is also observed in Table 7-4 to Table 7-6 that the corrected tapered cosine wavelet and the Morlet wavelet give relatively close results. This fits the previous studies which showed that the off-diagonal terms of spectral sensitivity *C* Matrix, frequency resolution and time resolution of the two wavelets are close each other.

In the other side, although the implementation of the Mexican Hat wavelet is able to match the spectra target, it tends to vastly change the velocity and the displacement time histories. A clear example on this is showed in Figure 7-10 for the 1992 Erzican, Erzican (GM #6) ground motion case, which shown that the use of the three wavelet candidates are able to match the target. However, in Figure 7-11 it is shown the use of the Mexican Hat wavelet greatly changes the acceleration, velocity and displacement time series.

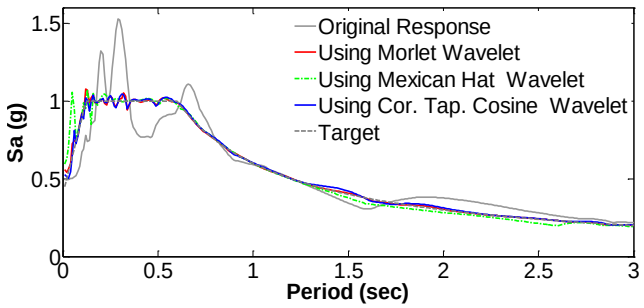

Figure 7-10 Matched Spectra Response of the 1992 Erzican, Erzican Ground Motion using 3 Wavelet Bases

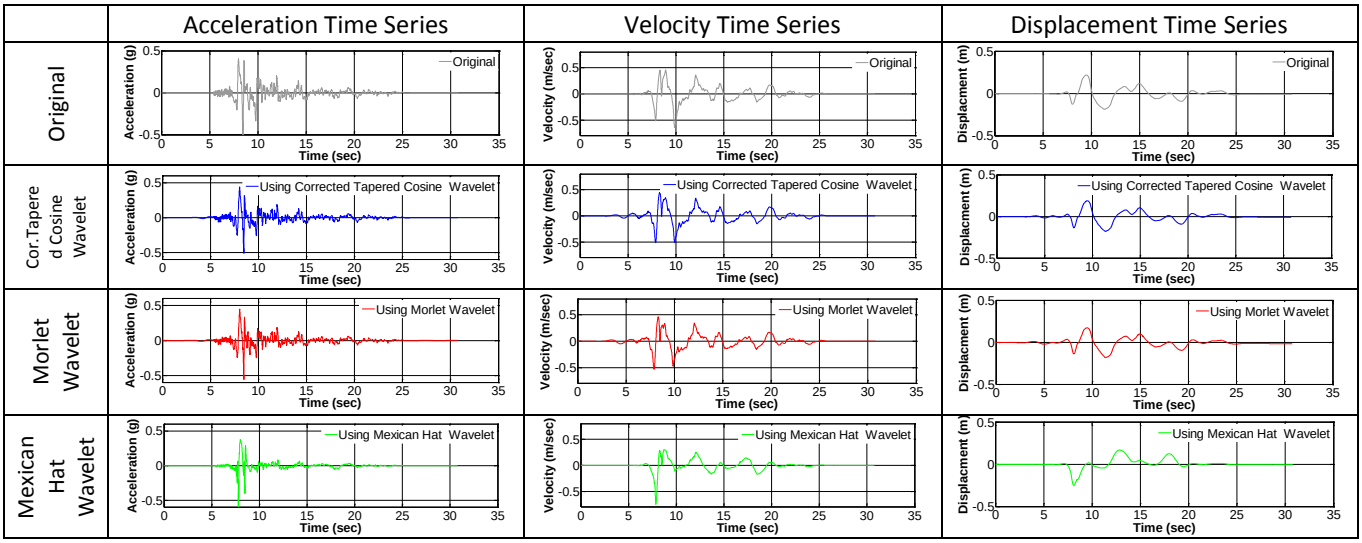

Figure 7-11 Spectra-compatible Time Series using 3 Wavelet Bases Candidates for the 1992 Erzican, Erzican GM

In term of computational time, in general the use of the Mexican hat wavelet requires longer time compared to the corrected tapered cosine wavelet and the Morlet wavelet. In term of average misfit, the corrected tapered cosine wavelet and the Morlet wavelet yield close results (approximately 0.012g on mean and 0.003g on standard deviation). The Mexican Hat wavelet yields higher average misfit and standard deviation (0.018g and 0.006g respectively).

On average, the Mexican Hat wavelet implementation also yields higher maximum misfits (0.109g compared to 0.088g and 0.094g for corrected tapered cosine and the Morlet wavelet respectively). In terms of displacement drift, as expected, the three candidates result almost zero values of displacement drifts.

Table 7-5 shows that for the near field ground motions, the corrected tapered cosine gives less change to the PGA compared to other wavelet candidates. The changes in the PSV are also smaller for the corrected tapered cosine wavelet and the Morlet wavelet. In term of PGD, the three wavelet bases generate close values.

In term of energy content, it can be seen in Table 7-6 that the three wavelet bases yields relatively close values, except for the 1992 Erzican, Erzican (GM #6) ground motion case where the use of the Mexican Hat

wavelet yields much lower Arias Intensity than the other wavelets. By closer examination in Figure 7-12, the Mexican Hat wavelet also changes the energy development for this particular ground motion.

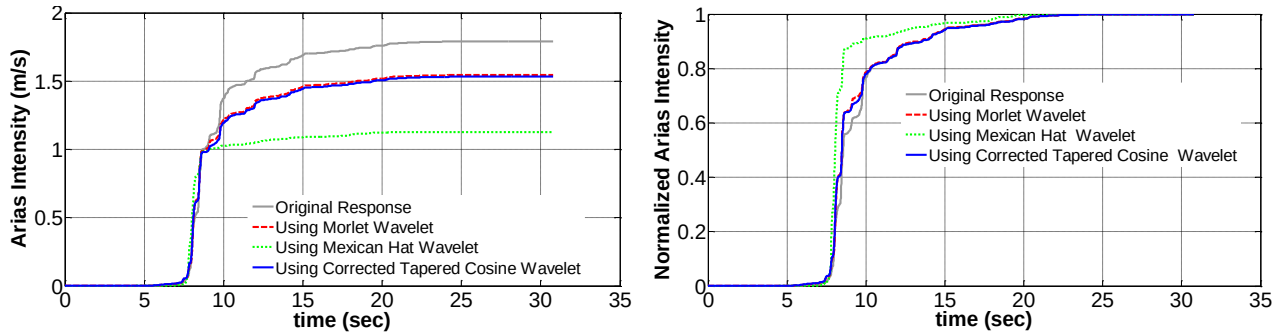

Figure 7-12 Arias Intensity and Normalized Arias Intensity for the 1992 Erzican, Erzican Ground Motion

As for the frequency content, it is observed in Table 7-6 that the corrected tapered cosine wavelet and the Morlet wavelet give relatively same spectrogram correlations, while the Mexican Hat wavelet yields lower correlations. This implies that the non-stationary contents are less preserved using the Mexican Hat wavelet. Figure 7-13 and Figure 7-14 present the wavelet coefficient spectrograms of the acceleration and displacement time series for the 1992 Erzican, Erzican (GM #6) ground motion. It can be seen here that the Mexican Hat wavelet tends to change the frequency content, which indicated by the changes in the spectrograms.

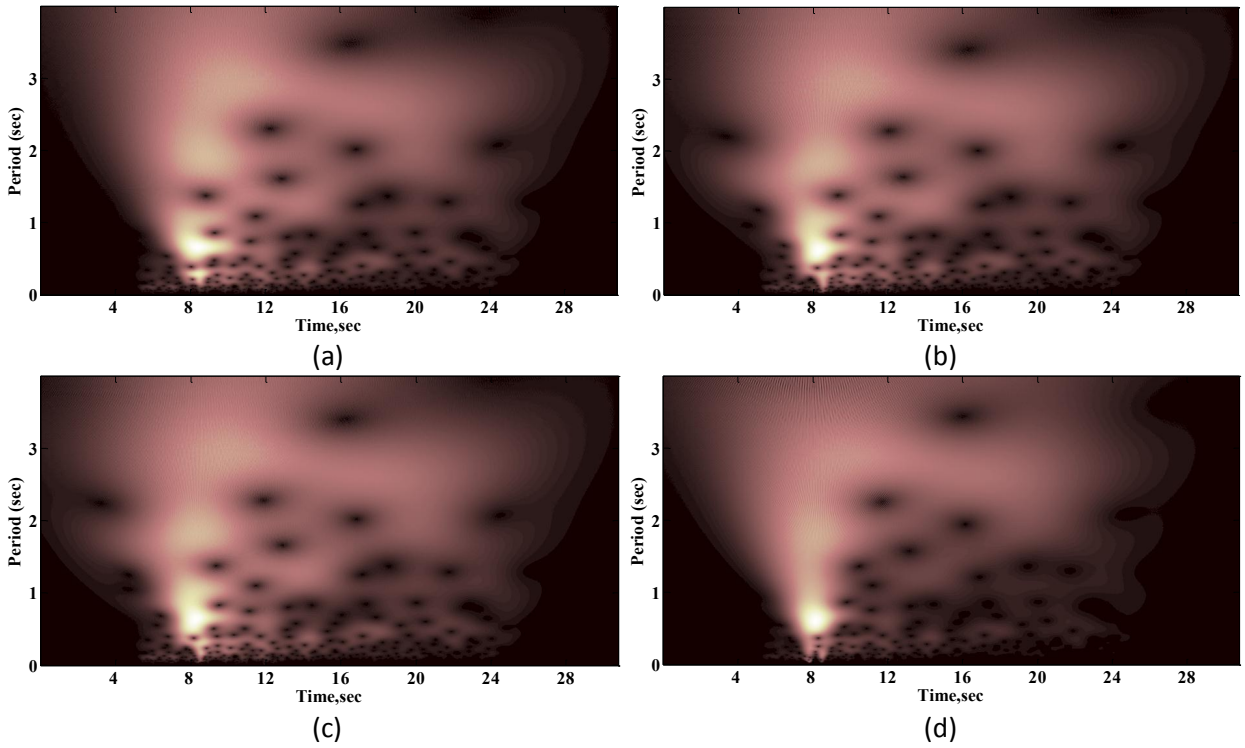

Figure 7-13 Acceleration Spectrogram for the Modified Erzican, Erzican Ground Motion using 3 Wavelet Bases
(a) Original (b) Using Corrected Tapered Cosine Wavelet (c) Using Morlet Wavelet (d) Using Mexican Hat Wavelet

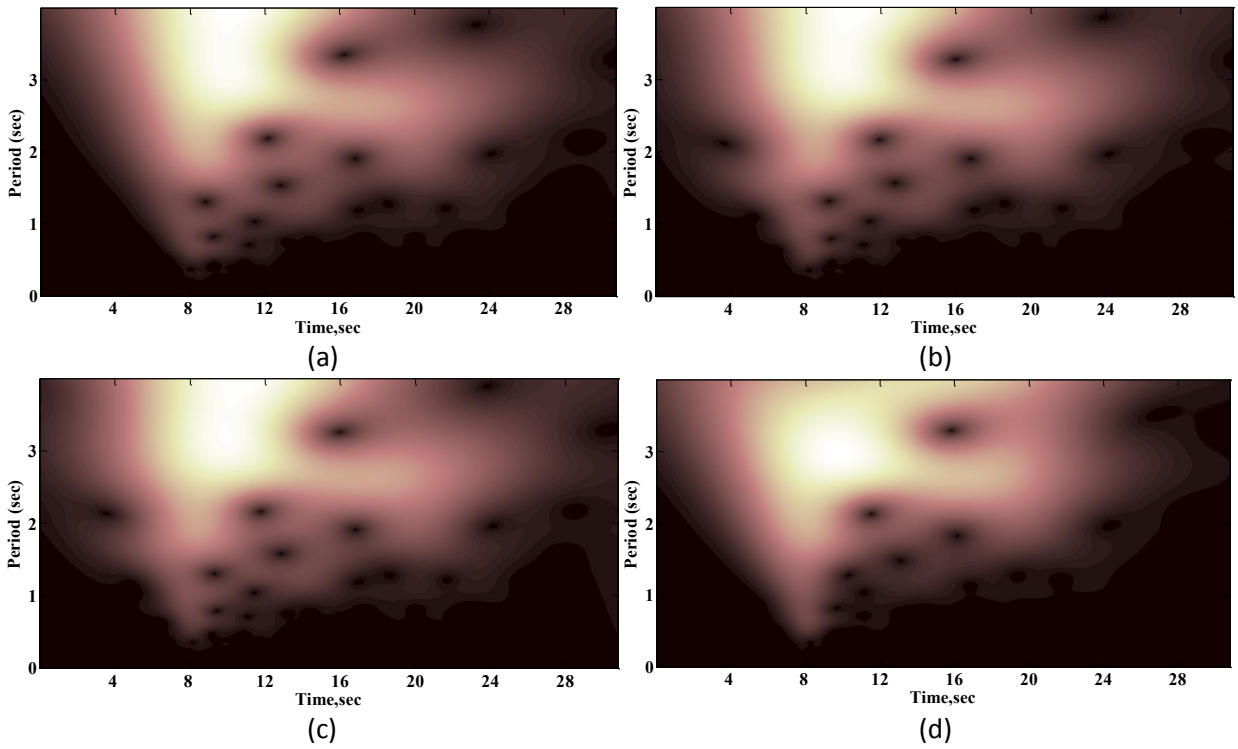

Figure 7-14 Displacement Spectrogram for the Modified Erzican, Erzican Ground Motion using 3 Wavelet Bases
(a) Original (b) Using Corrected Tapered Cosine Wavelet (c) Using Morlet Wavelet (d) Using Mexican Hat Wavelet

7.5 Options in Calculating Responses

The oscillator response can be calculated using a numerical method or an analytical formula. The decision of choosing which option to be used is depends on the time-efficiency and the result accuracy. For this comparison, the numerical method were calculated using the Newmark method while the analytical formula was solved using the generic formula from Wolfram Mathematica8 software. Both methods were executed using Matlab 2009a (Matlab 7.9, "The Language of Technical Computing," The Mathworks, Inc). Based on the proposed wavelet base, only the corrected tapered cosine wavelet was being compared.

By using the Duhamel's integral, the displacement response of a SDOF oscillator with angular frequency ω_{ni} and damping ratio ζ, as subjected to the wavelet adjustment $\psi_j(t)$ is given by:

$$u_{\psi ij}(t) = \int_0^t \frac{-1}{m\,\omega_{ni}} e^{(-\omega_i \zeta (t-\tau))}\, sin\big(\omega'_{ni}(t-\tau)\big)\psi_j(\tau - \Delta t)d\tau \tag{7.17}$$

Substituting the corrected tapered cosine wavelet function (Eqn. 7.5) to Eqn. 7.17 gives

$$u_{\psi ij}(t) = \int_0^t \frac{-1}{m\,\omega_{ni}} e^{(-\omega_i \zeta (t-\tau))}\, sin\big(\omega'_{ni}(t-\tau)\big) e^{-\left[\frac{(\tau - t_j)}{1.178\left(\frac{\omega_j}{2\pi}\right)^{-0.93}}\right]^2} cos\left(\omega_j\big(\tau - t_j\big)\right) d\tau \tag{7.18}$$

where m is the oscillator mass, ω'_{ni} is the damped angular frequency of ω_{ni} and ω_j is the wavelet acceleration frequency. Using Wolfram Mathematica 8 software (Mathematica 8 Documentation Centre, Wolfram Research Inc) , the generic formula is given in Figure 7-15.

```
Integrate[-1/m/wd*Exp[-wn*tetha*(t-x)]*Sin[wd*(t-x)]*Cos[wj*(x-tj)]*Exp[-(((x-tj)/(1.178*(wj/2/Pi)^-0.93))^2)], {x, 0, t}]
```

$$-\frac{1}{m\,wd\,wj^{0.93`}}\,e^{-0.023609938942365204`\,tj^2\,wj^{1.86`}-1.`\,t\,tetha\,wn}$$

$$\left(0.5`\left(e^{\frac{10.588760970974176`\,((0.`+1.`\,i)\,wd-(0.`+1.`\,i)\,wj+0.04721987788473041`\,tj\,wj^{1.86`}+tetha\,wn)^2}{wj^{1.86`}}}\right.\right.$$

$$\mathrm{Erfi}\left[\frac{1}{wj^{0.93`}}\left(3.254037641296452`\,wd-3.254037641296452`\,wj+((0.`+0.1536552600543346`\,i)\,t-(0.`+0.1536552600543346`\,i)\,tj)\,wj^{1.86`}-\right.\right.$$

$$\left.\left.(0.`+3.254037641296452`\,i)\,tetha\,wn\right)\right]\,(2.8838157741536987`\,\mathrm{Cos}[t\,wd-1.`\,tj\,wj]-(0.`+2.8838157741536987`\,i)\,\mathrm{Sin}[t\,wd-1.`\,tj\,wj])+$$

$$e^{\frac{10.588760970974176`\,((0.`-1.`\,i)\,wd+(0.`+1.`\,i)\,wj+0.04721987788473041`\,tj\,wj^{1.86`}+tetha\,wn)^2}{wj^{1.86`}}}$$

$$\mathrm{Erfi}\left[\frac{1}{wj^{0.93`}}\left(3.254037641296452`\,wd-3.254037641296452`\,wj+((0.`-0.1536552600543346`\,i)\,t+(0.`+0.1536552600543346`\,i)\,tj)\,wj^{1.86`}+\right.\right.$$

$$\left.\left.(0.`+3.254037641296452`\,i)\,tetha\,wn\right)\right]\,(2.8838157741536987`\,\mathrm{Cos}[t\,wd-1.`\,tj\,wj]+(0.`+2.8838157741536987`\,i)\,\mathrm{Sin}[t\,wd-1.`\,tj\,wj])\Bigg)-$$

$$0.5`\left(e^{\frac{10.588760970974176`\,((0.`+1.`\,i)\,wd-(0.`+1.`\,i)\,wj+0.04721987788473041`\,tj\,wj^{1.86`}+tetha\,wn)^2}{wj^{1.86`}}}\right.$$

$$\mathrm{Erfi}\left[\frac{(0.`+0.`\,i)+3.254037641296452`\,wd-3.254037641296452`\,wj-(0.`+0.1536552600543346`\,i)\,tj\,wj^{1.86`}-(0.`+3.254037641296452`\,i)\,tetha\,wn}{wj^{0.93`}}\right]$$

$$(2.8838157741536987`\,\mathrm{Cos}[t\,wd-1.`\,tj\,wj]-(0.`+2.8838157741536987`\,i)\,\mathrm{Sin}[t\,wd-1.`\,tj\,wj])$$

$$+e^{\frac{10.588760970974176`\,((0.`-1.`\,i)\,wd+(0.`+1.`\,i)\,wj+0.04721987788473041`\,tj\,wj^{1.86`}+tetha\,wn)^2}{wj^{1.86`}}}$$

$$\mathrm{Erfi}\left[\frac{(0.`+0.`\,i)+3.254037641296452`\,wd-3.254037641296452`\,wj+(0.`+0.1536552600543346`\,i)\,tj\,wj^{1.86`}+(0.`+3.254037641296452`\,i)\,tetha\,wn}{wj^{0.93`}}\right]$$

$$\left.(2.8838157741536987`\,\mathrm{Cos}[t\,wd-1.`\,tj\,wj]+(0.`+2.8838157741536987`\,i)\,\mathrm{Sin}[t\,wd-1.`\,tj\,wj])\right)+$$

$$0.5`\left(e^{\frac{10.588760970974176`\,((0.`+1.`\,i)\,wd+(0.`+1.`\,i)\,wj+0.04721987788473041`\,tj\,wj^{1.86`}+tetha\,wn)^2}{wj^{1.86`}}}\right.$$

$$\mathrm{Erfi}\left[\frac{3.254037641296452`\,(wd+wj+((0.`+0.04721987788473041`\,i)\,t-(0.`+0.04721987788473041`\,i)\,tj)\,wj^{1.86`}-(0.`+1.`\,i)\,tetha\,wn)}{wj^{0.93`}}\right]$$

$$(2.8838157741536987`\,\mathrm{Cos}[t\,wd+tj\,wj]-(0.`+2.8838157741536987`\,i)\,\mathrm{Sin}[t\,wd+tj\,wj])+$$

$$e^{\frac{10.588760970974176`\,((0.`-1.`\,i)\,wd-(0.`+1.`\,i)\,wj+0.04721987788473041`\,tj\,wj^{1.86`}+tetha\,wn)^2}{wj^{1.86`}}}$$

$$\mathrm{Erf}\left[\frac{1}{wj^{0.93`}}\left((0.`+3.254037641296452`\,i)\,wd+(0.`+3.254037641296452`\,i)\,wj+(0.1536552600543346`\,t-0.1536552600543346`\,tj)\,wj^{1.86`}-\right.\right.$$

$$\left.\left.3.254037641296452`\,tetha\,wn\right)\right]\,((0.`-2.8838157741536987`\,i)\,\mathrm{Cos}[t\,wd+tj\,wj]+2.8838157741536987`\,\mathrm{Sin}[t\,wd+tj\,wj])\Bigg)-$$

$$0.5`\left(e^{\frac{10.588760970974176`\,((0.`+1.`\,i)\,wd+(0.`+1.`\,i)\,wj+0.04721987788473041`\,tj\,wj^{1.86`}+tetha\,wn)^2}{wj^{1.86`}}}\right.$$

$$\mathrm{Erfi}\left[\frac{3.254037641296452`\,((0.`+0.`\,i)+wd+wj-(0.`+0.04721987788473041`\,i)\,tj\,wj^{1.86`}-(0.`+1.`\,i)\,tetha\,wn)}{wj^{0.93`}}\right]$$

$$(2.8838157741536987`\,\mathrm{Cos}[t\,wd+tj\,wj]-(0.`+2.8838157741536987`\,i)\,\mathrm{Sin}[t\,wd+tj\,wj])+$$

$$e^{\frac{10.588760970974176`\,((0.`-1.`\,i)\,wd-(0.`+1.`\,i)\,wj+0.04721987788473041`\,tj\,wj^{1.86`}+tetha\,wn)^2}{wj^{1.86`}}}$$

$$\mathrm{Erf}\left[\frac{0.`+(0.`+3.254037641296452`\,i)\,wd+(0.`+3.254037641296452`\,i)\,wj-0.1536552600543346`\,tj\,wj^{1.86`}-3.254037641296452`\,tetha\,wn}{wj^{0.93`}}\right]$$

$$\left.\left.((0.`-2.8838157741536987`\,i)\,\mathrm{Cos}[t\,wd+tj\,wj]+2.8838157741536987`\,\mathrm{Sin}[t\,wd+tj\,wj])\right)\right)$$

Figure 7-15 Mathematica8 Output Screen Shot

where *Erf* and *Erfi* are the error function and the imaginary error function respectively. This formula was implemented into Matlab 2009a where the *Erf* and *Erfi* function were executed as follow:

- The *Erf(z)* was executed using *erfz(z)*, where *z* is a complex number. The *erfz* function is available in Mathworks file exchange website (http://www.mathworks.com/matlabcentral/fileexchange/3574).
- The *Erfi(z)* was executed using *–i*erfz(i*z)* as defined by Mathematica, where *z* is a complex number. The same *erfz* Matlab function was used.

To verify the solution accuracy of the *erfz* function on Matlab, the error function values for several trivial cases resulted from Mathematica8 and *erfz* Matlab function were being compared, as presented in Table 7-7. It can be seen here that the *erfz* Matlab functions is accurate to calculate the imaginary error values.

Table 7-7 Comparison of Error Function Value

Formula	Mathematica8	Matlab *erfz* function
Erfi(2*i*)	0.995322265018952734162069256367 3*i*	0.995322265018953*i*
Erf(1+5*i*)	$1.07869311619854059759572757845 7\times10^{9}$ $-2.78377702922089652871014623 59\times10^{9}\,i$	$1.078693116198541\times10^{9}$ - $2.783777029220899\times10^{9}i$
Erfi(0.2+3.5*i*)	$7.6706146054\times10^{-7}$+0.99999990936*i*	0.000000767061461 + 0.999999909361285*i*
Erfi((2-5*i*)*$3^{0.97}$)	$-3.50297948396276891665563517 5\times10^{-79}$ -1.00000000000000*i*	-3.503×10^{-079} - 1*i*

The generic formula from the Mathematica8 output was implemented to Matlab 2009a (Matlab 7.9, "The Language of Technical Computing," The Mathworks Inc). It was found that for a range of frequency ratio $0.16667 < \frac{\omega_n}{\omega_j} < 6$, the formula gives close results to the Newmark method. However, it was also found that outside this frequency, the error function gives infinite values or 'Not a Number' (*NaN*) values, hence resulting in errors on the solution.

Figure 7-16 and Figure 7-17 give an illustration for the two calculation methods. In Figure 7-16, the oscillator period T_n was set as 0.4 sec and the wavelet period T_j was set as 0.5 sec. For this case, the two methods give very close results. However, where can be seen in Figure 7-17, when the ratio between the oscillator period and wavelet period was large, the generic formula gives error values on some range of time.

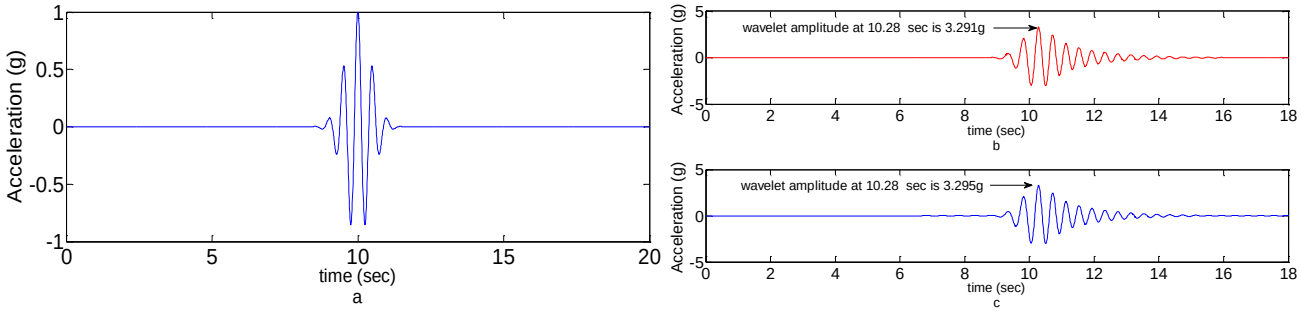

Figure 7-16 Comparison of Oscillator Response Calculated using Generic Formula and Newmark Method for Oscillator Period T_n=0.4 sec and wavelet period T_j =0.5sec
(a) Wavelet Acceleration Time Series (b) Acceleration Response using Mathematica8 Formula Output
(c) Acceleration Response using Newmark Method

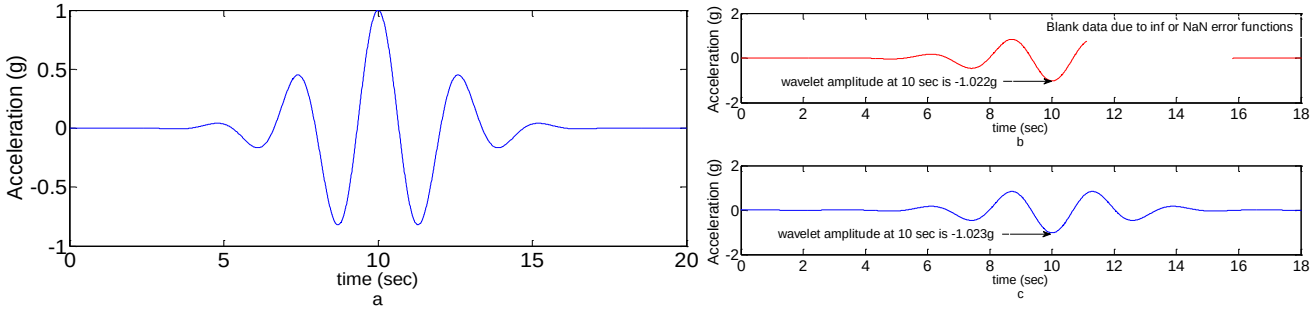

Figure 7-17 Comparison of Oscillator Response Calculated using Generic Formula and Newmark Method for Oscillator Period T_n=0.4 sec and wavelet period T_j =2.7sec
(a) Wavelet Acceleration Time Series (b) Acceleration Response using Mathematica8 Formula Output
(c) Acceleration Response using Newmark Method

It was recorded that the computational time is faster using Newmark method (0.00056 sec compared to 5.3sec for the generic formula). This may happen because the generic formula, executed using Matlab 2009a, recalls the error function several times which expenses the computational time. Another approach to calculate the error functions is by using the Maclaurin series (Wolfram, Mathwork Inc), which possibly result in better time-efficiency in calculating the error function. However, such derivation was not conducted in this study.

$$erf(z) = \frac{2}{\sqrt{\pi}} \sum_{n=0}^{\infty} \frac{(-1)^n z^{2n+1}}{n!(2n+1)} = \frac{2}{\sqrt{\pi}} \left(z - \frac{z^3}{3} + \frac{z^5}{10} - \frac{z^7}{42} + \frac{z^9}{216} - \cdots \right) \tag{7.19}$$

$$erfi(z) = -i + \frac{e^{z^2}}{\sqrt{\pi}} \left(z^{-1} + \frac{1}{2} z^{-3} + \frac{3}{4} z^{-5} + \frac{15}{8} z^{-7} + \cdots \right) \tag{7.20}$$

Considering the result accuracy and the computational time, it was selected to calculate the oscillator acceleration response as subjected to wavelet adjustment by using the Newmark method.

7.6 Summary of Wavelet Bases Study

Based on the study conducted, there are two candidates of wavelet bases that are suitable for the proposed method; the corrected tapered cosine wavelet and the Morlet wavelet. The summary of the wavelet bases are as follows:

- The Lilhanand and Tseng wavelet has some disadvantage features in terms of the baseline drift and its form that stops abruptly.
- The tapered cosine and the Suarez and Montejo wavelet have a good feature in which they have small value on the off-diagonal terms of *C* matrix. However, the two wavelets yield large baseline drifts.
- The Shannon wavelet has a very long time resolution, which might require large amount of zero padding at the ends of time histories, thus considered not efficient. This wavelet base also has large baseline drifts in velocity and displacement.
- The proposed algorithm that uses the Mexican Hat wavelet is able to match the target spectra and results in relatively zero displacement drifts. However, the use of the Mexican Hat wavelet tends to change the energy content and the frequency content of the original ground motions.
- The Morlet wavelet gives a slightly higher maximum misfit and a longer computational time compared to the corrected tapered cosine wavelet. The Morlet wavelet also tends to have close spectrogram correlations with the corrected tapered cosine wavelet.
- The fact that the corrected tapered cosine wavelet preserves the frequency contents and yields a realistic compatible acceleration time series, this wavelet base was selected for the proposed algorithm.
- The oscillator acceleration response due to wavelet adjustment was calculated using Newmark method.

CHAPTER 8. COMPARISON WITH OTHER METHODS

8.1 Comparison Result

This chapter compares the spectrum compatible acceleration time histories resulted from the proposed method and two existing methods that are commonly employed as practice; the RSPMatch in time domain and the frequency domain method. The comparing parameters were the computational time, the average misfit, the maximum misfit, the maximum error, the PGA, PGV, PGD, the Arias Intensity and the frequency content for both acceleration and displacement. The same ten ground motions as in Chapter 6 were used as the input. To reduce the distortion and minimize the chance of baseline drift during the spectral matching procedure, the ground motions were 5 sec zero padded at the beginning and end.

RSPMatch Configuration

The Manual for Program: RSPMatch ver 2005b explains the input parameters that can be used and adjusted by the user. One of the RSPMatch ver 2005b input parameters is the option to linearly scale the ground motion based on the ordinates of the original ground motion spectra and the target response spectra. There are 3 scaling options that can be chosen:

- Without scaling
- Scale the initial time history to fix the acceleration value before the spectral matching procedure and after each iteration
- Scale the initial time history to fix the acceleration value before the spectral matching procedure but do not scale after subsequent iterations

The default configuration, and was used in this comparison, is without scaling.

Another RSPMatch ver 2005b option is the PGA correction using sinusoidal waves. The RSPMatch ver 2005b Manual recommends not modifying the PGA. The reason is because the PGA is generally less well correlated with oscillator response than the spectral acceleration at the period(s) of the system being analyzed. Moreover, it is also difficult to obtain stable convergence of the adjustment procedure when the PGA is modified. The default configuration, and was used in this comparison, is without the PGA correction.

There are 3 phases of frequency bands in the default configuration, the first phase is from 1Hz to 100Hz, the second phase is from 0.2Hz to 100Hz and the last phase is from 1Hz to 100Hz. The default configuration was used in the comparison study. The periods of target spectra were spaced equally in log scale range from 0.06 sec to 3.0 sec.

Frequency Domain (MyRattle software) Configuration

The frequency domain method was calculated using the MyRattle software similar to Silva and Lee (1987). This software has no acceleration scaling or PGA correction options as in the previous method. For this study, the periods set were spaced equally in log scale, range from 0.06 sec to 3.0 sec. The maximum number of iteration was set as 10 (default configuration is 5). No baseline drifts corrections were employed on this method.

All methods were executed using a personal laptop with Intel i7 Quad-core 2.8Gz processor and 8192 Mb DDR3 RAM. The result comparisons are summarized in Table 8-1 to Table 8-3. Table 8-1 shows the computational time, the average misfit, the maximum misfit and the maximum error for each ground motion. Table 8-2 presents the PGA, PGV and PGD and the displacement drift resulted from the 3 different methods. Table 8-3 compares the energy content and the frequency content of the original acceleration and the spectrum compatible accelerations. The graphical results for each ground motion can be seen on APPENDIX A.

Table 8-1 Summary of Computational time, Misfit and Error

GM	Comp. Time (sec)			Average Misfit (g)			Maximum Misfit (g)			Max Error (%)		
	RSP-Match	Freq Meth.	Proposed	RSP-Match	Freq Meth	Proposed	RSP-Match	Freq Meth	Proposed	RSP-Match	Freq Meth	Proposed
1	11	28	26	0.006	0.011	0.009	0.073	0.082	0.073	7.31	11.94	9.97
2	21	32	18	0.008	0.012	0.014	0.213	0.169	0.083	28.78	18.19	11.01
3	10	21	19	0.010	0.018	0.011	0.068	0.110	0.091	11.46	12.86	9.70
4	11	33	19	0.008	0.018	0.011	0.051	0.099	0.084	6.82	15.67	8.37
5	10	23	50	0.008	0.008	0.010	0.099	0.106	0.105	11.32	11.34	10.50
6	8	18	31	0.006	0.008	0.007	0.063	0.099	0.050	6.27	5.58	5.64
7	31	25	19	0.027	0.015	0.007	0.098	0.119	0.045	26.27	8.34	8.44
8	10	19	36	0.011	0.012	0.015	0.090	0.075	0.091	9.01	18.93	10.94
9	31	23	33	0.010	0.014	0.011	0.074	0.065	0.106	9.98	9.74	10.62
10	12	20	21	0.012	0.017	0.015	0.074	0.086	0.092	13.01	11.99	11.96
Mean	15.5	24.2	27.2	0.011	0.013	0.011	0.090	0.101	0.082	13.02	12.46	9.72
Std Dev	8.9	5.3	10.4	0.006	0.004	0.003	0.046	0.029	0.021	7.97	4.20	1.82

Table 8-2 Summary of PGA, PGV, PGD and Drift

GM	PGA (g)				PGV (m/sec)				PGD (m)				Displacement Drift (m)		
	Original	RSP-Match	Freq Meth	Propo-sed	Original	RSP-Match	Freq Meth	Propo-sed	Original	RSP-Match	Freq Meth	Propo-sed	RSP-Match	Freq Meth	Propo-sed
1	0.23	0.48	0.49	0.51	0.29	0.46	0.83	0.63	0.23	0.23	1.7	0.37	0	1.69	-0.01
2	0.25	0.42	0.42	0.57	0.51	0.55	0.80	0.83	0.44	0.44	0.71	0.66	0.03	-0.64	-0.01
3	0.13	0.40	0.40	0.39	0.21	0.52	0.45	0.47	0.08	0.14	0.99	0.17	-0.01	-0.98	-0.02
4	0.21	0.40	0.43	0.48	0.19	0.46	0.51	0.42	0.13	0.20	0.66	0.24	0	0.66	0
5	0.41	0.40	0.34	0.43	0.65	0.64	0.60	0.64	0.28	0.23	0.66	0.25	0	-0.66	0
6	0.5	0.51	0.45	0.53	0.64	0.57	0.61	0.51	0.22	0.22	0.25	0.19	0	-0.18	0
7	0.59	0.70	0.60	0.53	0.48	0.59	0.45	0.58	0.22	0.34	0.85	0.24	0.09	0.85	-0.01
8	0.48	0.41	0.42	0.39	0.56	0.52	0.61	0.51	0.12	0.14	0.19	0.14	0.01	-0.02	0
9	0.98	0.56	0.46	0.52	0.46	0.48	0.43	0.55	0.10	0.16	0.18	0.17	0	-0.18	0
10	0.37	0.38	0.40	0.45	0.29	0.40	0.46	0.37	0.08	0.11	0.59	0.12	0	0.569	0.01
Median	0.39	0.42	0.43	0.50	0.47	0.52	0.56	0.53	0.18	0.21	0.66	0.22	0.00	0.65	0.01
Mean	0.42	0.47	0.44	0.48	0.43	0.52	0.58	0.55	0.19	0.22	0.68	0.26	0.01	0.64	0.01
Std Dev	0.25	0.10	0.07	0.06	0.17	0.07	0.14	0.13	0.11	0.10	0.45	0.16	0.03	0.48	0.01

Table 8-3 Summary of Arias Intensity and Correlation of Frequency Content

GM	Arias Intensity (m/sec)				Coefficient of Correlation for Acceleration Time Series			Coefficient of Correlation for Displacement Time Series		
	Original	RSPMatch	Freq Meth	Proposed	RSPMatch	Freq Meth	Proposed	RSPMatch	Freq Meth	Proposed
1	0.83	2.20	4.08	2.96	0.825	0.828	0.861	0.873	0.275	0.949
2	0.93	2.28	5.42	3.04	0.838	0.796	0.855	0.929	0.703	0.971
3	0.65	3.07	6.98	4.87	0.667	0.583	0.840	0.925	0.619	0.975
4	0.65	2.38	3.86	2.45	0.802	0.819	0.876	0.913	0.827	0.979
5	1.49	1.96	2.79	1.97	0.914	0.856	0.928	0.973	0.696	0.974
6	1.79	1.61	2.53	1.56	0.976	0.930	0.980	0.992	0.970	0.995
7	3.42	3.33	4.67	2.80	0.876	0.770	0.830	0.968	0.424	0.950
8	5.36	3.79	3.91	2.98	0.796	0.758	0.793	0.932	0.967	0.931
9	4.45	2.92	2.74	1.67	0.690	0.604	0.708	0.825	0.782	0.908
10	1.97	3.02	4.05	2.96	0.862	0.824	0.863	0.889	0.646	0.850
Median	1.64	2.65	3.98	2.88	0.832	0.808	0.858	0.927	0.700	0.961
Mean	2.15	2.66	4.10	2.73	0.825	0.777	0.853	0.922	0.691	0.948
Std Dev	1.68	0.68	1.35	0.94	0.094	0.108	0.073	0.050	0.219	0.043

8.2 Discussion

8.2.1 Computational time, Misfit and Error

It is observed in Table 8-1 that the proposed method can match the target spectrum. The average and the maximum misfits of the proposed method are 0.0110 g and 0.0821 g respectively. On average, the RSPMatch method gives a better result in term of average misfit, which is 0.0106g and 0.0903g for maximum misfit. This implies that for most cases, the RSPMatch method yields a smoother spectrum as indicated by the small average misfit. There is one case, which is the 1992 Cape of Mendocino, Petrolia (GM #7), where the RSPMatch generates a large misfit. Different period subsets and configuration may give better results. However, for the sake of consistency, during this comparison all ground motions were being matched with the same period subsets and configuration. Moreover, it is also showed that within 10 iterations, the frequency domain method can matched the target spectra with 0.0133g on the average misfit and 0.1010g on the maximum misfit. Since the proposed method calculates the initial solution (initial *b* vector) using the same calculation as in the RSPMatch method, the two methods may give close results.

To demonstrate the result of the three spectral matching methods, Figure 8-1 presents the spectra response for the 1999 Hector Mine, Hector (GM #1) and the 1971 San Fernando, LA Hollywood Store Hector (GM #4). It can be seen here that the RSPMatch generates smooth spectra response, the proposed method generates slightly more jagged spectra and the frequency domain method generates more jagged spectra. However, if desirable, the misfit can be reduced by using more iteration.

In terms of computational time, the proposed method runs longer compared to the other two methods. It requires approximately 75% and 13% longer time compared to the RSPMatch Method and the frequency

domain method respectively for the given configuration. The calculation of the full *C* matrix was giving the most contribution to the computational time in the proposed method. Another method of calculating the response and the initial *C* could be applied to reduce the computational time. The longer computational time may also due to the proposed method was executed in Matlab environment rather than in complied program.

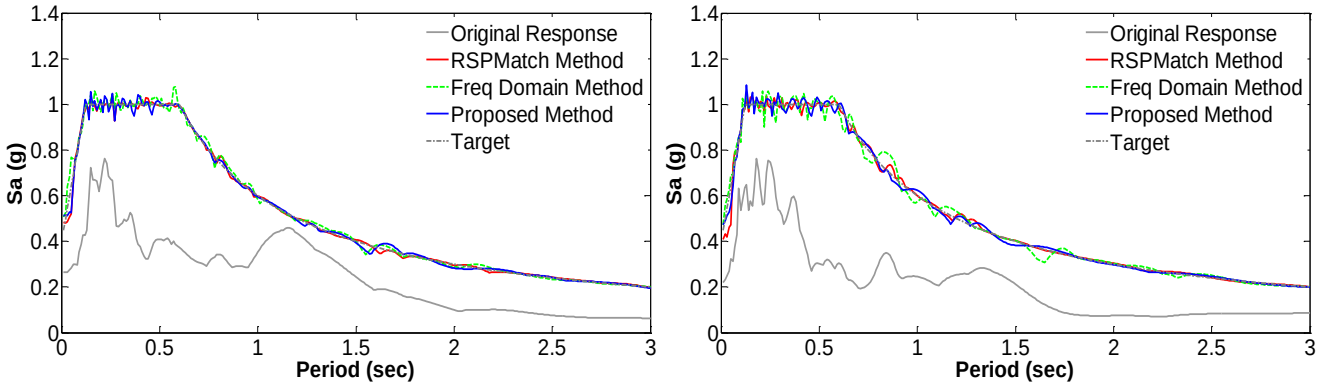

Figure 8-1 Comparison of Response Spectrum using the 3 Different Spectral Matching Methods for 1999 Hector Mine, Hector (left) and 1971 San Fernando, LA Hollywood Store (right) Ground Motion

8.2.2 PGA, PGV, PGD and Displacement Drift

The PGA comparison and their percentage change are presented in Table 8-4. It is observed here that all the three methods change the original PGA.

Table 8-4 PGA Comparison

GM	Type of Ground Motion	Original Spectra Shape Similarity to Target		PGA (g)				% Difference with Original		
		D_{rms}	SSE	Original	RSPMatch	Freq Metd	Proposed	RSPMatch	Freq Metd	Proposed
1	Far Field	0.029	230	0.23	0.48	0.49	0.51	108.7	113.0	121.7
2	Far Field	0.028	88	0.25	0.42	0.42	0.57	68.0	68.0	128.0
3	Far Field	0.021	359	0.13	0.40	0.40	0.39	207.7	207.7	200.0
4	Far Field	0.028	317	0.21	0.40	0.43	0.48	90.5	104.8	128.6
5	Near Field-Pulse	0.028	36	0.41	0.40	0.34	0.43	-2.4	-17.1	4.9
6	Near Field-Pulse	0.02	8	0.50	0.51	0.45	0.53	2.0	-10.0	6.0
7	Near Field-Pulse	0.033	79	0.59	0.70	0.60	0.53	18.6	1.7	-10.2
8	Near Field-No Pulse	0.027	113	0.48	0.41	0.42	0.39	-14.6	-12.5	-18.8
9	Near Field-No Pulse	0.053	189	0.98	0.56	0.46	0.52	-42.9	-53.1	-46.9
10	Near Field-No Pulse	0.023	60	0.37	0.38	0.40	0.45	2.7	8.1	21.6
Median				0.47	0.52	0.56	0.50	30.75	35.07	34.28
Mean				0.43	0.52	0.58	0.48	55.81	59.59	68.67
Std				0.17	0.07	0.14	0.06	65.85	66.19	69.74

On a closer examination, it is observed that the PGA tends to be greater than the original on the far field ground motion cases (GM #1 to #4). For these ground motions, all the three spectral matching methods generate 50% larger PGA. In other side, the PGA generally becomes smaller on the near field ground motion cases (GM #5 to #10). It is also observed that the three methods yield minor changes in the PGA (generally less than 50%) for the near field ground motions. By comparing the spectra shape similarity, it is observed that in

general, a ground motion with a small SSE will have minor changes in the PGA during the spectral matching. One exceptional case occurs for the 1971 San Fernando, LA Store (GM #4) ground motion case. It also observed that the proposed method yields a larger change on the PGA compared to the other two methods. This may happen because the proposed method applies linear scaling to the acceleration time series.

Table 8-5 shows the PGV comparison for the three methods. It can be seen that the frequency method generates higher PGV compared to other methods. This may happen because the frequency method uses a multiplicative scaling on the Fourier amplitude spectra. It is noticed that for zero damping, the Fourier amplitude spectra are very close to the pseudo-velocity spectra. Thus, by scaling the Fourier amplitude will also change the pseudo-velocity spectra. It is also examined that the proposed method yields larger changes on the PGV compared to the RSPMatch method. This may happen because the proposed method applies linear scaling to the acceleration time series. It is hard to see the correlation between the resulted PGV and the shape similarity, but generally the selection of a ground motion with a small SSE and a small D_{rms} aid a minor change in the PGV.

Table 8-5 PGV Comparison

GM	Type of Ground Motion	Original Spectra Shape Similarity to Target		PGV (m/sec)				% Difference with Original		
		D_{rms}	SSE	Original	RSPMatch	Freq Metd	Proposed	RSPMatch	Freq Metd	Proposed
1	Far Field	0.029	230	0.29	0.46	0.83	0.63	58.6	186.2	117.2
2	Far Field	0.028	88	0.51	0.55	0.80	0.83	7.8	56.9	62.7
3	Far Field	0.021	359	0.21	0.52	0.45	0.47	147.6	114.3	123.8
4	Far Field	0.028	317	0.19	0.46	0.51	0.42	142.1	168.4	121.1
5	Near Field-Pulse	0.028	36	0.65	0.64	0.60	0.64	-1.5	-7.7	-1.5
6	Near Field-Pulse	0.02	8	0.64	0.57	0.61	0.51	-10.9	-4.7	-20.3
7	Near Field-Pulse	0.033	79	0.48	0.59	0.45	0.58	22.9	-6.2	20.8
8	Near Field-No Pulse	0.027	113	0.56	0.52	0.61	0.51	-7.1	8.9	-8.9
9	Near Field-No Pulse	0.053	189	0.46	0.48	0.43	0.55	4.3	-6.5	19.6
10	Near Field-No Pulse	0.023	60	0.29	0.40	0.46	0.37	37.9	58.6	27.6
Median				0.47	0.52	0.56	0.53	16.93	32.90	24.21
Mean				0.43	0.52	0.58	0.55	44.10	61.85	52.36
Std				0.17	0.07	0.14	0.13	55.97	70.52	49.80

The PGD comparison is presented in Table 8-6. On average, it can be seen that the frequency domain method imposes high PGD (approximately about 3 times the original PGD), while the other two methods yield minor changes on the PGD. Most of the excessive PGD on the frequency domain results are due to the base-line drift. The RSPMatch method yields a slightly change in the PGD and is better than the other methods. This is based on the fact that the RSPMatch does not apply linear scaling to the acceleration time series.

Table 8-6 PGD Comparison

GM	Type of Ground Motion	Original Spectra Shape Similarity to Target		PGD (m)				% Difference with Original		
		D_{rms}	SSE	Original	RSPMatch	Freq Metd	Proposed	RSPMatch	Freq Metd	Proposed
1	Far Field	0.029	230	0.23	0.23	1.70	0.37	0.0	639.1	60.9
2	Far Field	0.028	88	0.44	0.44	0.71	0.66	0.0	61.4	50.0
3	Far Field	0.021	359	0.08	0.14	0.99	0.17	75.0	1137.5	112.5
4	Far Field	0.028	317	0.13	0.20	0.66	0.24	53.8	407.7	84.6
5	Near Field-Pulse	0.028	36	0.28	0.23	0.66	0.25	-17.9	135.7	-10.7
6	Near Field-Pulse	0.02	8	0.22	0.22	0.25	0.19	0.0	13.6	-13.6
7	Near Field-Pulse	0.033	79	0.22	0.34	0.85	0.24	54.5	286.4	9.1
8	Near Field-No Pulse	0.027	113	0.12	0.14	0.19	0.14	16.7	58.3	16.7
9	Near Field-No Pulse	0.053	189	0.10	0.16	0.18	0.17	60.0	80.0	70.0
10	Near Field-No Pulse	0.023	60	0.08	0.11	0.59	0.12	37.5	637.5	50.0
Median				0.18	0.21	0.66	0.22	27.68	211.04	50.00
Mean				0.19	0.22	0.68	0.26	31.54	345.72	47.81
Std				0.11	0.10	0.45	0.16	28.19	364.23	35.32

In terms of the displacement drift, as already showed in the previous study, the proposed method and the RSPMatch method yield a considerable small (near zero) drift. There is one case where the RSPMatch yields non-zero drift, which is for the 1992 Mendocino, Petrolia (GM #7) ground motion. For this ground motion, the RSPMatch yields about 0.09m drift. However, the RSPMatch ver 2005b has an option to minimize (or eliminate) this drift by activating the *dtflag* option which interpolates the acceleration time histories by dividing the time increment into smaller segments. This option reduces the numerical rounding. However, since the drift is still considered realistic and the *dtflag* option is not selected on the default configuration, such feature was not used in this comparison.

The frequency domain method generally imposes a large displacement drift which in some cases are considered unrealistic. Hence, a base-line drift correction is required before using the resulted acceleration time series. Moreover, Naeim and Lew (1995) discuss that when the displacement time history is implicitly involved in structural analysis, manipulating the acceleration time histories such that it corrupts the displacement time histories possibly lead to unreasonable structural displacement and drift.

Figure 8-2 shows an example of the displacement time histories, resulted from the three spectral matching methods using the 1992 Landers, Yermo Station (GM #2) ground motion as the input. It can be seen that the RSPMatch generates minor changes to the original displacement time series. The proposed method is giving slightly larger amplitude, due to the linear scaling on the acceleration time histories during the spectral matching procedure. Moreover, although the frequency domain method is able to retain the displacement time series shape, it creates an excessive displacement drift at the end of the ground motion.

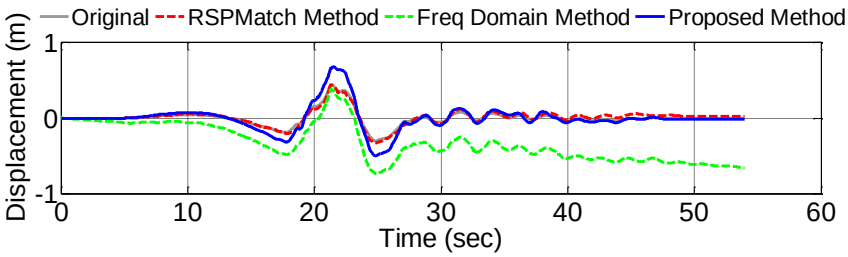

Figure 8-2 Displacement Time Histories for Spectrum-Compatible Acceleration Matching using the 1992 Landers, Yermo Fire Station Ground Motion

8.2.3 Energy Content

Table 8-7 presents the shape similarity of the original spectra to the target spectra, and the changes on the Arias Intensity. A new term was introduced here, which is the SE (sum of errors) term. The SE term is a modification of the SSE (sum of squared errors) by calculating the sum of errors between the logarithms of the original ground motion spectra and the target spectra, defined as

$$SE = \sum_{j=1}^{n} ln\, S_{atarget-j} - ln\, S_{aj}$$

where $ln\, S_{aj}$ is the log spectral acceleration of the original ground motion at period T_j, and ln $S_{atarget-j}$ is the log of target spectra. This SE term is intended to get better information whether the majority of the original spectra ordinates are under or over the target spectra and predicts the change in Arias Intensity. Positive SE implies that majority of the original spectra ordinates are under the target spectra, and vice versa. It is also noticed that the ln $S_{atarget-j}$ and ln S_{aj} may cancel out each other and yields near zero value, but not necessarily represents a good match with the target. Thus SE is not intended to be a direct measure of spectra shape similarity.

It is observed in Table 8-7 that a large SSE and SE correspond to a large change in the Arias Intensity. For instance, although the 1990 Manjil Abhar ground motion (GM #3) has a small Drms, it has a large SE value. It can be seen that the three methods yield major changes in the Arias Intensity (5 times, 11 times and 8 times of the original Arias Intensity for the RSPMatch, the frequency domain method and the proposed method respectively).

Another example is illustrated on the 1992 Landers, Yermo Fire Station (GM #2) and the 1989 Loma Prieta, Bran (GM #8) ground motions. It can be seen here although the GM #2 and GM #8 have close D_{rms} value, the GM #2 has a much larger SE term. This implies that the GM #2 has more ordinates that are under the target; hence requires more adjustments which lead to more additional energy to match the target than the GM #8 does.

It is also examined that the RSPMatch generates a minor change on Arias Intensity. This may happen due to no acceleration time series scaling is applied on the RSPMatch. On contrary, the proposed method is generating more energy than the RSPMatch method because it applies acceleration scaling during the process. It is also observed that the frequency domain generates major changes on the energy content. This is based on the fact that the frequency domain method scales the Fourier amplitude spectra.

Table 8-7 Percentage Different of Arias Intensity

GM	Type of Ground Motion	Original Spectra Shape Similarity to Target			Arias Intensity (m/sec)				% Difference with Original		
		D_{rms}	SSE	SE	Original	RSPMatch	Freq Metd	Proposed	RSPMatch	Freq Metd	Proposed
1	Far Field	0.029	230	245	0.83	2.2	4.08	2.96	165.1	391.6	256.6
2	Far Field	0.028	88	134	0.93	2.28	5.42	3.04	145.2	482.8	226.9
3	Far Field	0.021	359	314	0.65	3.07	6.98	4.87	372.3	973.8	649.2
4	Far Field	0.028	317	294	0.65	2.38	3.86	2.45	266.2	493.8	276.9
5	Near Field-Pulse	0.028	36	-6	1.49	1.96	2.79	1.97	31.5	87.2	32.2
6	Near Field-Pulse	0.02	8	-13	1.79	1.61	2.53	1.56	-10.1	41.3	-12.8
7	Near Field-Pulse	0.033	79	99	3.42	3.33	4.67	2.8	-2.6	36.5	-18.1
8	Near Field-No Pulse	0.027	113	95	5.36	3.79	3.91	2.98	-29.3	-27.1	-44.4
9	Near Field-No Pulse	0.053	189	160	4.45	2.92	2.74	1.67	-34.4	-38.4	-62.5
10	Near Field-No Pulse	0.023	60	116	1.97	3.02	4.05	2.96	53.3	105.6	50.3
Median					0.83	2.2	4.08	2.96	165.1	391.6	256.6
Mean					0.93	2.28	5.42	3.04	145.2	482.8	226.9
Std					0.65	3.07	6.98	4.87	372.3	973.8	649.2

The energy developments were being examined using the normalized Arias Intensity, which available on Appendix A. An example of the normalized Arias Intensity can be seen in Figure 8-3.

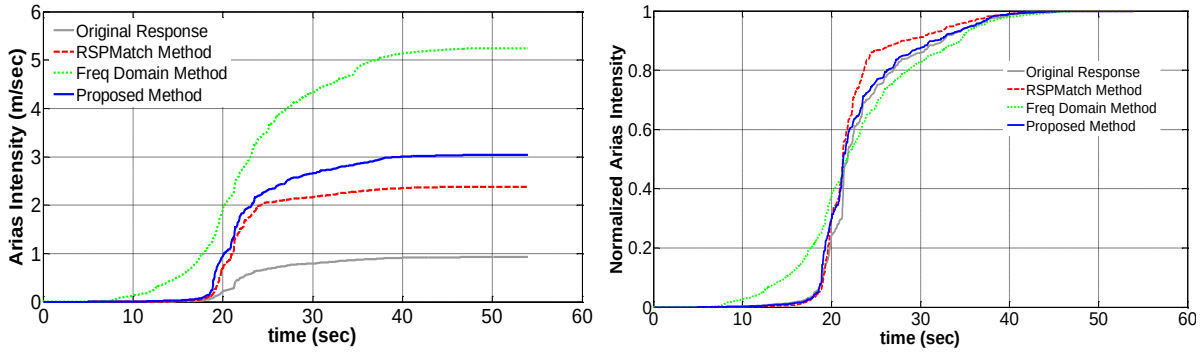

Figure 8-3 Comparison of Arias Intensity and Normalized Value for the 1992 Landers, Yermo Fire Station Ground Motion

It can be seen here that the frequency domain method tends to change not only the cumulative energy but also the energy development. For this particular ground motion, the energy development for the frequency domain method is increasing rapidly during the first 20 second followed by slower increments until the end of the ground motion.

It is also examined that for this particular ground motion, although the RSPMatch method induces a minor change on the cumulative Arias Intensity, this method changes the energy development. The change in energy development occurs between time t= 22sec to end of ground motion. This may happen because the RSPMatch employs no acceleration scaling which makes the method requires more wavelet adjustments. In the other side, the proposed method, which employs linear scaling, tends to preserve the energy development.

To examine the effect of the wavelet adjustments on the RSPMatch and the proposed methods, the wavelet acceleration adjustment and its Arias Intensity are presented on Figure 8-4. It is shown here that for this case the proposed method yields less wavelet adjustments than the RSPMatch method. The small wavelet adjustments on the proposed method induce low energy which tends to preserve the energy development.

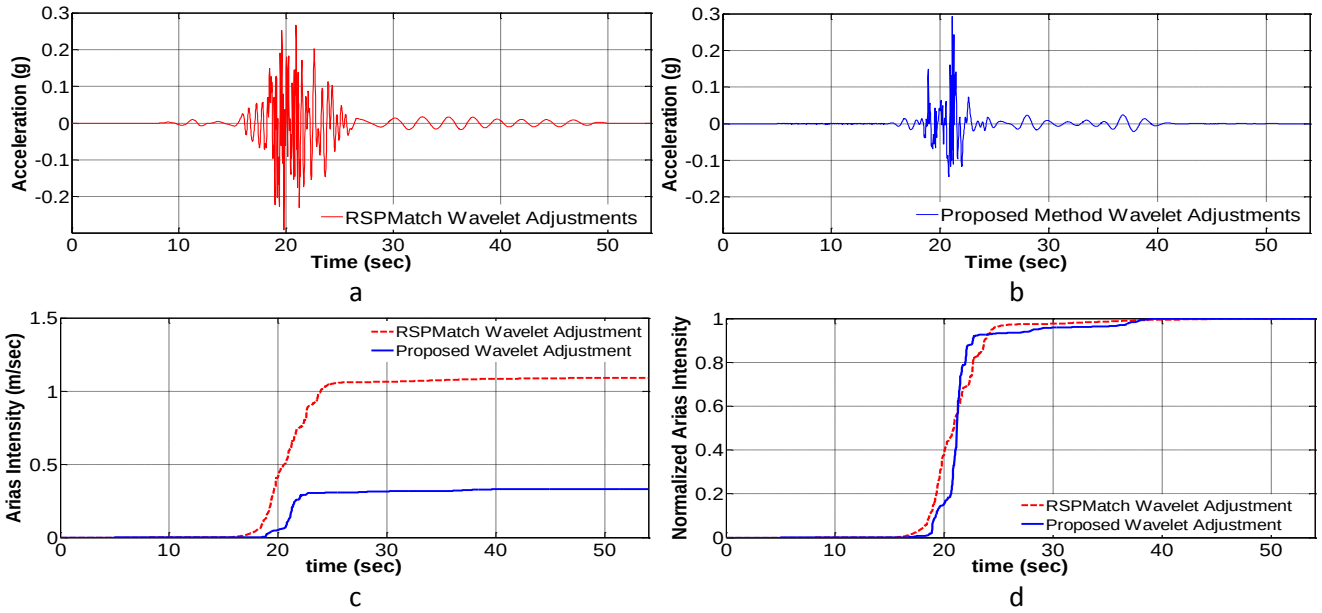

Figure 8-4 Comparison of Wavelet Adjustment and the Induced Energy
(a) Wavelet Adjustment from RSPMatch Method, (b) Wavelet Adjustment from Proposed Method,
(c) Arias Intensity, (d) Normalized Arias Intensity

From the previous discussion, it is noticed that the acceleration time series scaling is affecting the energy development. Here a study was conducted to examine this matter. For this reason, the scaling option on the RSPMatch was selected and results are being compared in Figure 8-5 and Table 8-8.

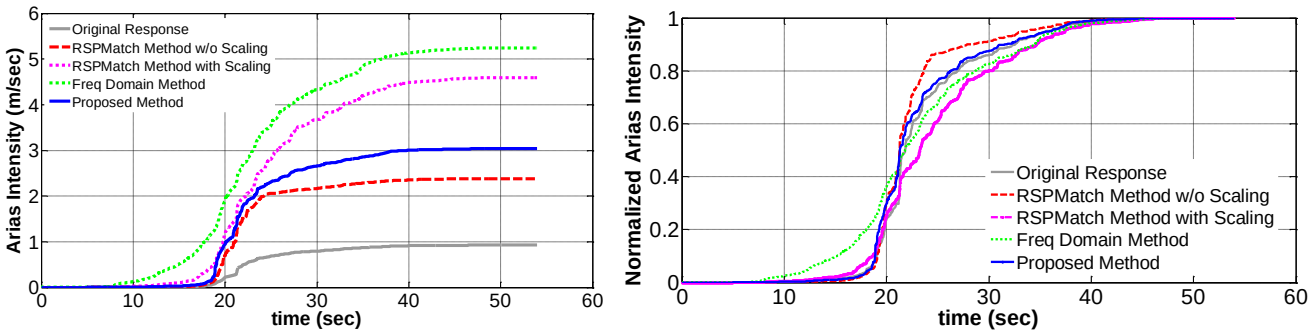

Figure 8-5 Comparison of Arias Intensity and Normalized Arias Intensity for the 1992 Landers, Yermo Fire Station Ground Motion with Scaling on RSPMatch

It can be seen that with the implementation of acceleration scaling, the RSPMatch method amplifies the total cumulative Arias Intensity (about 5 times the original), which is larger than if the scaling option was off. However, this Arias Intensity is smaller than on the frequency domain method. For this particular ground motion, the RSPMatch with the scaling also changes the energy development. However, unlike when the scaling is off, the energy development is smoother.

Table 8-8 Result Comparison for Landers, Yermo Fire Station Ground Motion

Methods	Average Misfit (g)	Max Misfit (g)	Displ. Drift (m)	PGA (g)	PGV (m/sec)	PGD (m)	Arias Intensity (m/sec)
Original				0.23	0.51	0.44	0.93
RSPMatch w/o Scaling	0.0082	0.2134	0.03	0.42	0.55	0.44	2.28
RSPMatch with Scaling	0.0109	0.1189	0.02	0.44	1.34	1.15	4.58
Freq. Domain	0.0120	0.1690	-0.64	0.42	0.80	0.71	5.42
Proposed Method	0.0137	0.0832	-0.01	0.57	0.83	0.66	3.04

8.2.4 Frequency Content

The frequency content preservation on acceleration and displacement time series were being quantified by comparing the wavelet coefficient spectrogram as described by Eqn. 7.16. Table 8-9 presents the comparison of the frequency content correlation between the original ground motions and the modified ones. It is observed that both the proposed method and the RSPMatch method are able to preserve the frequency contents better than the frequency domain method.

It is also noticed that for some ground motions, the three spectral matching methods failed to preserve the frequency content. It is suspected that the shape similarity between the ground motion spectra with the target spectra is affecting the frequency content preservation. Likewise the Arias Intensity comparison, spectra shape similarity were being quantified using $D_{rms,}$ SSE and SE terms as showed in Table 8-9.

It can be seen that the SSE terms are affecting the frequency content preservation, especially for the acceleration time series. The frequency contents are better preserved for a ground motion with a small SSE. For example, the 1979 Imperial Valley-1, El Centro Array 6 (GM #5) and the 1992 Erzican, Erzican (GM #6) ground motions have SSE value of 36 and 8 respectively. It is observed that by using the RSPMatch and the proposed method, the coefficient of correlation (*r*) for these ground motions are greater than 0.9. The proposed method coefficient of correlation even reaches 0.981 for GM #6, which implies the frequency content was only slightly altered.

Table 8-9 Comparison of Correlation on Frequency Content for 3 Spectral matching Methods

GM	Type of Ground Motion	Original Spectra Shape Similarity to Target			Coefficient of Correlation for Acceleration			Coefficient of Correlation for Displacement		
		D_{rms}	SSE	SE	RSPMatch	Freq Metd	Proposed	RSPMatch	Freq Metd	Proposed
1	Far Field	0.029	230	245	0.825	0.828	0.861	0.873	0.275	0.949
2	Far Field	0.028	88	134	0.838	0.796	0.855	0.929	0.703	0.971
3	Far Field	0.021	359	314	0.667	0.583	0.840	0.925	0.619	0.975
4	Far Field	0.028	317	294	0.802	0.819	0.876	0.913	0.827	0.979
5	Near Field-Pulse	0.028	36	-6	0.914	0.856	0.928	0.973	0.696	0.974
6	Near Field-Pulse	0.020	8	-13	0.976	0.930	0.980	0.992	0.970	0.995
7	Near Field-Pulse	0.033	79	99	0.876	0.770	0.830	0.968	0.424	0.950
8	Near Field-No Pulse	0.027	113	95	0.796	0.758	0.793	0.932	0.967	0.931
9	Near Field-No Pulse	0.053	189	160	0.690	0.604	0.708	0.825	0.782	0.908
10	Near Field-No Pulse	0.023	60	116	0.862	0.824	0.863	0.889	0.646	0.850
Median					0.832	0.808	0.858	0.927	0.700	0.961
Mean					0.825	0.777	0.853	0.922	0.691	0.948
Std					0.094	0.108	0.073	0.050	0.219	0.043

It is observed that D_{rms} terms are affecting the frequency content preservation. For instance, although the 1971 San Fernando LA, Hollywood Store (GM #4) ground motion has much larger SSE than the 1985 Nahanni, Station 1 (GM #9), the frequency content is better preserved on GM #4. This is based on the fact that the GM #4 has a better spectra shape similarity than the GM #9 (the D_{rms} of GM #4 and #9 are 0.028 and 0.053 respectively). Note that the D_{rms} implies the target similarity while the SSE implies the spectra ordinate differences. The spectra shape comparison is presented in Figure 8-6. It can be seen here that although the GM #4 has more ordinate errors, it has more similarity to the target than the GM #9 has. Matching a ground motion which spectra has a high dissimilarity to the target tends to cause a major change in the frequency content.

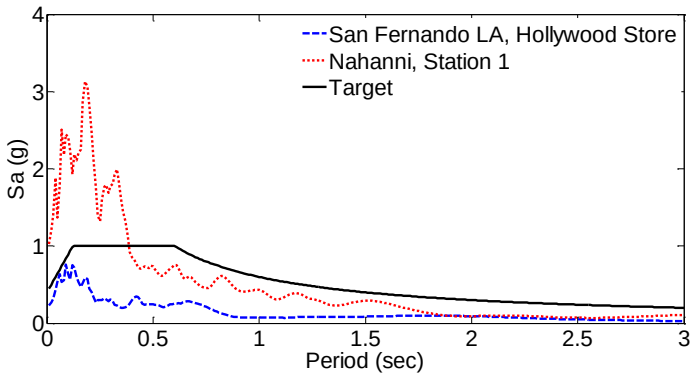

Figure 8-6 Response Spectra Comparison for San Fernando LA, Hollywood Store and Nahanni, Station 1

Table 8-9 also shows that the linear scaling on the acceleration time series aids to preserve the frequency content. The 1990 Manjil, Abhar ground motion (GM #3) gives a clear example for this. It can be seen that for this ground motion, the proposed method preserves the acceleration frequency content better than other methods. This may happen because the GM #3 has a large spectra misfit (indicates by large SSE and SE). Hence, by employing an acceleration scaling, the proposed method reduces the misfit and requires less adjustments. The frequency contents are not well preserved in the frequency domain method simply because this method applies multiplicative scale factors on the Fourier amplitude spectra.

The study also shows how important is the ground motions selection in the spectral matching method. A ground motion that is considered not appropriate (in terms of magnitudes, fault characteristic, fault distance, site condition and spectra shape) may lead to a major change on the original time histories. A clear example is given by the 1985 Nahanni, Station 1 ground motion (GM #9) where all the three methods failed to preserve the frequency content. This failure is affected by both D_{rms} and the SSE. It was discussed before that the GM #9 has a low spectral shape similarity to the target. The spectra responses of modified GM #9 resulted from the three methods are presented in Figure 8-7. The modified acceleration, velocity and displacement time series for GM #9 are presented in Figure 8-8. It can be seen here that the three methods give major changes on the original time histories.

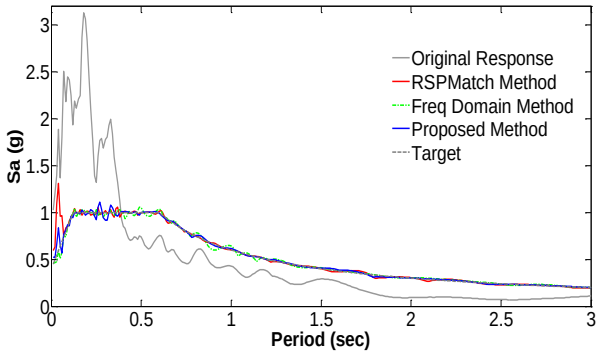

Figure 8-7 Time Series Comparison using 3 Spectral matching Methods for Nahanni, Station 1 Ground Motion

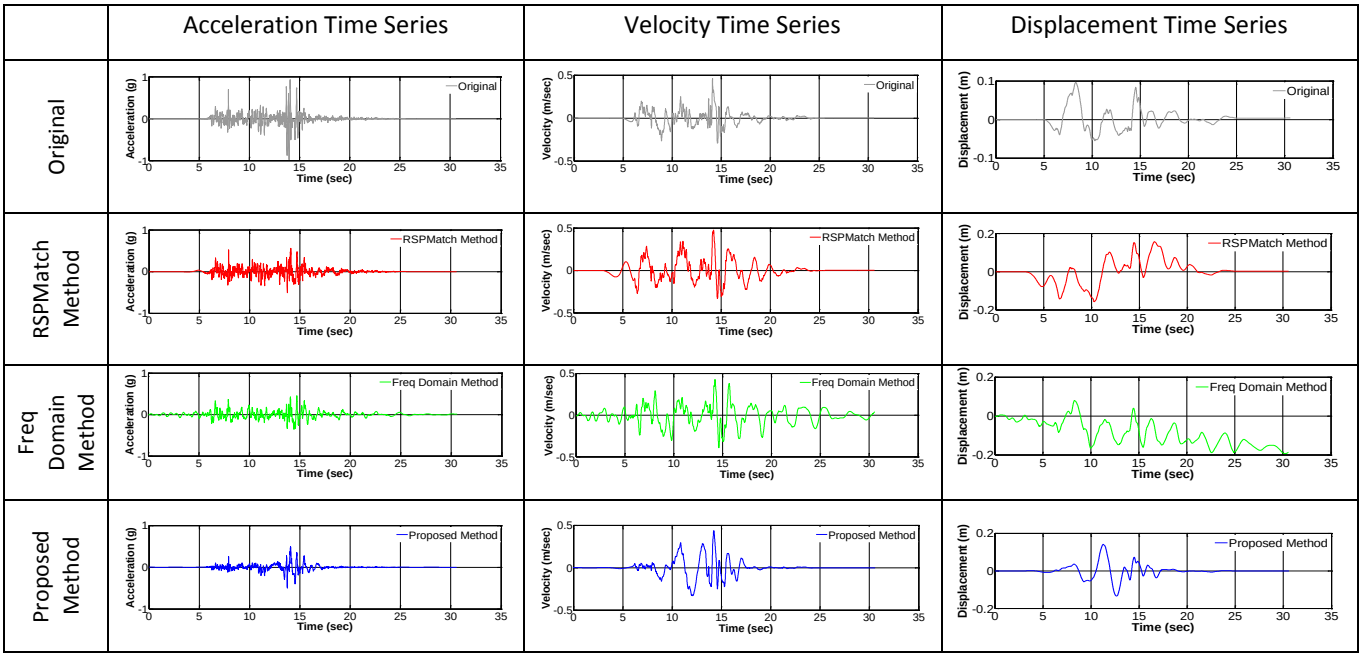

Figure 8-8 Time Series Comparison using 3 Spectral matching Methods for Nahanni, Station 1 Ground Motion

CHAPTER 9. SUMMARY, CONCLUSION AND RECOMMENDATION

9.1 Introduction

There are many approaches to obtain suitable acceleration time histories. If available, the engineer can use set of several recorded ground motions with appropriate magnitudes, fault characteristics, fault distance, and site conditions that are consistent with those that control the maximum considered earthquake for a site. However, there are few regions of the world where sets of recorded acceleration time histories are available with a wide range of site and source characteristics. It can therefore be desirable to either scale the existing ground motions or develop artificial earthquake acceleration time histories.

The most widely used approaches for creating spectrum-compatible ground motions are by generating artificial ground motions from white noise, and the use of manipulated real acceleration time histories. Creating artificial ground motions from white noise has a drawback in which the artificial acceleration time histories may have large number of cycles and thus possess very high energy content. Conversely, by using the real strong ground motions and applying some adjustments to match the target spectra, the modified acceleration time series tend to be more realistic.

One method that uses the real acceleration time series which is commonly employed is the spectral matching in the frequency domain. This method adjusts the Fourier amplitude spectra while keeping the Fourier phase spectra. However, adjusting the Fourier amplitude spectral may corrupt the velocity and displacement time histories, and the spectrum compatible acceleration time series tends to have very high energy.

An alternative approach of spectral matching is in the time domain by adding wavelets to the acceleration time histories. Adding discrete length wavelets to the acceleration records tends to preserve the non-stationary character of the original time histories.

9.2 Summary

This thesis presents and develops a proposed algorithm for spectral matching using wavelets coupled with the Broyden updating method. The main idea is to solve the spectral matching equations as a nonlinear system, by using the Broyden updating method. The nonlinearity comes from shifting in the time of peak response as the acceleration time histories are altered. The proposed method accounts for this nonlinearity by allowing the time of peak response to be shifted.

To be able to apply the Broyden method to spectral matching, the calculated spectral sensitivity matrix, *C* has to locate the peak response, regardless of the time it occurs. This is one of the main differences between the proposed method and the existing RSPMatch method.

A parametric study was carried out to obtain good set of several gain factors in the proposed algorithm that reduce the misfit and computational time. These gain factors include the gain factor on initial *C* matrix (α_C), the wavelet magnitude (ψ_M), the off-diagonal terms of *C* matrix reduction ($\alpha_{off\text{-}C}$), the gain factor on vector *b* updating (g_b) and the gain factor on *C* matrix updating (g_b). The efficient number of the outer-loop and the Broyden iterations were also been studied numerically. The parametric study was conducted using 10 different ground motions taken from FEMA P-695 list; contains 4 far field ground motions, 3 near field-pulse ground motions and 3 near field-no pulse ground motions. The criteria used to select the gain factors were the computational time, the average misfit and the maximum misfit. Both mean and standard deviation of each criteria were observed in the study.

The thesis also discusses the existing wavelet bases that were expected to be compatible in the procedure. The existing wavelet bases that were studied are the Lillhanand and Tseng wavelet, the tapered cosine wavelet, the corrected tapered cosine wavelet, the Morlet wavelet, the Mexican Hat wavelet, the Shannon wavelet and the Suarez and Montejo wavelet. To examine which wavelet base is giving better stability and efficiency in the algorithm, some characteristics of wavelet bases were observed including the frequency resolution, the time resolution, the off-diagonal terms of *C* matrix, the baseline drift as the products of wavelet integration, and also the ability to analytically integrate the wavelet.

After the wavelet base characteristics were compared, three candidates of wavelet bases were implemented in the proposed algorithm. The ground motion inputs were the same ten ground motions as used in the parametric study. The computational time, the misfit, the baseline drift, the PGA, PGV, PGD, the Arias Intensity and the frequency content were being compared. The preservation of the frequency contents were quantified using the Pearson's coefficient correlation of the modified wavelet spectrogram with the original. Both the frequency content of the acceleration and the displacement time series were compared. Based on this comparison, the corrected tapered cosine wavelet was selected to be used in the algorithm.

The proposed method was compared with the two other spectral matching methods that are commonly employed; the RSPMatch method in time domain and the frequency domain method. The comparing parameters were the same with the previous wavelet base study. The RSPMatch method was executed using RSPMatch ver. 2005b using the default configuration. The frequency domain method was executed using MyRattle software. The ground motion inputs were the same ten ground motions as used in the parametric

study. To reduce distortion and minimized the change of baseline drift, the ground motions were 5 sec zero padded at the beginning and end.

9.3 Conclusion

The spectral matching procedure is at its core a nonlinear problem, thus a nonlinear solving method was employed in the proposed algorithm. The Broyden updating method was selected as the nonlinear solving method because it does not require a differentiation analysis and it makes use of how much the *b* vector affect the misfit to update the spectra sensitivity *C* matrix. In the proposed method, the Broyden updating is coupled with wavelet functions to match the target spectra in the time domain. The main differences between the proposed method with the RSPMatch method is that it allows the time of peak response to be shifted and the *C* matrix locates the peak response, regardless of time it occurs.

It was also observed that the calculation efficiency is sensitive to the initial solution guess (initial vector *b*) and also several factors on the *C* matrix and inside the Broyden updating procedure. A high initial *C* matrix was selected to aid the algorithm not to overshoot the solution during the initial Broyden iterations. The initial *b* was calculated using the linear relationship between *b* vector and spectra misfit $S_{amisfit}$.

Based on the wavelet bases study, it was observed that the off-diagonal terms of the *C* matrix are affecting the solution nonlinearity. Ideally, these terms should be as small as possible to minimize the cross-correlation of wavelet adjustment. The reduction factor on these terms can be applied as consequences of losing the solution accuracy, due to under estimating the cross correlation of wavelet adjustments.

There were three candidates of the existing wavelet bases being studied that generate zero baseline drift and considered compatible with the proposed algorithm; the corrected tapered cosine wavelet, the Morlet wavelet and the Mexican Hat wavelet. The three wavelet bases were implemented in the algorithm and were used to match 10 ground motions taken from FEMA P-695. The corrected tapered cosine wavelet was selected based on the comparison.

The proposed method has been implemented and shows it capability to match the target within the given tolerance level. In term of computational efficiency, the proposed method requires longer time than the RSPMatch method. This may indicate there is some further room for improvement to the programming efficiency of the code or it may be related to computational efficiency of a compiled program versus a program running in the Matlab environment. It is expected that an efficient equation to analytically calculate the *C* matrix would make the proposed method runs faster. The calculation method of the initial *b* vector and initial *C* matrix are also affecting the computational time.

Using the 10 different ground motions, the proposed method yields an average misfit of 0.011g which is considerable close value compare to the other two methods (0.011g for the RSPMatch with default configuration and 0.013g for the frequency domain method). Based on the result, no baseline drift correction is needed on the resulted spectrum compatible acceleration time series.

The study also shows how important the ground motions selection is in spectral matching. A ground motion that is considered not appropriate in terms of magnitudes, fault characteristic, fault distance, site condition and spectra shape, may require the spectral matching procedure to generate major changes on the original time histories. The spectra shape can be quantified by D_{rms} and SSE terms to select appropriate ground motions that has good match with the target spectra.

The fact that the proposed method applies linear scaling to the time histories in between the Broyden loops, it is observed that the proposed method changes the cumulative Arias Intensity. Depends on the spectral shape similarity to the target, the proposed method yields an average change of 227% on the Arias Intensity. This value is larger than the RSPMatch (145%), which applies no scaling on the acceleration time series, but is smaller than the frequency domain method (483%).

In terms of preserving the frequency content, it was observed that depends on the D_{rms} and SSE terms of the original ground motion, the proposed method is generally able to preserve the frequency content of the acceleration and displacement time series (r = 0.853 and 0.948 respectively). These values are slightly better than the RSPMatch method (r = 0.825 and 0.922) and better than the frequency domain method (r = 0.777 and 0.691 respectively).

9.4 Recommendations

The following are some of the recommendations for future research to further develop the proposed spectral matching algorithm.

a. The fact that a reduction factor is being applied to the C matrix to provide calculation stability is a brief indication for future research to study on a new/existing wavelet base that has small value of the off-diagonal terms of C matrix yet has functional form that is readily integrate to zero velocity and displacement.
b. Expand the algorithm to simultaneously match 2 components of the same ground motion and recording station. This approach can match the maximum direction spectra or the geo-mean spectra target.
c. Expand the algorithm to simultaneously match several damping levels.

d. Compare the variability of a structure response as subjected to the spectra compatible time series with a structure response as subjected to the original time series that are linearly scaled. Compare the level of safety in design.

e. Study the convergence behavior between linearly spaced and logarithmic spaced periods set. Analyze how spectral matching methods fit the periods not in the matched set.

f. Compared the Arias Intensity after linear scaling and after spectral matching. Does adding wavelets always add energy to the original ground motions (increase the Arias Intensity)?

g. Study more strategic choices for period set based on the ground motions and target spectra, i.e. selected periods based on maximum misfit in a period band.

REFERENCES

ASCE 7-10, 2010, “Minimum Design Load for Building an Other Structures,” ASCE/SEI.

Abrahamson, N. A.,1992, “Non-stationary Spectral Matching,” Seismological Research Letters 63, 30.

Al Atik, L. and Abrahamson, N. A., 2010, “An Improved Method for Nonstationary Spectral Matching,” Earthquake Spectra 26 No. 3, 601-89.

Amiri, G.G. and Asadi, A., 2010, “Generating an Artificial Ground Motion Using (RBF) Neural Network And Wavelet Analysis,” 9th U.S. National and 10th Canadian Conference on Earthquake Engineering, 222.

Baker, J. W., 2011, “Conditional Mean Spectrum: Tool for Ground Motion Selection,” ASCE Journal of Structural Engineering (in press)

Bommer, J. and Acevedo, A.B., 2004, “The Use of Real Earthquake Accelerogram as Input to Dynamic Analysis,” Journal of Earthquake Engineering Vol 8, Special Issues 1 (43-91).

Broyden,C.G., 1965,“ A Class of Methods for Solving Nonlinear Simultaneous Equations,” Mathematics of Computation, Vol. 19, No. 92, 577-593.

FEMA, 2009, NEHRP Recommended Provisions for Seismic Regulations for New Buildings and other Structures. FEMA P695, “Quantification of Building Seismic Performance Factors.”

Goupillaud, P., Grossmann, A., Morlet, J., 1984. “Cycle-octave and Related Transforms in Seismic Signal Analysis,” Geoexploration 23:85-105

Hancock, J. et al, 2006, “An Improved Method of Matching Response Spectra of Recorded Earthquake Ground Motion using Wavelets,” Journal of Earthquake Engineering 10 (Special Issues 1), 67-89.

Haselton, et. al (2012), “Selecting and Scaling Earthquake Ground Motions for Performing Response-History Analyses”, 15th World Conference on Earthquake Engineering.

Kopecky, K.A.,2007, “Root Finding Methods”

Lilhanand, K. and Tseng, W. S., 1987, “Generation of Synthetic Time Histories Compatible with Multiple Damping Response Spectra,” SMiRT-9, Lausanne K2/10.

Lilhanand, K., and Tseng, W.S., 1988, “Development and Application of Realistic Earthquake Time Histories Compatible with Multiple Damping Response Spectra,” 9th World Conference on Earthquake Engineering, Tokyo, Japan, Vol 2, 819–824.

Mallat, S.G., 1999, “A Wavelet Tour of Signal Processing”, second ed. Academic Press, London, United Kingdom.

Manual for Program: RSPMatch2005, 2005

Mathematica 8 Documentation Centre, 2011, Wolfram Research Inc

Matlab, 7.9 (R2009a). “The Language of Technical Computing.” The Mathworks,Inc.

Morlet, J.,1981, “Sampling Theory and Wave Propagation,” Proc. 51st Annual Meet. Soc. Explor.Geophys., Los Angeles

Morlet, J.,1983, “Sampling Theory and Wave Propagation,” NATO ASI, Vol. F1, Issues on Acoustic Signal-Image Processing and Recognition, ed. C. H. Chert. Berlin: Springer

Naeim, F. and Lew, M., 1995, “On the Use of Design Spectrum Compatible Time Histories,” ASCE Journal of Structural Engineeering 110, 1533-1548.

Nakhaeim M. and Mohraz, B., 2010, “Damage-Based Spectral Matching,” 9th U.S. National and 10th Canadian Conference on Earthquake Engineering, 685.

Naga, P., 2010, “Analyzing the Effect of Moving Resonance on Seismic Response of Structures Using Wavelet Transforms,” Thesis, Virginia Polytechnic Institute and State University.

NIST, 2011, NIST GCR 11-917-15, “Selecting and Scaling Earthquake Ground Motions for Performing Response-Histories Analyses”

Preumont, A., 1984, “The Generation of Spectrum Compatible Accelerograms for the Design of Nuclear Power Plants,” Earthquake Eng. Struct. Dyn. 12, 481–497.

Shahbazian, A., and Pezeshk, S., 2010, “Improved Velocity and Displacement Time Histories in Frequency Domain Spectral-Matching Procedures,” Bulletin of the Seismological Society of America, Vol. 100, No. 6, 3213–3223,

Shama, A., 2012, “Spectrum Compatible Earthquake Ground Motions by Morlet Wavelet,” 20th Analysis & Computation Specialty Conference, ASCE.

Silva, W. J. and Lee, K., 1987, “WES RASCAL Code for Synthesizing Earthquake Ground Motions,” State-of-the-Art for Assessing Earthquake Hazards in the United Stated, Report 24, Miscellaneous Paper S-73-1. US Army Corps of Engineers, Vicksburg, Mississippi.

Suarez, L.E. and Montejo, L.A., 2005, “Generation of Artificial Earthquakes via the Wavelet Transform,” International Journal of Solids and Structures 42 (2005), 5905–5919.

Watson-Lamprey, J. and Abrahamson, N.A., 2006, “Selection of Ground Motion Time Series and Limits on Scaling,” Soil Dynamics and Earthquake Engineering 26, 477–482.

Yang, U. M., 1995, “A Family of Preconditioned Iterative Problem Solvers for Sparse Linear Systems”, Ph.D Thesis, University of Illinois at Urbana Champaign.

Zhou, Z., and Adeli, H., 2003, "Time-Frequency Signal Analysis of Earthquake Records Using Mexican Hat Wavelets," Computer Aided Civil and Infrastructure Engineering,” 18(5), 379-89

APPENDIX A. RESULTS COMPARISON

Hector Mine, Hector. 1999. M7.1, Component 000

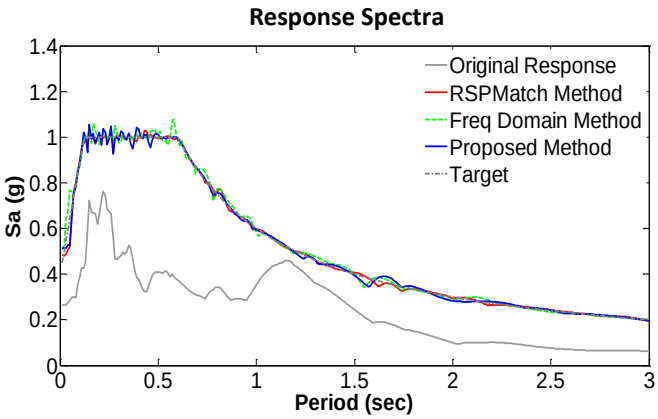

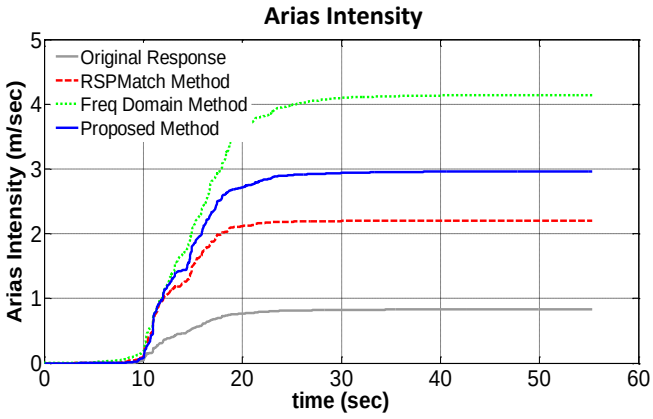

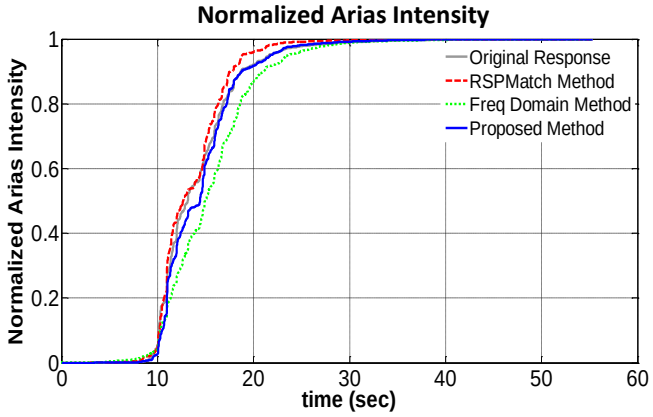

Summary

Method	Comp. Time (sec)	Average Misfit (g)	Maximum Misfit (g)	Displ Drift (m)
RSPMatch	11	0.0056	0.0731	0
Freq Method	28	0.0112	0.0820	1.69
Proposed Method	26	0.0088	0.0733	0

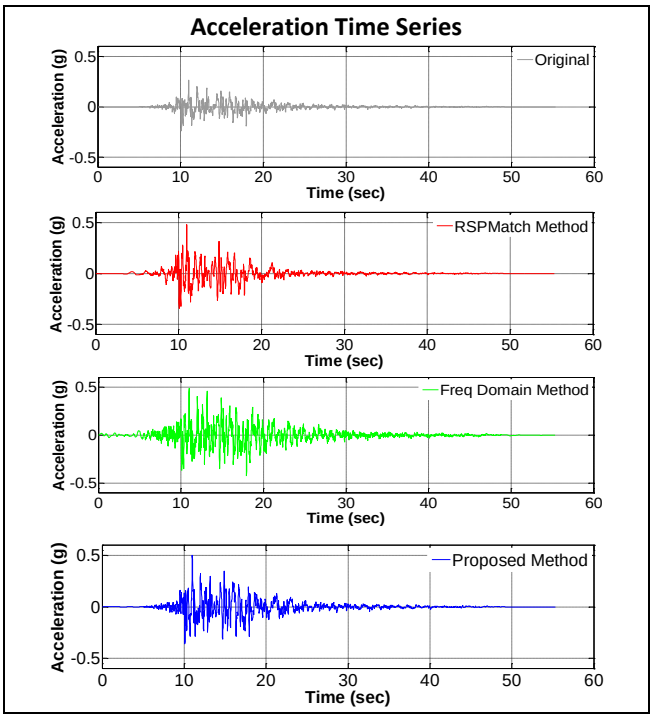

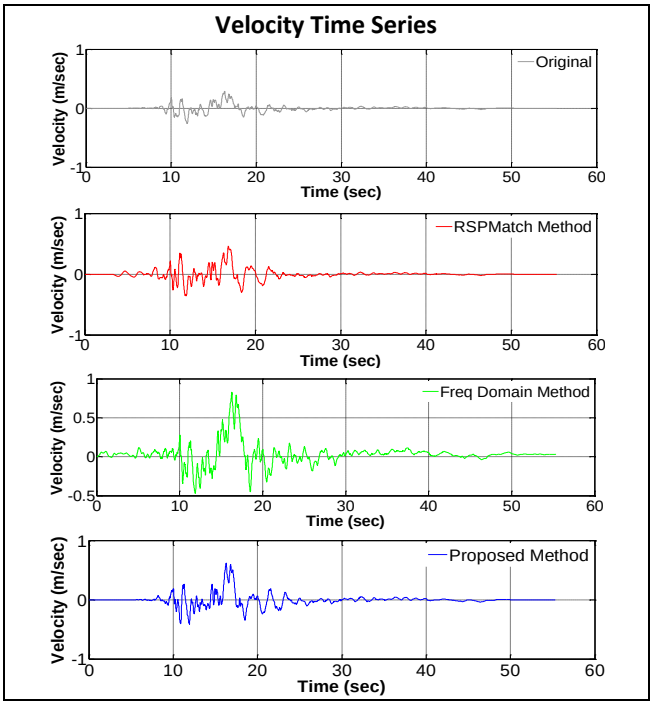

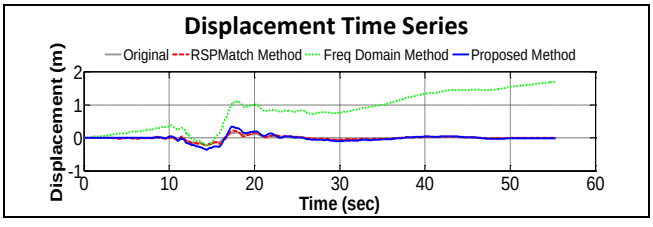

	Wavelet Coefficient of Acceleration Time Series	Wavelet Coefficient of Displacement Time Series
Original	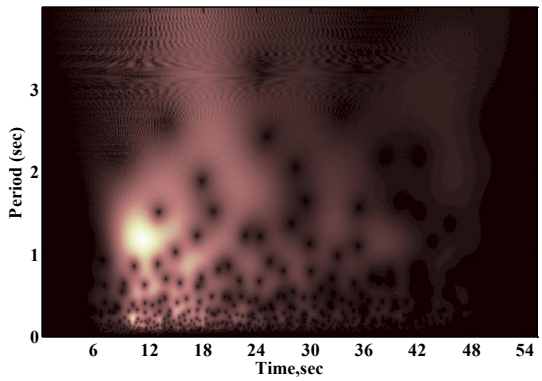	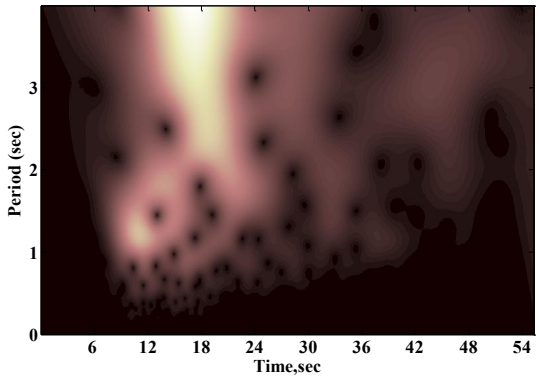
RSPMatch Method	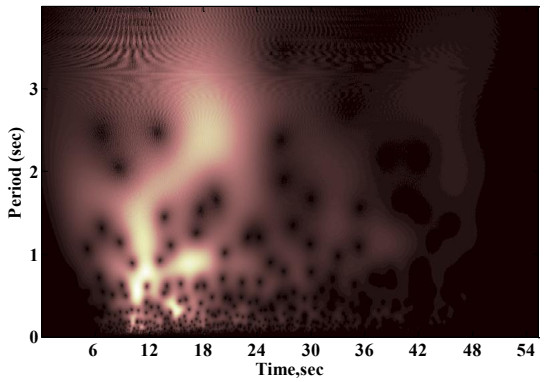	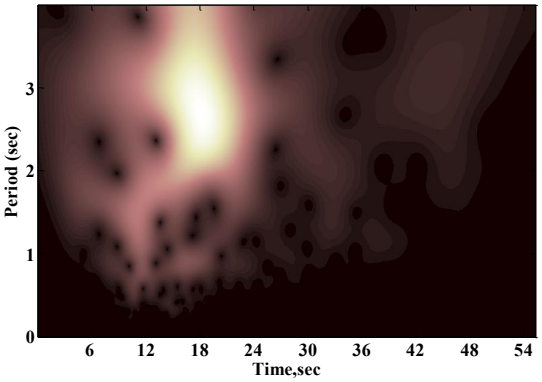
Freq Domain Method	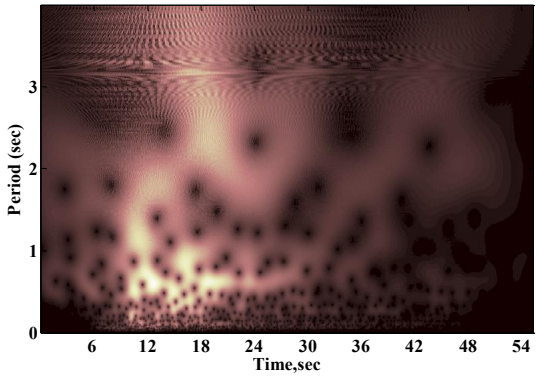	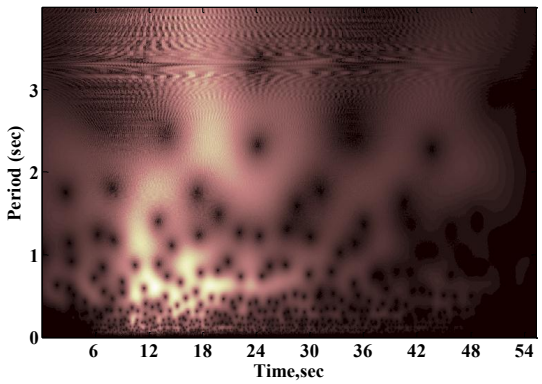

Proposed Method	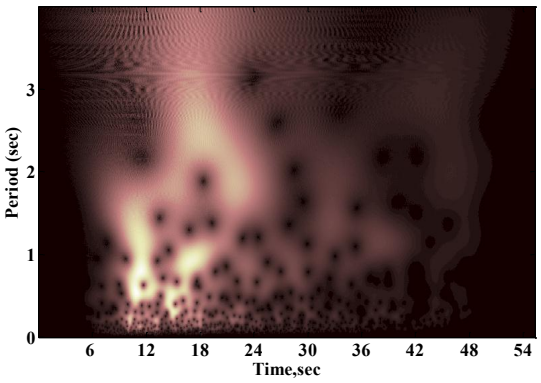	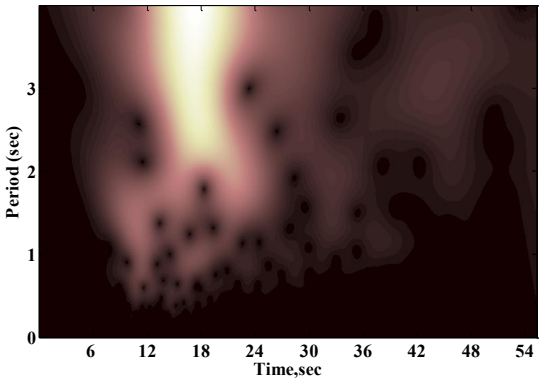

Lander, Yermo Fire Station. 1992. M7.2, Component 270

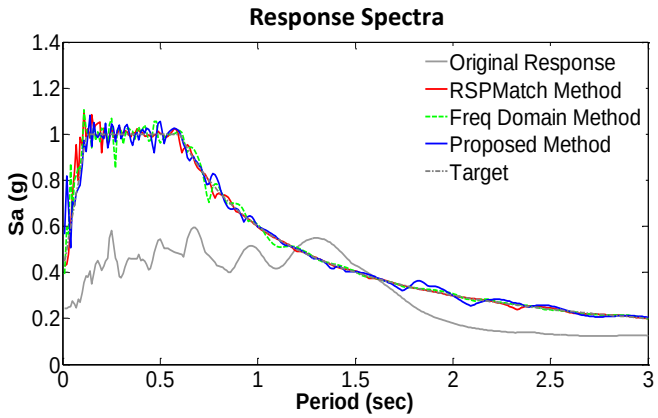

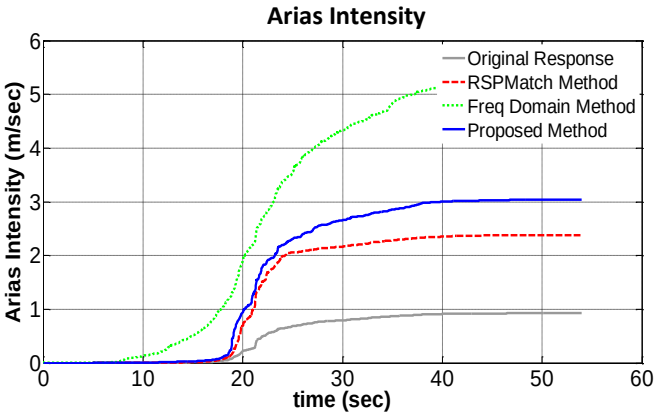

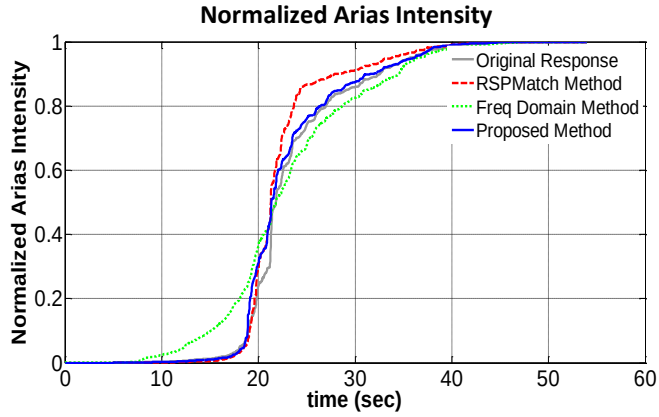

Summary

Method	Comp. Time (sec)	Average Misfit (g)	Maximum Misfit (g)	Displ. Drift (m)
RSPMatch	21	0.0082	0.2134	0.03
Freq Method	32	0.0120	0.1690	-0.64
Proposed Method	18	0. 0137	0.0832	-0.01

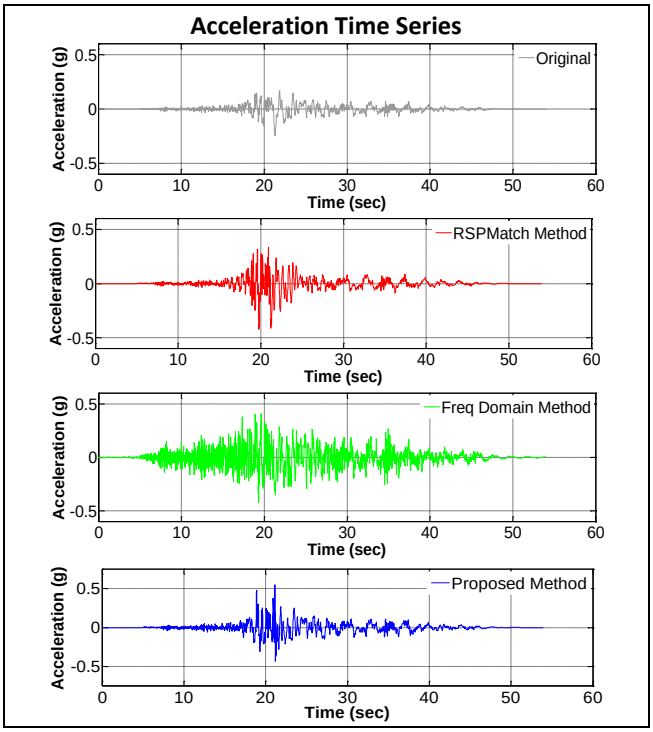

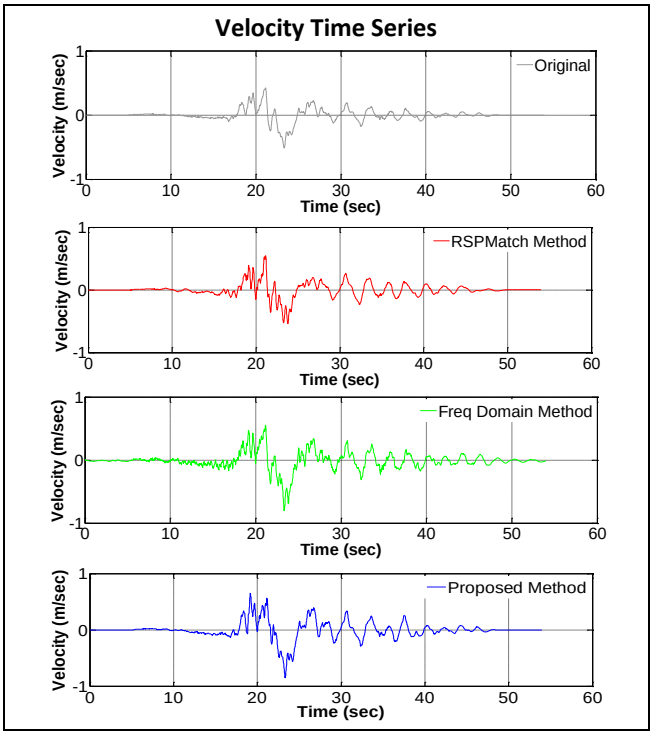

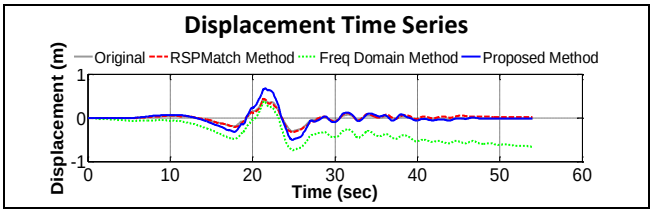

	Wavelet Coefficient of Acceleration Time Series	Wavelet Coefficient of Displacement Time Series
Original	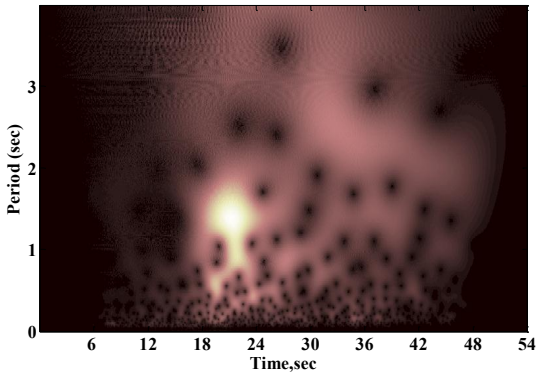	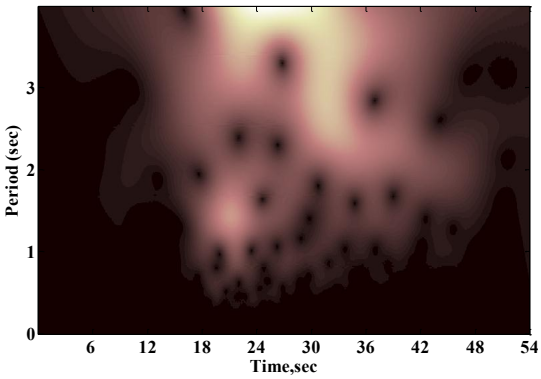
RSPMatch Method	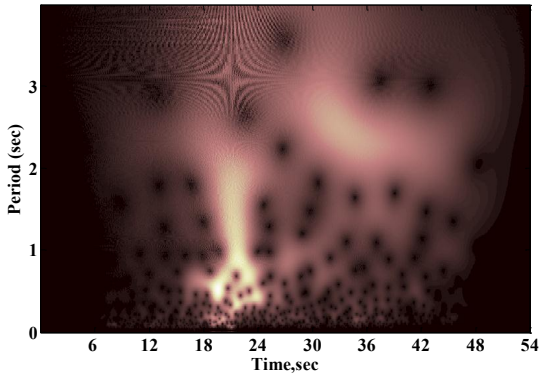	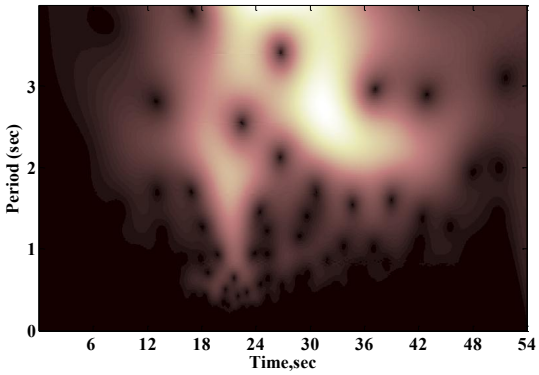
Freq Domain Method	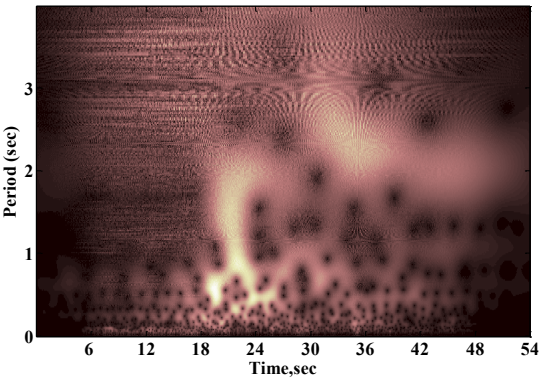	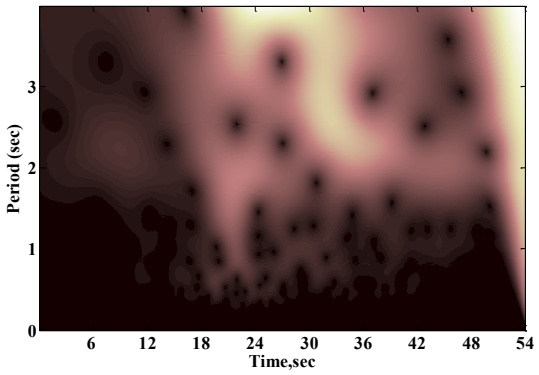
Proposed Method	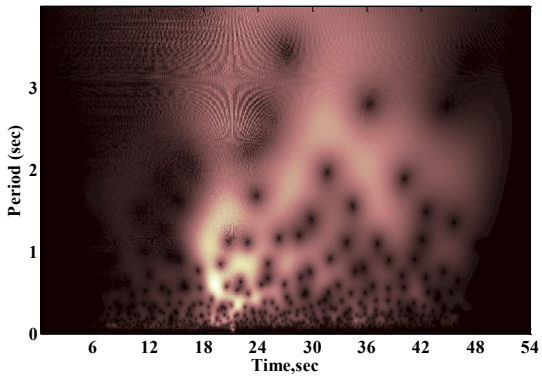	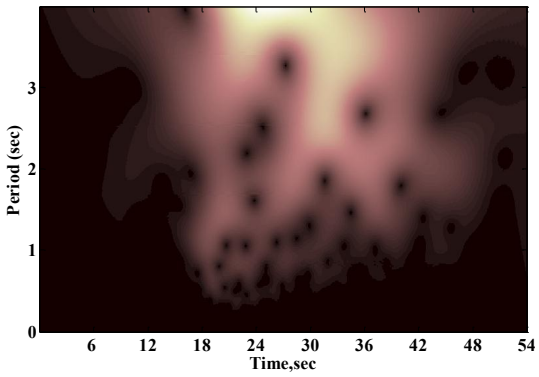

Manjil Iran, Ahbar. 1990. M7.4, Component 057

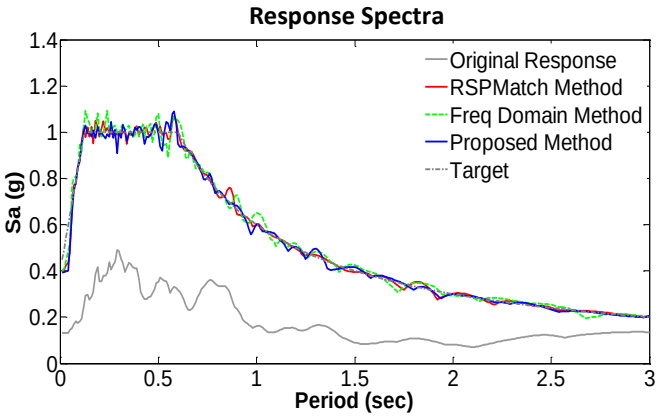

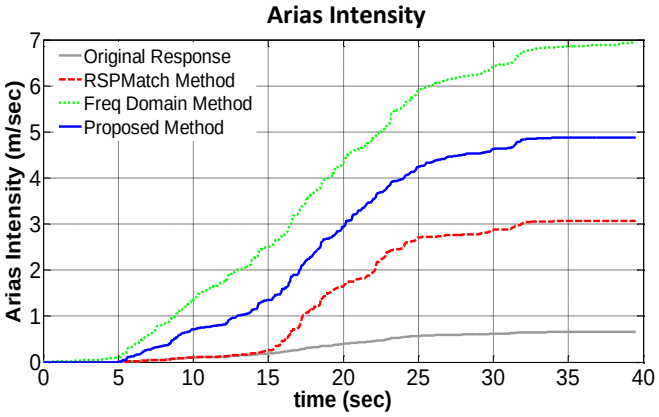

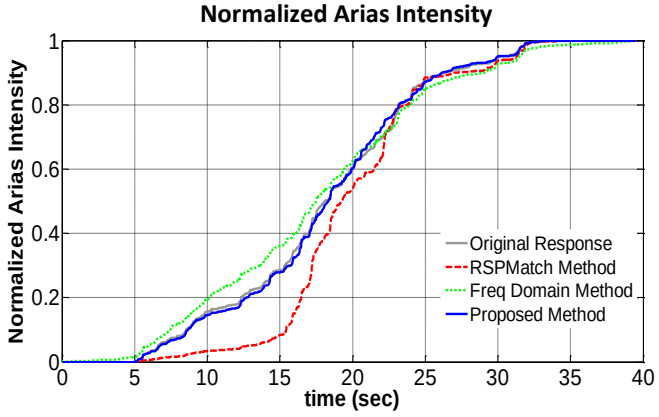

Summary

Method	Comp. Time (sec)	Average Misfit (g)	Maximum Misfit (g)	Displ Drift (m)
RSPMatch	10	0.0103	0.0683	-0.01
Freq Method	21	0.0176	0.1100	-0.98
Proposed Method	19	0.0113	0.0912	-0.01

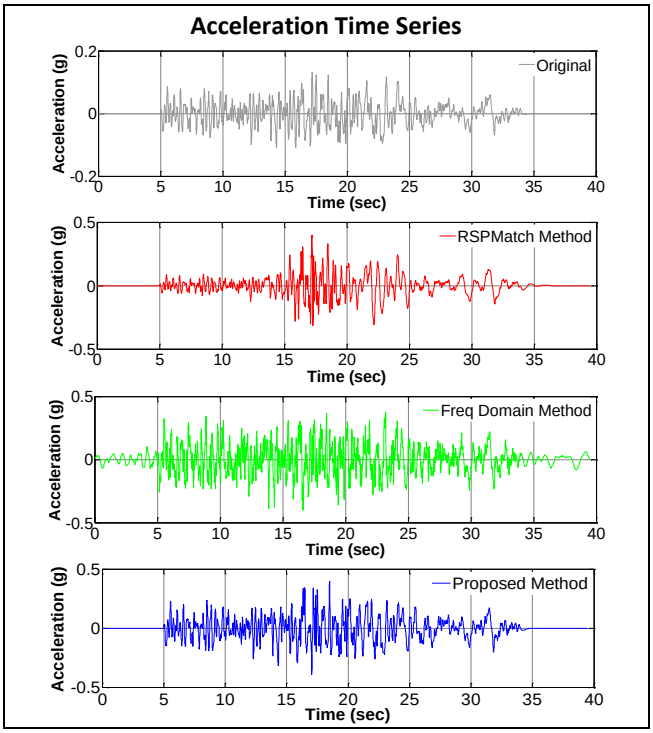

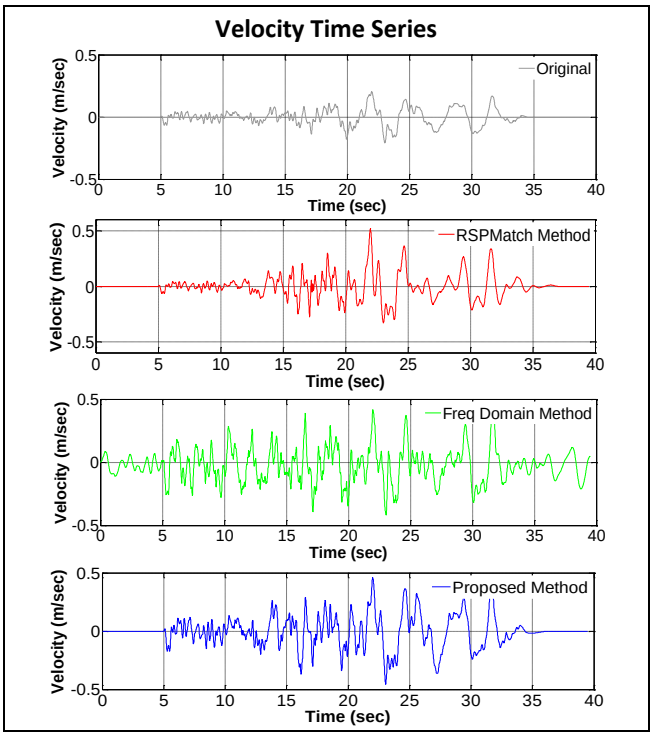

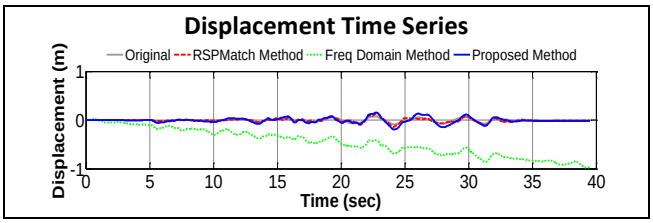

	Wavelet Coefficient of Acceleration Time Series	Wavelet Coefficient of Displacement Time Series
Original	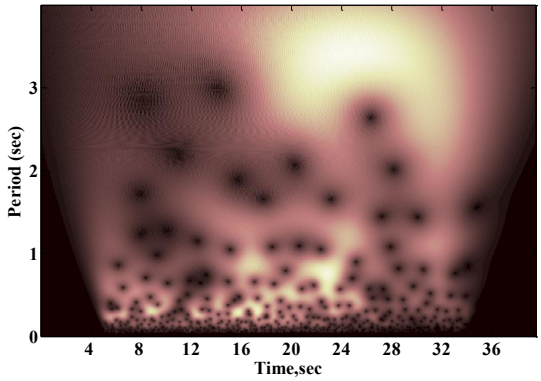	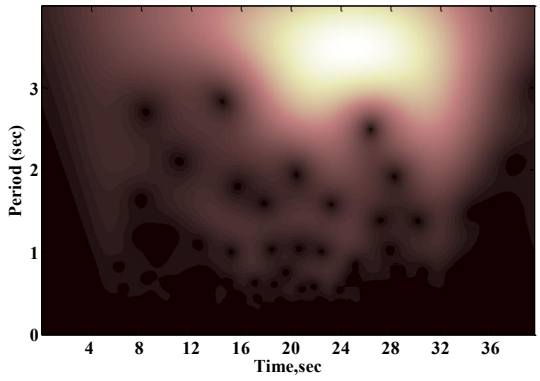
RSPMatch Method	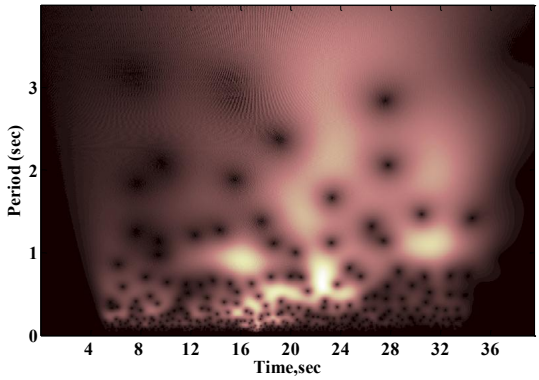	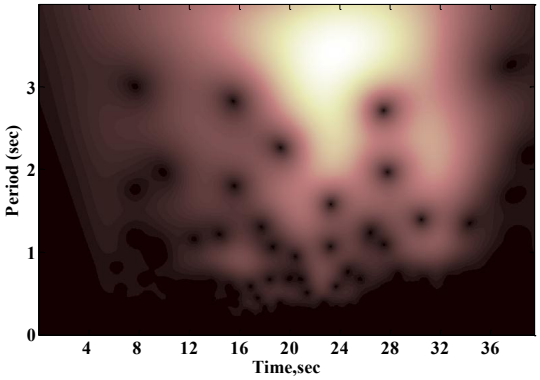
Freq Domain Method	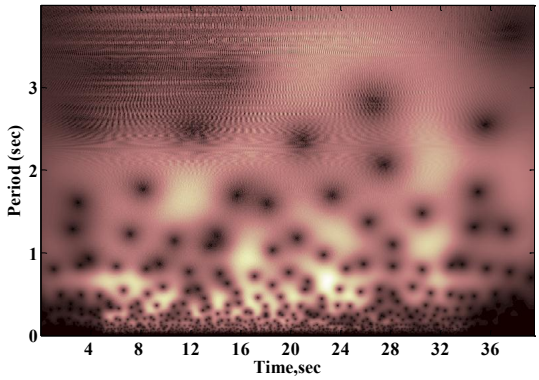	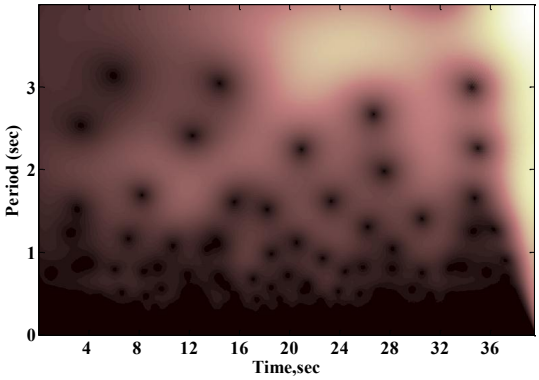

Proposed Method	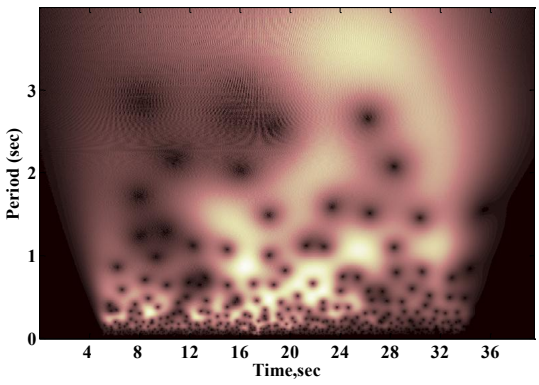	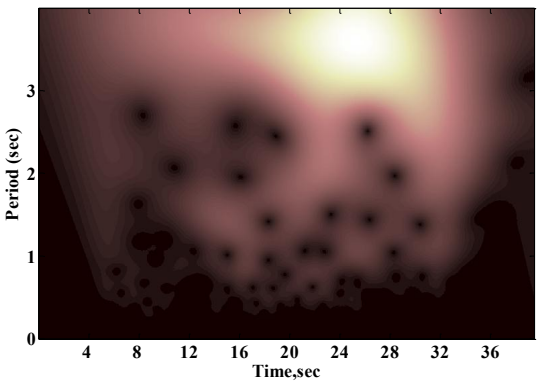

San Fernando, LA Hollywood Stor. 1971. M6.6, Component 090

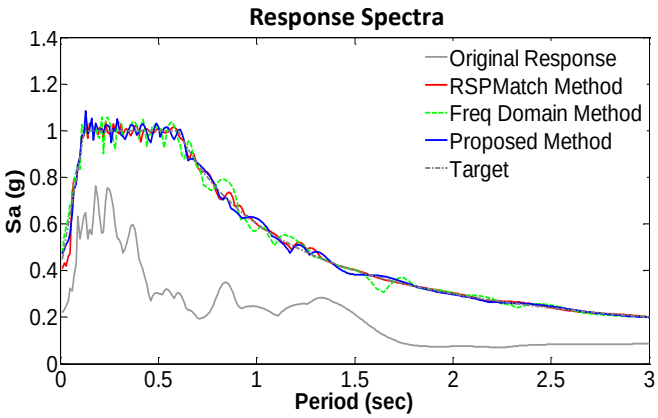

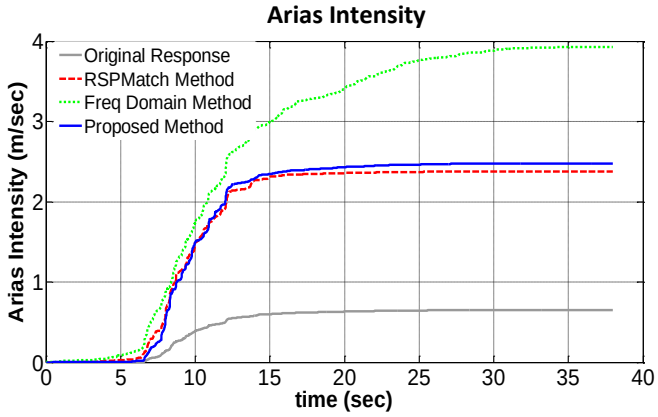

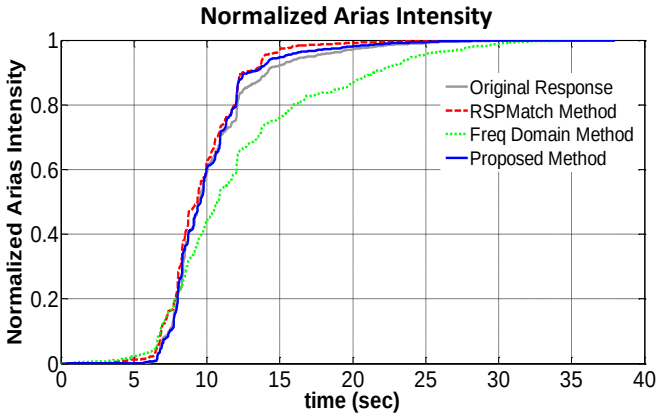

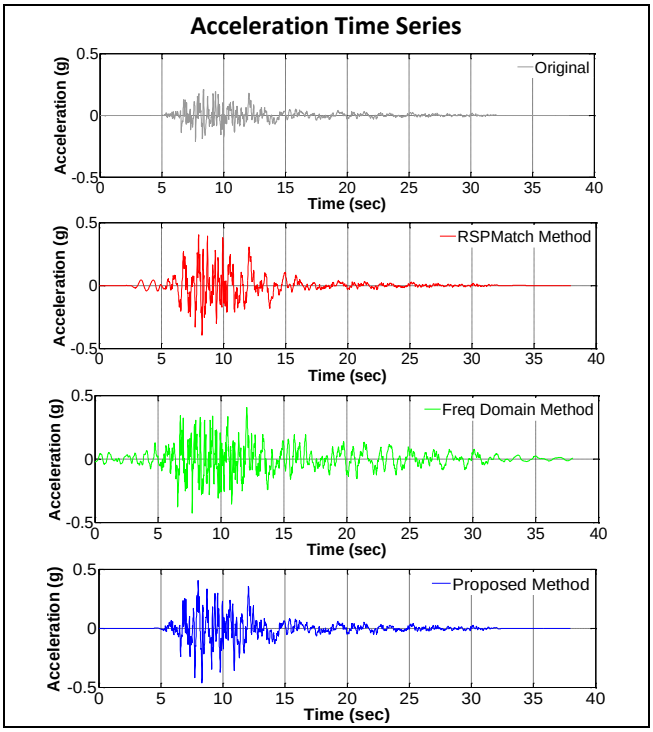

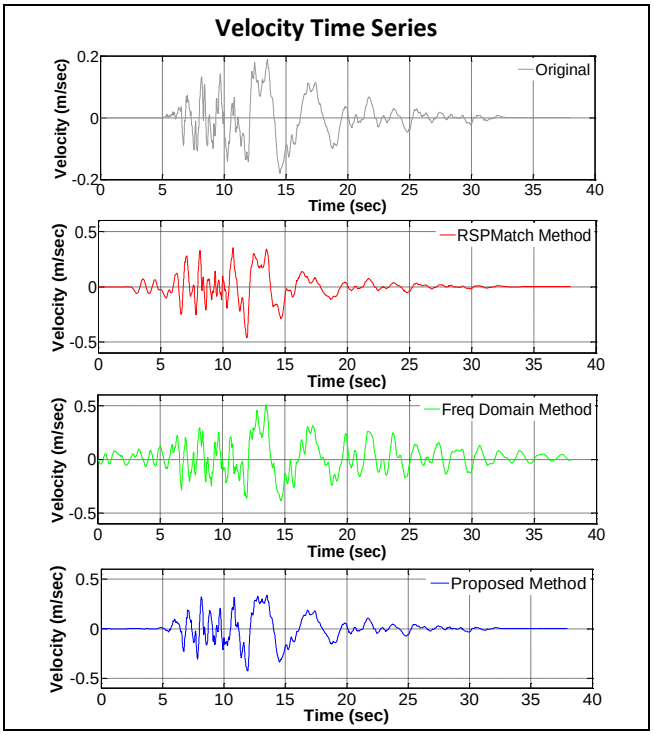

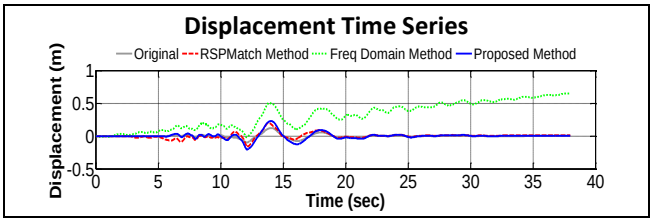

Summary

Method	Comp. Time (sec)	Average Misfit (g)	Maximum Misfit (g)	Displ. Drift (m)
RSPMatch	11	0.0075	0.0506	0
Freq Method	33	0.0182	0.0991	0.66
Proposed Method	19	0.0106	0.0837	0

	Wavelet Coefficient of Acceleration Time Series	Wavelet Coefficient of Displacement Time Series
Original	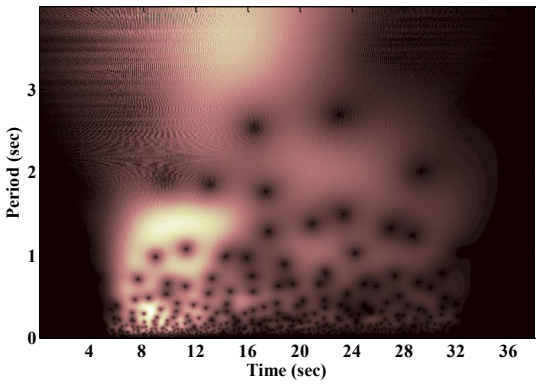	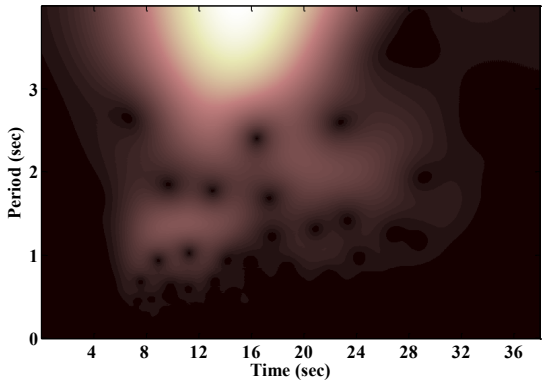
RSPMatch Method	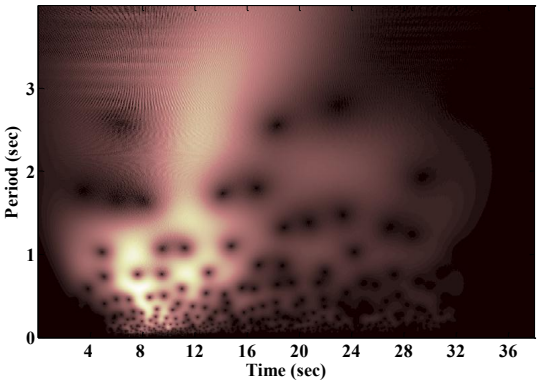	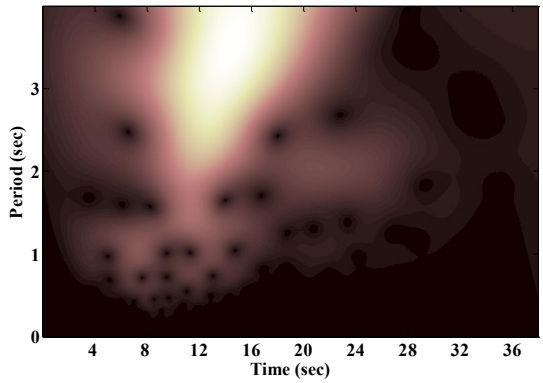
Freq Domain Method	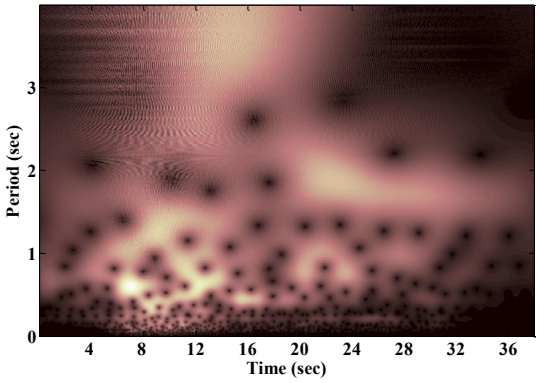	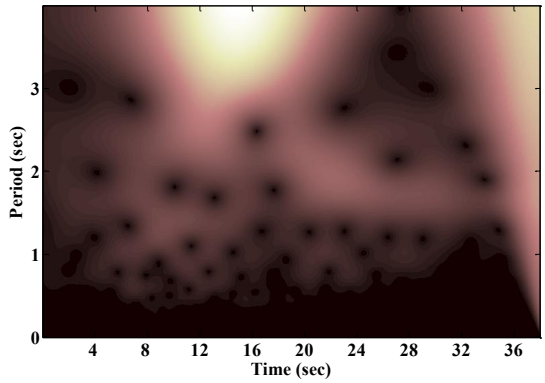
Proposed Method	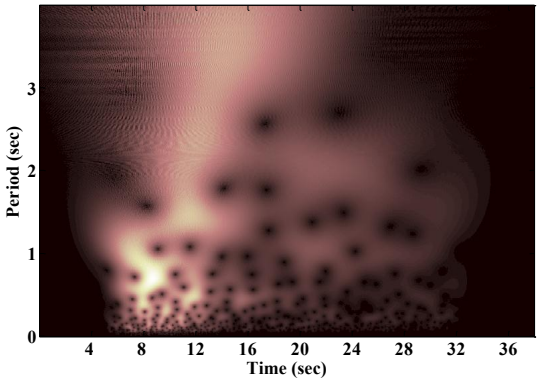	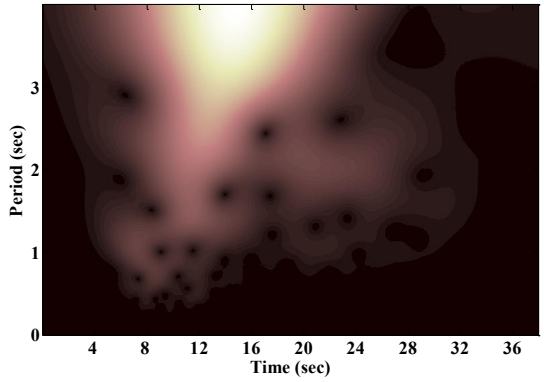

Imperial Valley-06, ElCentro #6. 1979. M6.5, Component 140

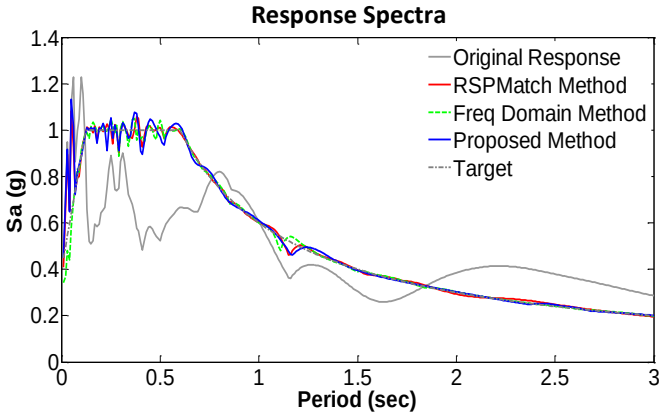

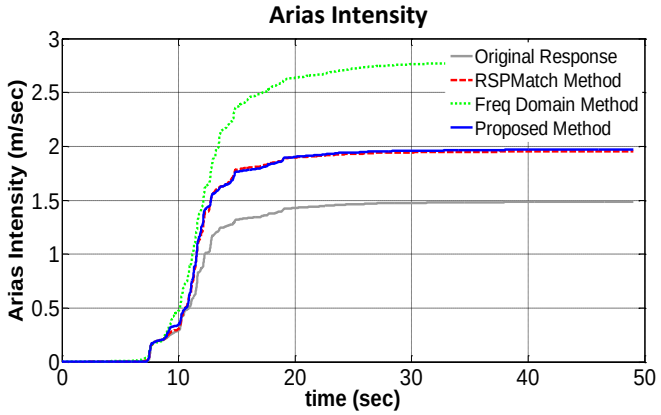

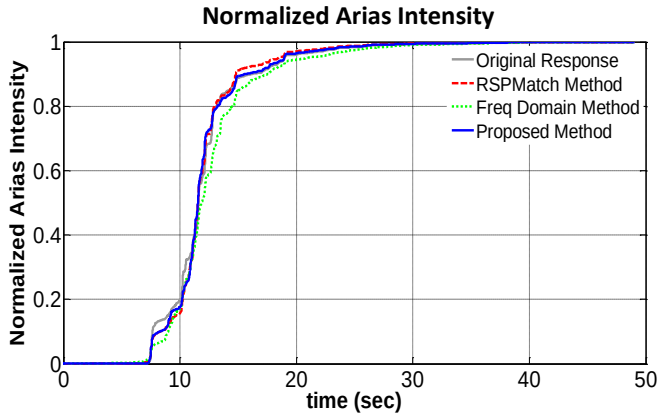

Summary

Method	Comp. Time (sec)	Average Misfit (g)	Maximum Misfit (g)	Displ. Drift (m)
RSPMatch	10	0.0084	0.0993	0
Freq Method	23	0.0077	0.1136	-0.66
Proposed Method	50	0.0104	0.1050	0

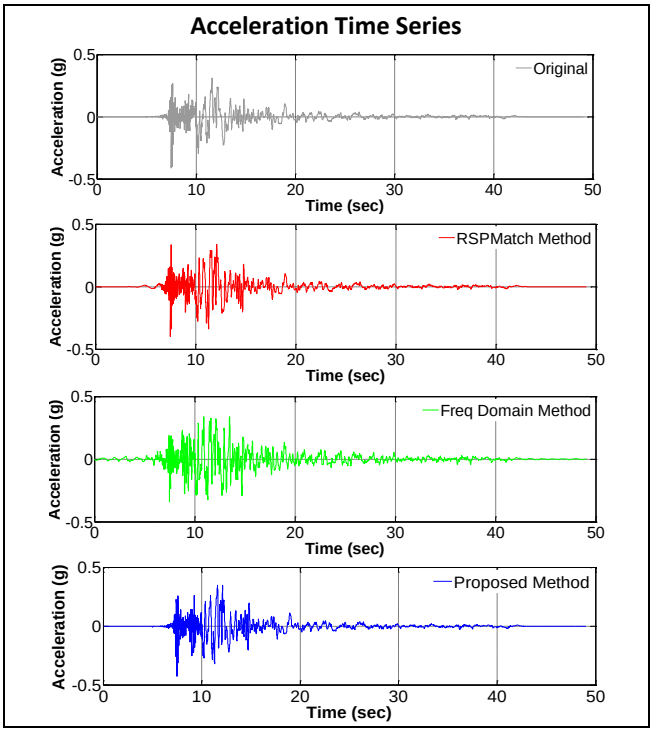

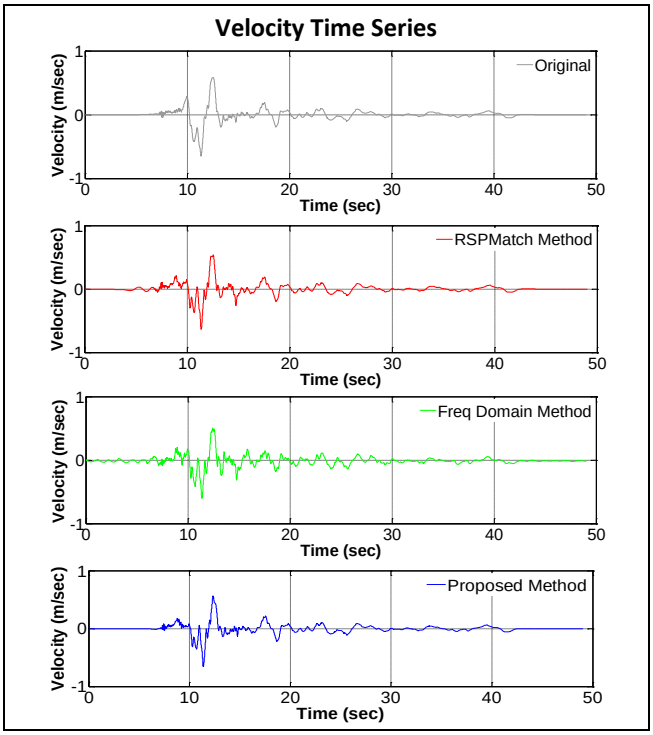

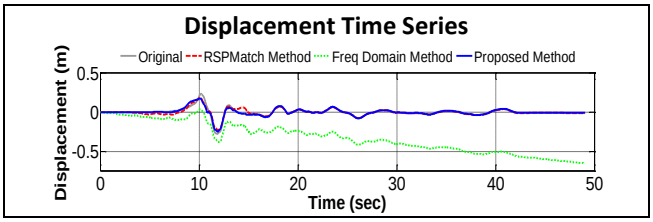

	Wavelet Coefficient of Acceleration Time Series	Wavelet Coefficient of Displacement Time Series
Original	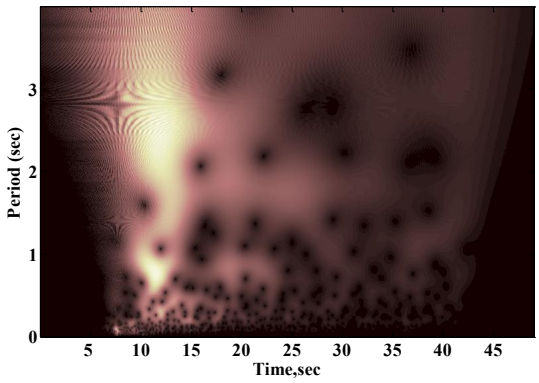	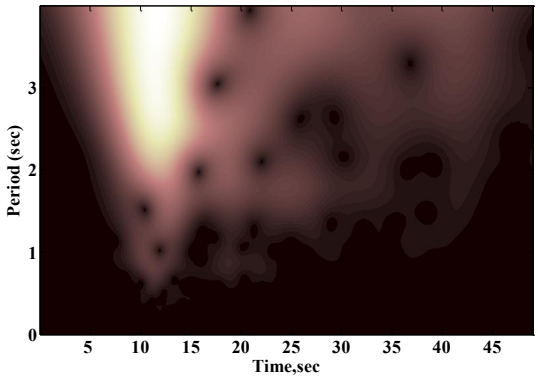
RSPMatch Method	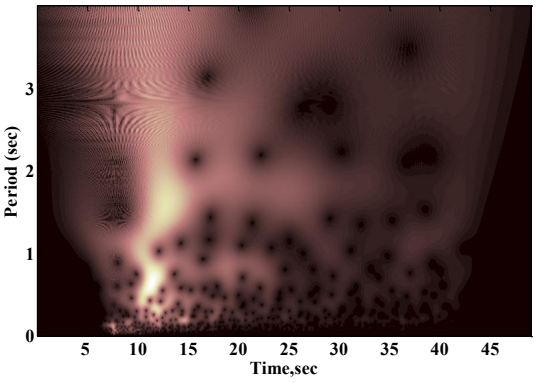	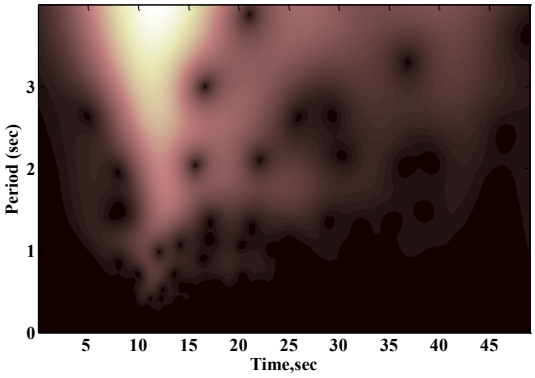
Freq Domain Method	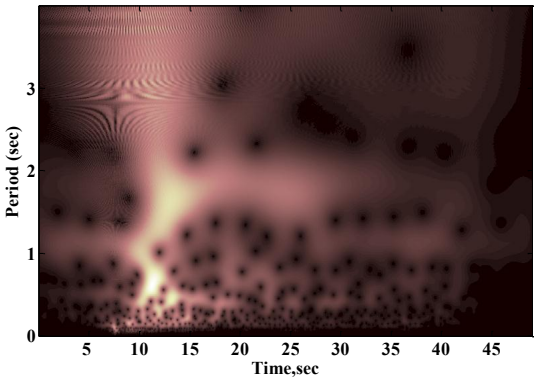	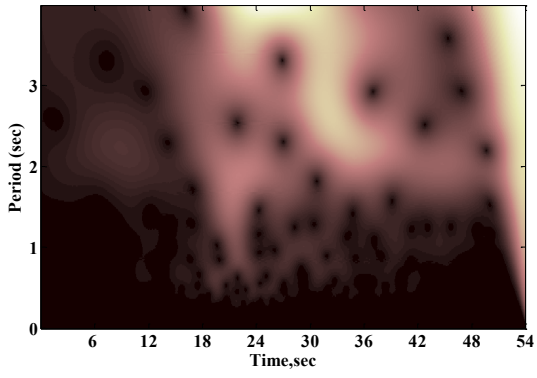
Proposed Method	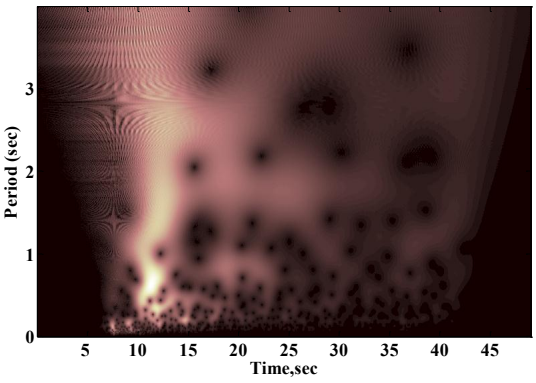	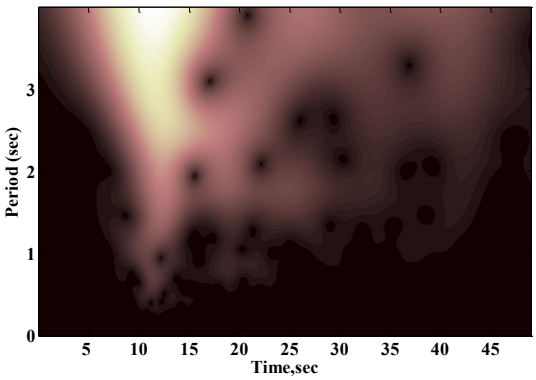

Erzican, Turkey , Erzincan. 1992. M6.7, Component EW

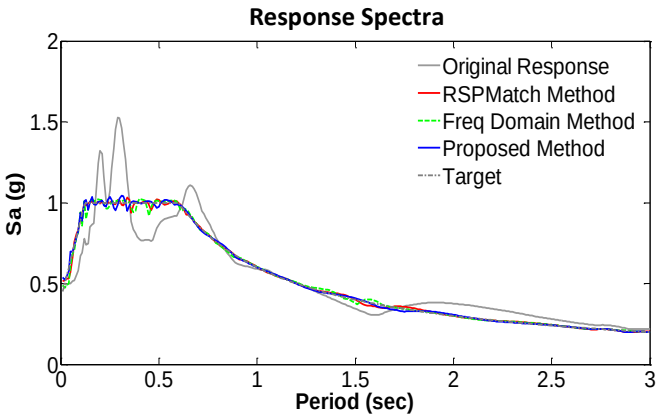

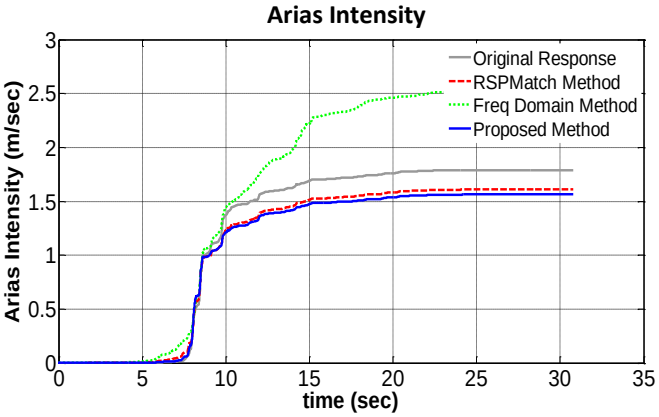

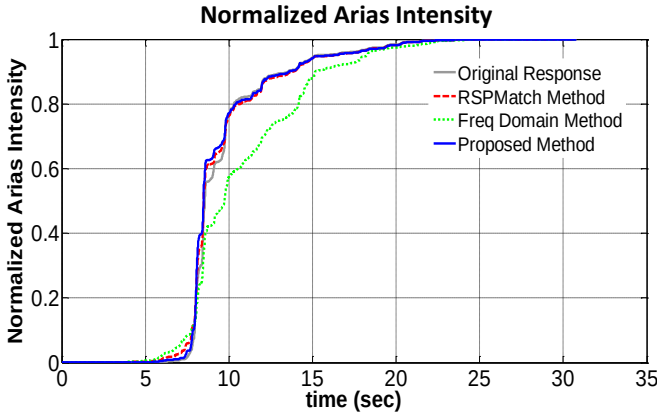

Summary

Method	Comp. Time (sec)	Average Misfit (g)	Maximum Misfit (g)	Displ. Drift (m)
RSPMatch	8	0.0061	0.0627	0
Freq Method	18	0.0084	0.0993	-0.18
Proposed Method	31	0.0071	0.0501	0

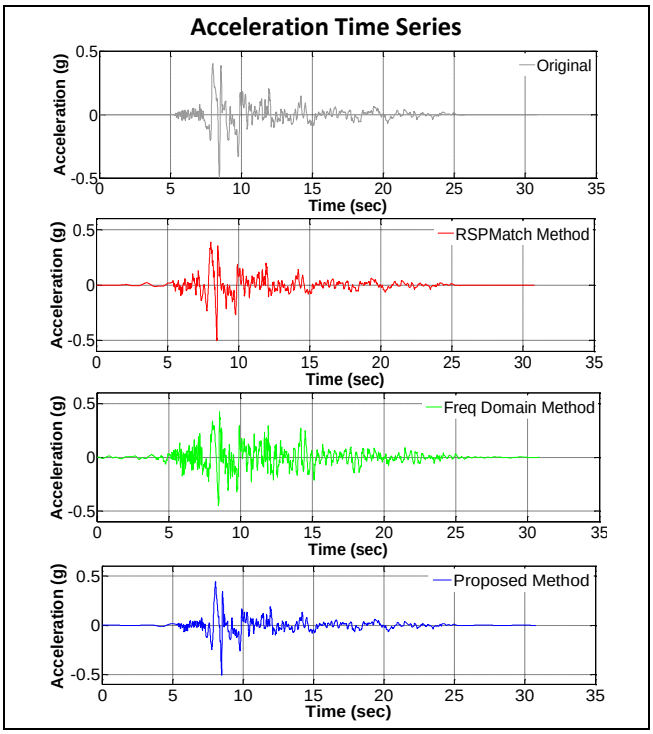

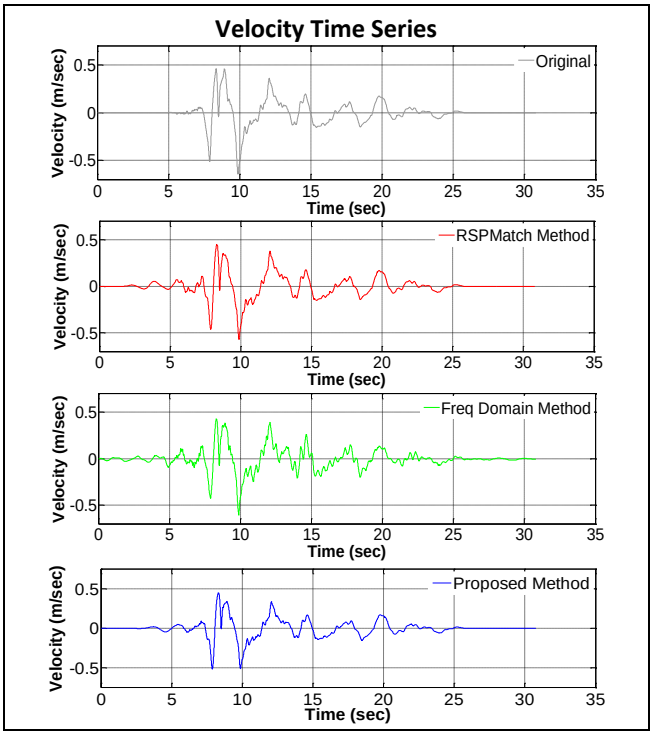

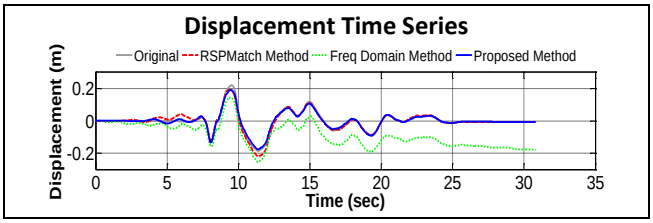

	Wavelet Coefficient of Acceleration Time Series	Wavelet Coefficient of Displacement Time Series
Original	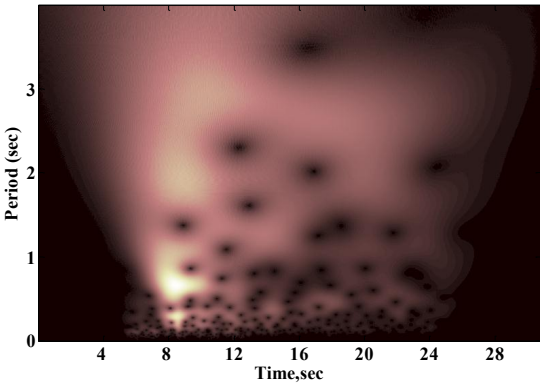	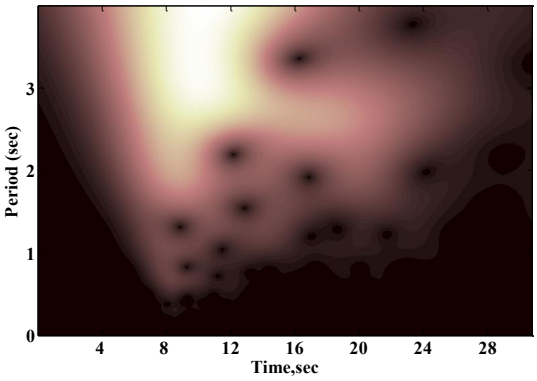
RSPMatch Method	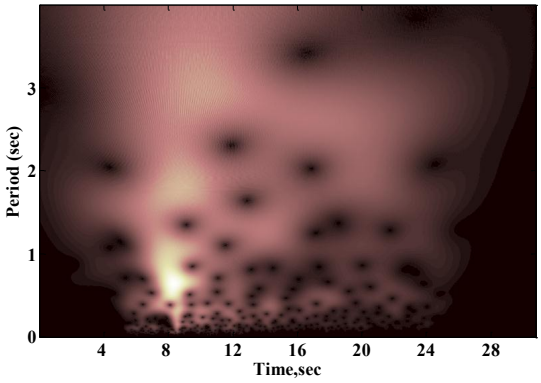	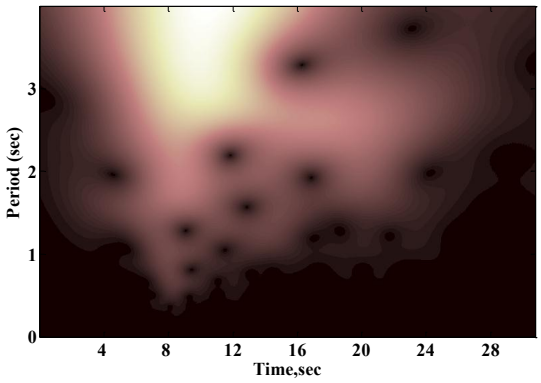
Freq Domain Method	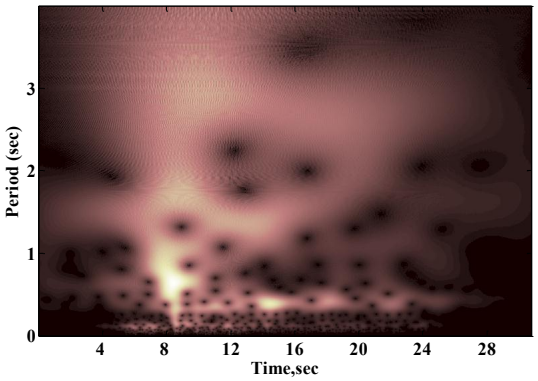	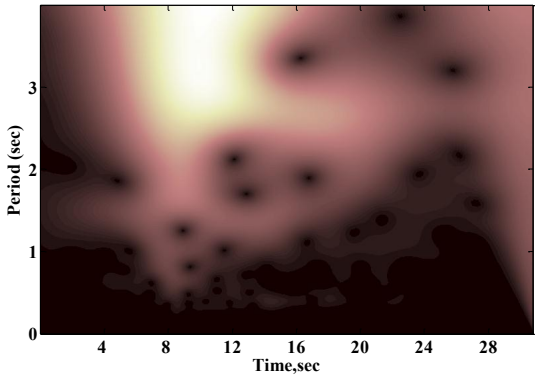
Proposed Method	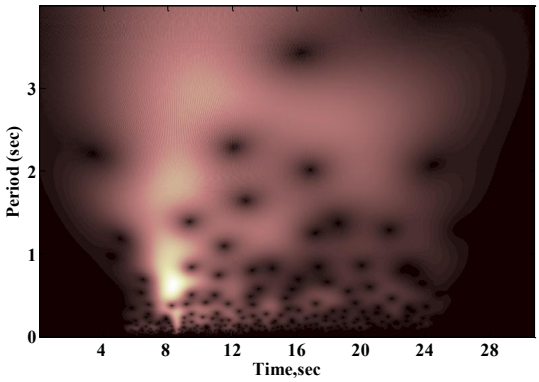	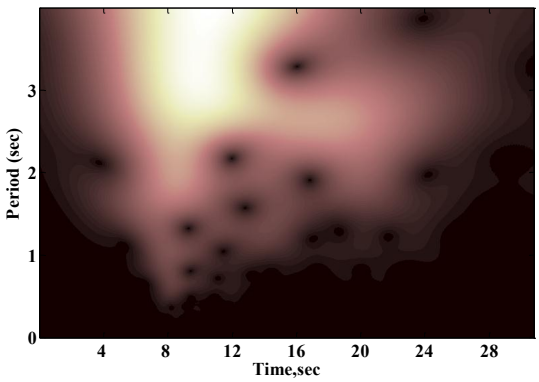

Cape Mendocino, Petrolia. 1992. M7.0, Component 000

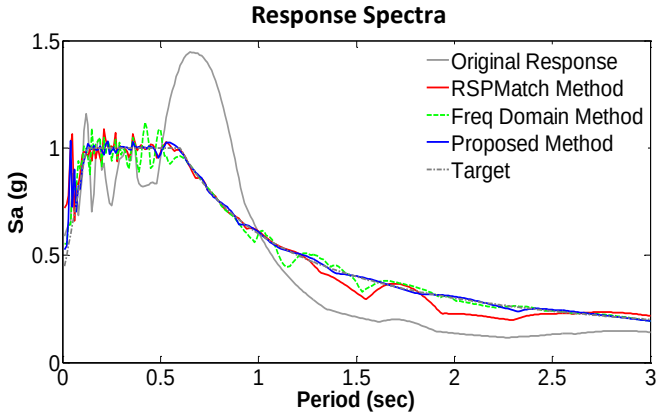

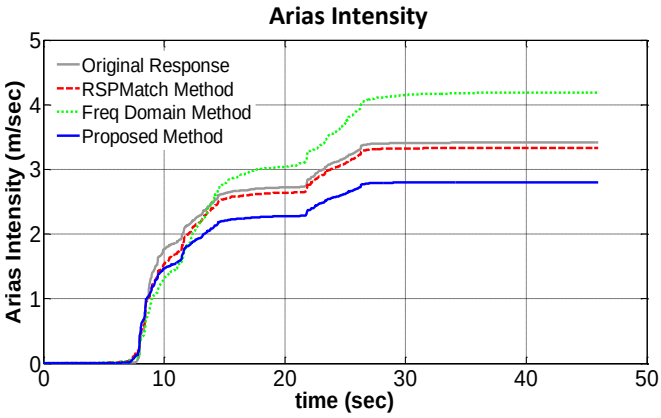

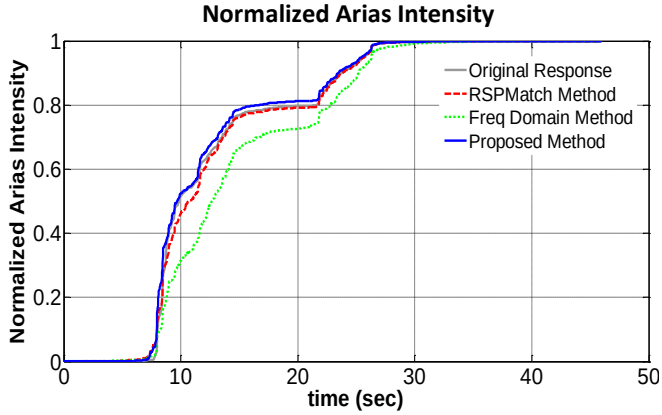

Summary

Method	Comp. Time (sec)	Average Misfit (g)	Maximum Misfit (g)	Displ. Drift (m)
RSPMatch	31	0.0274	0.0984	0.09
Freq Method	25	0.0151	0.1191	0.85
Proposed Method	19	0.0073	0.0453	-0.01

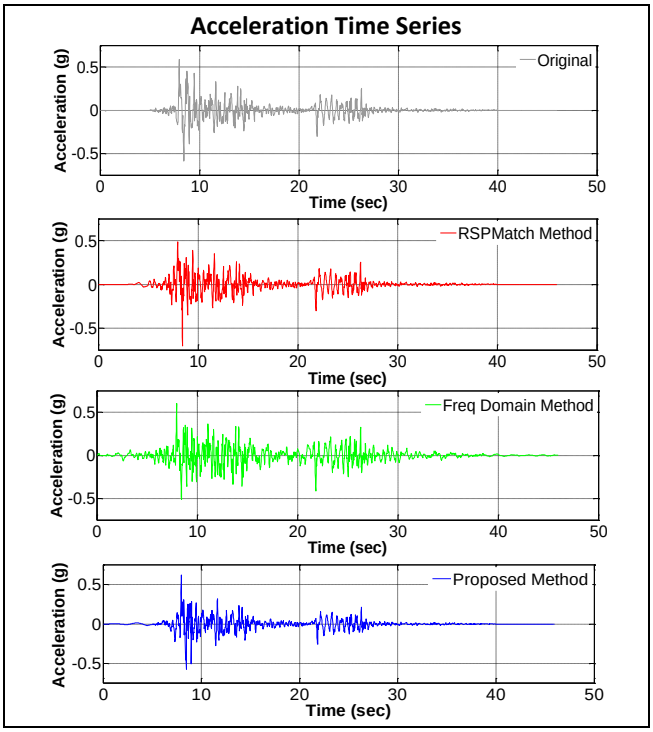

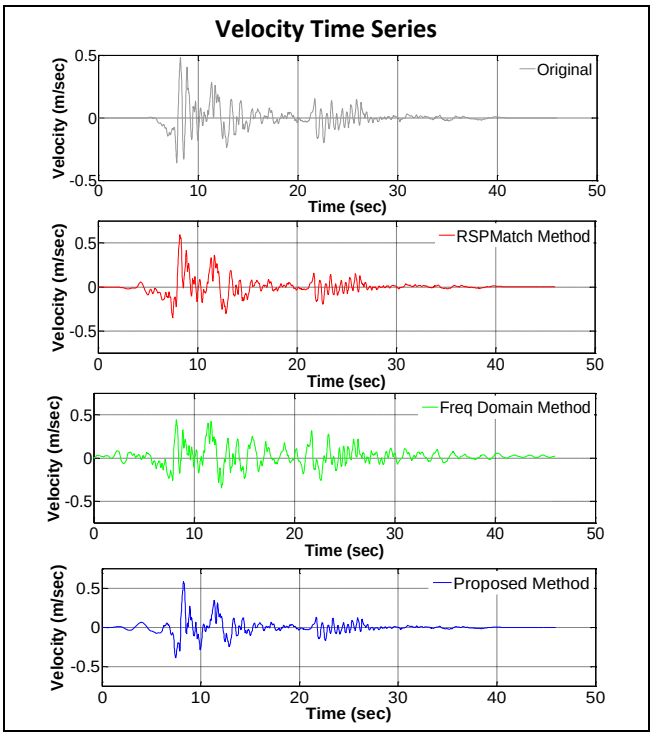

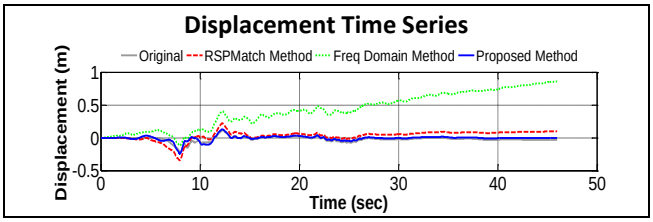

	Wavelet Coefficient of Acceleration Time Series	Wavelet Coefficient of Displacement Time Series
Original	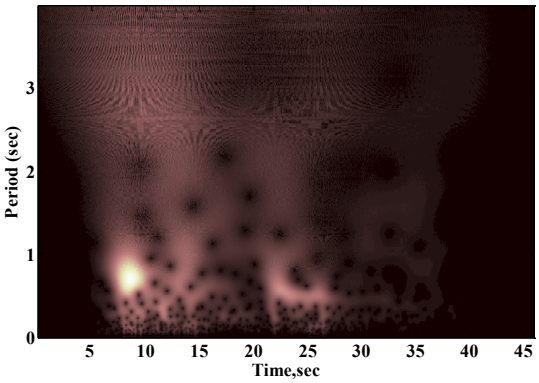	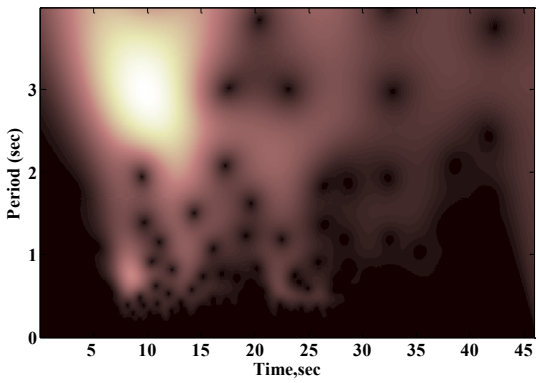
RSPMatch Method	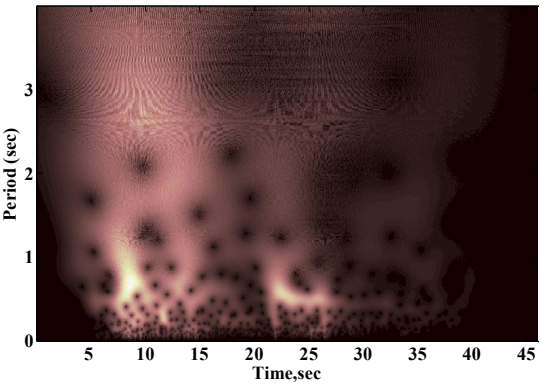	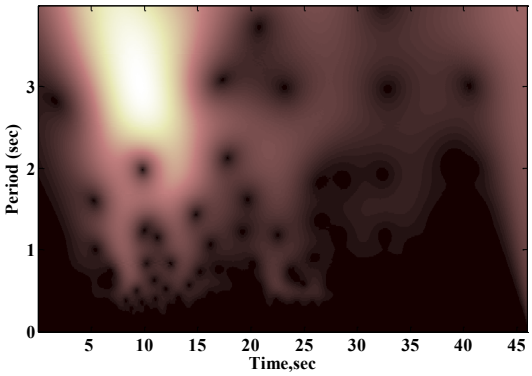
Freq Domain Method	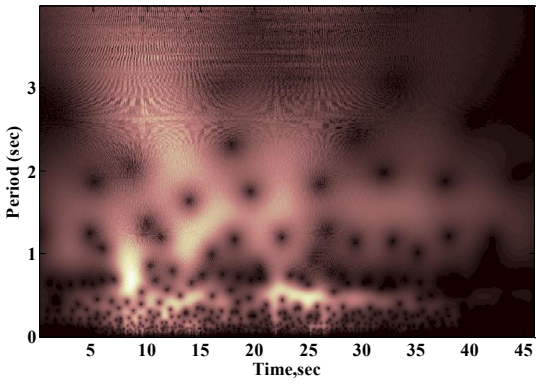	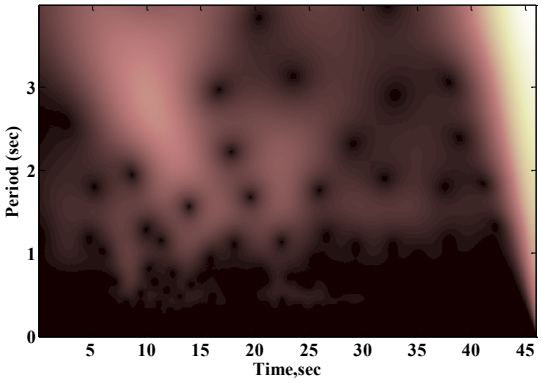
Proposed Method	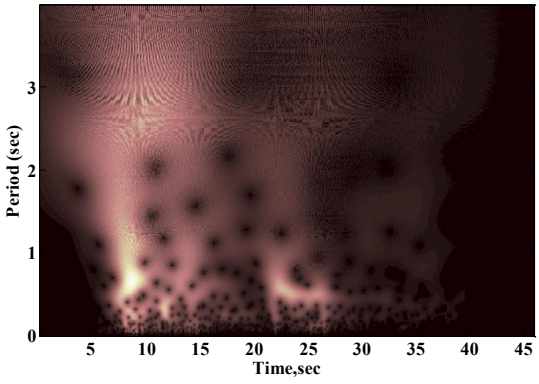	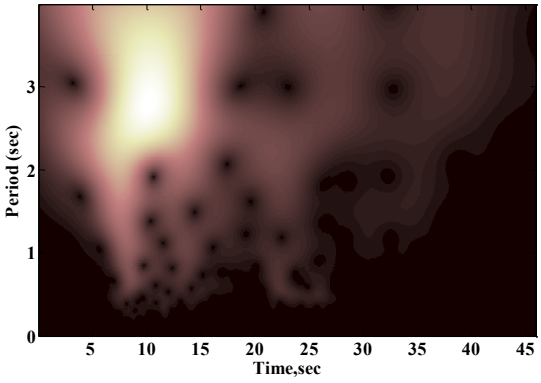

Loma Prieta, BRAN. 1989. M6.9, Component 000

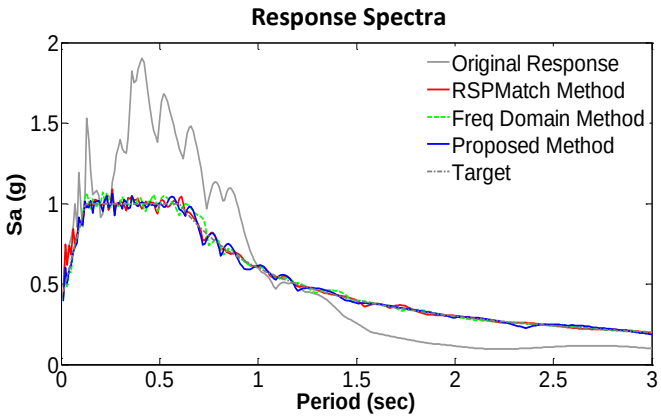

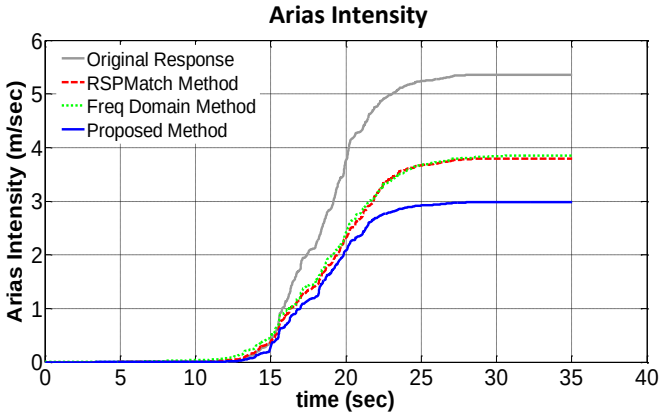

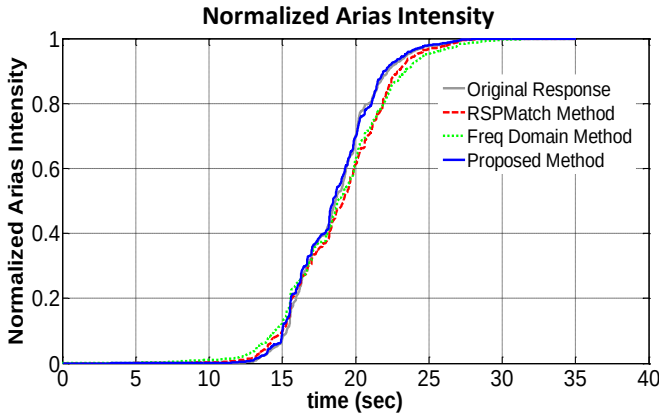

Summary

Method	Comp. Time (sec)	Average Misfit (g)	Maximum Misfit (g)	Displ. Drift (m)
RSPMatch	10	0.0107	0.090	0.01
Freq Method	19	0.0123	0.0747	-0.02
Proposed Method	36	0.0148	0.0912	0

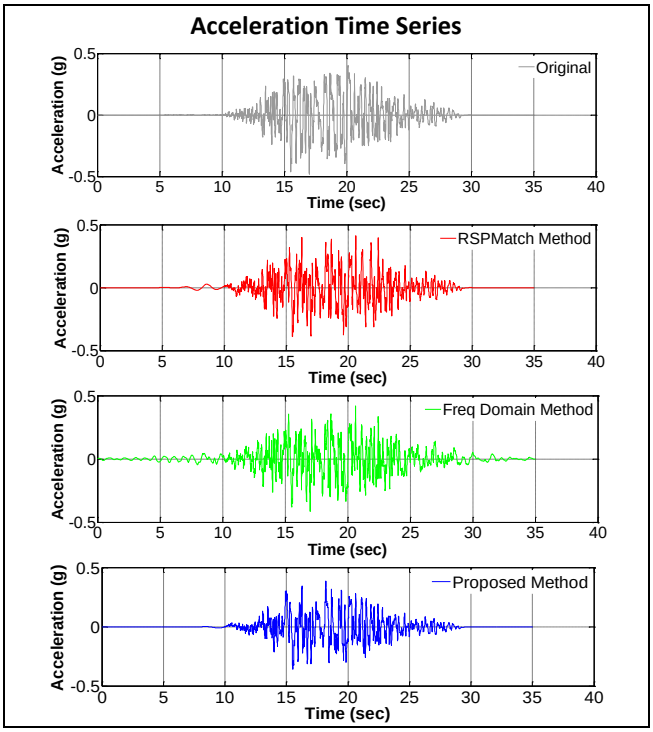

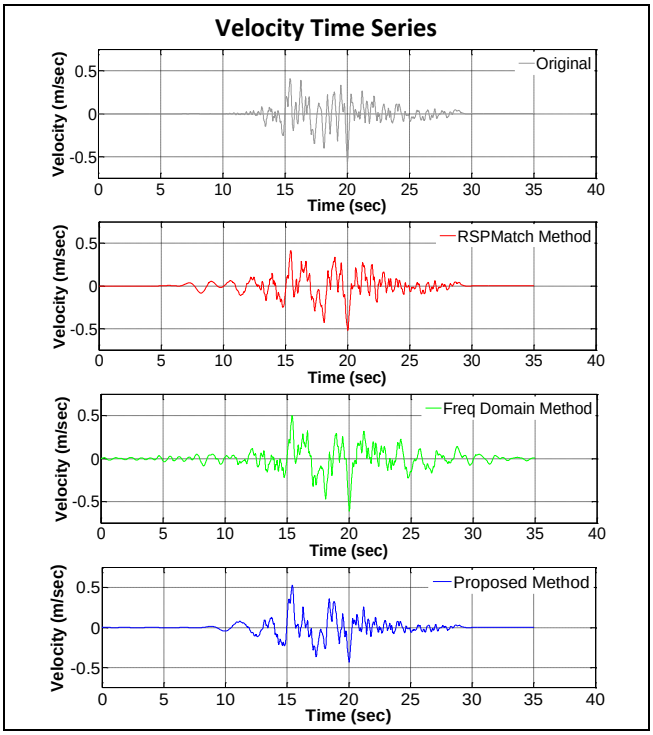

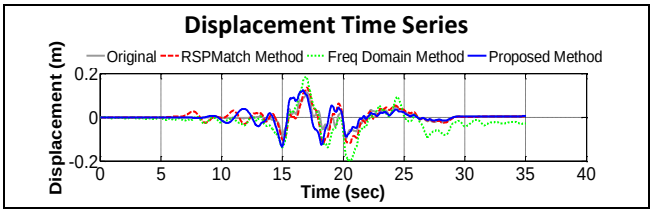

	Wavelet Coefficient of Acceleration Time Series	Wavelet Coefficient of Displacement Time Series
Original	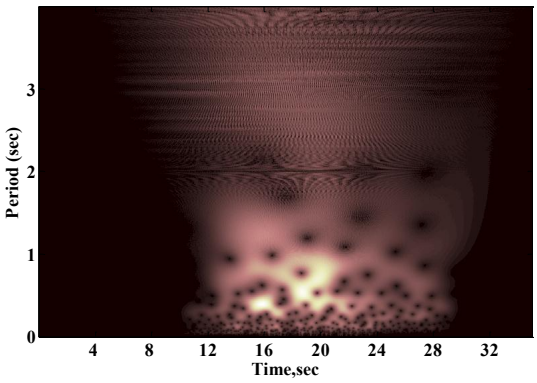	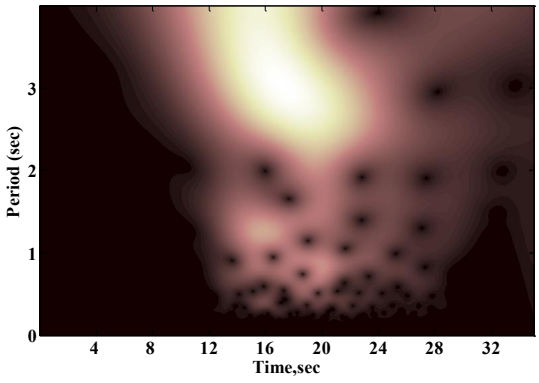
RSPMatch Method	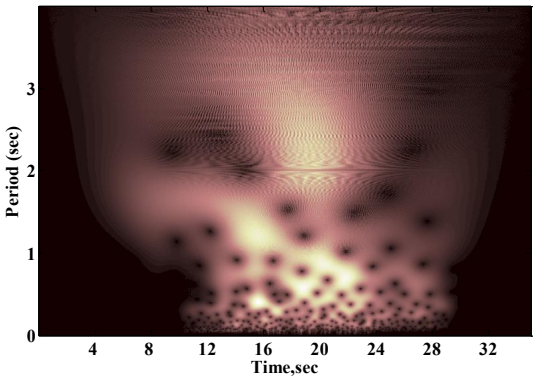	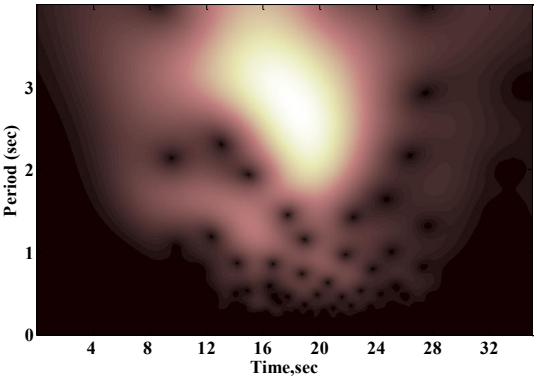
Freq Domain Method	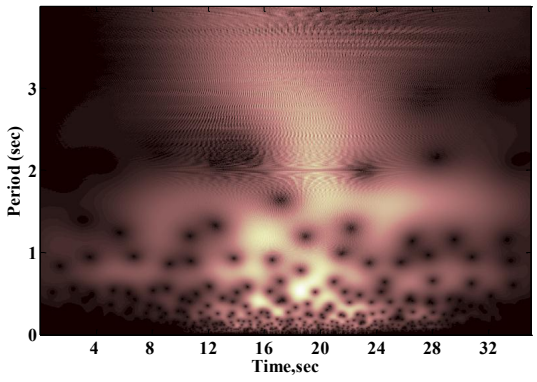	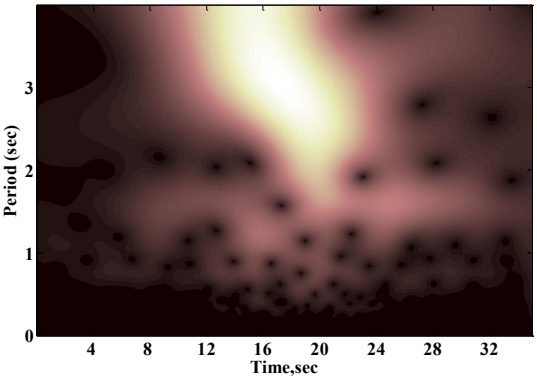
Proposed Method	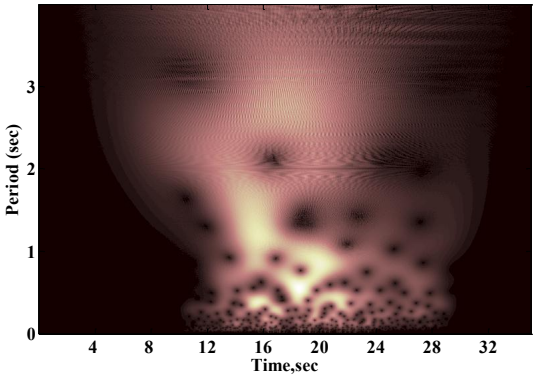	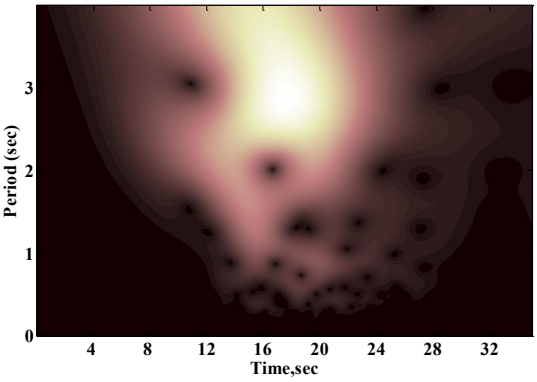

Nahanni Canada, Site 1. 1985. M6.8, Component 019

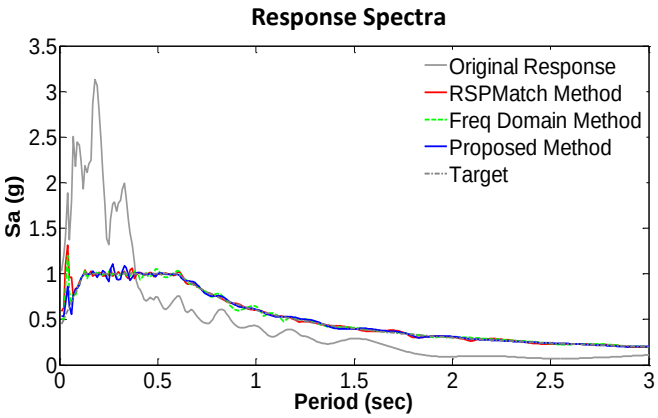

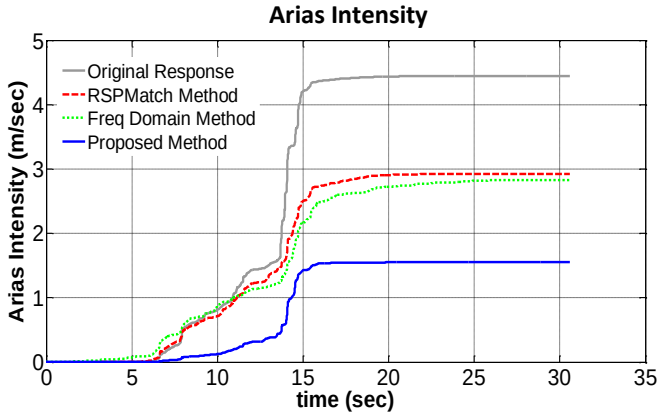

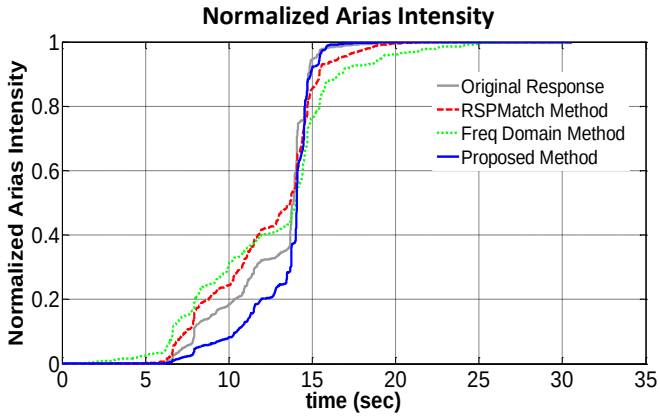

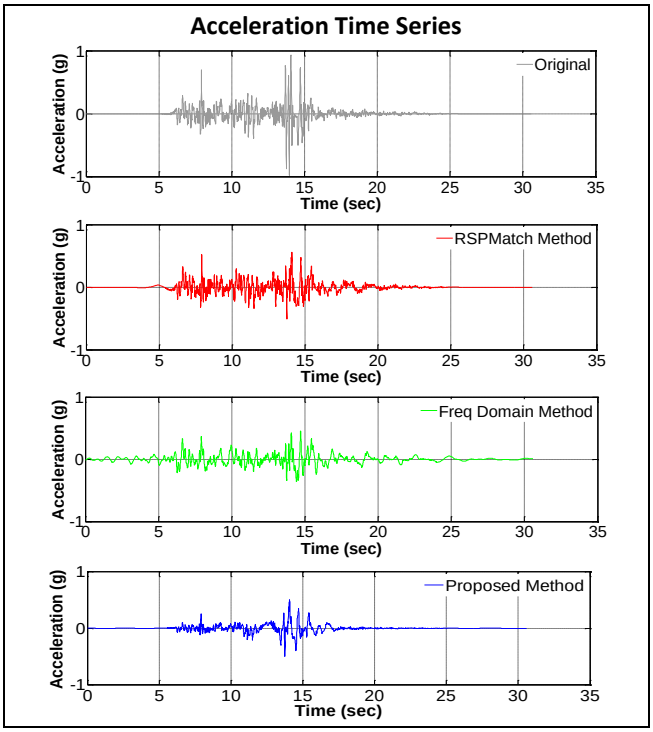

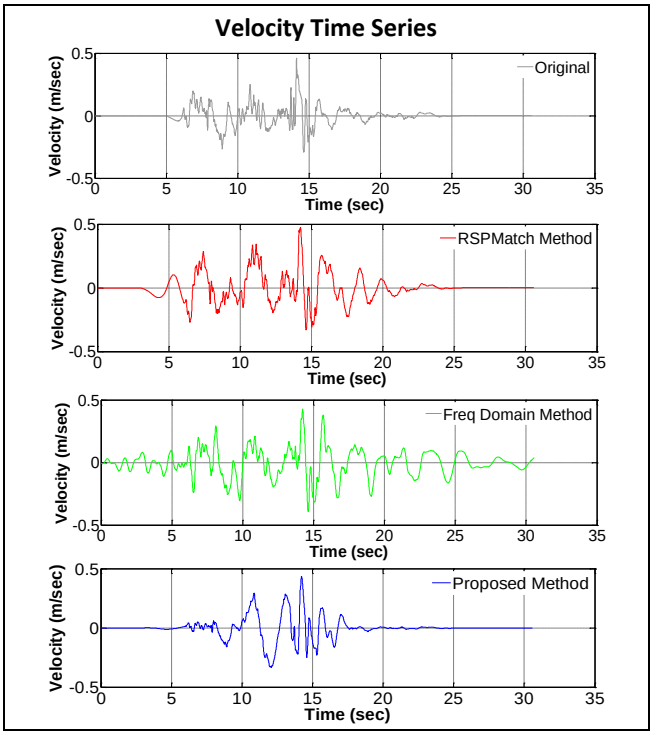

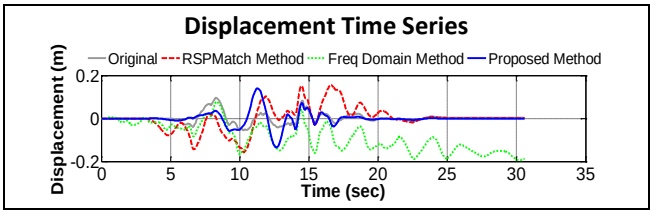

Summary

Method	Comp. Time (sec)	Average Misfit (g)	Maximum Misfit (g)	Displ. Drift (m)
RSPMatch	31	0.0097	0.0737	0
Freq Method	23	0.0136	0.0651	-0.18
Proposed Method	33	0.0112	0.1062	0

	Wavelet Coefficient of Acceleration Time Series	Wavelet Coefficient of Displacement Time Series
Original	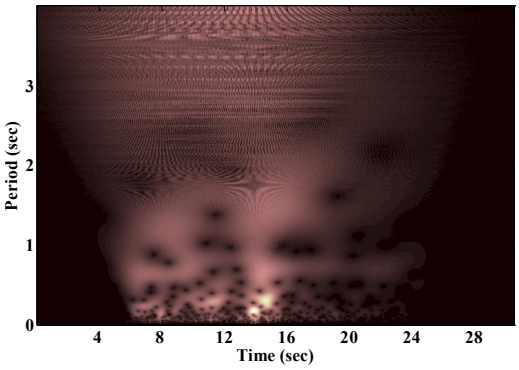	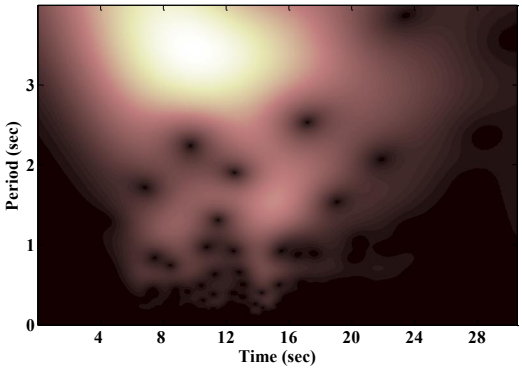
RSPMatch Method	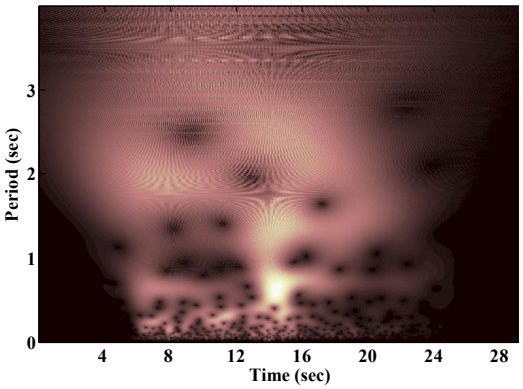	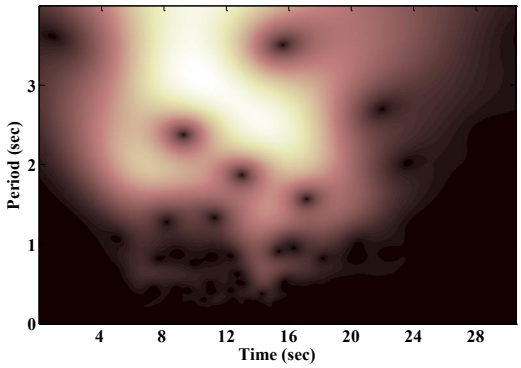
Freq Domain Method	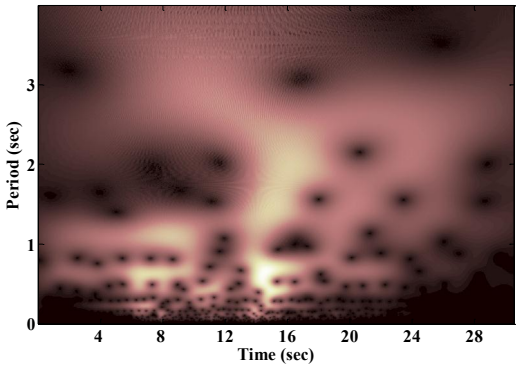	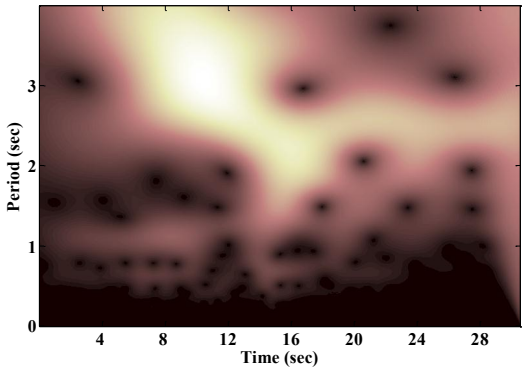
Proposed Method	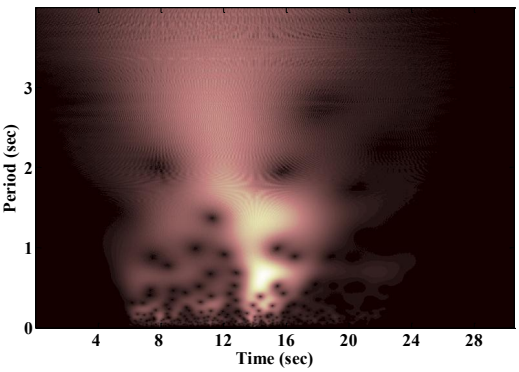	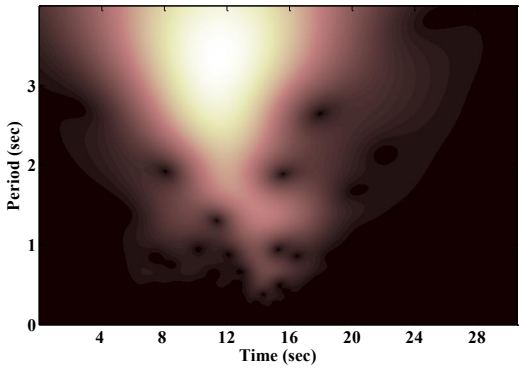

Northridge-01, Northridge-Saticoy. 1994. M6.7, Component 090

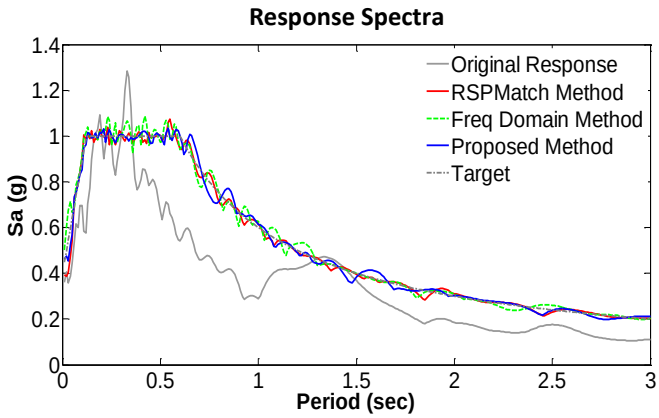

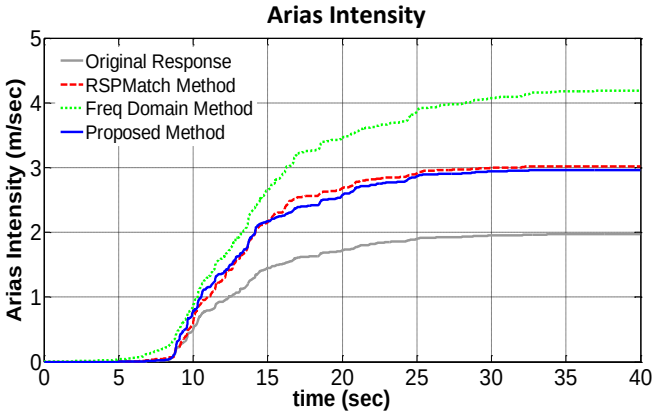

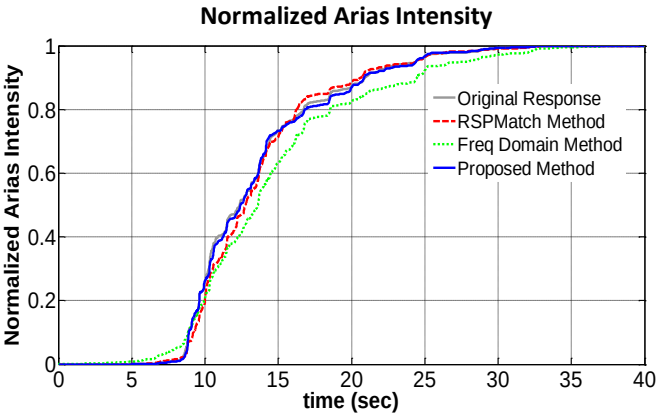

Summary

Method	Comp. Time (sec)	Average Misfit (g)	Maximum Misfit (g)	Displ. Drift (m)
RSPMatch	12	0.0119	0.0737	0
Freq Method	20	0.0172	0.0861	0.57
Proposed Method	21	0.0152	0.0921	0

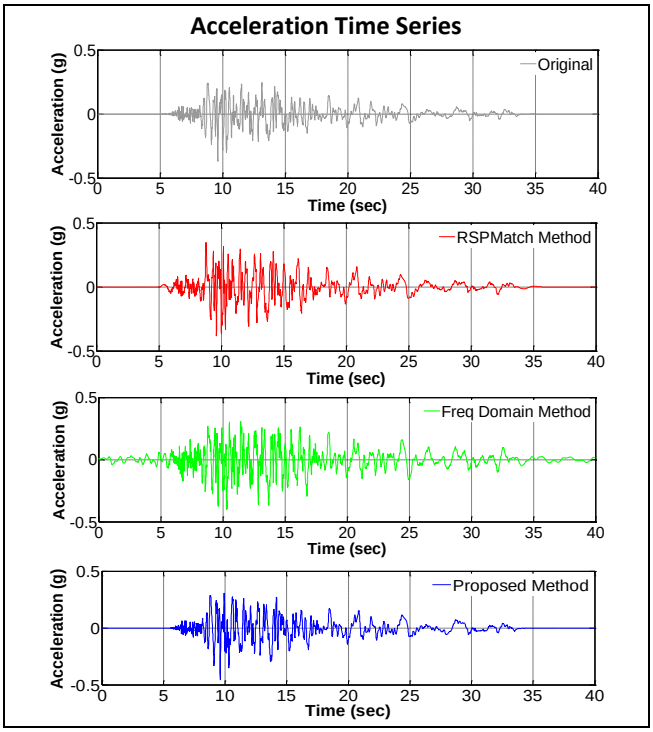

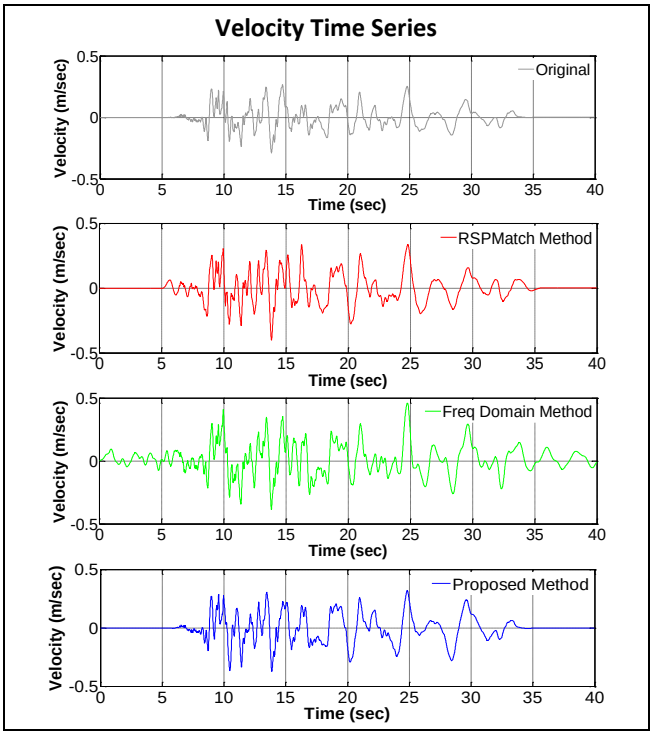

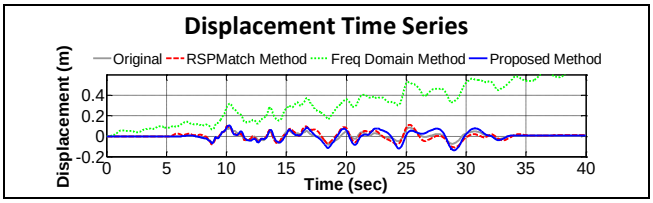

	Wavelet Coefficient of Acceleration Time Series	Wavelet Coefficient of Displacement Time Series
Original	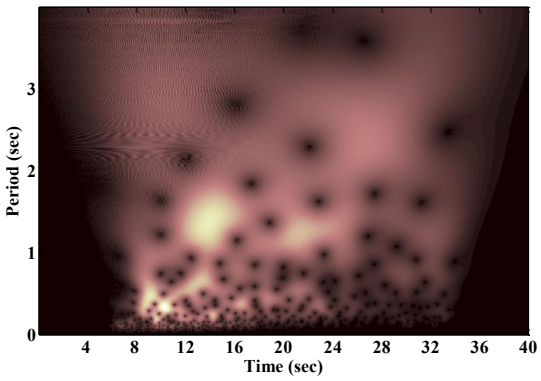	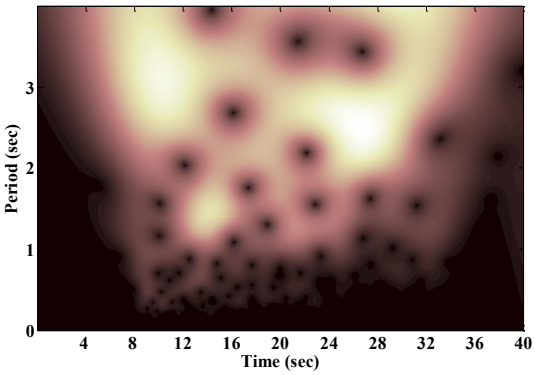
RSPMatch Method	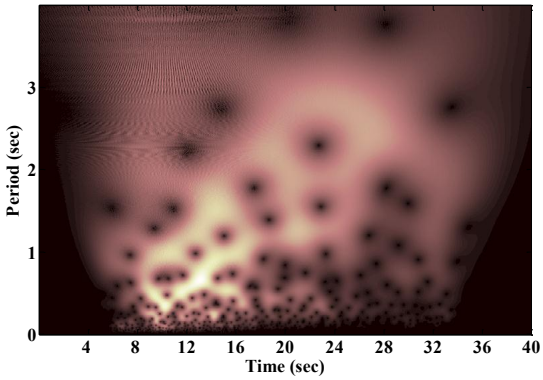	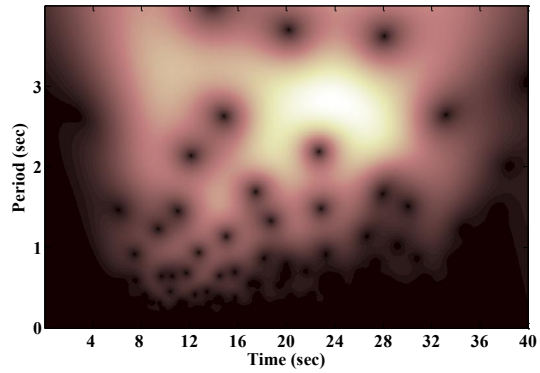
Freq Domain Method	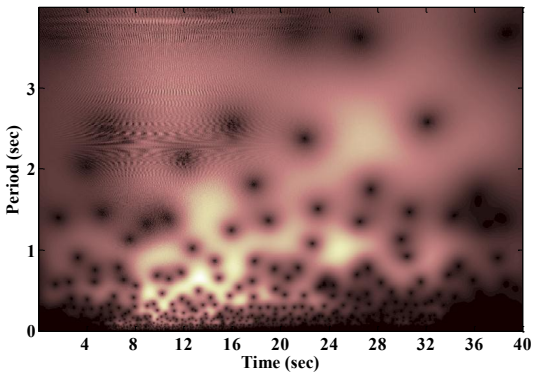	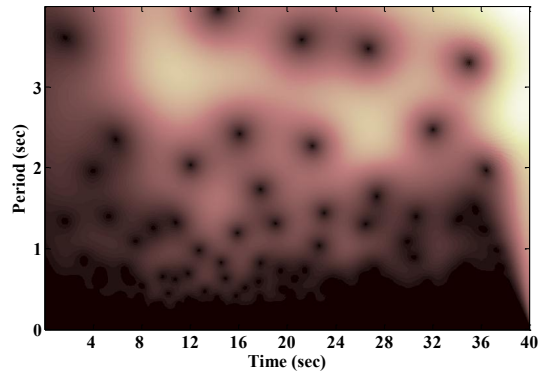
Proposed Method	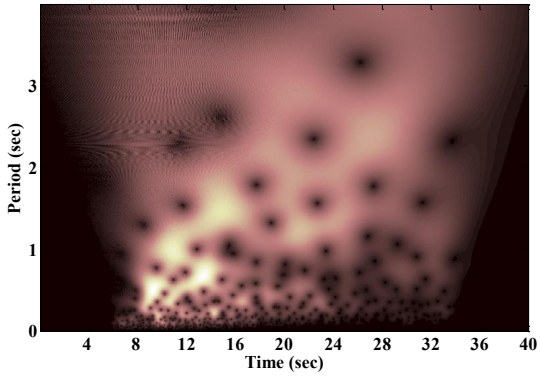	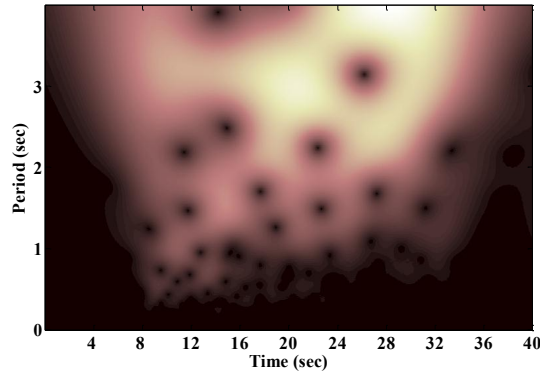

APPENDIX B. FREQUENCY RESOLUTION

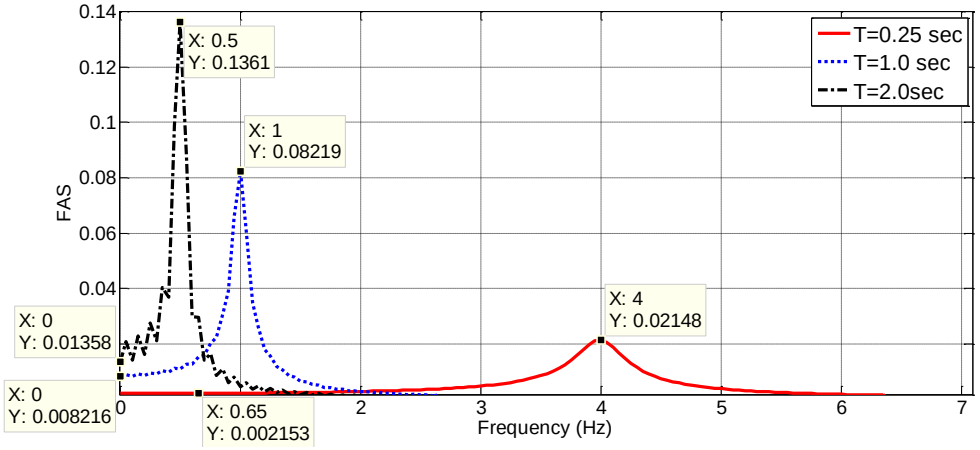

Figure B-1 Frequency Resolution of Lilhanand and Tseng Wavelet

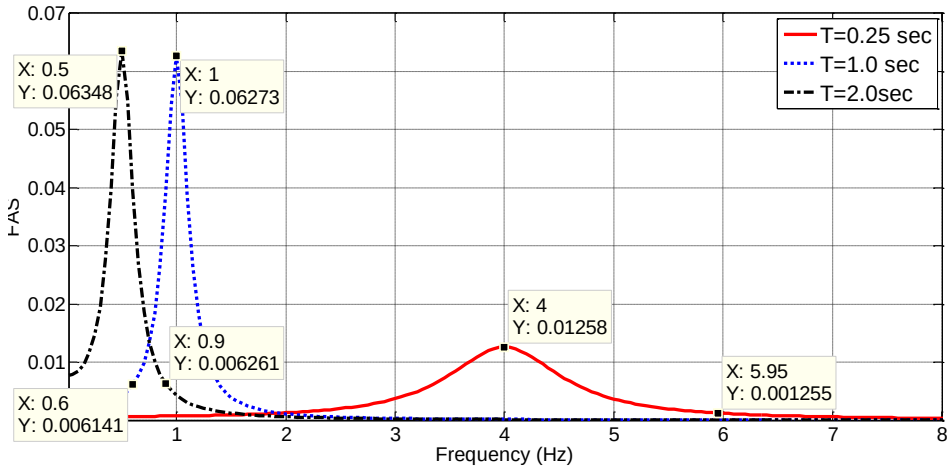

Figure B-2 Frequency Resolution of Tapered Cosine Wavelet

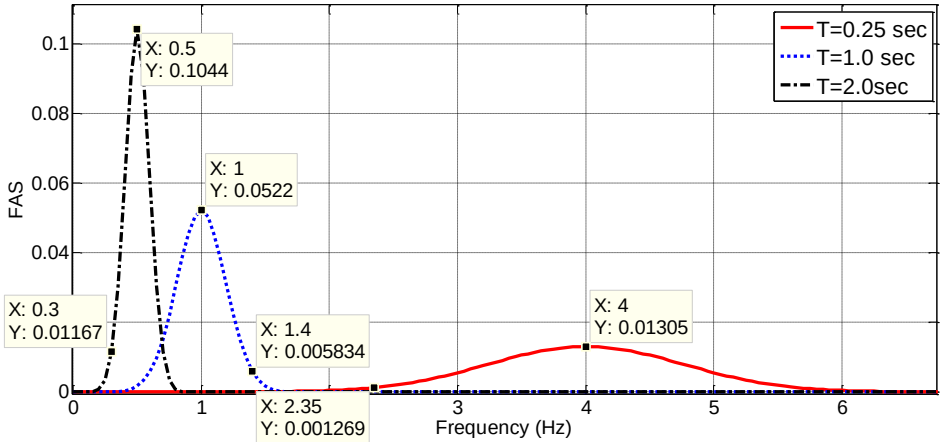

Figure B-3 Frequency Resolution of Corrected Tapered Cosine Wavelet

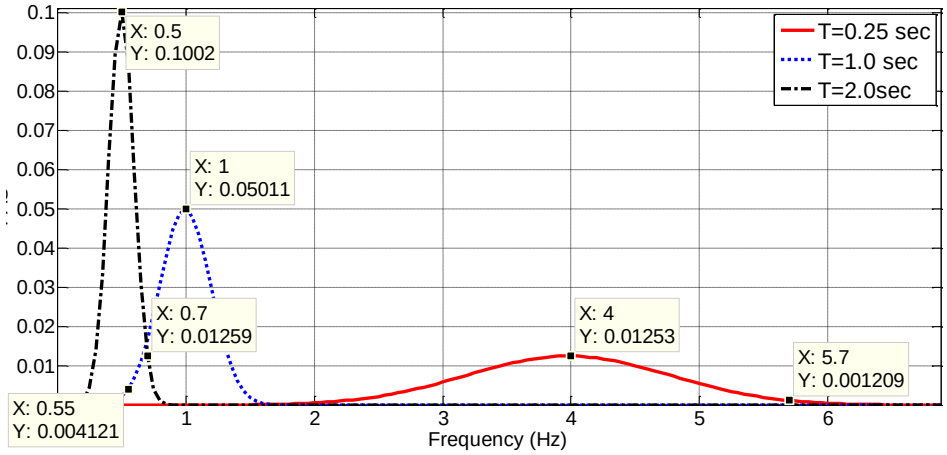

Figure B-4 Frequency Resolution of Morlet Wavelet

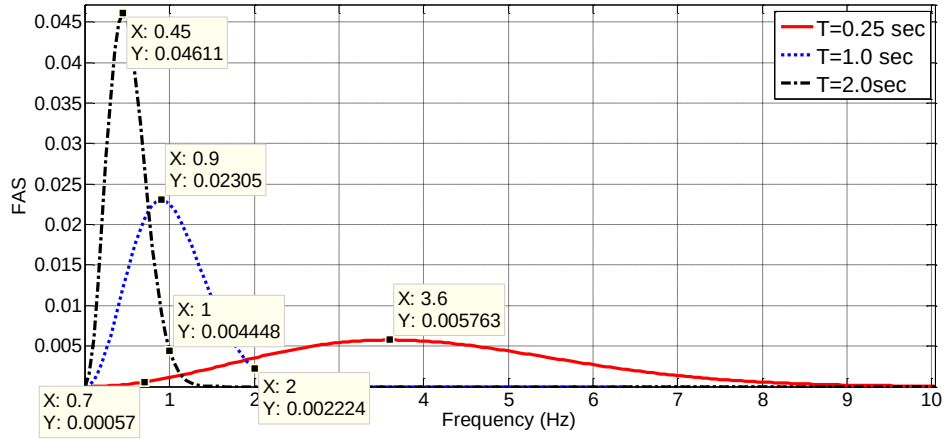

Figure B-5 Frequency Resolution of Mexican Hat Wavelet

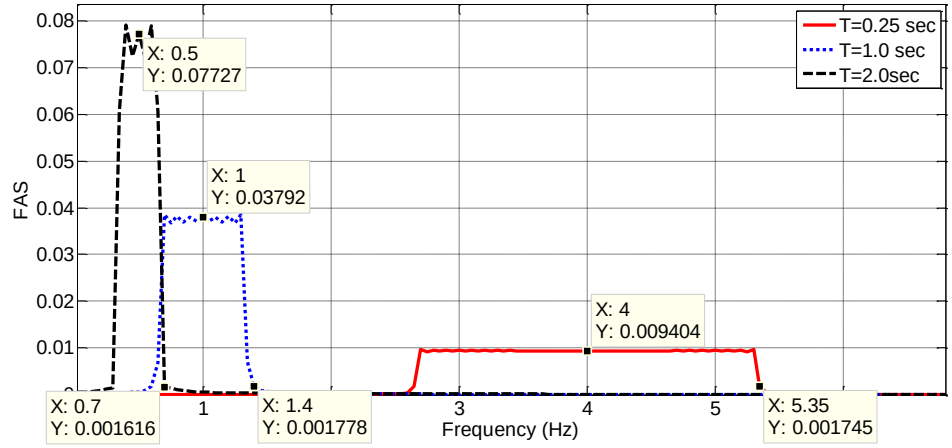

Figure B-6 Frequency Resolution of Shannon Wavelet

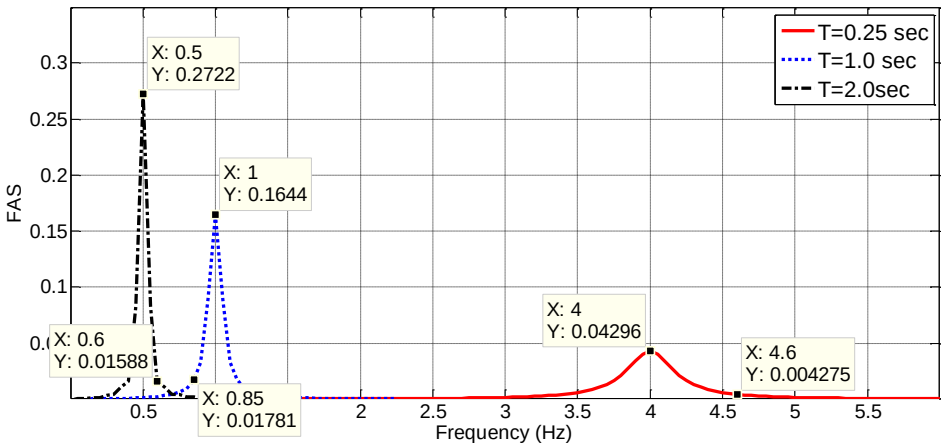

Figure B-7 Frequency Resolution of Suarez and Montejo Wavelet

APPENDIX C. FLOW CHART OF THE LINEAR ALGORITHM

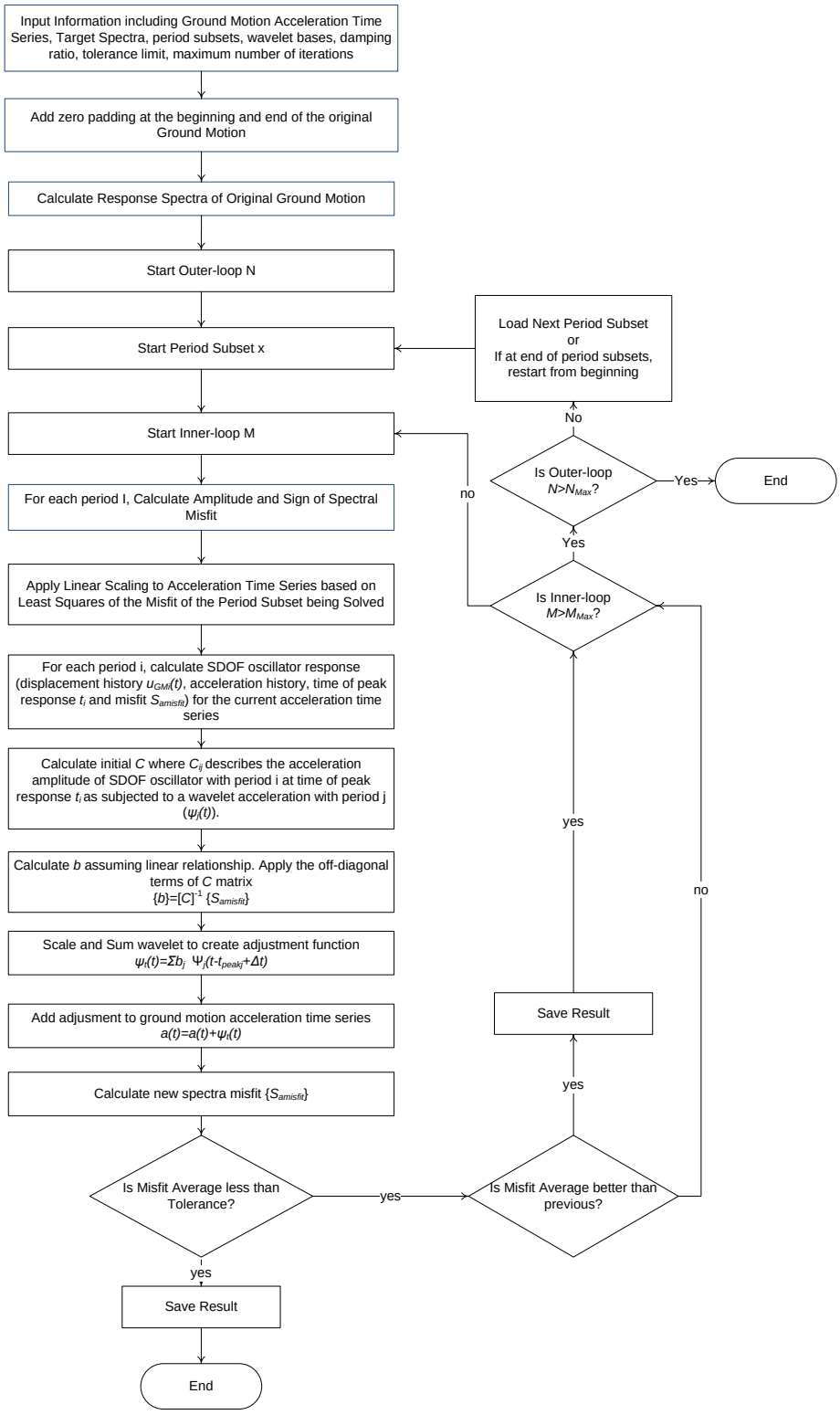

Figure C-1 Linear Algorithm Flow Chart